

# Mechanistic Studies of Monolayer Formation on H-Si(111) Surfaces

**Thesis committee****Thesis supervisor**

Prof. dr. H. Zuilhof  
Professor of Organic Chemistry  
Wageningen University

**Other members**

Prof. dr. ir. F.A.M. Leermakers	Wageningen University
Prof. dr. A.M. Brouwer	University of Amsterdam
Prof. dr. L.W. Jenneskens	Utrecht University
Dr. ir. L.C.P.M. de Smet	Delft University of Technology

This research was conducted under the auspices of the graduate school VLAG.

# Mechanistic Studies of Monolayer Formation on H-Si(111) Surfaces

Bart Rijkssen

## **Thesis**

submitted in fulfillment of the requirements for the degree of doctor  
at Wageningen University  
by the authority of the Rector Magnificus  
Prof. dr. M.J. Kropff  
in the presence of the  
Thesis Committee appointed by the Academic Board  
to be defended in public  
on Wednesday 11 April 2012  
at 1.30 p.m. in the Aula.

Bart Rijksen

Mechanistic Studies of Monolayer Formation on H-Si(111) Surfaces

PhD thesis, Wageningen University, Wageningen, The Netherlands, 2012

With references, with summaries in Dutch and English

ISBN: 978-94-6173-200-2

## Table of Contents

<b>Chapter 1</b>	General Introduction	7
<b>Chapter 2</b>	Silicon Radical Surface Chemistry	15
<b>Chapter 3</b>	Mimicking the Silicon Surface: Reactivity of Silyl Radical Cations towards Nucleophiles	73
<b>Chapter 4</b>	Reactivity of Silyl Radicals Towards Unsaturated Hydrocarbons: Understanding Monolayer Formation on H-Terminated Silicon (111)	97
<b>Chapter 5</b>	Hexadecadienyl Monolayers on H- Si(111): Faster Monolayer Formation and Improved Surface Coverage Using the Enyne Moiety	115
<b>Chapter 6</b>	General Discussion	137
<b>Appendices</b>		143
<b>Summary</b>		151
<b>Samenvatting</b>		155
<b>Curriculum Vitae</b>		159
<b>List of Publications</b>		161
<b>Overview Training Activities</b>		163
<b>Dankwoord</b>		165



# Chapter 1

## General Introduction

## 1.1 Self-Assembled Monolayers

Thin films of materials have already been known and studied for centuries.<sup>1,2</sup> Within the area of thin layers, monolayers form a special class, since these layers are exactly one molecule thick. One of the most widely known examples of monolayers are Langmuir films, which are layers formed by surfactants that are spread on a liquid (mostly water) surface. This thesis, however, will focus on more stable, organic monolayers that are formed on solid surfaces (more specifically silicon) by self assembly from solutions or neat liquid material. Self assembly is a process in which components assemble into highly ordered structures without any assistance or guidance from pre-ordered structures (see Figure 1).<sup>1-6</sup> This can happen both for molecules,<sup>7-9</sup> 2D structures,<sup>2,10-12</sup> and even three-dimensional, mesoscale-sized objects.<sup>13-15</sup>

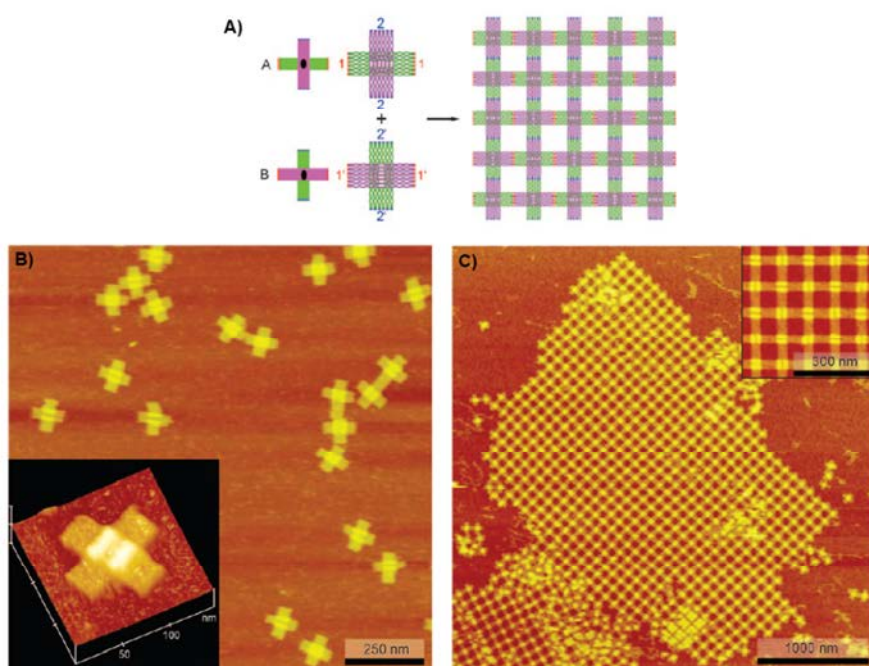


**Figure 1.** Example of self-assembly of DNA-structures, so-called DNA-origami;<sup>7</sup> **a.** Schematic structure of the two types of tiles (A and B), and how these self-assemble into networks; **b.** Atomic force microscopy (AFM) pictures of the individual tiles; and **c.** AFM pictures of an array of tiles with dimensions of  $2 - 3 \mu\text{m}^2$ .<sup>8</sup>



Starting from a bare surface, adsorbed molecules will initially lie flat, which lowers the free energy of the bare surface,<sup>16</sup> and minimizes the free space between the attached chains so as to optimize the Van der Waals interactions between the chains. As more molecules adsorb, the chains will stand more upright, until finally all chains are in an upright position (see Figure 2a). Densely packed monolayers express a high ordering of the chains (see Figure 2b). The speed of monolayer formation, as well as the stability of resulting layers, depends largely on how the chains are attached to the surface. Molecules can be kept in place by electronic interactions of the head group with the surface, or even form covalent bonds with the substrate. Typical examples of reversible attachment are alkanethiol monolayers on metal surfaces such as gold,<sup>10,17</sup> silver,<sup>18-20</sup> copper,<sup>20,21</sup> and platinum.<sup>22</sup> Gold surfaces are historically the most studied, because the material is easy to use (no oxidation under ambient conditions), high-quality monolayers are relatively easily obtained, and the material is compatible with spectroscopic techniques like surface plasmon resonance (SPR) and reflective IR techniques.<sup>10</sup>

However, non-metal surfaces, such as glass and silicon,<sup>24-27</sup> are very suitable alternative substrates, from both application and cost perspectives, but also since monolayers can be covalently attached to the surface (see Figure 3). This covalent linkage of the chains greatly increases the stability of the monolayer. Typically, chains are attached to such  $\text{SiO}_x$  surfaces by using chloro-silane or alkoxy-silane head groups that react with oxides at the surface, and can crosslink between the chains.<sup>26,28,29</sup> The thus formed network is more stable than thiol-gold bonds, but is still susceptible to hydrolysis. In the case of silicon, however, an alternative possibility is direct attachment of carbon chains to the oxide-free hydrogen-terminated silicon (H-Si) surface. Already in the early nineties, Chidsey and coworkers discovered that 1-alkenes and 1-alkynes react with the silicon surface to form monolayers, attached via Si-C bonds.<sup>24,25</sup> Shortly after that, Lewis and co-workers showed that alkylation of a silicon surface can also be performed by first halogenating the surface followed by a reaction with an alkyl Grignard reagent.<sup>30</sup> In the following decades understanding of the reactions that take place, as well as the techniques to prepare these layers have seen major development.<sup>26,27,31-37</sup> It has been shown that this reaction works well, both for porous H-Si,<sup>38,39</sup> H-Si(100)<sup>40-42</sup> and H-Si(111) surfaces.<sup>24,43</sup> The carbon-silicon bond is not susceptible to hydrolysis, and in fact monolayers can withstand prolonged exposure to acidic solutions, as well as exposure to HF, and – depending on the surface and monolayer quality – also to basic conditions. Moreover, these layers remain stable under ambient conditions for months, while oxidation of the surface proceeds very slowly. Furthermore, the direct attachment of the carbon chains to H-Si makes electronic coupling to the silicon bulk via the organic layer possible, which offers a great potential for electronic devices and sensors.<sup>26,32,34,35</sup> Examples of how the properties of silicon surfaces can be tuned for specific applications will be discussed in more detail in chapter 2.

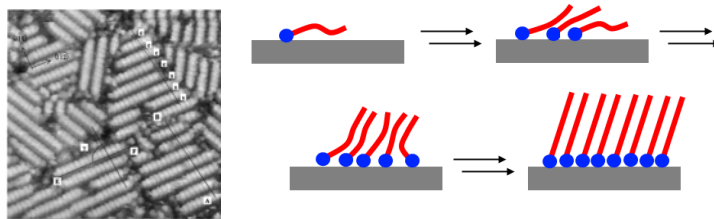


**Figure 2a.** Self assembly of a monolayer on a solid surface; and **b.** STM image ( $220 \times 220$  Å) of 1,6-hexanedithiol monolayer on Au(111), showing a clear pattern of lines.<sup>23</sup>

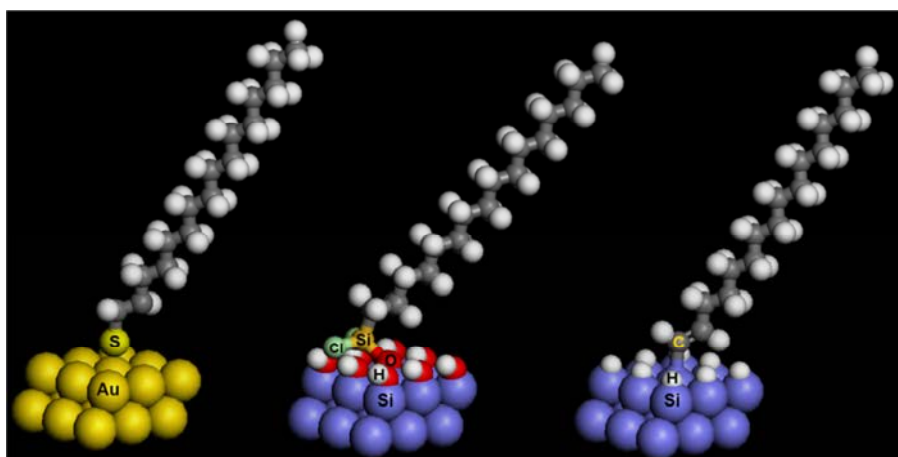


**Figure 3.** Reversible binding of an alkanethiol chain to gold (left), and covalent binding of tri-chlorosilane molecule to silicon oxide (here simplified representation by surface silanol groups), resulting in Si-O-C linkage (middle), and direct attachment of a 1-alkyne to hydrogen-terminated silicon (right).

## 1.2 Outline of this thesis

As discussed in previous paragraph, this thesis will mainly focus on covalently attached organic monolayers on H-Si surfaces, and H-Si(111) in particular. The reactions underlying the formation of these monolayers, typically involve surface-centered silyl radicals, as indicated in Figure 4.

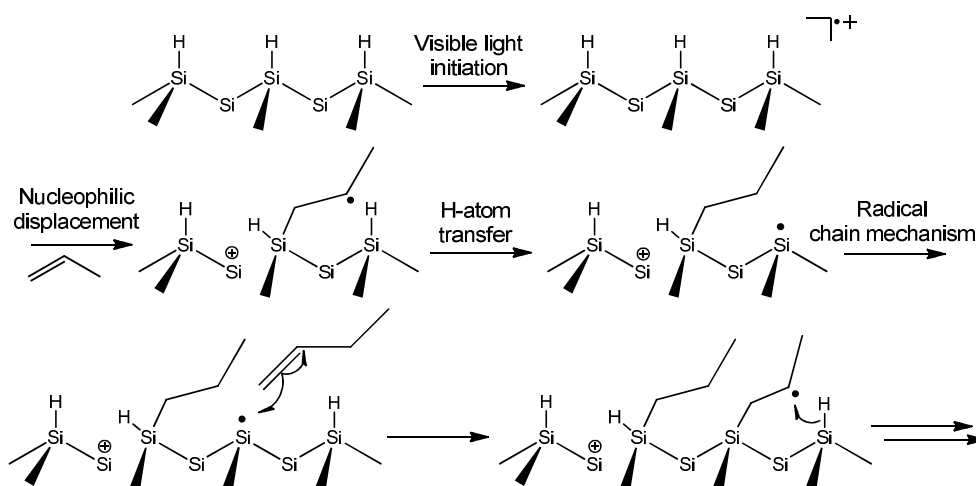


**Figure 4.** Monolayer formation onto H-terminated Si: radical cation-induced initiation,<sup>44</sup> followed by the radical chain propagation mechanism.

The main goal of the research presented in this thesis is to deepen the understanding of the critical factors in this attachment, with the aims to improve both the speed of monolayer formation on HSi(111), and the quality of the monolayers. Firstly, to achieve speed-up, the underlying mechanisms need to be unraveled. The radical cation mechanism as proposed by Zuilhof and coworkers in 2005 (see Figure 4) may serve as a good starting point for a more detailed mechanistic study. However, only little is known about reactivity of silyl radical cations (chapter 3) and silyl radicals (chapter 4) towards alkenes and alkynes. Let alone, about identifying tunable parameters that allow the actual speed-up of monolayer formation. And secondly, to further improve the quality (more densely packed layers), beyond the current highest quality monolayers on silicon,<sup>45</sup> requires a systematic study that combines theory and experiments (chapter 5). This resulted in the following outline for this thesis:

Chapter 2 gives a detailed overview of the important role of silyl radical reactivity in controlling the processes that take place at the silicon surface. By understanding this reactivity, also unwanted side-reactions such as the oxidation of the Si surface can be harnessed. Furthermore, different preparation methods, and their practical advantages for certain applications are presented. The chapter concludes with an overview of different strategies for functionalization of monolayers, making these surfaces suitable for application in sensory devices.

Though the radical chain mechanism has been widely accepted, the actual initiation of this mechanism has been the source of many debates over the last few years.<sup>46,47</sup> The various

proposed mechanisms are discussed in chapter 2; however, the most feasible mechanism will be studied in more detail in chapter 3. This chapter describes the study of an exciton-initiated mechanism, which is more commonly known as the radical cation mechanism. The goal is to establish the feasibility of this mechanism, and to assess whether this knowledge can be used to speed up monolayer formation. This study is the first to present stable radical cations of branched oligo silanes (up to 9 Si atoms in the chain) and their reactivity towards a number of nucleophiles commonly used in monolayer fabrication. The combination of kinetics and product studies shows that nucleophilic attack to silyl radical cations occurs rapidly, and leads to the formation of silicon-centered radicals that can undergo follow-up reactivity. In addition, following from this study of model systems new candidates are proposed that could indeed lead to better and faster monolayer formation.

In chapter 4, theoretical and experimental studies are combined to study silyl radical reactivity in more detail. The goal of this study is to identify parameters that can be used to gain more control over the radical reaction at the H-Si surface. More control will not only lead to faster monolayer formation, it will also lead to more tailor-made strategies for the functionalization of surfaces. To this aim, the reaction rates of silyl radicals, with various precursors (1-alkenes, 1-alkynes, etc.) commonly used in monolayer research, are tested and validated. A theoretical model is then used to predict the reactivity of novel precursor molecules.

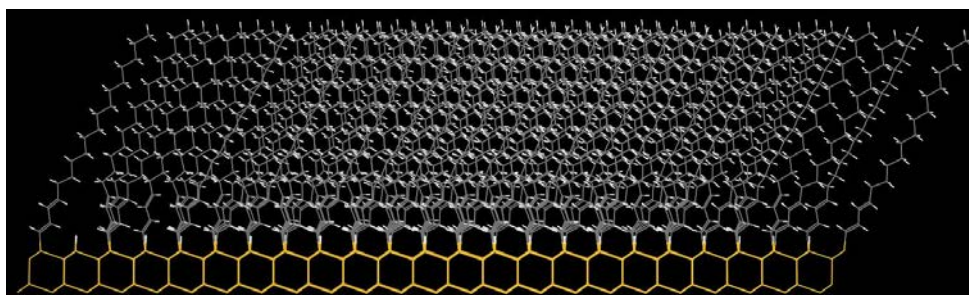


**Figure 5.** Molecular modeling representation of a C18 dieny l monolayer on H-Si(111).

Chapter 5 forms the completion of the puzzle, as it combines the knowledge gathered from the previous chapters to improve monolayer formation. In this study a novel precursor containing a 3-en-1-yne functionality is tested in monolayer formation. This molecule was specifically designed to have an enhanced reactivity towards silyl radicals and radical cations, and also fulfills the geometric constraints required for a highly ordered layer. The chapter presents a study on both the kinetics of monolayer formation, as well as a detailed study on the quality of the resulting layers. Theoretical modeling (see Figure 5) is then used

to get a better understanding of the interactions taking place at the surface, and to evaluate the properties of this monolayer in comparison with previously used nucleophiles.

Finally, in chapter 6 the main results of this study are summarized, and placed in a wider context. The findings will be related to current and future research, and to the potential of applications of Si-C based monolayers for (bio-)electronic devices.

## References

- (1) Schreiber, F. *Prog. Surf. Sci.* **2000**, 65, 151.
- (2) Ulman, A. *An Introduction to Ultrathin Organic Films: From Langmuir-Blodgett to Self-Assembly*; Academic Press: Boston, 1991.
- (3) Fenter, P.; Eberhardt, A.; Eisenberger, P. *Science* **1994**, 266, 1216.
- (4) Zimmerman, S. C.; Zeng, F. W.; Reichert, D. E. C.; Kolotuchin, S. V. *Science* **1996**, 271, 1095.
- (5) Genzer, J.; Efimenko, K. *Science* **2000**, 290, 2130.
- (6) Lopinski, G. P.; Wayner, D. D. M.; Wolkow, R. A. *Nature* **2000**, 406, 48.
- (7) Rothmund, P. W. K. *Nature* **2006**, 440, 297.
- (8) Liu, W. Y.; Zhong, H.; Wang, R. S.; Seeman, N. C. *Angew. Chem. Int. Edit.* **2011**, 50, 264.
- (9) Chen, J. H.; Seeman, N. C. *Nature* **1991**, 350, 631.
- (10) Love, J. C.; Estroff, L. A.; Kriebel, J. K.; Nuzzo, R. G.; Whitesides, G. M. *Chem. Rev.* **2005**, 105, 1103.
- (11) Schwartz, D. K. *Annu. Rev. Phys. Chem.* **2001**, 52, 107.
- (12) Fraxedas, J. *Adv. Mater.* **2002**, 14, 1603.
- (13) Bowden, N.; Terfort, A.; Carbeck, J.; Whitesides, G. M. *Science* **1997**, 276, 233.
- (14) Bowden, N. B.; Weck, M.; Choi, I. S.; Whitesides, G. M. *Acc. Chem. Res.* **2001**, 34, 231.
- (15) Clark, T. D.; Tien, J.; Duffy, D. C.; Paul, K. E.; Whitesides, G. M. *J. Am. Chem. Soc.* **2001**, 123, 7677.
- (16) Adamson, A. W.; Gast, A. P. *Physical Chemistry of Surfaces*; 6th ed. ed.; Wiley-Interscience: New York, 1997.
- (17) Nuzzo, R. G.; Allara, D. L. *J. Am. Chem. Soc.* **1983**, 105, 4481.
- (18) Walczak, M. M.; Chung, C. K.; Stole, S. M.; Widrig, C. A.; Porter, M. D. *J. Am. Chem. Soc.* **1991**, 113, 2370.
- (19) Fenter, P.; Eisenberger, P.; Li, J.; Camillone, N.; Bernasek, S.; Scoles, G.; Ramanarayanan, T. A.; Liang, K. S. *Langmuir* **1991**, 7, 2013.
- (20) Laibinis, P. E.; Whitesides, G. M.; Allara, D. L.; Tao, Y. T.; Parikh, A. N.; Nuzzo, R. G. *J. Am. Chem. Soc.* **1991**, 113, 7152.
- (21) Campos, M. A. C.; Trilling, A. K.; Yang, M. L.; Giesbers, M.; Beekwilder, J.; Paulusse, J. M. J.; Zuilhof, H. *Langmuir* **2011**, 27, 8126.
- (22) Li, Z. Y.; Chang, S. C.; Williams, R. S. *Langmuir* **2003**, 19, 6744.

- (23) Leung, T. Y. B.; Gerstenberg, M. C.; Lavrich, D. J.; Scoles, G.; Schreiber, F.; Poirier, G. E. *Langmuir* **2000**, *16*, 549.
- (24) Linford, M.; Fenter, P.; Eisenberger, P. M.; Chidsey, C. E. D. *J. Am. Chem. Soc.* **1995**, *117*, 3145.
- (25) Linford, M. R.; Chidsey, C. E. D. *J. Am. Chem. Soc.* **1993**, *115*, 12631.
- (26) Buriak, J. M. *Chem. Rev.* **2002**, *102*, 1271.
- (27) Ciampi, S.; Harper, J. B.; Gooding, J. J. *Chem. Soc. Rev.* **2010**, *39*, 2158.
- (28) Wasserman, S. R.; Whitesides, G. M.; Tidswell, I. M.; Ocko, B. M.; Pershan, P. S.; Axe, J. D. *J. Am. Chem. Soc.* **1989**, *111*, 5852.
- (29) Wasserman, S. R.; Tao, Y. T.; Whitesides, G. M. *Langmuir* **1989**, *5*, 1074.
- (30) Bansal, A.; Li, X.; Lauermann, I.; Lewis, N. S.; Yi, S. I.; Weinberg, W. H. *J. Am. Chem. Soc.* **1996**, *118*, 7225.
- (31) Sieval, A. B.; Linke, R.; Zuilhof, H.; Sudholter, E. J. R. *Adv. Mater.* **2000**, *12*, 1457.
- (32) Boukherroub, R. *Curr. Opin. Solid St. M.* **2005**, *9*, 66.
- (33) Shirahata, N.; Hozumi, A.; Yonezawa, T. *Chem. Rec.* **2005**, *5*, 145.
- (34) Wayner, D. D. M.; Wolkow, R. A. *J. Chem. Soc. Perk. T. 2* **2002**, 23.
- (35) Hamers, R. J. *Annu. Rev. Anal. Chem.* **2008**, *1*, 707.
- (36) Rijksen, B.; Caipa Campos, M. A.; Paulusse, J. M. J.; Zuilhof, H. In *Encyclopedia of Radicals in Chemistry, Biology and Materials*; Chatgililoglu, C., Struder, A., Eds.; Wiley: Chichester, 2012.
- (37) Li, Y.; Calder, S.; Zuilhof, H. *Langmuir* **in Press**.
- (38) Stewart, M. P.; Buriak, J. M. *Angew. Chem. Int. Edit.* **1998**, *37*, 3257.
- (39) Stewart, M. P.; Buriak, J. M. *J. Am. Chem. Soc.* **2001**, *123*, 7821.
- (40) Sieval, A. B.; Opitz, R.; Maas, H. P. A.; Schoeman, M. G.; Meijer, G.; Vergeldt, F. J.; Zuilhof, H.; Sudholter, E. J. R. *Langmuir* **2000**, *16*, 10359.
- (41) Sieval, A. B.; Vleeming, V.; Zuilhof, H.; Sudholter, E. J. R. *Langmuir* **1999**, *15*, 8288.
- (42) Ng, A.; Ciampi, S.; James, M.; Harper, J. B.; Gooding, J. J. *Langmuir* **2009**, *25*, 13934.
- (43) Scheres, L.; Giesbers, M.; Zuilhof, H. *Langmuir* **2010**, *26*, 4790.
- (44) Sun, Q.-Y.; De Smet, L. C. P. M.; Van Lagen, B.; Giesbers, M.; Thuene, P. C.; Van Engelenburg, J.; De Wolf, F. A.; Zuilhof, H.; Sudhölter, E. J. R. *J. Am. Chem. Soc.* **2005**, *127*, 2514.
- (45) Scheres, L.; Arafat, A.; Zuilhof, H. *Langmuir* **2007**, *23*, 8343.
- (46) Wang, X. Y.; Ruther, R. E.; Streifer, J. A.; Hamers, R. J. *J. Am. Chem. Soc.* **2010**, *132*, 4048.
- (47) Lee, M. V.; Scipioni, R.; Boero, M.; Silvestrelli, P. L.; Ariga, K. *Phys. Chem. Chem. Phys.* **2011**, *13*, 4862.

## Chapter 2

# Silicon Radical Surface Chemistry

**Abstract.** Over the past two decades, covalently attached self-assembled organic monolayers on silicon (Si) surfaces have gained much interest, because of their potential use in electronic devices. The formation of these layers is commonly accepted to proceed mainly via a radical chain mechanism at the Si surface. This chapter deals with relevant issues regarding the preparation and the functionalization of such monolayers on Si, with an emphasis on the involved radical chemistry. The attachment modes of olefins, and mechanisms thereof, depend largely on the surface geometry. Section 1 deals with the different surface geometries and the required surface pretreatment prior to monolayer formation (etching steps). Monolayer formation finds itself in competition with oxidation of the surface. Both the oxidation and monolayer attachment are described by surface radical chain reactions. The hydrosilylation reaction at the surface is explained in detail in Section 2. Surface radicals were typically initiated by direct cleavage of the Si-H bonds at the Si surface (at high temperatures or UV irradiation). However, as reaction conditions have become milder, the radical mechanism has also been shown to be in effect under mild initiation conditions that do not allow direct cleavage of Si-H bonds. Several mechanisms are discussed in Section 3, which range from initiation by adventitious oxygen and reactive species to exciton-mediated mechanisms. To support these theories, many theoretical and experimental modeling studies are reported in literature. Those relevant to the initiation routes presented here, are discussed in detail in Section 4. Monolayers on Si form an ideal scaffold for further surface functionalization and patterning. Section 5 gives an overview of the progress that has been made, in expanding the versatility of  $\text{Si-CH}_2\text{-}$  functionalizations, in recent years (mostly > 2005). Finally, Section 6 presents perspectives for further research and new applications.

**This chapter is published as:**

“Silicon Radical Surface Chemistry”, Rijkssen, B.; Caipa Campos, M.A.; Paulusse, J.M.J.; Zuilhof, H. in Encyclopedia of Radicals in Chemistry, Biology and Materials, Wiley, Chichester, 2012.

## 2.1 Introduction

Radical chemistry is the method of choice for the preparation of numerous organic molecules and polymers, as well as inorganic complexes. It has also found its way into the area of surface science. In particular the radical chemistry of silicon surfaces has attracted much attention, due to the relative ease of application, i.e. mild reaction conditions, high chemo- and regioselectivity, the absence of metal catalysts, while no by-products are formed.<sup>1-4</sup> This chapter reviews different aspects of the radical chemistry involved to make organic monolayers onto silicon surfaces, specifically Si-C linked monolayers.

Ever since the development of the first integrated circuit in 1958, the demand for novel semiconductor-based electronic devices with ever smaller dimensions has continuously increased. Silicon and germanium are the preferred metalloids due to their semiconductor properties and tunable electron mobility, while current state of the art devices have reached feature sizes below 30 nm. As a consequence, the impact of surface effects is becoming increasingly important.<sup>2,3,5</sup> The surface chemistry associated with these semiconductors, silicon in particular, has been explored as a potential means towards the fabrication of molecular electronic devices.<sup>6,7</sup> For many sensitive electronic applications, however, it is also of great importance that the silicon surface remains oxide-free.<sup>8-10</sup> Silicon oxide acts as an insulator, and a thin layer of oxide on top of a silicon-based electronic device prevents direct electronic contact between the organic functionality and the substrate, and thereby diminishes signal intensity. Controlling the nature of the surface can be achieved in a number of ways, of which the attachment of self-assembled monolayers (SAMs) may be considered the most sophisticated.<sup>11-15</sup> Such monolayers allow for the precise attachment of (bio)molecules and the subsequent detection of their counterparts. Moreover, high-quality SAMs may also prevent oxygen and water from reaching the surface, thereby improving the lifetime and robustness of such sensing devices.

Whereas the familiar SAMs on gold<sup>16</sup> are mostly based on the reversible gold-thiol bond, SAMs on silicon are covalently attached to the surface.<sup>2,3,5</sup> In effect, obtaining high-quality monolayers is not trivial. Siloxane-based SAMs are commonly applied in order to attach functional molecules onto silicon substrates in a rapid way, but these bonds are prone to hydrolysis and do not provide for oxide-free silicon substrates.<sup>17-20</sup> The use of monolayers based on silicon-carbon bonds offers an exciting alternative. Si-C bonds are known to be both thermally and chemically robust, due to the low polarity of this strong bond. This is essential in the formation of well-defined, highly stable, robust organic monolayers on silicon.<sup>2,21</sup>

In the current chapter various methods for the preparation of organic Si-C monolayers, including relevant issues concerning oxidation of the silicon surface, are presented. The



radical mechanisms at the silicon surface based on experimental and theoretical studies are discussed. In addition, the importance of high-quality oxide-free monolayers on silicon surfaces as well as the introduction of functional groups to the monolayer are addressed. At last, applications and future research are presented, describing the main remaining challenges.

### 2.1.1 Silicon Surfaces

Two types of silicon are most commonly used available, flat (single crystal) and porous silicon surfaces. The most widely employed type is flat silicon due to its variety of orientations, the possibility of adding dopants in a controlled manner and their commercial availability.<sup>1,22,23</sup> The most common surface orientations are Si(100) and Si(111). Freshly cut surfaces are rapidly coated with a thin native oxide layer upon exposure to air. The initial step in the formation of organic monolayers on silicon involves what may be called an activating passivation of the silicon surface, which opens up the surface reactivity to only a selected series of desirable reactions. In general, hydrogen is the most commonly employed passivating agent,<sup>24</sup> however, halogens such as iodine and chlorine have also been investigated.<sup>25,26</sup> Oxide-free, hydrogen-terminated silicon surfaces may be obtained via the adsorption of atomic hydrogen under ultra-high vacuum conditions at elevated temperatures ( $> 1100\text{ }^{\circ}\text{C}$ ).<sup>27</sup> Alternatively, wet chemical reactions using fluoride-containing solutions yield hydrogen-terminated silicon surfaces under rather mild conditions (i.e. ambient temperature and pressure). Important features of these hydrogen-terminated silicon surfaces include high chemical homogeneity ( $> 99\%$  H-termination), their relative stability in air and water during brief rinsing procedures, and their low reactivity towards several organic solvents.<sup>21,28-31</sup> Treatment of Si(100) surfaces with dilute aqueous HF (1-3%) yields predominantly dihydride-terminated Si(100) surfaces that display nanometer-scale roughness, Figure 1.<sup>29</sup> However, mono- and tri-hydride orientations are also present. The preparation of mono- and di-hydrated atomically flat surfaces is only possible employing ultra-high vacuum techniques. Recently, Hines and co-workers used scanning tunneling microscopy (STM) and FT infrared spectroscopy to demonstrate that aqueous solution of  $\text{NH}_4\text{F}$  (40%) selectively passivates Si(100) surfaces, eventually producing a hydrogen-terminated surface of near-atomic flatness.<sup>32</sup> Conversely, after only brief immersion of Si(111) surfaces in degassed aqueous  $\text{NH}_4\text{F}$  solution (40%), atomically flat surfaces, nearly exclusively occupied with Si-H groups, are readily obtained, Figure 1<sup>28,29</sup> The roughness of the surface has been studied by STM and FTIR spectroscopy. The ATR-FTIR spectra of the hydrogen-terminated Si(111) surface show a very sharp, narrow stretch silicon-hydrogen vibration  $\nu(\text{Si-H})$  at  $2083.7\text{ cm}^{-1}$ , indicating a high degree of chemical homogeneity, while

the STM image of the silicon surface shows atomically flat terraces with monoatomic steps, Figure 2.

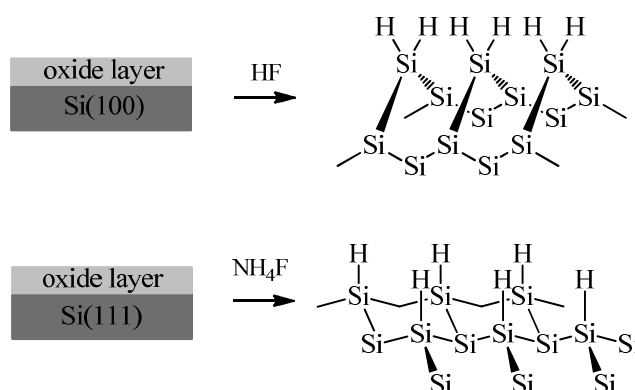


**Figure 1.** Preparation of hydrogen-terminated Si(100) and Si(111) surfaces by chemical etching in fluoride-containing solutions.<sup>28,29,32,33</sup>

In addition, the etching mechanism has been resolved based on in-situ STM and electrochemical measurements. Etching involves two components, one chemical and the other electrochemical; both are highly dependent on pH.<sup>34,35</sup> Other passivating agents can be employed such as HF and NaOH, however, these treatments lead to increased surface roughness, as well as the formation of mono-, di-, and tri-hydride-terminated Si(111) surfaces.<sup>36,37</sup>

Other silicon surfaces, such as porous silicon, are also of great interest due to their luminescent properties and high surface area.<sup>38</sup> These surfaces are prepared from crystalline silicon substrates (mainly Si(100)) using chemical or electrochemical methods. Surfaces typically consist of  $-\text{SiH}_3$ ,  $=\text{SiH}_2$ , and  $-\text{SiH}$  groups in different orientations and environments. Over the last few years, porous silicon has attracted much attention as a platform for biomolecules.<sup>39</sup> The refractive index can be tuned, turning substrates into photonic devices,<sup>40</sup> which can be subsequently modified by attachment of complex biomolecules.<sup>39-42</sup>

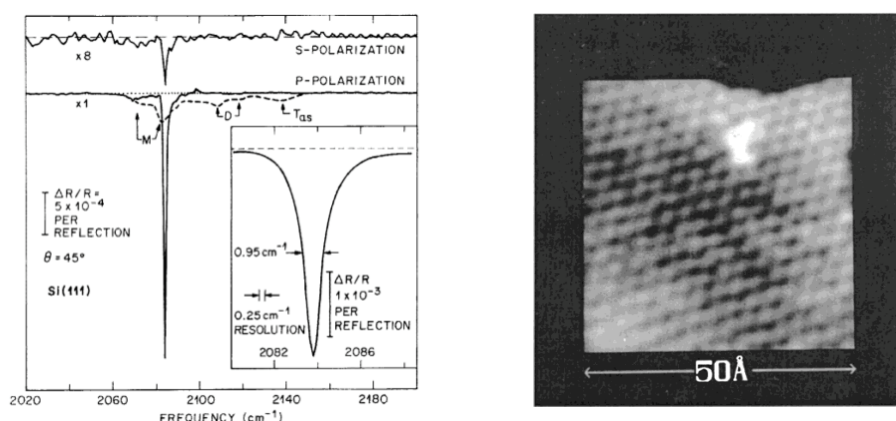


**Figure 2.** ATR-FTIR spectra of the hydrogen-terminated Si(111) surface, prepared through the 40%  $\text{NH}_4\text{F}$  (aq) etching procedure, taken with both s- and p-polarized IR light (left) and STM image of the flat Si(111)-H surface, prepared through etching with 40%  $\text{NH}_4\text{F}$  (aq). The gray scale represents a height change of 0.5 Å.<sup>28,29</sup>

### 2.1.2 Oxidation of Silicon Surfaces

The oxidation of hydrogen-terminated silicon surfaces has been studied in detail.<sup>43</sup> However the mechanism still has not been completely unraveled. Currently, the most accepted mechanism involves a radical mechanism, analogous to the auto-oxidation of tris(trimethylsilyl)silane ((TMS)<sub>3</sub>SiH or TTMS).<sup>44</sup> In this mechanism, molecular oxygen reacts with a surface-centered radical (surface **1**) to form peroxy radical **2**, Figure 3.

This radical either abstracts a neighboring hydrogen leaving a dangling bond at the surface (**3**), which may either react again with oxygen, or splits up under insertion of oxygen into a silicon backbond inside the surface (**4**). In the latter case, the silyloxy radical may abstract a hydrogen atom, resulting in a silanol group (surface **5**). Alternatively, this oxygen may be inserted in an available silicon backbond, resulting in surface **6**, the analog of which has been observed when TTMS was employed in a model study.<sup>23</sup> Both situations result in the formation of dangling bonds at the surface that are prone to attack by oxygen.

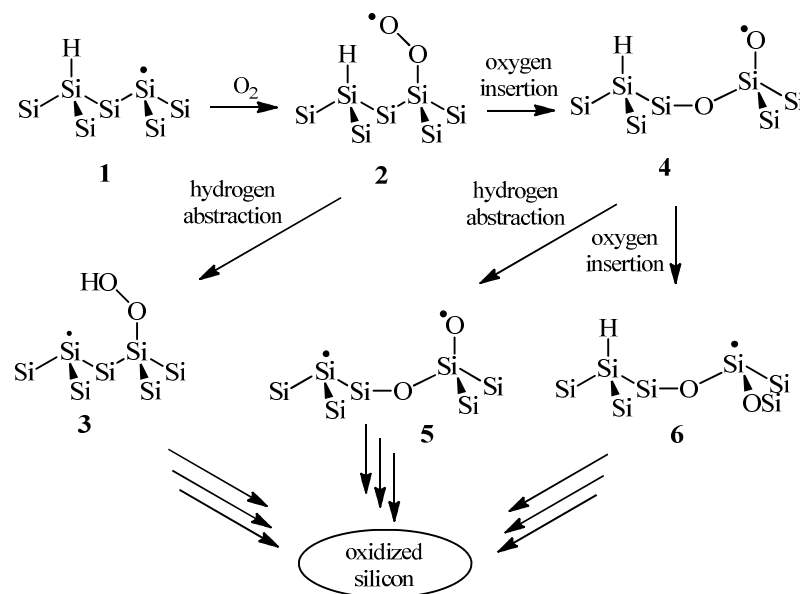


**Figure 3.** Oxidation of the hydrogen-terminated Si(111) surface.<sup>45</sup>

The radical mechanism of oxidation of silicon surfaces was further investigated by FTIR.<sup>43</sup> H-Si(111) surfaces were exposed to air, either in the dark or under irradiation at specific wavelengths. The intensity of the Si-H stretch vibration did not decrease significantly in the dark, nor upon irradiation using 450 nm light. This is in agreement with the energy required for homolytic cleavage of Si-H bonds, which was found to be  $84 \text{ kcal mol}^{-1}$ ,<sup>46</sup> requiring irradiation at wavelengths below 350 nm. This was further confirmed by a small decrease in signal observed upon irradiation at this wavelength, which is as expected as 350 nm is apparently just barely enough for photolysis. Dramatic loss of the Si-H signal was observed upon irradiation at 254 nm, indicating that oxidation of the surface involves such homolytic cleavage of the Si-H bond. Interestingly, oxidation of porous silicon initially leaves the Si-H bonds intact, which shows that oxygen directly attacks the Si-Si bonds. FTIR spectra taken after irradiation of a freshly etched porous Si sample in the presence of oxygen ( $\lambda = 365 \text{ nm}$ , 60 min.), show a large increase of the silicon oxide band ( $\nu_{\text{Si-O}}$  between  $1000$  and  $1200 \text{ cm}^{-1}$ ) and a correspondingly loss of the  $\text{SiH}_2$  signal ( $\nu_{\text{Si-H}_2} = 2116 \text{ cm}^{-1}$ ). However, the ingrowth of a  $\nu_{\text{O-Si-H}}$  band ( $2200 \text{ cm}^{-1}$ ) equals the loss of the  $\text{SiH}_2$  signal, resulting in no net loss of surface hydride species.<sup>47</sup> This different reactivity - which may be a reflection of slightly changed thermodynamics related to the surface structure of porous Si - also likely entails consequences for the attachment of hydrocarbons to this substrate, via the occurrence of other reaction mechanisms.

## 2.2 Radical Chain Propagation

Alkyl monolayers grown on appropriately prepared hydrogen-terminated Si(111) typically reflect the atomic flatness of the underlying silicon substrate. Several studies have focused on methods of chemical passivation of silicon through formation of Si-C bonds.<sup>3,48-50</sup> Hydrosilylation of alkenes or alkynes has been achieved via radical initiation,<sup>51</sup> thermally<sup>51,52</sup> or photochemically induced,<sup>53-56</sup> or by utilizing Lewis acid catalysts.<sup>57,58</sup> The first example of wet-chemical preparation of covalently attached organic monolayers on silicon surfaces, without an intermediate oxide layer, was reported in 1993 by Linford and Chidsey.<sup>59</sup> The carbon chains were bound to the hydrogen-terminated silicon surface via radical reaction. Diacylperoxide is cleaved by pyrolysis (100 °C) to form carbon-centered radicals (and CO<sub>2</sub>), which abstract hydrogen from the surface, yielding surface-centered radicals (Figure 4). These silicon radicals in turn react with the abundantly present alkyl radicals to form stable Si-C bonds. As a result, densely packed monolayers were obtained, which showed good resistance to boiling chloroform, acid, base and even treatment with HF.

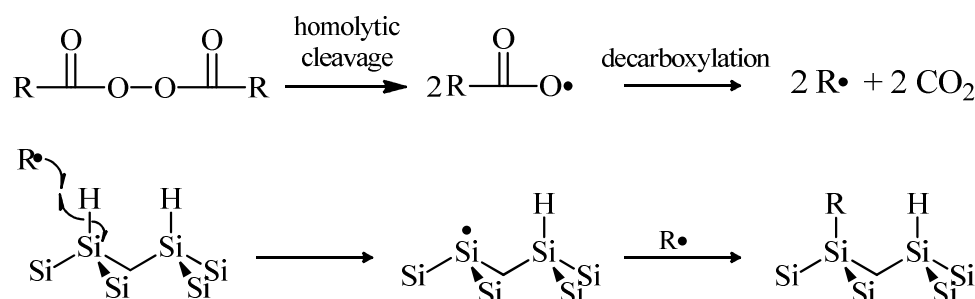


**Figure 4.** Formation of alkyl radicals from diacyl peroxide.

### 2.2.1 Attachment of Alkenes to Silicon Surfaces

Addition of alkenes and alkynes to silyl radicals was already reported as early as 1947.<sup>60-62</sup> This reaction proved very useful in the synthesis of organosilicon compounds (specifically from trichlorosilanes). Because of their reactivity towards silyl radicals,<sup>63</sup> alkenes and alkynes were used in a follow-up study on monolayer formation on silicon. Indeed, these compounds yielded high quality monolayers in the absence and in the presence of various concentrations of diacyl peroxide. Deuterium labeling of the peroxide demonstrated that the attachment of unsaturated carbon chains is preferred over attachment of alkyl radicals

stemming from diacyl peroxide. Moreover, at higher temperatures ( $> 150\text{ }^{\circ}\text{C}$ ) dense monolayers were also obtained from alkenes in the absence of diacyl peroxide.<sup>51</sup> Formation of surface radicals was explained by either homolytic cleavage of the Si-H bonds or reaction with adventitious oxygen. As known from the literature, radical addition to a double or triple carbon-carbon bond results in the formation of a  $\beta$ -carbon radical.<sup>64</sup> This radical subsequently abstracts a hydrogen atom, either from unreacted olefin in solution or from an adjacent Si-H site. However, the latter is preferred, owing to the lower bond dissociation energy of  $84\text{ kcal mol}^{-1}$  for Si-H<sup>65</sup> in comparison to the terminal C-H bond in alkenes and alkynes ( $101$  and  $111\text{ kcal mol}^{-1}$ , respectively<sup>66</sup>); this finally results once more in a surface-centered radical. Chidsey and coworkers proposed a radical chain reaction which is depicted in Figure 5.<sup>51</sup> The feasibility of hydrogen transfer from the surface to the alkyl chain was later demonstrated on porous silicon by the group of Buriak.<sup>67</sup> After attachment of perdeuterated styrene to a hydrogen-terminated surface, they observed methylene vibrations at  $2917$  and  $2846\text{ cm}^{-1}$  according to FTIR corresponding to consumption of Si-H sites.

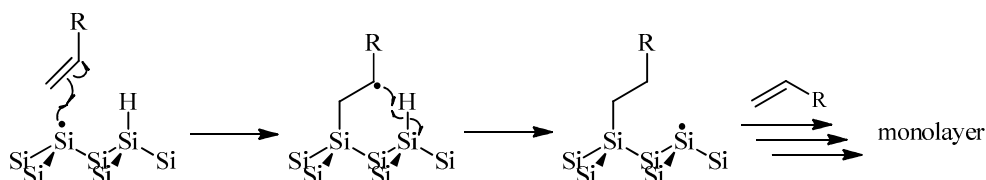


**Figure 5.** Reaction mechanism of the addition of 1-alkenes to hydrogen-terminated Si(111), as proposed by Chidsey and coworkers.<sup>51,68</sup>

Additional evidence for the radical propagation reaction was obtained from scanning tunneling microscopy (STM) studies performed under ultra high vacuum (UHV) on Si(100). To this purpose, dangling bonds (basically surface-centered silyl radicals) were created at the surface with an STM tip, which subsequently were exposed to styrene. STM showed lines of attached styrene molecules growing from these dangling bonds (see Figure 6).<sup>69</sup> Growth of these lines halted at surface defects, supporting the proposed hydrogen-abstraction mechanism. The observed pattern originates from the geometry of the hydrogen-terminated Si(100) surface, which consists of parallel aligned  $\text{SiH}_2$  sites, as shown in Figure 7.

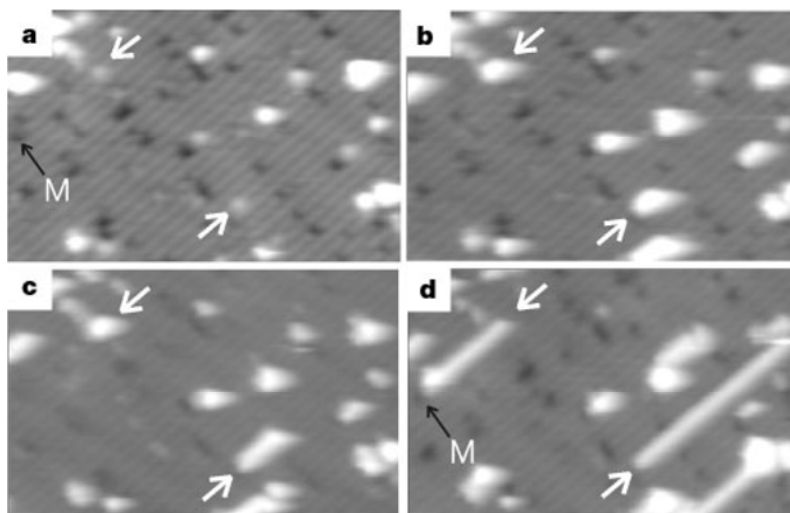


**Figure 6.** Growth of styrene lines on a hydrogen-terminated Si(100) surface with a small number of single Si dangling bonds. A sequence of STM images is shown for prolonged exposure to styrene: 3 L (a), 28 L (b), 50 L (c) and 105 L (d). White arrows denote two particular dangling-bond sites, leading to growth of long styrene lines. The missing dimer defect (marked M) terminates line-growth in the top left-hand corner of the image.<sup>69</sup>

Further evidence for the radical propagation mechanism was provided by Wolkow and coworkers, who studied the attachment of styrene on Si(111) with STM (see Figure 8).<sup>68</sup> In this case, the reaction of styrene with dangling bonds at the surface led to the formation of islands. This indicates unidirectional growth of the monolayer, dictated by the geometry of the surface. The hexagonal array of Si-H sites on atomically flat terraces provides for six equivalent Si-H sites near any starting Si-H site at the surface. From a single alkylation site the reaction thus propagates via one of these available Si-H sites, in six possible directions, as observed in Figure 7. This chain reaction was found to be self-limiting, and is proposed to terminate, when no neighboring hydrogen atom is available for abstraction by the alkyl radical, for instance because of the chain running into itself. Additional studies performed by Zuillhof and coworkers, based on alkyl monolayers fabricated from alkenes via white-light induced reaction, showed that island formation on Si(111) is generic for this kind of reactions, and is thus neither specific for styrene nor requires the use of an STM tip to induce a radical reaction.<sup>70</sup> Monte Carlo simulations showed that on average 76 chains attached to the surface before the chain reaction terminated.<sup>54</sup>

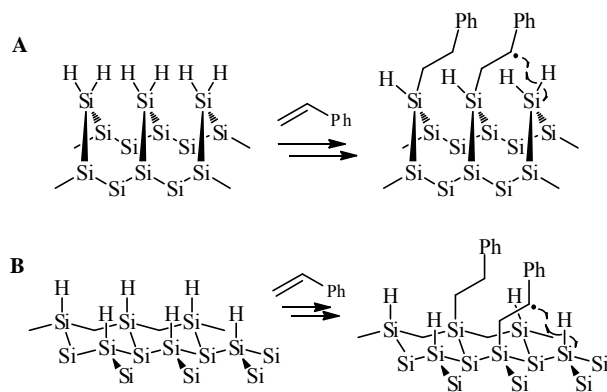


**Figure 7.** Styrene attachment onto hydrogen-terminated silicon surfaces; A: Si(100), B: Si(111).

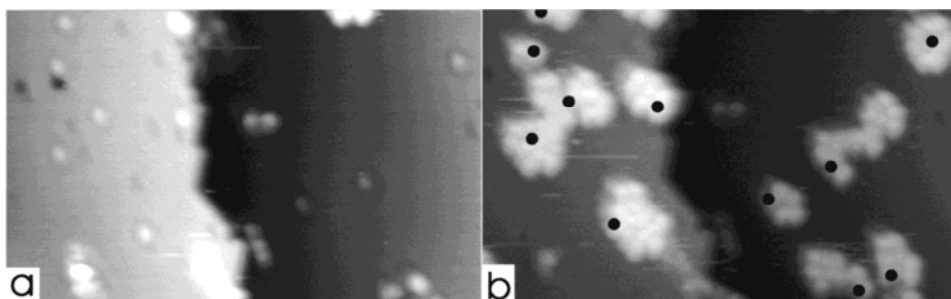


**Figure 8.** Occupied state STM images of an hydrogen-terminated Si(111) surface with isolated dangling bonds created by desorption activated by STM tip; (a) before dosing with styrene and (b) after exposure to 12 langmuirs of styrene. The black dots in (b) mark the positions of the initial dangling bonds, showing that these sites serve to nucleate the growth of styrene islands.<sup>68</sup>

### 2.2.2 Surface Reactions of Vinyl Radicals

The attachment of alkyne moieties to the surface form a special case, since the resulting product, which is obtained after addition and subsequent hydrogen transfer, is an alkenyl group. This unsaturated carbon is able to react again with a neighboring silyl radical,



forming bridged Si-C-Si or Si-C-C-Si structures.<sup>71</sup> This reaction competes with hydrosilylation of alkyne molecules present near the surface; this would then leave alkenyl chains at the surface (Figure 9, reaction a). However, alkyne monolayers on Si(100) did not show the presence of double bonds (no absorption between 1500 and 1700  $\text{cm}^{-1}$  according to FTIR-ATR studies), indicating saturation of the alkyl chains. There are two additional possibilities for double attachment of alkynes, as depicted in Figure 9 (routes b and c).<sup>71</sup> The first route involves the formation of a 1,2-bridged structure obtained after reaction of the  $\beta$ -carbon in the double bond with the surface radical, resulting in a 7-membered ring (route b). Attachment via the  $\alpha$ -carbon (route c), on the other hand, follows an anti-Markovnikov mechanism resulting in a six-membered ring. Route a is less favorable, since it does not follow for anti-Markovnikov type of addition, which is typically observed in reactions of silyl radicals.<sup>64</sup> In addition, this route leads to the formation of a seven-membered ring, which is less favorable than a six-membered ring. The high strain is mainly located on the Si-C and C-C bonds, as the silicon atoms are constrained within the crystal lattice. Moreover, DFT calculations confirmed that 1,1-bridged species are 5-7  $\text{kcal mol}^{-1}$  lower in energy, than 1,2 conformations.<sup>71</sup> It is important to note that both attachment modes are expected, since the energy differences are easily overcome at the high temperatures employed in these experiments. The characteristics of these alkyne-derived monolayers differ from alkene-derived monolayers prepared under these circumstances on H-Si(100) with respect to the tilt angles, which are on average higher for alkyne-derived monolayers ( $40^\circ$ ,  $27^\circ$ ,  $33^\circ$  for C12, C16 and C18-alkynes, as compared to  $32^\circ$ ,  $39^\circ$  and  $18^\circ$  for the alkene-analogues). For more recently developed reactions that take place under milder conditions on H-Si(111),<sup>72</sup> precisely the opposite is observed, pointing to the idea that attachment in those cases indeed only involves the terminal carbon atom, while here several bonding schemes are simultaneously operative (vide infra, Section 3.3.3).

On Si(111) surfaces double  $\alpha$ -attachment is unlikely, since the resulting bridged structure would form a highly strained four-membered ring. On the other hand,  $\beta$ -attachment would yield a five-membered ring, which is significantly lower in energy than the four-membered ring, though still too high in energy to form. Mono-attachment of alkynes as depicted in Figure 9 (B) is therefore considered to be predominant. The presence of a C=C double bond in alkyne-derived monolayers on Si(111) was demonstrated by FTIR spectroscopy (C=C stretch at  $1600.8 \text{ cm}^{-1}$ )<sup>51</sup> and infrared reflection absorption spectroscopy (IRRAS) (C=C stretch at  $1601 \text{ cm}^{-1}$ ).<sup>72,73</sup>

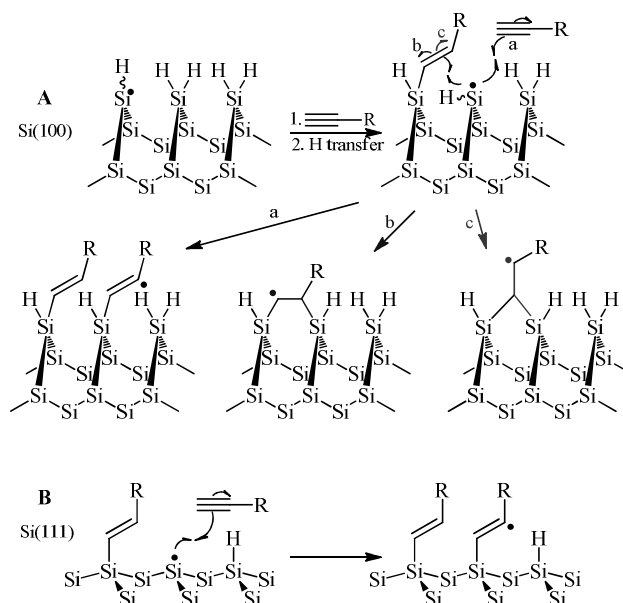


**Figure 9.** Reaction of alkynes with silicon surfaces; (A) Si(100) and (B) Si(111).

### 2.2.3 Siloxyl Monolayers

Siloxyl monolayers are generally prepared by reacting chlorosilanes<sup>74</sup> or trialkoxysilanes<sup>75-77</sup> with an oxide-covered silicon surface. However, as a result of the poorly defined underlying silicon-oxide surface, the resulting monolayers are less uniform than alkyl monolayers linked via Si-C bonds. Several groups reported solutions to this problem by attaching  $\alpha$ -alcohols<sup>34,78,79</sup> or aldehydes directly onto oxide-free silicon.<sup>34,79-81</sup> Although both moieties lead to the formation of Si-O-C linkages, the mechanisms of formation are entirely different. The attachment of a carbonyl moiety to the silicon surface is expected to proceed via a very efficient radical chain mechanism, similar to reaction with unsaturated alkyl chains (Figure 10, A). In the case of alcohols, attachment is likely to proceed via nucleophilic attack of the OH-group to the silicon, leading to a pentavalent silicon intermediate. Subsequent release of di-hydrogen results in oxidative addition. Attachment via this pathway does not lead to the formation of a new reactive site, as is the case in the radical chain mechanism. This mechanism is consequently less efficient, overall resulting in slower and incomplete monolayer fabrication, as elegantly shown for the attachment of

methanol to Si(111) upon prolonged heating at elevated temperatures (65 °C, 12 h), which leads to partial coverage of the surface (max. 33% of available Si-H sites).<sup>82</sup>

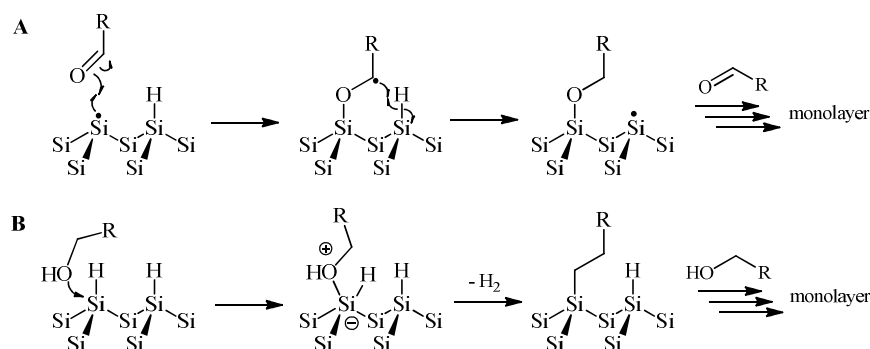


**Figure 10.** Formation of siloxyl monolayers from aldehydes (A) and alcohols (B).

### 2.2.4 Competing Reactions by Halogen Impurities

Neat alkenes and alkynes may easily contain traces of the starting material such as bromo- or chloro-alkanes. From the experiments performed by Chatgililoglu and coworkers it is known that silyl radicals can react very fast with such halocarbons. The rate of reaction of a primary alkyl bromide towards the TTMSS radical is in the order of  $10^7 \text{ s}^{-1}$ , whereas the chlorides were shown to react much slower ( $10^5 \text{ s}^{-1}$ ).<sup>83</sup> The reactivity of bromine compounds easily overshadows the reactivity of aldehydes, alkenes and alkynes, which are in the range of  $10^4 - 10^6 \text{ s}^{-1}$  (see Table 3.1 in paragraph 3). Traces of bromoalkanes, present in the reaction mixture, lead to holes in the monolayer (see Figure 11). These Si-Br sites are susceptible to hydrolysis, resulting in oxygen bound to the silicon surface, which for certain applications is undesirable and decreases monolayer stability.

The reactivity of silyl radicals towards chlorocarbons is much lower (as described above), and lies within the range of aldehydes and alkenes. This may explain that traces of chlorine compounds are typically not a big problem in monolayer formation. Even at a higher concentration of such chlorine compounds present in the reaction mixture, no significant chlorination of the surface was observed.<sup>51,84</sup> It is, in fact, well possible to make chlorine-terminated carbon monolayers ( $\text{Si}-(\text{CH}_2)_n\text{-Cl}$ ), from chlorine-containing compounds like 1-chloroundecene, and such Cl-termination was reported to be of good quality.<sup>2</sup> However, when high-quality oxide-free surfaces are required, chlorine traces still may cause undesired holes in the monolayer that may facilitate oxidation.

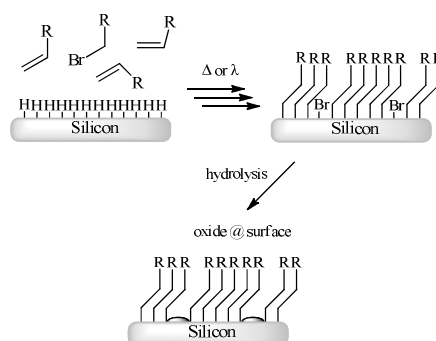


**Figure 11.** Bromine impurities in the reaction mixture lead to the formation of Si-Br causing holes in the monolayer. Furthermore the surface-bound bromine is susceptible to hydrolysis leading to oxidation of the surface.

## 2.3 Formation of Surface-Centered Silyl Radicals

### 2.3.1 Thermal Attachment

As previously mentioned, initial experiments demonstrated that monolayer formation also takes place at elevated temperatures ( $>200\text{ }^{\circ}\text{C}$ ) with linear alkenes  $\text{C}_n\text{H}_{2n+2}$  ( $n = 12 - 20$ ), and does not require the use of peroxides.<sup>51</sup> Zuilhof, Sudhölter and co-workers showed the formation of high-quality alkene monolayers on silicon employing a solution of alkene (2.5%) in toluene or mesitylene.<sup>85</sup> The use of alkene solutions signifies a reduction of the amount of material required per wafer (40-fold), and allows for the use of solid alkenes. This thermal method for monolayer formation on silicon is fast, yields high-quality monolayers and is relatively easy to employ. However, due to limitations in thermal budget, the required temperatures limit the application of this method in ultra-small IC manufacturing.<sup>48</sup> In addition, the direct attachment of functional alkenes and complex molecules may lead to the formation of side-products, or (to a varying degree) result in so-called upside-down attachment (see Figure 12), drastically influencing monolayer quality (i.e. density and uniformity). Typically, therefore these complex molecules are attached to a pre-functionalized surface. These procedures will be explained in more detail in paragraph 5. Side reactions may slow down the monolayer formation, resulting in incomplete layers. The occurrence of bare patches on the surface has major consequences for the monolayer stability, since these patches are not protected against oxidation.

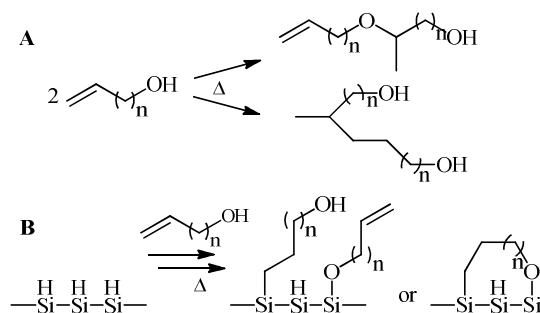


**Figure 12.** Side reactions of functional molecules as a result of high reaction temperatures (A); undesired reactions at the surface: upside-down attachment and bridge-formation (B).

### 2.3.2 UV Attachment

In search of milder reaction conditions for the attachment of alkenes and alkynes, the use of UV irradiation was considered. Early work of Chidsey and coworkers already showed that UV irradiation of Si(111) and Si(100) surfaces resulted in direct cleavage of the Si-H bond.<sup>54</sup> In their study they found that the drastically enhanced formation of  $\text{SiO}_2$  as observed by XPS (X-ray photoelectron spectroscopy) coincided with a decrease in Si-H signal at  $2112 \text{ cm}^{-1}$  in FTIR. A range of alkenes and alkynes was successfully attached to the surface, yielding monolayers of comparable quality as those obtained via thermal reaction. This UV method has several advantages over thermal attachment, such as significantly lower input of thermal energy required, as these reactions are performed at room temperature without increase of reaction times. Considering the aforementioned thermal budget, this method is very suitable for the IC manufacturing industry.<sup>48</sup> Arguably the most important advantage is the ability of direct photo-patterning of the surface. Use of a mask allows for local irradiation, and thus local monolayer formation, as shown in Figure 3.2. This was demonstrated by the selective functionalization of H-Si(111) with octadecanal using UV irradiation through a mask ( $\lambda = 385 \text{ nm}$ ).<sup>80</sup> The remaining unmodified patches were shown to still be reactive, by attaching 1-octadecene in a following step. The different wettabilities of the monolayer-covered areas and the uncovered silicon areas were observed under a microscope.

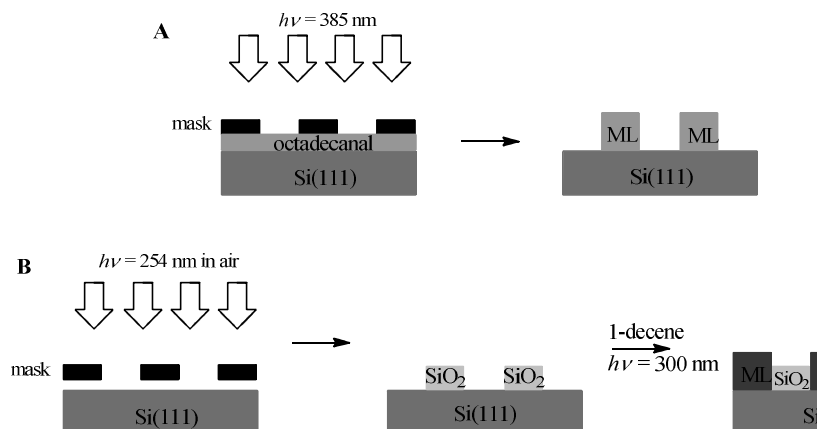


**Figure 13.** Direct patterning via monolayer formation (A),<sup>80</sup> patterning of oxide layer and subsequent filling of unmodified patches with a monolayer from 1-decene (B).<sup>86</sup>

Interestingly, Wayner and coworkers successfully demonstrated the opposite approach by selectively oxidizing the silicon surface by irradiating through a mask under ambient atmosphere (see Figure 13 B). This resulted in oxidized, non-reactive patches, and non-irradiated reactive patches.<sup>86</sup> After growing a monolayer on the reactive patches, a pattern containing hydrophobic and hydrophilic domains was obtained, which was observed by scanning electron microscopy (SEM) and scanning auger electron microscopy (SAES, see Figure 14). Side-reactions also occur during UV initiated monolayer formation. Photolysis of functional moieties may occur, and upside-down attachment has also been demonstrated, similar to the thermal methods.<sup>87</sup> Moreover, prolonged UV irradiation may cause cleavage of Si-C bonds resulting in degradation of the newly formed monolayers. This has also been observed for monolayers on porous silicon.<sup>58,88</sup>

Bedzyk and coworkers reported that upon reaction with undecenoic acid bromo-ethyl ester, less than 10% of the ester was attached via the alkene moiety while retaining the bromine (see Figure 15c, A).<sup>87</sup> For the remaining sites, up to 50% reacted with bromine (B), 27% reacted with de-brominated ester (C) and 13% of the sites showed upside-down attachment (D). Again the usefulness of these reactions depends on the application of the monolayer. When the function of the monolayer is simply to serve as a scaffold layer, and the resulting packing density and presence of surface oxides are not important, this method provides a fast and easy way to obtain such a layer.

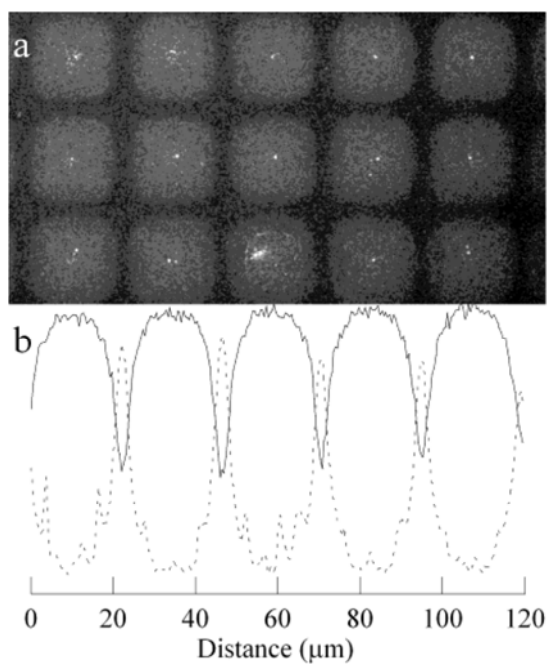


**Figure 14.** (a) SEM picture of a surface patterned by oxide and monolayer patches; (b) SAES line scan of the modified surface depicting the relative abundance of carbon (dashed) and oxygen (solid) as a function of distance.<sup>86</sup>

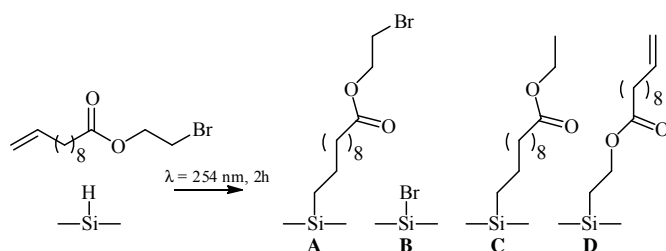


**Figure 15.** UV attachment of undecenoic acid bromo-ethylester to silicon, resulting in normal attachment (A), bromination of the surface (B), normal attachment of a de-brominated alkene molecule (C), and upside-down attachment of a de-brominated compound.<sup>87</sup>

An alternative mechanism to the UV-induced cleavage of Si-H bonds, was recently reported by Hamers and coworkers.<sup>53</sup> They argue that UV irradiation leads to electron donation from the silicon surface into the acceptor levels of carbon-carbon double bonds present near the surface. This leaves a positive charge on the surface, in the form of a silyl cation, which is susceptible to nucleophilic attack (Figure 16). Attack of an alkene to this surface cation and a (concerted or successive) hydride shift from the silicon surface to the carbon chain yields again a silyl cation, close to the alkylation center. This cation is available for a following nucleophilic attack. This proposed mechanism has, however, not yet been investigated in full detail.

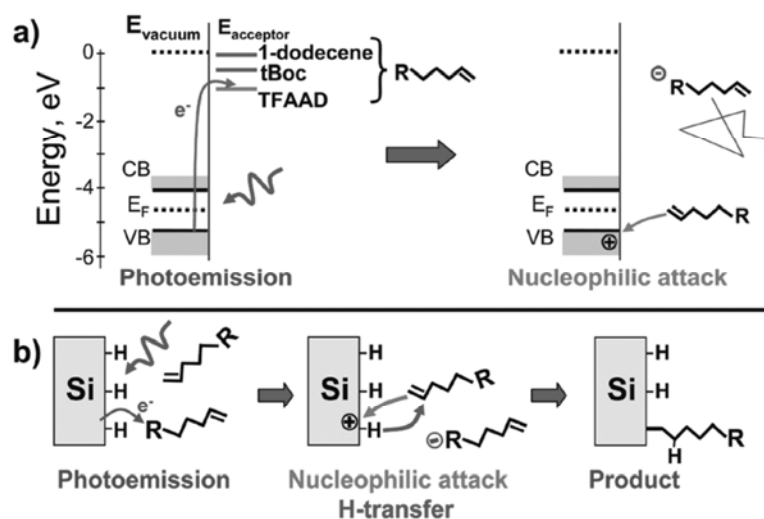


**Figure 16.** Photoemission mechanism for UV-initiated grafting of alkenes to hydrogen-terminated silicon surfaces<sup>53</sup>: (a) photoemission to an acceptor level followed by nucleophilic attack of another alkene; (b) overall grafting mechanism. Acceptor levels in (a) are from refs <sup>89</sup> and <sup>90</sup>.

### 2.3.3 Other Initiation Mechanisms

The need for more versatile and milder approaches towards functional monolayers on silicon still continues. Significant success has been achieved via the development of methods that make use of lower temperatures ( $< 150\text{ }^{\circ}\text{C}$ ), white light ( $\lambda > 450\text{ nm}$ )<sup>91-93</sup> or even proceed without any significant external activation (i.e. at room temperature, in the



dark),<sup>72</sup> frequently making these approaches, next to the toluene/mesitylene-based method discussed before,<sup>85</sup> the methods of first choice for Si-C based monolayer formation onto hydrogen-terminated Si. Since these conditions do not allow regular crossing of high activation barriers, direct cleavage of Si-H bonds is not predominantly involved. Several mechanisms that have been proposed in order to explain mild attachment will be discussed in this paragraph.

#### 2.3.3.1 Initiation by adventitious oxide and activation by glass reaction vessels

The theory of adventitious oxide being able to create dangling bonds on the silicon surface dates back to the initial experiments performed by Linford and Chidsey.<sup>51</sup> In their experiments in the absence of radical initiator they still observed efficient monolayer formation from alkenes and alkynes. These reactions were attributed to the presence of traces of oxygen in the reaction mixture, which reacts with the silicon surface as previously described in Section 1.3. Although these reactions indeed result in initiation of a radical chain reaction, recent studies show that the extensive exclusion of oxygen from the reaction mixture has no apparent influence on reactivity.<sup>72</sup> In fact, the quality of the monolayers is increased as oxidation of the surface is minimized. Therefore, still another initiation mechanism must be in effect that may coincide with oxygen initiation. Based on these findings Miscki *et al.* proposed a mechanism that involved degradation of the unsaturated hydrocarbons by reaction with silanol groups of the glass reaction vessel at elevated temperature.<sup>94</sup> This mechanism was supported by the observed drop in reaction rate and monolayer quality upon employing PTFE reaction-vessels.

#### 2.3.3.2 Diazonium salts

Aryldiazonium salts have been used for direct grafting of aryl groups onto hydrogen-terminated silicon surfaces.<sup>95-97</sup> These reactions form a special case, and show that solution reactions and surface reactions, may have very different outcomes. Reactions with the silicon surface lead to hydrosilylation products, whereas solution reactions with silanes generally lead to substitution of a silicon-bound hydrogen with the counterion of the diazonium salt (see Figure 17).<sup>98</sup> The reaction most likely proceeds via a one-electron reduction of the aryldiazonium cation, yielding an aryl radical and N<sub>2</sub>. The difference between surface reactions and reactions with silanes lies in nature and fate of the electron donor. In solution, electron donation by the silane leads to the formation of a silyl radical cation, which is attacked by the counterion of the diazonium salt. The dissociated hydrogen atom subsequently combines with the aryl radical (Figure 17A). In contrast, electron

donation from the surface leaves a hole that is highly delocalized and is able to migrate into the silicon bulk. The aryl radical picks up a hydrogen atom from the surface, leaving a surface silicon-centered silyl radical, which reacts with an unreacted aryl radical to form a Si-C bond (see Figure 18A). Although direct evidence of this reaction has not been demonstrated, formation of radicals at the surface has been evidenced, by trapping the radicals with alkenes and alkynes, leading to alkyl and alkenyl monolayers (see figure 18B).<sup>99</sup>

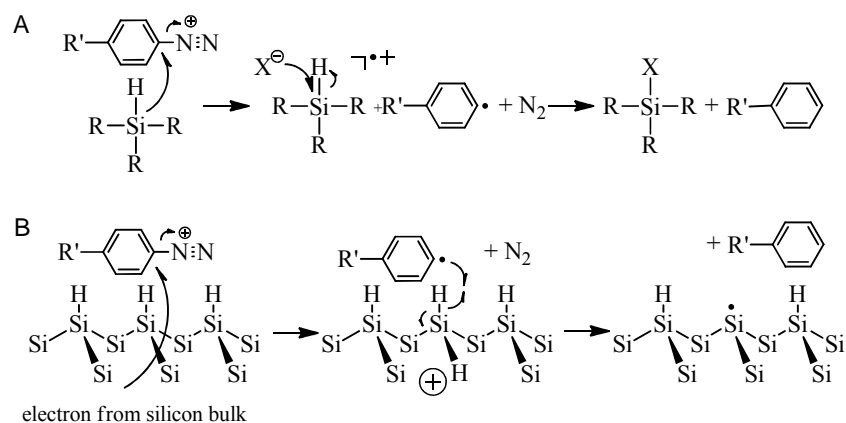


**Figure 17.** Reactions of diazonium salts with silane molecules (A) and with the silicon surface (B).

Moreover, the electron injection from the silicon bulk into accepting orbitals in solution is in good agreement with the findings of Hamers and co-workers described above.<sup>53</sup> This is a very elegant example of fabrication of alkyl and alkenyl monolayers at room temperature, via controlled radical initiation at the surface. When carboxylate and hydroxyl  $\omega$ -functionalized alkenes are employed, mainly Si-C bonds are formed. This procedure allows for the use of different functional groups without affecting monolayer quality. Diazonium-initiated attachment occurs fast, as evidenced by formation of a complete aryl monolayer in 3 h,<sup>99</sup> where aryldiazonium salts act as both initiators and reagents (see Figure 18B), making this an excellent approach to aryl monolayers. For high-quality alkyl monolayers other methods may be more suited, given the instability of alkyl diazonium salts, which thus require the involvement of aryl salts that will themselves also show reactivity towards H-Si surfaces and thus to distortions within the formed monolayer. In fact, a parallel can be drawn to the presence of halogen impurities discussed in Section 2.4. Though the aryl attachment is not susceptible to hydrolysis, the disruption of the layer will allow faster penetration of oxygen resulting in oxidation.

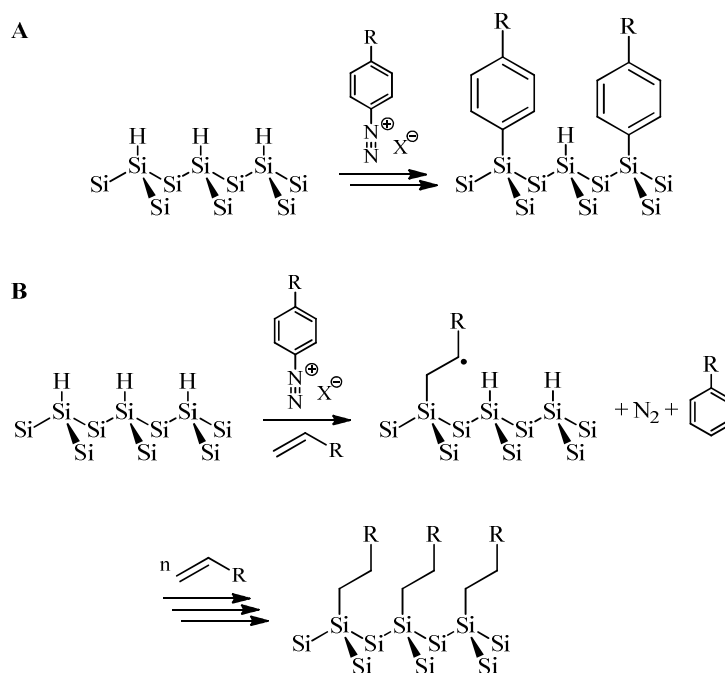


**Figure 18.** Recombination of surface centered radicals with abundant aryl radicals lead to formation of arylmonolayers on silicon (A). In small amounts diazonium salts initiate formation of silicon-centered radicals that are trapped by alkenes leading to the formation of an alkyl monolayer (B).

### 2.3.3.3 Exciton-mediated initiation

Buriak and coworkers found that alkenes attach to porous silicon under irradiation at wavelengths higher than 450 nm.<sup>67,91</sup> They proposed a mechanism involving excitons, in which electron/hole pairs form near the silicon surface (Figure 19), leading to positive charges on the surface. Nucleophilic attack on a positively charged silicon atom may then result in the formation of a  $\beta$ -carbocation on the attached alkyl chain. Transfer of a hydride from the surface to the  $\beta$ -carbocation yields a neutral alkyl chain. This mechanism, however, does not lead a chain reaction, as the attachment of a single chain does not lead to the formation of a new reactive site at the surface.

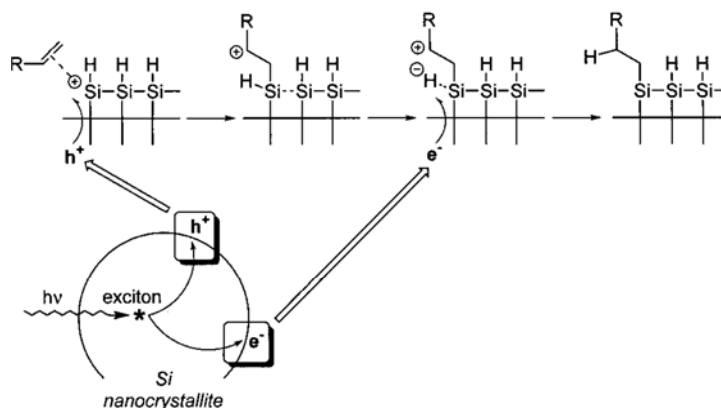


**Figure 19.** Proposed mechanism for the exciton-mediated hydrosilylation reaction. An unbound exciton produced by light absorption leads to a surface-localized supra-band gap positive charge. This surface charge subsequently interacts with an alkene and forms a silylated  $\beta$ -carbocation upon Si-C bond formation. This carbocation then abstracts a hydride (formally  $\text{H}\bullet$  and an electron from the exciton) from an adjacent Si-H bond, leading to a neutral alkyl chain.<sup>91</sup>

Zuilhof and coworkers also demonstrated the attachment of alkenes and alkynes onto Si(100)<sup>93</sup> and Si(111),<sup>92</sup> by irradiation at 658 nm (white-light reaction). This process is also based on the exciton formation, though the charge separation was considered to take place both at the surface as well as deeper in the silicon bulk. The electronic band structure of silicon would then cause separation of the electron/hole pair, followed by migration of electrons to the silicon bulk. In contrast, the holes move towards the surface, resulting in delocalized radical cations at the silicon surface. Nucleophilic attack of alkenes onto these radical cations results in cleavage of a silicon backbond, and formation of a Si-C bond and a  $\beta$ -carbon radical (see Figure 20). Hydrogen transfer from the surface to this radical yields a surface centered radical, which propagates the radical chain mechanism.<sup>92</sup> A recent mechanistic study confirms the reactivity of alkenes and alkynes towards delocalized radical cations, and will be discussed in more detail in Section 4.3.<sup>100</sup> The studies on monolayer formation at room temperature in the dark can only be explained by radical cation initiation.<sup>72</sup> Degradation of alkenes or alkynes by reaction with silanol<sup>94</sup> can be excluded at this temperature. Also initiation by adventitious oxygen can be excluded, as great care was taken to remove oxygen from the reaction mixture. Indeed, XPS shows that oxidation of the silicon surface is below the detection limits.

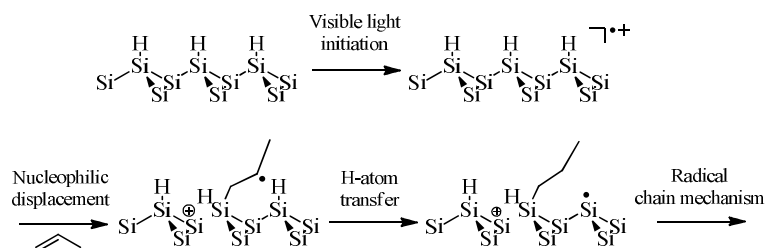


**Figure 20.** Proposed radical cation mechanism for initiation of light-induced reaction.<sup>92</sup>

This mild technique, introduced by Zuilhof and co-workers, was shown to result in hexadecenyl monolayers of very high quality (water contact angles  $\sim 111^\circ$ , and  $\text{CH}_2$  stretch vibrations at  $\nu_{\text{C-H}} = 2919$  and  $2850 \text{ cm}^{-1}$ ). In order to determine the origin of this enhancement of the self-assembly process, the difference in reactivity between alkenes and alkynes, as well as the resulting quality of the monolayers, were studied in detail.<sup>73,101</sup> To this aim, the rate of monolayer formation from both alkenes and alkynes was studied (see Figure 21). A clear difference in reactivity of alkenes and alkynes is observed both for samples prepared under visible-light irradiation (Figure 21 left), and in the dark (Figure 21 right). Under irradiation, 1-hexadecyne monolayers have come to completion after 8 h, whereas the alkene layers are still far from completion (contact angles of  $\sim 111^\circ$  and  $\sim 100^\circ$  resp.).<sup>73</sup> Comparison of these results to the results from the experiments in the dark shows a clear effect of irradiation. Under dark conditions, alkyne-derived monolayers are fully formed (contact angle  $\sim 111^\circ$ ) after 24 h, whereas the contact angles of the alkene layers do not exceed  $97^\circ$ . These differences in reactivity of the alkenes and alkynes are contributed to differences in nucleophilicity, and lower barriers in the hydrogen abstraction reaction at the surface, as will be discussed in more detail in Section 4.2 and 4.3.

In addition, the structural differences between alkene-derived and alkyne-derived monolayers were studied in detail. A combination of surface analysis techniques (ATR-IR, XPS, ellipsometry and water contact angles) was used to determine accurate surface coverages of monolayers prepared from a series of alkenes and alkynes ( $\text{C}_{12}$  to  $\text{C}_{18}$ ).<sup>73</sup> Figure 22 shows the influence of the number in carbons in the chain on the thickness of the monolayer (Figure 22, left), and the influence on the surface coverage (Figure 22, right). Alkynes lead to thicker layers, indicating that the chains are in a more vertical position than the chains in the alkene layers (tilt angles  $22\text{--}35^\circ$  and  $37\text{--}40^\circ$  for alkynes and alkenes, respectively). This is in agreement with the observed surface coverages, which are significantly higher for alkynes (55 to 65% for  $\text{C}_{12}$  to  $\text{C}_{18}$ ) as compared to alkenes (50 to 55% for  $\text{C}_{12}$  to  $\text{C}_{18}$ ).

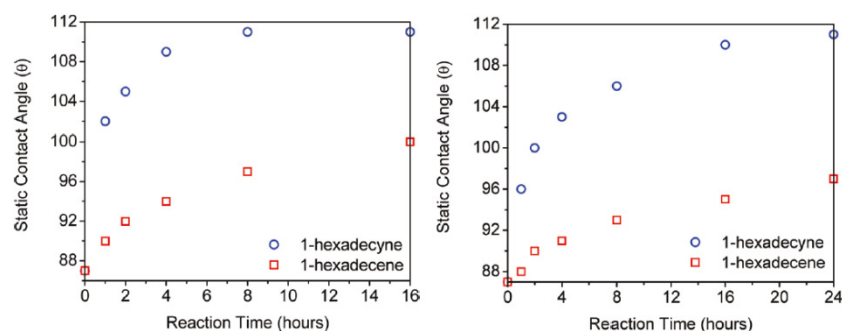


**Figure 21.** Static contact angles of 1-hexadecyne (○) and 1-hexadecene-derived (□) monolayers on H-Si(111) at 20 °C (left) under ambient light, and (right) in the dark, as a function of reaction time.<sup>73</sup>

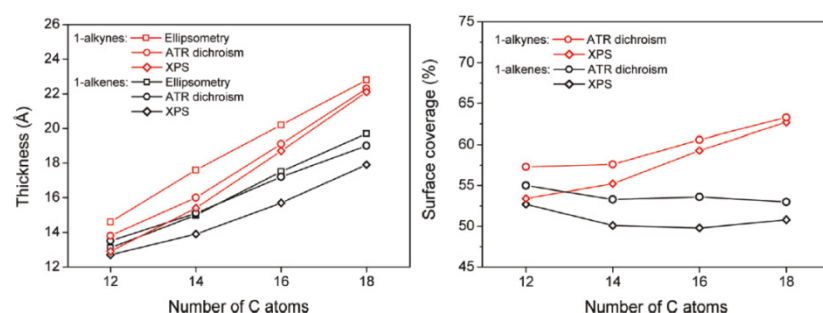


**Figure 22.** (left) Layer thickness and (right) surface coverages as a function of the number of carbons in alkyne-derived and alkene-derived monolayers, as determined by XPS, ATR and ellipsometry.<sup>73</sup>

Supportive evidence was found in a modeling study, performed by the same group.<sup>101</sup> Molecular mechanics simulations of the monolayers combined with quantum chemical calculations showed that alkynes indeed should lead a higher theoretical surface coverage than alkenes (up to 69% for alkynes vs. 50-55% for alkenes), for a variety of reasons. First, the Van der Waals radius of a  $\text{-HC=CH-}$  group is smaller than a  $\text{-CH}_2\text{-CH}_2\text{-}$ . Second, the  $\text{sp}^2$  hybridization of the carbon bound to the surface results in a more favorable angle ( $60^\circ$  vs. surface normal) over a  $\text{sp}^3$  hybridized carbon ( $76^\circ$  vs. surface normal), which lowers the strain energy in the Si-C link. Third, as shown by G3 calculation, the driving force for Si-C bond formation is  $\sim 10 \text{ kcal mol}^{-1}$  higher for 1-alkynes than for 1-alkenes. These factors combined drive monolayer formation for 1-alkynes to a significantly higher degree of surface coverage and correspondingly improved surface properties.

### 2.3.3.4 Fluoride-catalyzed and neutral attachment

Though Cerofolini and coworkers support the strong case of radical propagation, they argue that the Si-H bond is too strong for homolytic cleavage at 150 °C.<sup>102</sup> Therefore they investigated two alternatives, catalytic activity of trace fluoride, and a neutral concerted mechanism, that describe attachment to the silicon surface without initial cleavage of the Si-H bond.<sup>81</sup> Nucleophilic attack of F<sup>-</sup> onto the silicon surface is suggested to result in the formation of pentavalent silicon. This intermediate then releases a hydride that attacks a carbon-carbon double bond, yielding an  $\alpha$ -carbanion, which in turn attacks the silicon, substituting fluoride (see Figure 23). The result is a neutral alkyl chain and a fluoride anion, which is available for the next attachment. The proposed alternative mechanism, however, proceeds via a neutral transition state. In a concerted mechanism, the Si-C bond is formed, and the hydrogen is transferred to the alkyl chain. The two mechanisms were found to be indistinguishable in apolar media, whereas the activation energies may indeed be reached at these elevated temperatures.<sup>103</sup> However, both reactions result in a neutral product, which does not lead to propagation of the reaction. Neutral attachment and fluoride-catalyzed attachment can thus not be important in monolayer formation at ambient and slightly elevated temperatures, as under such conditions the formation of lines and islands of monolayers have been shown, e.g. by aforementioned STM results.<sup>70</sup> In the case of aldehydes, alkenes and alkynes, the attachment therefore most likely proceeds mainly via the radical mechanism, as described in Section 2.<sup>92,104</sup>

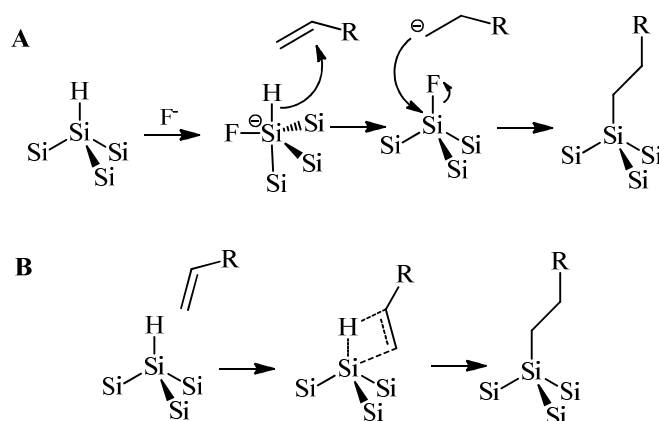


**Figure 23.** Fluorine-catalyzed attachment of alkenes to silicon (A), and attachment and hydrogen transfer in a concerted reaction (B).

## 2.4 Experimental and Theoretical Modeling Studies

In order to better understand the reactions taking place during monolayer formation, modeling studies were undertaken by several research groups. Most theoretical studies make use of a silicon slab or crystal to represent the silicon surface.<sup>102,105-107</sup> An alternative suitable model is tris(trimethylsilyl)silane (TTMSS), which may provide a good representation of the H-Si(111) surface. Moreover, the chemistry of the TTMSS radical has already been studied in detail,<sup>45,63,108-110</sup> allowing for a clear interpretation of novel reactivity patterns. Recently, Fouassier and coworkers extended these reactivity studies to a wide range of alkenes and combined them with density functional theoretical (DFT) calculations.<sup>111,112</sup> The calculations of reaction barriers showed good correlation with experimental reaction rates. However, this study was not directed towards monolayer formation on silicon, and the used reagents are not representative of precursors commonly used in monolayer formation experiments. The experimental set-up, however, may be very useful in modeling the radical reaction at the silicon surface.

### 2.4.1 Quantum-Chemical Calculations on the Surface Radical Mechanism

While the methods for monolayer fabrication developed into milder and more efficient attachments, the actual kinetics of the reactions at the silicon surface remained until recently largely hidden. In order to gain a better understanding of the propagation mechanism at the silicon surface, Selloni and coworkers conducted a theoretical investigation into the radical chain reaction on silicon surfaces. With First-Principles String Molecular Dynamics (FPSMD) the trajectory of acetylene and ethylene in the addition reaction with Si(111) was modeled, as well as the subsequent hydrogen transfer (see Figure 24).<sup>106,113</sup> A significantly higher addition barrier was found for acetylene than for ethylene (3.5 and 0.9 kcal mol<sup>-1</sup> respectively), which seemed to contrast observed experimental reactivity of the surface, where alkynes display a 9-fold higher reactivity.<sup>114</sup> However, the barrier for hydrogen transfer from the surface to the  $\beta$ -carbon radical is much higher for the attached ethylene (16.4 kcal mol<sup>-1</sup>) than for acetylene (12.5 kcal mol<sup>-1</sup>). In fact, the barrier of hydrogen transfer to the ethylene moiety is even higher than the return barrier for dissociation from the surface (9.7 kcal mol<sup>-1</sup>). Therefore the authors suggest that ethylene is more likely to desorb from the surface, than to accept a hydrogen atom from a neighboring Si-H. This is in agreement with experimental findings of 1-hexene monolayers on silicon, which were shown to dissociate under UHV conditions (no heat or UV required) in a STM setup.<sup>115</sup> Although ethylene reacts faster with silyl radicals on the silicon surface, acetylene results in a faster overall reaction, as was also observed in the aforementioned monolayer experiments.<sup>114</sup> In a follow-up study, the barrier energies of formaldehyde addition (0.7



kcal mol<sup>-1</sup>) and hydrogen transfer (8.1 kcal mol<sup>-1</sup>) were calculated. These barriers are lower than the barrier for ethylene or acetylene addition, indicating that reactions of aldehydes are likely to proceed even faster. However, a recent experimental study by Horrocks and coworkers revealed the contrary.<sup>116</sup> Monolayer formation was studied by employing alkene and aldehyde moieties in equimolar amounts in the reaction mixture. The final attachment ratio reflects the rates of alkene and aldehydes addition. The addition of alkenes was found to proceed approximately nine times faster than aldehyde addition. Further modeling studies are therefore required to explain these differences in reactivity.

The group of Selloni further demonstrated that stabilization of the  $\beta$ -radical is key to increasing the reactivity of unsaturated carbon-carbon bonds towards silyl radicals.<sup>105,106</sup> The reaction barriers for the addition of both styrene and phenylacetylene were shown to disappear as a result of the stabilization by the conjugated system. This indicates that addition will proceed rapidly. The barriers for hydrogen abstraction (6.9 and 5.8 kcal mol<sup>-1</sup> for styrene and phenylacetylene, respectively) are also significantly lower than for the analogous non-conjugated compounds. Furthermore the authors present the theoretically favorable reaction pathway as strong supportive evidence that the with STM observed styrene-lines indeed are formed in a radical reaction. They show that hydrogen transfer between the  $\beta$ -carbon radical and the nearest Si-H site is very likely, and that addition of styrene to a dangling bond is also very favorable. As was discussed in the previous chapter, the direction of propagation on Si(100) is directed by the surface geometry, resulting in the formation of lines.

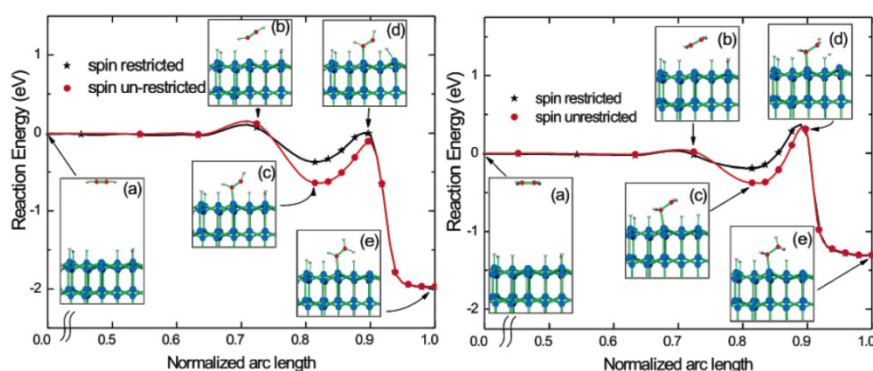


**Figure 24.** Potential energy profile along the minimum energy pathway for the reaction of acetylene (left) and ethylene (right) with the H-Si(111) surface. Black and red lines respectively correspond to spin-unpolarized and spin-polarized calculations. The zero-point energy corresponds to a non-interacting surface - molecule system. Blue: silicon atoms; red: carbon atoms; hydrogen atoms: white.<sup>106</sup>

### 2.4.2 TTMS as a Model for the Si(111) Surface: Combining Experiment and Theory

Inspired by the mechanistic investigations into the chemistry of the  $(\text{TMS})_3\text{Si}\bullet$  radical (**8**), Zuilhof and coworkers combined experimental and theoretical results of reactions of silyl radicals with precursors commonly used in monolayer formation<sup>117</sup>. The objective was to link observed reactivity to a theoretical model, in order to explain and predict experimental findings. Since the formed  $\beta$ -carbon radical in linear alkenes and alkynes does not display UV absorbance above 250 nm, its reactivity cannot be measured directly. Competition reactions involving the silyl radical and two monolayer-precursor molecules (e.g. an alkene and an alkyne) resulted in relative reaction rates (see Figure 25). Since terminal alkenes are most commonly used in monolayer fabrication, the reactivity of 1-decene was used for reference (see Table 4.1).<sup>3,48,52,89</sup> The observed reactivity order of 1-decyne, 1-decene and 1-undecanal is in good agreement with monolayer experiments (aldehyde < alkene < alkyne).<sup>73,114,116</sup> In addition, the introduction of conjugated bonds has a strong effect on reactivity. A 10-fold increase in reactivity was observed for phenylacetylene as compared to 1-decene. The predictive potential of these reactivity experiments was demonstrated by the high reactivity of two novel potential pre-cursors for monolayers, hexadeca-3-en-1-yne and 1,3-hexadecadiyne. The introduction of conjugated bonds leads to a dramatic increase of reactivity (200- and 1400-fold increase for the ene-yne and diyne respectively), making these compounds very suitable for accelerated monolayer fabrication. Very recently, Rijksen, Pujari, et al. have indeed shown that this is the case.<sup>118</sup>

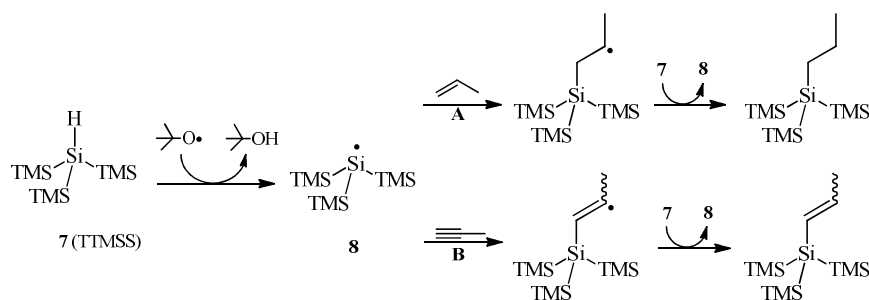


**Figure 25.** Competition experiments of TTMS radical (**8**) with alkene and alkyne. The reactivity ratio is determined by the product ratio of reactions A and B.<sup>117</sup>

In order to investigate the rates for the addition reaction, DFT calculations were carried out on a simplified model of **8** (see Figure 26). The study showed the importance of taking reaction entropy into account for calculation of the rates, as the rates calculated with inclusion of both enthalpic and entropic effects show a very good correlation with the reactivity ratios (Table 1), while calculations that only account for enthalpic effects do not

yield a proper correlation with experimental results. Moreover, the theoretical rates closely resemble experimental rates from literature ( $8 \times 10^4$ ,  $1 \times 10^5$  and  $5 \times 10^7 \text{ s}^{-1}$  for addition of acetone, alkene and styrene to **8**). The predictive power of the theoretical model was demonstrated by calculation of the rates for the diyne and yne-ene species. The employed models may prove useful in determining which functionalities are compatible, while avoiding undesired side reactions (upside-down attachment).

**Table 1.** Experimental reactivity ratios (determined at 20 °C) and calculated reaction rates (calculated for 20 °C) for the addition of silyl radicals to monolayer precursors.

Reagent	Reactivity ratio vs. 1-Decene (-)	Calculated Rate ( $\text{M}^{-1}\text{s}^{-1}$ )
<b>1-undecanal</b>	0.03	$4.2 \times 10^4$
<b>1-decene</b>	1.0	$6.5 \times 10^5$
<b>1-decyne</b>	7.5	$3.2 \times 10^6$
<b>styrene</b>	-	$1.8 \times 10^7$
<b>phenylacetylene</b>	91	$4.8 \times 10^7$
<b>hexadeca-3-en-1-yne</b>	203	$1.1 \times 10^8$
<b>1,3-hexadecadiyne</b>	1430	$1.0 \times 10^9$

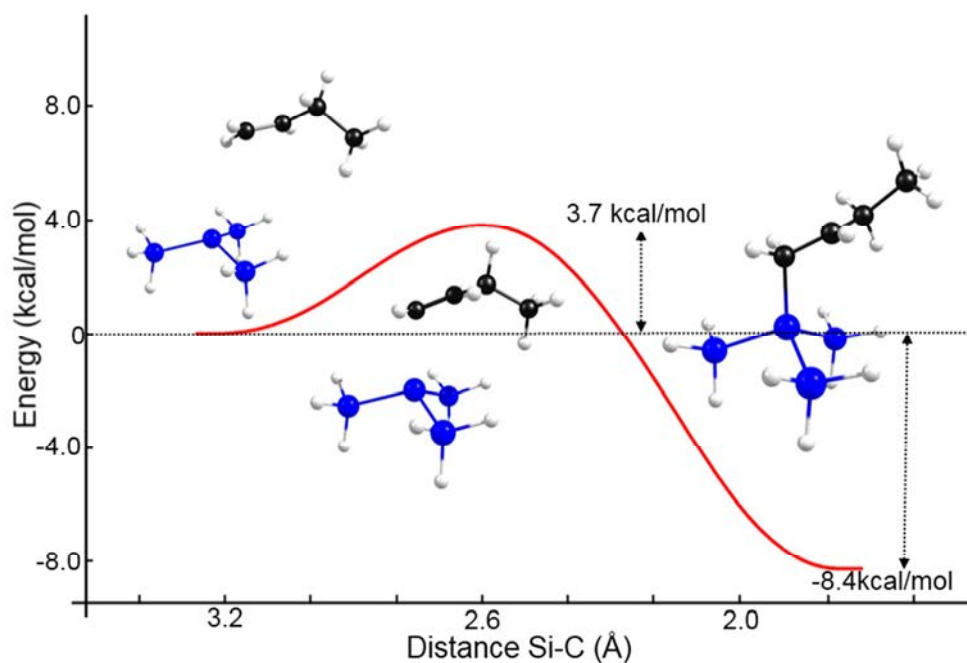


**Figure 26.** Si<sub>4</sub>-model derived from TTMSS, which is used for calculating the reaction barrier for addition of unsaturated carbons to the silyl radical.

### 2.4.3 Experimental Modeling of Radical Cation Initiation

As was discussed already in Section 3, early methods for monolayer formation were based on a substantial input of energy in order to directly cleave Si-H bonds at the silicon surface. However, the success of new mild procedures shows that there must be another mechanism that coincides with direct cleavage of Si-H bonds. Section 2.3 already gives a detailed overview of mechanisms proposed to explain mild attachment, which are supported by experimental findings. Recently, our group reported an experimental kinetics study on the reactivity of silyl radical cations, demonstrating the feasibility of radical cation initiation.<sup>101</sup> The molecules used in this study were designed to represent the top-layer of the hydrogen-terminated silicon surface (see Figure 27).

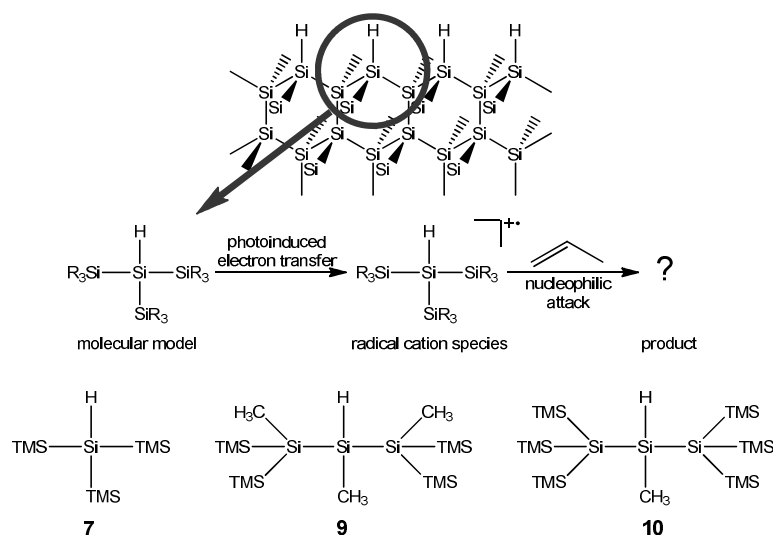


**Figure 27.** Selection of models used to represent the Si(111) surface (**7**, **9** & **10**) and the subsequent study of the silyl radical cations. Note: TMS = Si(CH<sub>3</sub>)<sub>3</sub>.<sup>101</sup>

Silyl radical cations of **7**, **9** & **10**, were efficiently generated by photo-induced electron transfer using N-methyl quinolinium salts (NMQ; 355 nm) and toluene as sensitizer and co-sensitizer, respectively.<sup>119</sup> These radical cations subsequently were shown to react readily with a variety of nucleophiles, regularly used in monolayer fabrication. These experiments showed that alkenes and alkynes react with silyl radical cations with high rates ( $k_2 \sim 10^6 \text{ M}^{-1} \text{ s}^{-1}$ ). This reactivity is in line with the initiation of monolayer formation by alkenes and alkynes onto hydrogen-terminated surfaces. However, the significantly higher reactivity of oxygen-centered nucleophiles ( $k_2 > 10^7 \text{ M}^{-1} \text{ s}^{-1}$ ) contrasts with the difference in reactivity, of aldehydes compared to alkenes, that is observed in monolayer experiments (attachment via alkene moieties was shown to be one order of magnitude more favorable than attachment of aldehydes,<sup>116</sup> whereas carboxylic acids do not attach at all).<sup>120</sup> Therefore, it can be concluded that, while the radical cation mechanism properly explains the initiation of the visible-light induced reaction, the propagation step in the preparation of Si-C linked monolayers does not involve radical cation, but only surface-centered radicals. Furthermore, experiments with deuterium-labeled **9** and **10** (Si-D instead of Si-H), showed a (secondary) kinetic isotope effect of 1.2, indicating that cleavage of the Si-H (or Si-D) bonds does not occur in the rate-limiting step of the initiation, but that nucleophilic attack takes place close to the Si-H site. This was confirmed by analysis of the reaction mixtures of **7**, which showed products of substitution reactions (substitution of a TMS group, see Figure 28A). The presence of hydrosilylation products could be contributed predominantly

to radical formation by nucleophilic attack to the silyl radicals (see Figure 28B), and only in a minor degree to spontaneous dissociation of **11**.

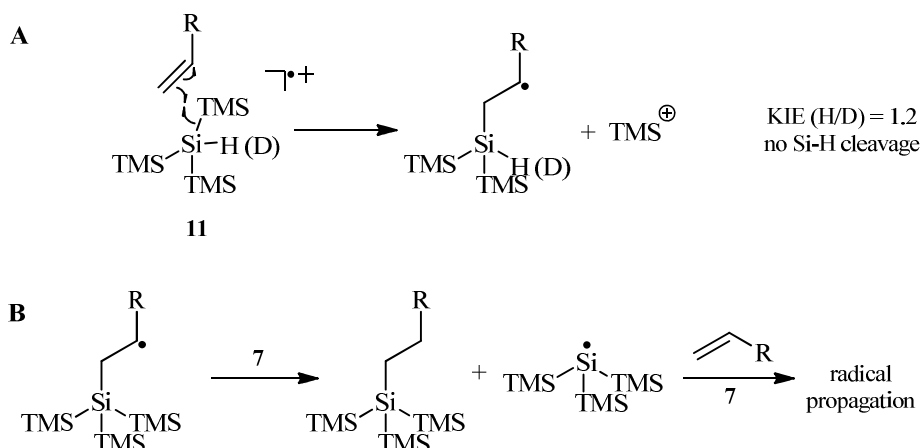


**Figure 28.** (A) Nucleophilic attack of alkene to the Si center of the TTMSS radical cation (**11**), results in the substitution of a TMS group, and the formation of a  $\beta$ -carbon radical. The Si-H (or Si-D) bond remains intact, which is in line with the secondary KIE of 1.2; (B) the  $\beta$ -carbon radical intermediates (like those obtainable via A) abstracts hydrogen from TTMSS (**7**), resulting in the formation of the TTMSS radical.

## 2.5 FUNCTIONALIZED MONOLAYERS ON SILICON SURFACES

The formation of functional monolayers on silicon surfaces has attracted significant attention over the past decades, since functional surfaces are essential in the development of new biosensors and molecular electronics.<sup>121-123</sup> The presence of functional molecules on silicon surfaces allows for selective binding and detection of target biomolecules.<sup>124-127</sup> In addition, these functional assemblies provide a way to gain control over surface properties such as wettability, friction and adhesion.<sup>128</sup> Incorporation of functional moieties on the surface is, however, far from trivial and often relies on the use of protective groups or the use of a reactive intermediate, to which the desired functional molecules are then coupled. Direct attachment of functionalities onto the silicon surface is not desirable, since side reactions readily take place resulting for example in upside-down attachment, drastically affecting packing of the alkyl chains in the monolayer, as discussed in the following sections.

### 2.5.1 C-H Bond Activation

The incorporation of functional groups into the silicon surface was initially studied by Chidsey and co-workers.<sup>129,130</sup> Two strategies were studied, both involving C-H activation of terminal methyl groups in an octadecyl monolayer on Si(111). The first method entails illumination of the octadecyl monolayer at 350 nm for 15 minutes in the presence of 4'-[3-trifluoromethyl-3H-diazirin-3-yl]-benzoic acid *N*-hydroxysuccinimide ester (TDBA-OSu), (see Figure 29). This aryl-diazirine crosslinker, inserts into the carbon-hydrogen bonds of the terminal methyl groups of the octadecyl monolayer through a highly reactive singlet-state carbene intermediate. This reaction was carried out using carbon tetrachloride as solvent and resulted in a surface with amino-reactive *N*-hydroxysuccinimidyl moieties. Although this method is fast, it leads to rather ill-defined structures on the surface. Moreover, only low surface coverages of amino-reactive groups are achieved (approximately 10%), and as a result, the surfaces remain hydrophobic, affecting further functionalizations. However, this route allowed for the successful immobilization of amino-functional biomolecules, such as amino-modified DNA, making these systems suitable for biological scanning probe microscopy (SPM),<sup>126,130,131</sup> while further improvements on the coverage may be feasible.

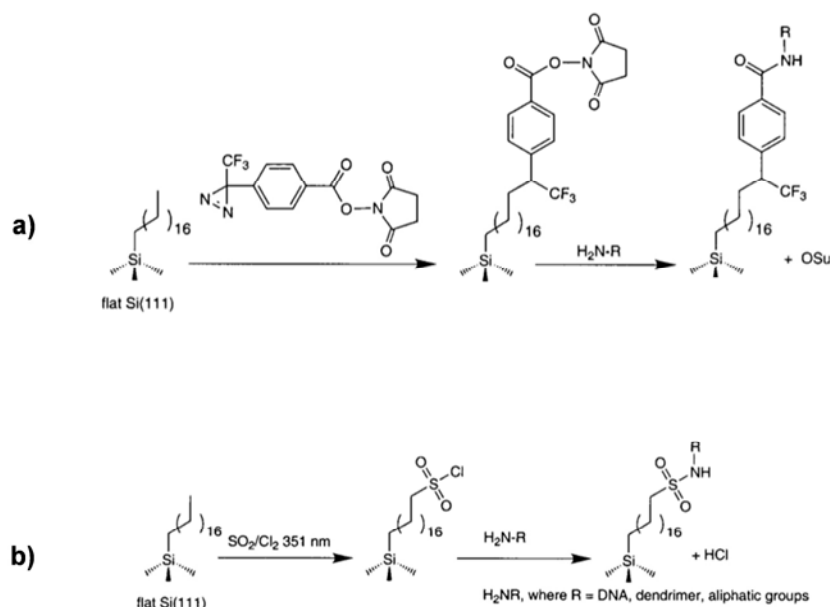


**Figure 29.** Functionalization of octadecyl monolayers on silicon through C-H bond activation, followed by amide (a) and sulfonamide (b) formation.<sup>2</sup>

Alternatively, a gas-phase free radical chlorosulfonation reaction was employed to introduce *in situ* highly reactive sulfonylchloride groups onto the octadecyl monolayer by irradiating the surface with 350 nm UV light with chlorine gas in sulfur dioxide. Subsequent reaction with primary amines leads to sulfonamide formation, Figure 29b. This route also results in less disordered amino-modified monolayers, than aminopropyltriethoxysilane based organic films on silicon oxide surfaces. Another advantage of this approach is that the density of sulfonylchloride groups can be controlled by irradiation time, while the conjugation reaction depends on amine concentration, and reaction time, allowing for ample control over surface coverage. The amine-terminated alkyl monolayers obtained after reaction of the sulfonylchloride groups with ethylenediamine, provide a facile route to a wide range of heterobifunctional crosslinkers such as benzoylbenzoic acid and N-hydroxysuccinimide or direct conjugation of amino-functional biomolecules. Oxidation of terminal methyl groups present on hexadecyl monolayers on Si(111) was recently studied by Zuilhof, Schubert and co-workers as a functionalization method.<sup>132</sup> Densely packed hexadecyl monolayers were locally oxidized using an electrically biased Pt-coated atomic force microscopy (AFM) probe in contact mode. Oxidation behavior was studied as a function of applied voltage. At low voltages, these monolayers remained unchanged.

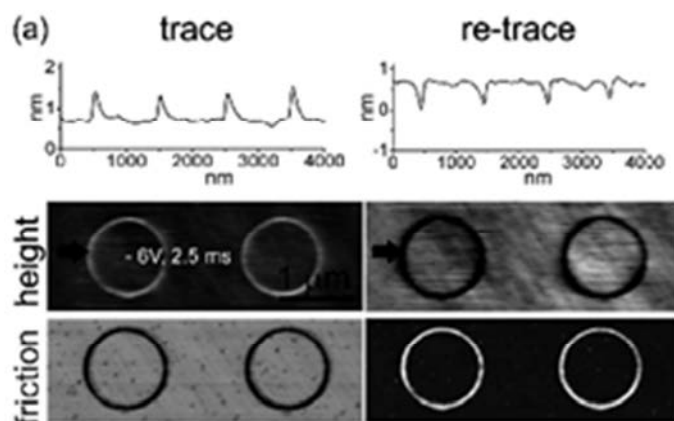


**Figure 30.** Contact-mode AFM height and friction images of a patterned hexadecylated silicon surface. Two circles showing monolayer oxidation ( $\sim 6$  V bias at a pixel duration of 2.5 ms), and section profiles along the arrow above the height images. All patterns were obtained in a pixel resolution of  $\sim 205$  pixels/ $\mu\text{m}$ .<sup>132</sup>

However, upon increasing the bias voltage, oxidation of the terminal methyl groups occurred, resulting in carboxylic acid moieties. Depending on the voltage employed, as well



as the length of the oxidation pulse, a highly controlled partial to complete degradation of the monolayer was achieved, with concomitant control over the oxidation of the underlying silicon (partial monolayer degradation to yield a.o. carboxylic acid moieties does not lead to surface oxidation yet). Figure 30 shows the contact-mode height and friction images in both directions (trace and re-trace) obtained after local probe oxidation of the hexadecyl monolayer.

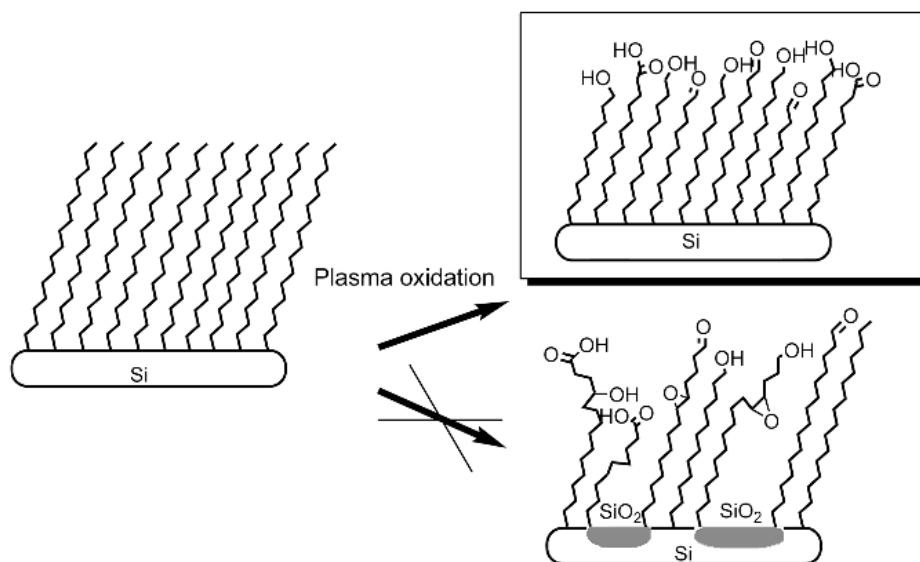


**Figure 31.** Schematic representation of the surface reactions during plasma treatment of alkyl monolayers on silicon.<sup>133</sup>

This method allows even milder local probe oxidations using labile functional groups that are oxidized already at very low bias voltages (for example NHS moieties, discussed in the following Section). While this process is carried out on the microscale, plasma treatment of alkyl monolayers on silicon gives access to functionality over much larger areas. Hexadecyl monolayers on Si(111) or Si(100) underwent a short plasma treatments (1-3 seconds), which resulted in oxidation of the terminal methyl groups into hydroxyl, aldehydes and carboxylate functionalities, Figure 31.<sup>133</sup> Importantly, on Si(111) substrates this did not damage the underlying oxide-free silicon as evidenced by the  $C_{1s}$  and  $Si_{2p}$  XPS narrow scan analysis. After 1 s of oxidation, C=O bonds represent a significant part of the surface functionalities, in the form of aldehydes groups. Oxidation of the silicon substrate was indeed observed for Si(100) surfaces. After 3 s of plasma treatment, 5% of the total  $Si_{2p}$

signal corresponds to  $\text{SiO}_2$ . Carbon atoms with a single bond to oxygen (C-O) are mostly formed during plasma treatment. This was further evidenced by reacting these monolayers with *p*-trifluoromethylbenzylamine (TFBA), resulting in conjugation with 35-40% of the C=O groups introduced by plasma treatment.

Packing of the alkyl monolayers was not significantly affected by the plasma treatment, as observed by IRRAS. Initially, symmetric and antisymmetric C-H stretching vibrations of the  $\text{CH}_2$ -moieties are observed at  $2851\text{ cm}^{-1}$  and  $2920\text{ cm}^{-1}$ , respectively. Upon plasma oxidation, the intensity of these vibrations gradually decreases, while the  $\text{CH}_3$  vibration at  $2965\text{ cm}^{-1}$  disappears entirely already after 3 s of plasma treatment. The underlying alkyl chains retain their initial packing as indicated by the symmetric  $\text{CH}_2$  vibration at  $2920\text{ cm}^{-1}$ . To demonstrate the reactivity of aldehyde-terminated monolayers (1 s plasma-treatment), reaction with cysteamine was carried, resulting in thiol-terminated surfaces. These surfaces were successfully employed in the attachment of gold nanoparticles (Au NPs). In addition, the binding of Au NPs was used to demonstrate the ability of surface patterning using plasma. To this purpose, a soft contact mask was employed during the plasma treatment allowing the formation of patterns with micrometer-sized features, as observed by AFM in Figure 32. This novel and facile route gives access to patterning of high-quality functional silicon surfaces.

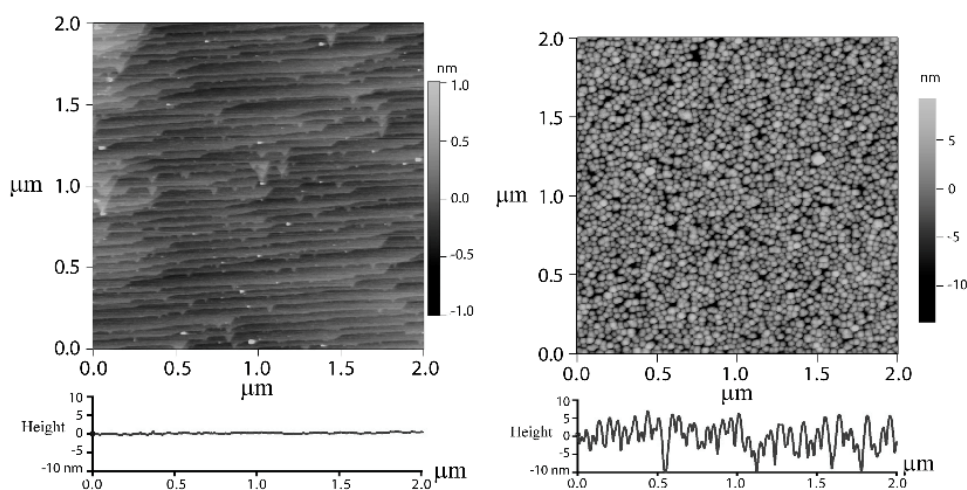


**Figure 32.** AFM images and sections measured on monolayer-coated silicon(111) surfaces. After exposure to cysteamine and gold nanoparticles without plasma treatment (left); and after 1 s of air-based plasma followed by reaction with cysteamine and gold nanoparticles (right).<sup>133</sup>

### 2.5.2 Carboxylic Acids

Carboxylic acid-terminated monolayers have proven to be a very useful scaffold for further functionalization of silicon surfaces.<sup>120,134,135</sup> However, the quality of the corresponding monolayers depends largely on the method employed for their fabrication. Early investigations by Zuilhof, Sudhölter and co-workers showed that thermal attachment (200°C, 2h) resulted in significant upside-down attachment. According to FTIR studies, these monolayers display poor packing as compared to alkyl monolayers.<sup>52</sup> On the other hand, when employing photochemical methods ( $\lambda = 300$  nm, 3h), high-quality monolayers were obtained without significant upside-down attachment.<sup>134</sup> This suggests that the acid moiety is able to react with surface Si-H at elevated temperatures, whereas it displays a strongly diminished reactivity at room temperature. This compatibility of carboxylic acid moieties with the hydrosilylation reaction was further studied by Bowden and coworkers who functionalized the silicon surface with a mixture of 1-octadecene and a fluoro-capped carboxylic acid in the presence of TEMPO (see Figure 33).<sup>120</sup> The thus obtained surfaces were characterized by XPS and IR spectroscopy. The silicon surface did not oxidize, since no signal was observed at 101-104 eV region in the Si<sub>2p</sub> narrow scan.<sup>136</sup> In addition, the F<sub>1s</sub> narrow scan did not display any signals in the 684-694 eV region, indicating the absence of fluorine atoms, which confirms the limited reactivity of acid moieties towards silyl radicals. Chazalviel and coworkers studied the preparation of mixed monolayers employing photochemical methods ( $\lambda = 312$  nm) with 1-alkenes and acid-terminated 1-alkenes. A drawback of this method is the use of numerous rinsing steps with hot acetic acid to remove physisorbed carboxylic acid molecules from the silicon surface.<sup>137</sup>

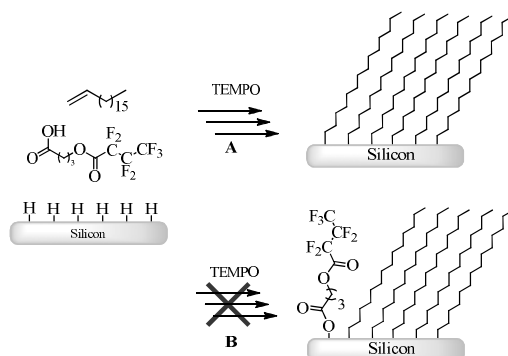


**Figure 33.** TEMPO-initiated monolayer formation of 1-octadecene and fluorine-capped carboxylic acid results solely in the formation of octadecyl layers (A). No attachment of the carboxylic acids (B) was observed with STM (no fluorine signal in the 684-694 eV region).<sup>120</sup>

### 2.5.3 Esters: Hydrolysis, Reduction and Cleavage

As discussed in the previous Section, direct attachment of carboxylic acids during hydrosilylation of the silicon surface is problematic due to the formation of silyl esters on the silicon surface.<sup>59,138-140</sup> Instead, the use of 1-alkenes bearing ester moieties such as methyl and propyl esters of 10-undecylenic acid have been successfully employed in the formation of monolayers on silicon; subsequent hydrolysis of the esters yielded carboxylic acid-functionalized silicon surfaces, Figure 34.<sup>138</sup>

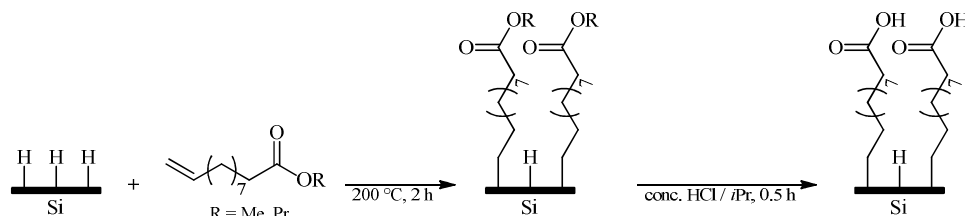


**Figure 34.** Attachment of 10-undecenyl ester on Si(100) surfaces and formation of acid-terminated monolayers on silicon after hydrolysis.<sup>138</sup>

These ester-terminated monolayers on Si(100) were prepared under thermal conditions (200 °C). The resulting silicon monolayers are well-ordered as demonstrated by the antisymmetric and symmetric methylene stretching vibrations in the FTIR spectra (for methyl ester-terminated monolayers:  $\nu_a$  2923  $\text{cm}^{-1}$ ,  $\nu_s$  2854  $\text{cm}^{-1}$ , and for propyl ester-terminated monolayers:  $\nu_a$  2920  $\text{cm}^{-1}$ ,  $\nu_s$  2850  $\text{cm}^{-1}$ ). The ester moieties do not significantly affect packing of the monolayers. Subsequent hydrolysis of the ester groups led to the formation of acid-terminated monolayers (Figure 34). It may be desirable to use acidic conditions, since strongly alkaline solutions may damage the silicon surface. Acetate-functionalized monolayers on Si(100) have been studied as well. These monolayers were prepared from 10-undecenyl acetate employing thermal conditions (Figure 35).<sup>138</sup> A close packing of the alkyl chains in the monolayer was observed by FTIR spectroscopy. Hydrolysis of these surfaces was foreseen to provide a route to alcohol-terminated surfaces. However, under acidic conditions the acetate moieties were not hydrolyzed, most likely due to inaccessibility of the esters due to steric hindrance. Use of  $\text{LiAlH}_4$ , however, conveniently yielded hydroxyl-terminated monolayers.

In addition to these studies, Boukherroub and Wayner investigated the modification of Si(111) surfaces with ethyl undecylenate employing UV irradiation.<sup>141</sup> Several reactions on the ester moieties using standard chemical and solid-phase chemical procedures were performed to generate functional silicon surfaces (Figure 36). For example, alcohol-terminated monolayers are obtained after reduction of the ester moieties with  $\text{NaBH}_4$ , while

reaction with an alkyl Grignard reagent gives a tertiary alcohol that can be acylated with acetyl chloride. Finally, hydrolysis of the ester leads to a carboxylic acid-terminated surface that could be coupled to a protected amino acid (glycine methyl ester) using a standard solid phase amide coupling protocol. The surface density of the ester function can be controlled by dilution of the reacting ester with a long-chain alkene. This has the beneficial effects of minimizing the disruption of the alkyl chain packing in the monolayers and avoiding steric blocking of the ester group.

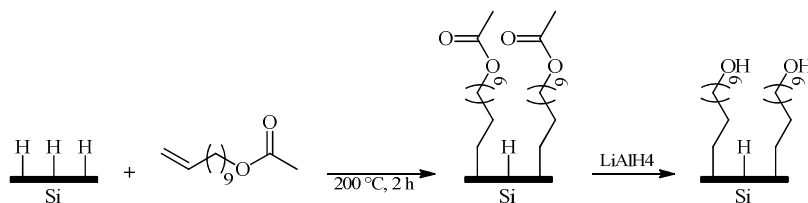


**Figure 35.** Attachment of 10-undecenyl acetate on Si(100) surfaces and subsequent hydrolysis to provide alcohol-terminated silicon surfaces.<sup>138</sup>

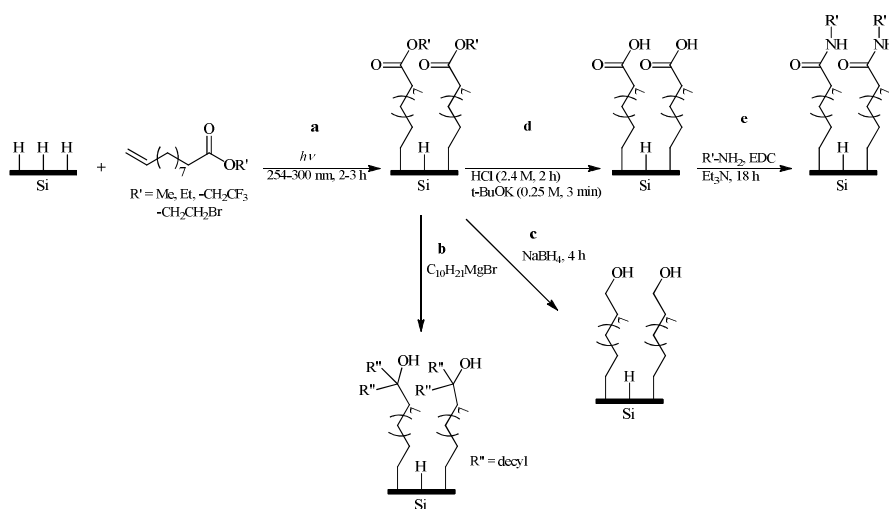


**Figure 36.** Modification and reactivity of 10-undecenyl ester-derived monolayers on Si(100) and Si(111) surfaces. Formation of alcohol-(b,c) and acid-terminated monolayers (d) and subsequent immobilization of biomolecules (e) using conventional solid phase amide coupling protocols.<sup>141</sup>

### 2.5.4 Active Esters

Ester and amide linkages are the most frequently employed groups for the conjugation of functional molecules onto surfaces. As described previously, the ester groups present in an alkyl monolayer are easily hydrolyzed, giving access to alcohols and carboxylic acid functionalities. Carboxylic acid-terminated monolayers may further react with alcohols or amines to form esters or amides, respectively. These reactions are of great interest, because they facilitate the attachment of biomolecules such as proteins, peptides, antibodies, and DNA.<sup>142,143</sup> However, activation of the carboxylic acid moieties is required. In general, acid-terminated surfaces are activated by carbodiimide reagents, such as 1-ethyl-3-(3-(dimethylaminopropyl)-carbodiimide (EDC) or *N,N'*-dicyclohexylcarbodiimide (DCC) to form a reactive *O*-acylurea intermediate. Upon reaction with amines, stable amide bonds are formed, Figure 37.<sup>144,145</sup> These reactions are often carried out in organic solvents, but aqueous solutions are also suitable. Hydrolysis of the *O*-acylurea intermediate may, however, take place in water, limiting the efficiency of conjugation. Alternatively, *N*-hydroxysuccinimide (NHS) has been employed to activate acid moieties. In contrast to the *O*-acylurea intermediate resulting from carbodiimide activation, an NHS ester is formed. These NHS esters are very reactive towards amines and much less prone to hydrolysis than the carbodiimide esters.

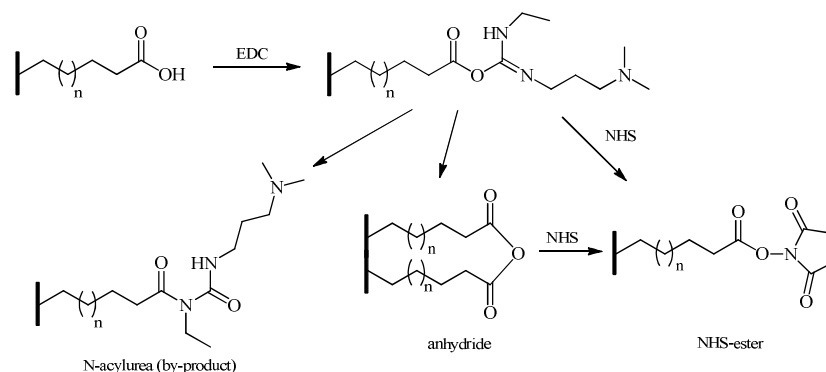


**Figure 37.** Activation of acid-terminated surfaces employing carbodiimide (EDC) reagents and alternative reaction pathways.

The activation of acid-terminated monolayers using NHS/EDC chemistry on silicon, initially introduced by Boukherroub and coworkers,<sup>146</sup> is widely employed as a common platform for the *in situ* attachment of amines, so as to obtain functional monolayers on silicon.<sup>135,147-149</sup> Similarly, several approaches have been developed towards the formation of NHS-activated silicon surfaces.<sup>138,150,151</sup> Many of these procedures rely on the use of  $\omega$ -

ester or  $\omega$ -acid-terminated 1-alkenes/1-alkynes, requiring several steps and rather harsh conditions that affect monolayer quality, either after the hydrolysis step (for ester-terminated 1-alkene/1-alkyne monolayers) or due to upside-down attachments (in the case of acid-terminated 1-alkene/1-alkyne),<sup>147,152</sup> although recently direct photochemical attachment of undecylenic acid was reported to proceed without upside-down attachment.<sup>137</sup> The use of photochemical methods enables the direct attachment of NHS-esters onto silicon in a one-step reaction by irradiation of the silicon surface immersed in  $\omega$ -NHS-functionalized 1-alkene. Although irradiation with 254 nm light<sup>153-155</sup> leads to the formation of NHS-activated silicon surfaces, partial decomposition of the NHS-ester-terminated monolayer (30%) and formation of SiO<sub>2</sub> takes place, linked to the photoreactivity of the NHS moiety under these circumstances. Recently, the mild and quantitative preparation of NHS-ester functionalized monolayers on silicon surfaces using mild photochemical methods (447 nm) was reported.<sup>156</sup> This method offers an alternative to prepare well-defined mixed monolayers from NHS-functionalized 1-alkene and 1-alkenes at room temperature. Under these conditions, no degradation of the NHS-ester moieties was detected. Further functionalization of the resulting surfaces with a variety of primary amines, as well as biotin hydrazide was investigated (Figure 38).

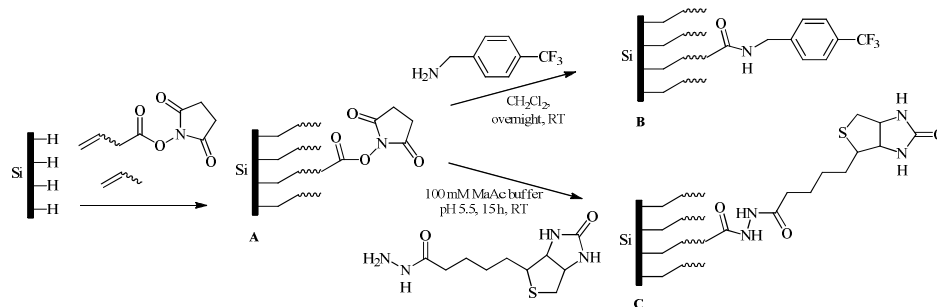


**Figure 38.** Schematic representation of the formation of a mixed monolayer terminated with NHS-ester moieties (A) and of the subsequent substitution of the NHS-ester moiety by *p*-trifluoromethyl benzylamine (TFBA) (B) or biotin hydrazide (C).<sup>156</sup>

Apart from the attachment of small molecule amines, NHS-esters have been used for immobilization of substituted hydrazide derivatives and even in the covalent coupling of antibodies.<sup>157</sup> This method is often applied to the immobilization of proteins, including native proteins, since no additional coupling reagents are required, and the conjugation proceeds in a single step. Achieving high conversion remains an issue however, due to hydrolysis of the NHS-esters. Very recently, Sam *et al.*<sup>158</sup> reported on the activation of acid-terminated monolayers via NHS/EDC route on porous silicon (Figure 39). In these

studies, infrared spectroscopy was used to investigate the formation of succinimidyl ester-terminated chains by varying the EDC and NHS concentrations in order to avoid by-products.

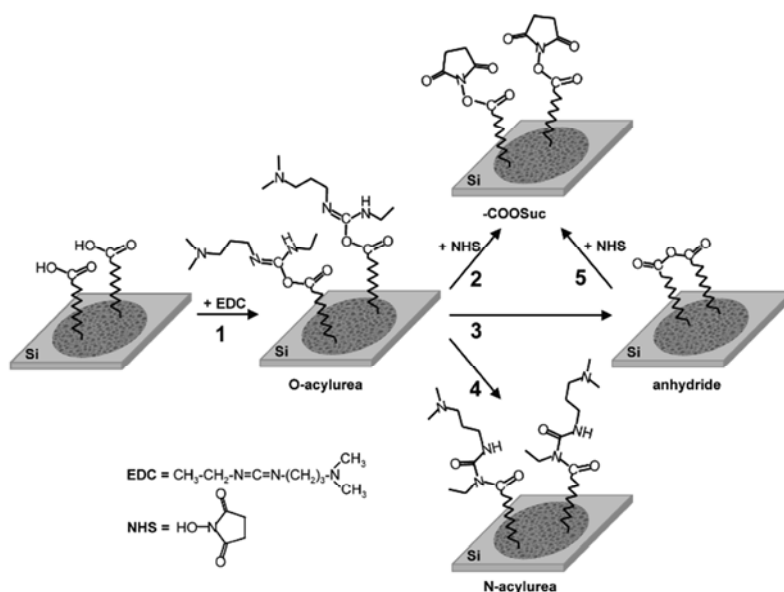


**Figure 39.** Schematic representation of activation reactions the surface: Interaction between acid-terminated moieties and EDC forming the O-acylurea intermediate (**1**) and subsequent reaction paths (**2-5**) for the experimentally detected products (succinimidyl ester, anhydride, urea). The kinetic competition between the various paths determines the final surface composition.<sup>158</sup>

Equimolar mixing of EDC and NHS in a range of 5 mM was found to be optimal to achieve high conversions. These results are explained in terms of kinetic competition between different reaction pathways, taking into account that sites where NHS adsorbs at the surface become inactive. The applicability of these findings to flat hydrogenated silicon surfaces remains to be demonstrated. Several alternative strategies have been reported towards activation of acid-terminated monolayers on silicon. For instance, an anhydride-terminated monolayer was obtained after reaction of the terminal acid moieties present in the monolayer with trifluoroacetic anhydride, in the presence of triethylamine.<sup>159</sup> These surfaces were further reacted with allylamine in order to yield alkene moieties available for further reactions. Yet another approach relies on the covalent attachment of protected



semicarbazide-functionalized alkenes on Si(111) surfaces via photochemical methods (254 nm, 2 h) as depicted in Figure 40a.<sup>160</sup>

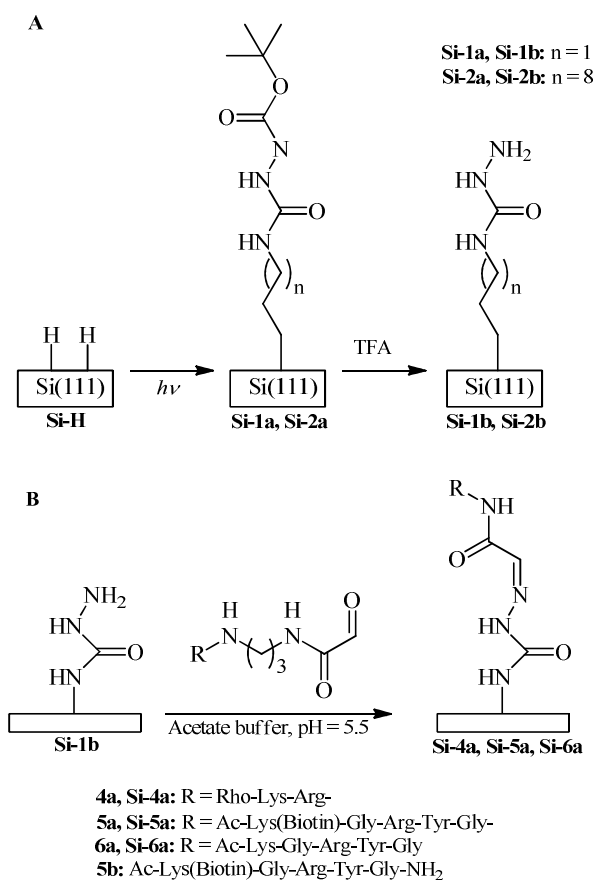


**Figure 40.** Schematic representation of the functionalization of silicon surfaces with semicarbazide groups (A) and immobilization with different peptides (B).<sup>160</sup>

Successful covalent binding of the organic layer onto the silicon surface was demonstrated by XPS and FTIR spectroscopy. However, the silicon surface did not remain oxide-free, especially after the acidic treatment to remove the protecting groups of the semicarbazide moieties. The deprotected semicarbazide-terminated monolayer was then further reacted with peptides bearing a glyoxylyl group for site-specific R-oxo semicarbazone ligation, Figure 40b. Successful peptide immobilization was confirmed by AFM and fluorescence experiments.

### 2.5.5 Acid Fluoride Monolayers

A highly useful functionalization of oxide-free silicon surfaces using acid-fluoride-terminated alkynes was recently investigated.<sup>161</sup> The acid fluoride functionality is stable under ambient conditions, but reacts readily with strong nucleophiles (amines and anionic nucleophiles). In addition, acid-fluoride-terminated monolayers do not form dimeric structures, since hydrogen bonding interactions do not occur, which prevent extensive washing steps as required for carboxylic-acid containing alkenes/alkynes. These  $\text{-C(=O)-F}$  terminated monolayers were prepared from 10-undecynoyl fluoride on oxide-free Si(111) under mild conditions (80 °C, 16 h, see Figure 41). These surfaces remain oxide-free as indicated by the  $\text{Si}_{2p}$  narrow scan, in which no signals are observed in the 101–104 eV region. The terminal alkyne functionality of 10-undecynoyl fluoride reacts with H-Si under mild conditions and yields stable Si-C=C bonds on Si(111) that are known to inhibit the oxidation of the underlying Si substrate.<sup>54,72</sup> The ellipsometric layer thickness of 12 Å is consistent with the length of the molecule and the expected tilt angle of 30–35° with respect to the surface normal confirm the formation of the monolayer. Upside-down attachment are excluded as indicated by attenuated total reflection infrared spectroscopy measurements (ATR-IR), which showed the double-bond stretching vibration of the Si-C=C moiety ( $\nu_{\text{C=C}}$  1603  $\text{cm}^{-1}$ ) and  $\text{CH}_2$  stretching vibrations that indicate a high-quality packing that is rare for functionalized surfaces, whereas the more easily visible alkyne C-H stretch (expected around  $\nu_{\text{C-H}} = 3309 \text{ cm}^{-1}$ ) remained absent. These acid-fluoride-terminated monolayers were also employed as a reactive platform for further functionalization and patterning with primary amines. The high efficiency of amide formation was shown by quantitative amide formation upon application of reactive microcontact printing ( $\mu\text{CP}$ ) with a flat PDMS stamp (20 s), i.e. indistinguishable from surfaces that were immersed in a solution of N-decylamine (1 h). Both surfaces showed an increase of water contact angle from 83° (acid-fluoride layer) to 104°, which is indicative of a methyl-terminated layer. Furthermore layer thickness increased in both cases from 12 to 26 Å. ATR-IR showed complete conversion of the conversion of acid fluorides (complete disappearance of acid fluoride absorption at 1843  $\text{cm}^{-1}$ , and appearance of the amide N-H stretch at 3313  $\text{cm}^{-1}$ ). The stability of the resulting N-hexadecylamide-terminated monolayers in water was investigated by XPS, which displays as most characteristic feature the lack of oxide formation, even after amide formation (no traces of  $\text{SiO}_2$  at the surface around 102 eV). The high reactivity towards amines makes acid-fluoride-terminated monolayers excellent platforms for reactive  $\mu\text{CP}$ , while the high selectivity of the amide formation makes them excellent intermediates for introducing a broad range of functionalities on oxide-free silicon surfaces, including complex biomolecules, such as fluorescently labeled oligo-DNA on oxide-free silicon, which is still accessible for hybridization.<sup>161</sup>

For more information regarding  $\mu$ CP, the reader is kindly referred to the work of Zhu and coworkers ( $\mu$ CP of alcohols on Si-Cl surfaces),<sup>162</sup> Mizuno and Buriak ( $\mu$ CP of 1-octadecyne directly on Si(111) and Si(100) by use of catalyst-impregnated stamps),<sup>163</sup> and the work of Toone and coworkers (catalytic conversion of terminal groups on the monolayer by chemically modified stamps).<sup>56,164</sup>

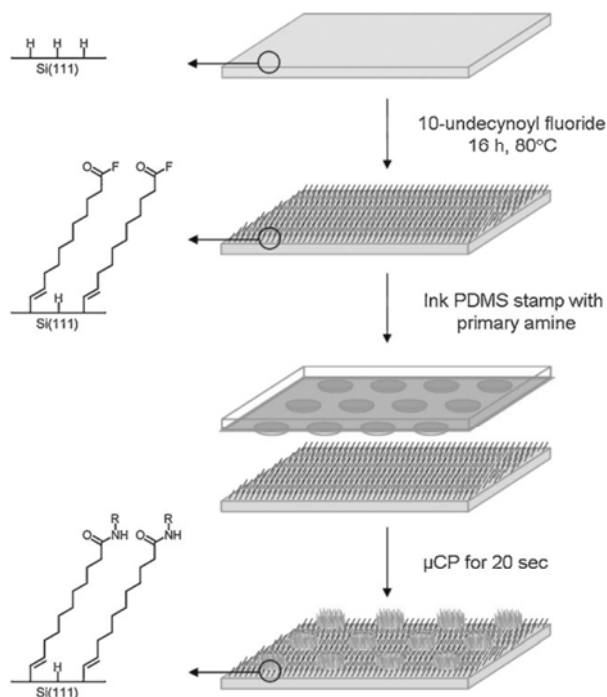


**Figure 41.** Schematic representation of the procedure used for  $\mu$ CP on oxide-free silicon via highly reactive acid-fluoride-functionalized monolayers.<sup>161</sup>

### 2.5.6 Click Chemistry

Due to the relatively sensitive nature of silicon surfaces, the wide range of desirable functionalizations requires versatile reactions that proceed under mild conditions. Hence, in addition to e.g. the amide-forming reactions from NHS esters or acid fluorides (see above), click reactions have attracted considerable attention for orthogonal and site-selective

immobilization of functional moieties.<sup>165</sup> Click reactions are identified by the mild reaction conditions needed, their high chemo- and regioselectivity, and their efficiency.<sup>165,166</sup> Gooding and coworkers prepared alkyne-terminated monolayers on Si(100) through thermal addition of 1,9-nonadiyne. Subsequently, the Cu-catalyzed azide-alkyne cycloaddition was employed to attach a variety of functional azides onto these monolayers.<sup>167,168</sup> Very robust oxide-free modified silicon surfaces were produced via the hydrosilylation reaction. Moreover, these surfaces are stable to allow the preparation of redox assemblies for aqueous environments and antifouling surfaces.<sup>168,169</sup>

The radical addition reaction of thiols to alkenes or alkynes has recently emerged as an elegant and appealing alternative coupling reaction. Very mild reaction conditions, the absence of a metal catalyst, and the ready availability of thiol-functional (bio)molecules are distinctive features of this coupling chemistry.<sup>166,170,171</sup> In addition, these radical reactions have been used as an efficient strategy towards immobilization and patterning of biomolecules on inorganic substrates such as gold, glass and silicon.<sup>166,169,172</sup> For example, Bertin and Schlaad used thiol-ene chemistry as a method to rapidly functionalize glass substrates with polymers.<sup>173</sup> Dendrimeric and polymeric approaches have been reported demonstrating both thiol-ene and thiol-yne chemistry. Waldmann and co-workers for example used polyamidoamine dendrimers attached covalently to silicon oxide surfaces to develop a new method for the site-specific immobilization and patterning of proteins.<sup>174,175</sup> Patton and co-workers used silicon substrates functionalized with silanes to generate a library of polyfunctional, patterned and multicomponent polymer brush surfaces.<sup>176</sup> Recently, Ravoo and co-workers reported the immobilization of functional thiols on alkene- and alkyne-terminated self-assembled monolayers on silicon oxide substrates by photochemical microcontact printing.<sup>177</sup> Although these strategies are not specific for oxide-free silicon surfaces, the versatility of the employed coupling strategies allows for their easy extension to these surfaces. This was shown for example by Buriak and coworkers who used thiol-ene chemistry for the layer-by-layer assembly of  $\alpha,\omega$ -dithiols and  $\alpha,\omega$ -diene molecules on oxide-free silicon, silicon oxide and germanium surfaces.<sup>177</sup> The Si(100) surfaces were modified using photochemical methods (254 nm, 3 h) by reacting the hydrogen-terminated silicon surface with the desired  $\alpha,\omega$ -diene (i.e. 1,7-octadiene, 1,11-dodecadiene). The alkene-terminated monolayers thus obtained were immersed in neat  $\alpha,\omega$ -dithiols, and after UV irradiation for 0.5 h, thiol-terminated monolayers were generated. Subsequent reaction of these silicon surfaces with  $\alpha,\omega$ -dienes led to the formation of alkene-terminated monolayers, and this procedure was continued until the desired number of layers was reached, Figure 42. This layer-by-layer approach provides an interesting platform for growing covalently bound films of controlled thickness onto oxide-free silicon.

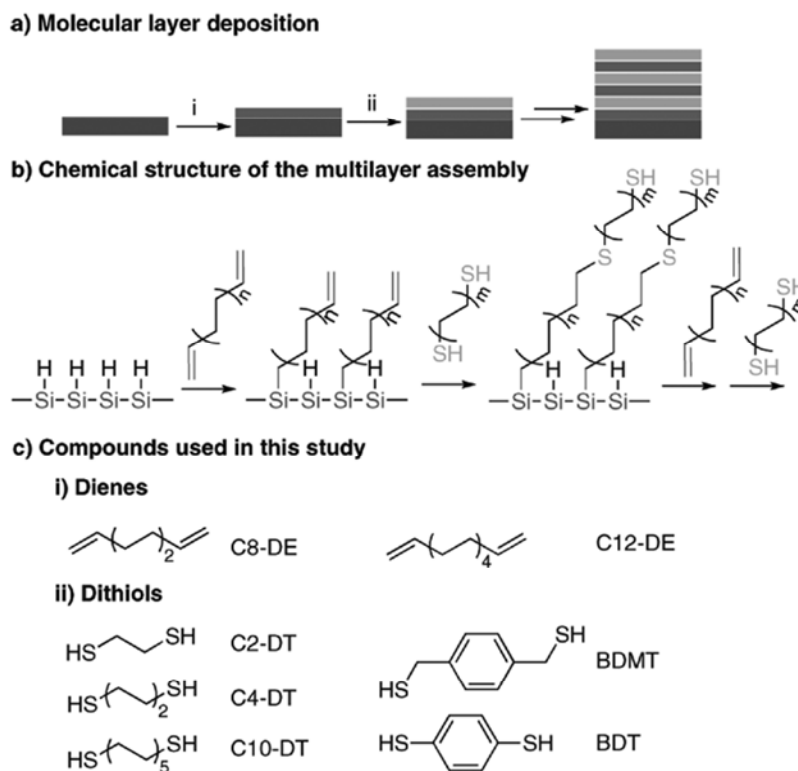


**Figure 42.** (a) Schematic representation of the covalent molecular layer deposition assembly of a thiol-ene multilayer; (b) Chemical structure of the multilayer assembly and (c) Dienes and dithiols employed in this study.<sup>177</sup>

Recently, Zuillhof and co-workers reported on a versatile approach employing thiol-ene click chemistry as a versatile, efficient, and patternable route to functionalize silicon surfaces under ambient atmosphere without the introduction of silicon oxide.<sup>178</sup> In these studies, alkene-terminated monolayers on oxide-free Si(111) were obtained after reaction of hydrogen-terminated Si(111) with neat 1,13-tetradecadiene under thermal conditions (80 °C, 16 h). The alkene-terminated monolayers were further exposed to 365 nm light in the presence of different functional thiols and 2,2-dimethoxy-2-phenylacetophenone (DMPA), which acts as a photoinitiator (Figure 43). This lead to a wide range of functionalized surfaces, which in all cases displayed a high surface coverage (45-75%; typically limited by the steric bulk of the functional group with respect to the alkene chains), while the silicon surfaces did not undergo any discernable oxidation.

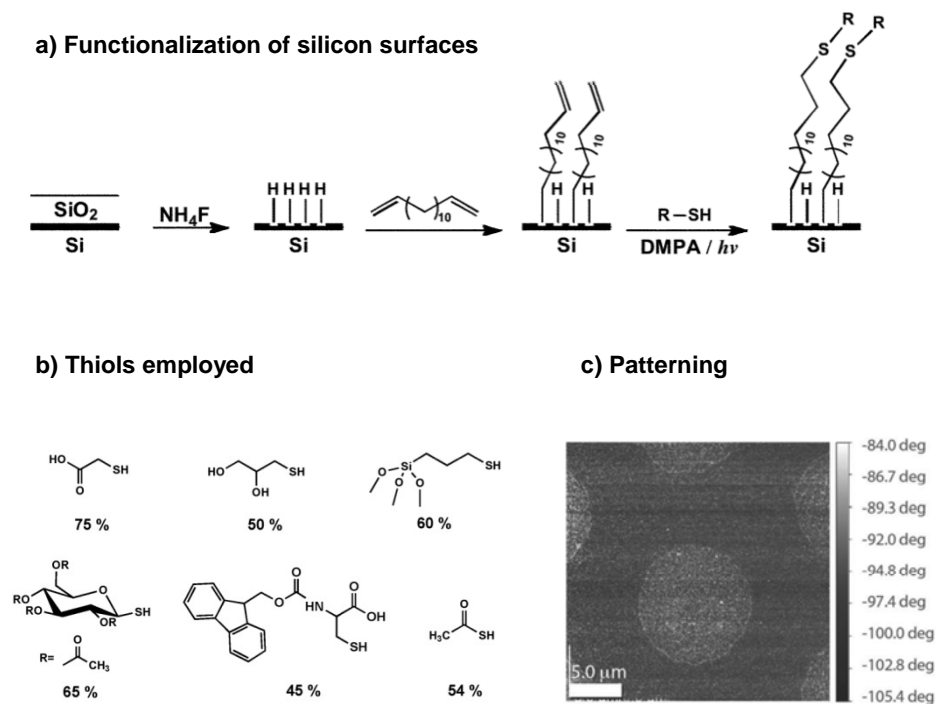


**Figure 43.** (a) Schematic representation of functionalization of silicon surfaces using thiol-ene chemistry; and (b) thiols employed in surface functionalization, with corresponding surface coverages. (c) AFM phase image of the patterned silicon monolayer with thioglycolic acid.<sup>178</sup>

In addition, microcontact-printing of thioglycolic acid onto an alkene-terminated monolayer was investigated. A PDMS stamp with 10  $\mu\text{m}$  pillar-like features was covered with a mixture of thioglycolic acid and DMPA in ethanol, subsequently brought into contact with the alkene-functional silicon substrate, and next the surface was irradiated through the stamp for 5 min. After thorough cleaning of the substrate, the surface displays a 10  $\mu\text{m}$  sphere-pattern in the AFM phase image, confirming successful transfer of the pattern as shown in Figure 43c.<sup>178</sup> This further demonstrates that thiol-ene chemistry provides an efficient method for metal-free light-induced patterning onto silicon.

## 2.6 Perspectives

The rapidly progressing development of novel approaches to form covalently attached monolayers on silicon surfaces parallel deepening insights into silyl radical chemistry. The high stability of Si-C bonds in combination with the versatile chemistry available for the functionalization of monolayers, make these systems ideal platforms for electronic and sensory devices. This paragraph outlines the currently unresolved “hot” topics in this area.

Since the pioneering research in the early 90's, monolayer fabrication has seen major developments. Starting from experiments using relatively harsh reaction conditions (temperatures  $> 200\text{ }^{\circ}\text{C}$ ),<sup>51,59</sup> methods progressed into much milder methods for generation of surface-centered silyl radicals. Si-H bonds were also shown to cleave under UV irradiation,<sup>54,80,86</sup> and eventually monolayer formation was demonstrated to occur without the direct cleavage of these bonds (white-light method and attachment in the dark).<sup>67,72,91-93</sup> These increasingly milder methods have resulted in the direct attachment of sensitive molecules, such as complex sugars and peptides that would otherwise degrade.<sup>179</sup> At this moment experimentalists have a wealth of mild methods and techniques available.<sup>3,4,48</sup> Depending on the desired properties, ease of use, and availability of precursors, several options exist for the fabrication of monolayers on silicon.

A major challenge, however, still lies in speeding up monolayer formation. Where typical formation of SAMs from thiols on gold using stamps takes minutes,<sup>180</sup> attachment onto silicon is still in the range of hours. Experiments have shown that up to 90% of the layer is formed within minutes, yet filling up the remaining holes (and thus completing the layer) is a slow process.<sup>70,181</sup> Looking from a radical chemistry perspective, basically there are two approaches to achieve this speed-up. The first approach is to change reaction conditions in order to initiate more dangling bonds at the silicon surface. Radical addition and the subsequent hydrogen transfer have been shown to be efficient reactions for covalent attachment of precursors. In this respect, addition of radical initiators and/or catalysts may prove valuable in increasing the reaction rates, as long as no undesired side reactions take place. Additionally, irradiation (UV or visible light) possibly assisted by electronic modification of the surface properties (bias voltages) may also catalyze the formation of surface-centered radicals.

A promising second approach to the speed-up may lie in the modification of the precursors. An enhanced reactivity in both the addition and hydrogen transfer steps may lead to larger islands and longer lines, depending on the surface (Si(111) and Si(100), respectively).<sup>117,118</sup> Moreover, recent studies show that modification of these precursors - in order to reduce the number of close contacts near the surface - also contributes to higher surface coverages and increased packing of the monolayers.<sup>101</sup>

Another “hot” topic is the functionalization of monolayers. With the advent of efficient coupling chemistry, also new moieties are readily introduced in the monolayers. Functionality of these layers has progressed from aldehydes and acids to azides and alkenes, which can be used in “click” chemistry (alkyne-azide, thiol-ene, etc.) for the attachment of more complex molecules. However, the ever increasing demand for high-quality monolayers on oxide-free silicon, requires side reactions of functional moieties to be reduced to an absolute minimum, as indicated, for example, by the attachment of  $\omega$ -aldehyde functionalized alkenes to Si(111).<sup>116</sup> Since aldehydes are also reactive towards silyl radicals, up to 10% of the pre-cursors attaches via this moiety instead of the desired attachment via the alkene. For aldehyde-functionalized alkynes, however, this ratio is expected to further shift in favor of the alkyne attachment. In general, alkyne-derived Si-C linked monolayers display superior linking properties as compared to alkene-based monolayers in terms of packing density,<sup>73,101</sup> rate of formation<sup>72,73,101,117</sup> and stability towards oxidation,<sup>126</sup> and alkyne precursors are thus expected to be at the basis of novel functional monolayers on silicon surfaces.

## References

- (1) Waltenburg, H. N.; Yates, J. T. *Chem. Rev.* **1995**, 95, 1589.
- (2) Buriak, J. M. *Chem. Rev.* **2002**, 102, 1271.
- (3) Ciampi, S.; Harper, J. B.; Gooding, J. J. *Chem. Soc. Rev.* **2010**, 39, 2158.
- (4) Gooding, J. J.; Ciampi, S. *Chem. Soc. Rev.* **2011**, 2704.
- (5) Cummings, S. P.; Savchenko, J.; Ren, T. *Coord. Chem. Rev.* **2011**, 1587.
- (6) Ball, P. *Nat. Mater.* **2005**, 4, 119.
- (7) Ruess, F. J.; Oberbeck, L.; Simmons, M. Y.; Goh, K. E. J.; Hamilton, A. R.; Hallam, T.; Schofield, S. R.; Curson, N. J.; Clark, R. G. *Nano Lett.* **2004**, 4, 1969.
- (8) Ron, I.; Pecht, I.; Sheves, M.; Cahen, D. *Acc. Chem. Res.* **2010**, 43, 945.
- (9) Vilan, A.; Yaffe, O.; Biller, A.; Salomon, A.; Kahn, A.; Cahen, D. *Adv. Mater.* **2009**, 22, 140.
- (10) Yaffe, O.; Scheres, L.; Puniredd, S.; Stein, N.; Biller, A.; Lavan, R.; Shpaisman, H.; Zuilhof, H.; Haick, H.; Cahen, D. *Nano Lett.* **2009**, 9, 2390.
- (11) Liu, Y.-J.; Yu, H. Z. *ChemPhysChem* **2002**, 3, 799.
- (12) Liu, Y.-J.; Yu, H. Z. *ChemPhysChem* **2003**, 4, 335.
- (13) Faber, E. J.; de Smet, L. C. P. M.; Olthuis, W.; Zuilhof, H.; Sudhölter, E. J. R.; Bergveld, P.; van den Berg, A. *ChemPhysChem* **2005**, 6, 2153.
- (14) Faber, E. J.; Sparreboom, W.; Groeneveld, W.; de Smet, L. C. P. M.; Bommer, J.; Olthuis, W.; Zuilhof, H.; Sudhölter, E. J. R.; Bergveld, P.; van den Berg, A. *ChemPhysChem* **2007**, 8, 101.
- (15) Salomon, A.; Böcking, T.; Chan, J.; Chan, C. K.; Amy, F.; Girshevitz, O.; Cahen, D.; Kahn, A. *Phys. Rev. Lett.* **2005**, 95.



- (16) Love, J. C.; Estroff, L. A.; Kriebel, J. K.; Nuzzo, R. G.; Whitesides, G. M. *Chem. Rev.* **2005**, *105*, 1103.
- (17) Halik, M.; Klauk, H.; Zschieschang, U.; Schmid, G.; Dehm, C.; Schutz, M.; Maisch, S.; Effenberger, F.; Brunnbauer, M.; Stellacci, F. *Nature* **2004**, *431*, 963.
- (18) Lee, G.; Chrisey, L.; Colton, R. *Science* **1994**, *266*, 771.
- (19) Sagiv, J. *J. Am. Chem. Soc.* **1980**, *102*, 92.
- (20) Ulman, A. *Chem. Rev.* **1996**, *96*, 1533.
- (21) Linford, M.; Fenter, P.; Eisenberger, P. M.; Chidsey, C. E. D. *J. Am. Chem. Soc.* **1995**, *117*, 3145.
- (22) Hu, D. Q.; MacPherson, C. D.; Leung, K. T. *Surf. Sci.* **1992**, *273*, 21.
- (23) Hamers, R. J.; Wang, Y. *Chem. Rev.* **1996**, *96*, 1261.
- (24) Yablonovitch, E.; Allara, D. L.; Chang, C. C.; Gmitter, T.; Bright, T. B. *Phys. Rev. Lett.* **1986**, *57*, 249.
- (25) Bansal, A.; Li, X.; Lauermann, I.; Lewis, N. S.; Yi, S. I.; Weinberg, W. H. *J. Am. Chem. Soc.* **1996**, *118*, 7225.
- (26) Cai, W.; Lin, Z.; Strother, T.; Smith, L. M.; Hamers, R. J. *J. Phys. Chem. B* **2002**, *106*, 2656.
- (27) Wolkow, R. A. *Annu. Rev. Phys. Chem.* **1999**, *50*, 413.
- (28) Higashi, G. S.; Becker, R. S.; Chabal, Y. J.; Becker, A. J. *Appl. Phys. Lett.* **1991**, *58*, 1656.
- (29) Higashi, G. S.; Chabal, Y. J.; Trucks, G. W.; Raghavachari, K. *Appl. Phys. Lett.* **1990**, *56*, 656.
- (30) Bateman, J. E.; Eagling, R. D.; Worrall, D. R.; Horrocks, B. R.; Houlton, A. *Angew. Chem., Int. Ed.* **1998**, *37*, 2683.
- (31) Sieval, A. B.; Vleeming, V.; Zuilhof, H.; Sudhölter, E. J. R. *Langmuir* **1999**, *15*, 8288.
- (32) Clark, I. T.; Aldinger, B. S.; Gupta, A.; Hines, M. A. *J. Phys. Chem. C* **2010**, *114*, 423.
- (33) Allongue, P.; Kieling, V.; Gerischer, H. *Electrochim. Acta* **1995**, *40*, 1353.
- (34) Allongue, P.; Henry de Villeneuve, C.; Morin, S.; Boukherroub, R.; Wayner, D. D. M. *Electrochim. Acta* **2000**, *45*, 4591.
- (35) Allongue, P.; Kieling, V.; Gerischer, H. *Electrochim. Acta* **1993**, *40*, 1353.
- (36) Burrows, V. A.; Chabal, Y. J.; Higashi, G. S.; Raghavachari, K.; Christman, S. B. *Appl. Phys. Lett.* **1988**, *53*, 998.
- (37) Allongue, P.; Costa-Kieling, V.; Gerischer, H. *J. Electrochem. Soc.* **1993**, *140*, 1009.
- (38) Canham, L. T. *Appl. Phys. Lett.* **1990**, *57*, 1046.
- (39) Jane, A.; Dronov, R.; Hodges, A.; Voelcker, N. H. *Trends Biotechnol.* **2009**, *27*, 230.
- (40) Di Francia, G.; La Ferrara, V.; Manzo, S.; Chiavarini, S. *Biosens. Bioelectron.* **2005**, *21*, 661.
- (41) De Stefano, L.; Arcari, P.; Lamberti, A.; Sanges, C.; Rotiroli, L.; Rea, I.; Rendina, I. *Sensors-Basel* **2007**, *7*, 214.
- (42) Kilian, K. A.; Boecking, T.; Gooding, J. J. *Chem. Commun.* **2009**, 630.
- (43) Cicero, R. L.; Linford, M. R.; Chidsey, C. E. D. *Langmuir* **2000**, *16*, 5688.

- (44) Chatgililoglu, C.; Guarini, A.; Guerrini, A.; Seconi, G. *J. Org. Chem.* **1992**, *57*, 2207.
- (45) Chatgililoglu, C. *Organosilanes in Radical Chemistry*; Wiley: Chichester (UK), 2004.
- (46) Chatgililoglu, C. *Chem. Rev.* **1995**, *95*, 1229.
- (47) Harper, J.; Sailor, M. J. *Langmuir* **1997**, *13*, 4652.
- (48) Buriak, J. M. *Chem. Rev.* **2002**, *102*, 1271.
- (49) Ulman, A. *Chem. Rev.* **1996**, *96*, 1533.
- (50) Boukherroub, R. *Curr. Opin. Solid St. M.* **2005**, *9*, 66.
- (51) Linford, M. R.; Fenter, P.; Eisenberger, P. M.; Chidsey, C. E. D. *J. Am. Chem. Soc.* **1995**, *117*, 3145.
- (52) Sieval, A. B.; Demirel, A. L.; Nissink, J. W. M.; Linford, M. R.; van der Maas, J. H.; de Jeu, W. H.; Zuilhof, H.; Sudholter, E. J. R. *Langmuir* **1998**, *14*, 1759.
- (53) Wang, X. Y.; Ruther, R. E.; Streifer, J. A.; Hamers, R. J. *J. Am. Chem. Soc.* **2010**, *132*, 4048.
- (54) Cicero, R. L.; Linford, M. R.; Chidsey, C. E. D. *Langmuir* **2000**, *16*, 5688.
- (55) Terry, J.; Linford, M. R.; Wigren, C.; Cao, R. Y.; Pianetta, P.; Chidsey, C. E. D. *Appl. Phys. Lett.* **1997**, *71*, 1056.
- (56) Shestopalov, A. A.; Clark, R. L.; Toone, E. J. *Langmuir* **2010**, *26*, 1449.
- (57) Holland, J. M.; Stewart, M. P.; Allen, M. J.; Buriak, J. M. *J. Solid State Chem.* **1999**, *147*, 251.
- (58) Buriak, J. M.; Allen, M. J. *J. Am. Chem. Soc.* **1998**, *120*, 1339.
- (59) Linford, M. R.; Chidsey, C. E. D. *J. Am. Chem. Soc.* **1993**, *115*, 12631.
- (60) Sommer, L. H.; Pietrusza, E. W.; Whitmore, F. C. *J. Am. Chem. Soc.* **1947**, *69*, 188.
- (61) Burkhard, C. A.; Kriebel, R. H. *J. Am. Chem. Soc.* **1947**, *69*, 2687.
- (62) Barry, A. J.; Depree, L.; Gilkey, J. W.; Hook, D. E. *J. Am. Chem. Soc.* **1947**, *69*, 2916.
- (63) Chatgililoglu, C. *Acc. Chem. Res.* **1992**, *25*, 188.
- (64) Kopping, B.; Chatgililoglu, C.; Zehnder, M.; Giese, B. *J. Org. Chem.* **1992**, *57*, 3994.
- (65) Laarhoven, L. J. J.; Mulder, P.; Wayner, D. D. M. *Acc. Chem. Res.* **1999**, *32*, 342.
- (66) Lide, D., A. *CRC Handbook of Chemistry and Physics*; CRC Press: Boca Raton, FL, 2005.
- (67) Stewart, M. P.; Buriak, J. M. *Angew. Chem. Int. Edit.* **1998**, *37*, 3257.
- (68) Cicero, R. L.; Chidsey, C. E. D.; Lopinski, G. P.; Wayner, D. D. M.; Wolkow, R. A. *Langmuir* **2002**, *18*, 305.
- (69) Lopinski, G. P.; Wayner, D. D. M.; Wolkow, R. A. *Nature* **2000**, *406*, 48.
- (70) Eves, B. J.; Sun, Q.-Y.; Lopinski, G. P.; Zuilhof, H. *J. Am. Chem. Soc.* **2004**, *126*, 14318.
- (71) Sieval, A. B.; Opitz, R.; Maas, H. P. A.; Schoeman, M. G.; Meijer, G.; Vergeldt, F. J.; Zuilhof, H.; Sudholter, E. J. R. *Langmuir* **2000**, *16*, 10359.
- (72) Scheres, L.; Arafat, A.; Zuilhof, H. *Langmuir* **2007**, *23*, 8343.
- (73) Scheres, L.; Giesbers, M.; Zuilhof, H. *Langmuir* **2010**, *26*, 10924.
- (74) Netzer, L.; Iscovici, R.; Sagiv, J. *Thin Solid Films* **1983**, *100*, 67.

- (75) Siewierski, L. M.; Brittain, W. J.; Petrash, S.; Foster, M. D. *Langmuir* **1996**, *12*, 5838.
- (76) Heid, S.; Effenberger, F.; Bierbaum, K.; Grunze, M. *Langmuir* **1996**, *12*, 2118.
- (77) Onclin, S.; Ravoo, B. J.; Reinhoudt, D. N. *Angew. Chem. Int. Ed.* **2005**, *44*, 6282.
- (78) Cleland, G.; Horrocks, B. R.; Houlton, A. *J. Chem. Soc. Faraday T.* **1995**, *91*, 4001.
- (79) Hacker, C. A.; Anderson, K. A.; Richter, L. J.; Richter, C. A. *Langmuir* **2005**, *21*, 882.
- (80) Effenberger, F.; Gotz, G.; Bidlingmaier, B.; Wezstein, M. *Angew. Chem. Int. Ed.* **1998**, *37*, 2462.
- (81) Boukherroub, R.; Morin, S.; Wayner, D. D. M.; Bensebaa, F.; Sproule, G. I.; Baribeau, J. M.; Lockwood, D. J. *Chem. Mater.* **2001**, *13*, 2002.
- (82) Michalak, D. J.; Amy, S. R.; Aureau, D.; Dai, M.; Esteve, A.; Chabal, Y. J. *Nat. Mater.* **2010**, *9*, 266.
- (83) Chatgililoglu, C.; Griller, D.; Lesage, M. *J. Org. Chem.* **1989**, *54*, 2492.
- (84) Di Bella, S.; Condorelli, G. G.; Motta, A.; Ustione, A.; Cricenti, A. *Langmuir* **2006**, *22*, 7952.
- (85) Sieval, A. B.; Vleeming, V.; Zuilhof, H.; Sudholter, E. J. R. *Langmuir* **1999**, *15*, 8288.
- (86) Wojtyk, J. T. C.; Tomietto, M.; Boukherroub, R.; Wayner, D. D. M. *J. Am. Chem. Soc.* **2001**, *123*, 1535.
- (87) Jin, H.; Kinser, C. R.; Bertin, P. A.; Kramer, D. E.; Libera, J. A.; Hersam, M. C.; Nguyen, S. T.; Bedzyk, M. J. *Langmuir* **2004**, *20*, 6252.
- (88) Buriak, J. M.; Stewart, M. P.; Geders, T. W.; Allen, M. J.; Choi, H. C.; Smith, J.; Raftery, D.; Canham, L. T. *J. Am. Chem. Soc.* **1999**, *121*, 11491.
- (89) Wang, X. Y.; Colavita, P. E.; Streifer, J. A.; Butler, J. E.; Hamers, R. J. *J. Phys. Chem. C* **2010**, *114*, 4067.
- (90) Colavita, P. E.; Sun, B.; Tse, K. Y.; Hamers, R. J. *J. Am. Chem. Soc.* **2007**, *129*, 13554.
- (91) Stewart, M. P.; Buriak, J. M. *J. Am. Chem. Soc.* **2001**, *123*, 7821.
- (92) Sun, Q.-Y.; De Smet, L. C. P. M.; Van Lagen, B.; Giesbers, M.; Thuene, P. C.; Van Engelenburg, J.; De Wolf, F. A.; Zuilhof, H.; Sudhölter, E. J. R. *J. Am. Chem. Soc.* **2005**, *127*, 2514.
- (93) Sun, Q.-Y.; de Smet, L. C. P. M.; van Lagen, B.; Wright, A.; Zuilhof, H.; Sudhölter, E. J. R. *Angew. Chem. Int. Ed.* **2004**, *43*, 1352.
- (94) Mischki, T. K.; Lopinski, G. P.; Wayner, D. D. M. *Langmuir* **2009**, *25*, 5626.
- (95) Allongue, P.; de Villeneuve, C. H.; Pinson, J.; Ozanam, F.; Chazalviel, J. N.; Wallart, X. *Electrochim. Acta* **1998**, *43*, 2791.
- (96) de Villeneuve, C. H.; Pinson, J.; Bernard, M. C.; Allongue, P. *J. Phys. Chem. B* **1997**, *101*, 2415.
- (97) Stewart, M. P.; Maya, F.; Kosynkin, D. V.; Dirk, S. M.; Stapleton, J. J.; McGuinness, C. L.; Allara, D. L.; Tour, J. M. *J. Am. Chem. Soc.* **2004**, *126*, 370.
- (98) Nakayama, J.; Yoshida, M.; Simamura, O. *Tetrahedron* **1970**, *26*, 4609.
- (99) Wang, D.; Buriak, J. M. *Langmuir* **2006**, *22*, 6214.
- (100) Rijksen, B.; Van Lagen, B.; Zuilhof, H. *J. Am. Chem. Soc.* **2011**, accepted.

- (101) Scheres, L.; Rijksen, B.; Giesbers, M.; Zuilhof, H. *Langmuir* **2011**, *27*, 972.
- (102) Coletti, C.; Marrone, A.; Giorgi, G.; Sgamellotti, A.; Cerofolini, G.; Re, N. *Langmuir* **2006**, *22*, 9949.
- (103) Cerofolini, G. F.; Galati, C.; Reina, S.; Renna, L.; Condorelli, G. G.; Fragala, I. L.; Giorgi, G.; Sgamellotti, A.; Re, N. *Appl. Surf. Sci.* **2005**, *246*, 52.
- (104) de Smet, L. C. P. M.; Pukin, A. V.; Sun, Q. Y.; Eves, B. J.; Lopinski, G. P.; Visser, G. M.; Zuilhof, H.; Sudholter, E. J. R. *Appl. Surf. Sci.* **2005**, *252*, 24.
- (105) Kanai, Y.; Takeuchi, N.; Car, R.; Selloni, A. *J. Phys. Chem. B* **2005**, *109*, 18889.
- (106) Takeuchi, N.; Kanai, Y.; Selloni, A. *J. Am. Chem. Soc.* **2004**, *126*, 15890.
- (107) Yan, H.; Shi, Y. C.; Liu, G.; Yuan, S. L. *Mol. Simulat.* **2008**, *34*, 525.
- (108) Chatgililoglu, C.; Griller, D.; Lesage, M. *J. Org. Chem.* **1988**, *53*, 3641.
- (109) Chatgililoglu, C. *Chem-Eur. J.* **2008**, *14*, 2310.
- (110) Baguley, P. A.; Walton, J. C. *Angew. Chem. Int. Ed.* **1998**, *37*, 3073.
- (111) Lalevee, J.; Allonas, X.; Fouassier, J. P. *J. Org. Chem.* **2007**, *72*, 6434.
- (112) Lalevee, J.; Blanchard, N.; Graff, B.; Allonas, X.; Fouassier, J. P. *J. Organomet. Chem.* **2008**, *693*, 3643.
- (113) Kanai, Y.; Tilocca, A.; Selloni, A.; Car, R. *J. Chem. Phys.* **2004**, *121*, 3359.
- (114) Ng, A.; Ciampi, S.; James, M.; Harper, J. B.; Gooding, J. J. *Langmuir* **2009**, *25*, 13934.
- (115) Hossain, M. Z.; Kato, H. S.; Kawai, M. *J. Am. Chem. Soc.* **2007**, *129*, 3328.
- (116) Hong, Q.; Rogero, C.; Lakey, J. H.; Connolly, B. A.; Houlton, A.; Horrocks, B. R. *Analyst* **2009**, *134*, 593.
- (117) Rijksen, B.; Paulusse, J. M. J.; Zuilhof, H. **submitted**.
- (118) Rijksen, B.; Pujari, S.; Paulusse, J. M. J.; Zuilhof, H. **in preparation**.
- (119) Dinnocenzo, J. P.; Simpson, T. R.; Zuilhof, H.; Todd, W. P.; Heinrich, T. *J. Am. Chem. Soc.* **1997**, *119*, 987.
- (120) Perring, M.; Dutta, S.; Arafat, S.; Mitchell, M.; Kenis, P. J. A.; Bowden, N. B. *Langmuir* **2005**, *21*, 10537.
- (121) Sassolas, A.; Leca-Bouvier, B. D.; Blum, L. J. *Chem. Rev.* **2008**, *108*, 109.
- (122) Ron, I.; Sepunaru, L.; Itzhakov, S.; Belenkova, T.; Friedman, N.; Pecht, I.; Sheves, M.; Cahen, D. *J. Am. Chem. Soc.* **2010**, 265.
- (123) Sun, T.; Qing, G.; Su, B.; Jiang, L. *Chem. Soc. Rev.* **2011**.
- (124) Ashkenasy, G.; Cahen, D.; Cohen, R.; Shanzer, A.; Vilan, A. *Acc. Chem. Res.* **2002**, *35*, 121.
- (125) Roth, K. M.; Yasseri, A. A.; Liu, Z.; Dabke, R. B.; Malinovskii, V.; Schweikart, K.-H.; Yu, L.; Tiznado, H.; Zaera, F.; Lindsey, J. S.; Kuhr, W. G.; Bocian, D. F. *J. Am. Chem. Soc.* **2003**, *125*, 505.
- (126) Haick, H.; Cahen, D. *Prog. Surf. Sci.* **2008**, *83*, 217.
- (127) Vilan, A.; Yaffe, O.; Biller, A.; Salomon, A.; Kahn, A.; Cahen, D. *Adv. Mater.* **2009**, *22*, 140.
- (128) Yang, L.; Lua, Y.-Y.; Lee, M. V.; Linford, M. R. *Acc. Chem. Res.* **2005**, *38*, 933.
- (129) Cicero, R. L.; Wagner, P.; Linford, M. R.; Hawker, C. J.; Waymouth, R. M.; Chidsey, C. E. D. *Polym. Prepr.* **1997**, *38*, 904.
- (130) Wagner, P.; Nock, S.; Spudich, J. A.; Volkmuth, W. D.; Chu, S.; Cicero, R. L.; Wade, C. P.; Linford, M. R.; Chidsey, C. E. D. *J. Struct. Biol.* **1997**, *119*, 189.

- (131) Hegner, M.; Dreier, M.; Wagner, P.; Semenza, G.; Guen-Therodt, H.-J. *J. Vac. Sci. Technol. B* **1996**, 1418.
- (132) Yang, M.; Wouters, D.; Giesbers, M.; Schubert, U. S.; Zuilhof, H. *Acs Nano* **2009**, 3, 2887.
- (133) Rosso, M.; Giesbers, M.; Schroën, K.; Zuilhof, H. *Langmuir* **2010**, 26, 866.
- (134) Voicu, R.; Boukherroub, R.; Bartzoka, V.; Ward, T.; Wojtyk, J. T. C.; Wayner, D. D. M. *Langmuir* **2004**, 20, 11713.
- (135) Bocking, T.; Wong, E. L. S.; James, M.; Watson, J. A.; Brown, C. L.; Chilcott, T. C.; Barrow, K. D.; Coster, H. G. L. *Thin Solid Films* **2006**, 515, 1857.
- (136) Sieval, A. B.; Linke, R.; Zuilhof, H.; Sudholter, E. J. R. *Adv. Mater.* **2000**, 12, 1457.
- (137) Faucheux, A.; Gouget-Laemmel, A. C.; de Villeneuve, C. H.; Boukherroub, R.; Ozanam, F.; Allongue, P.; Chazalviel, J. N. *Langmuir* **2006**, 22, 153.
- (138) Sieval, A. B.; Demirel, A. L.; Nissink, J. W. M.; Linford, M. R.; van der Maas, J. H.; de Jeu, W. H.; Zuilhof, H.; Sudhölter, E. J. R. *Langmuir* **1998**, 14, 1759.
- (139) Lee, E. J.; Ha, J. S.; Sailor, M. J. *J. Am. Chem. Soc.* **1995**, 117, 8295.
- (140) Lee, E. J.; Bitner, T. W.; Ha, J. S.; Shane, M. J.; Sailor, M. J. *J. Am. Chem. Soc.* **1996**, 118, 5375.
- (141) Boukherroub, R.; Wayner, D. D. M. *J. Am. Chem. Soc.* **1999**, 121, 11513.
- (142) Sullivan, T. P.; Huck, W. T. S. *Eur. J. Org. Chem.* **2003**, 17.
- (143) Böcking, T.; James, M.; Coster, H. G. L.; Chilcott, T. C.; Barrow, K. D. *Langmuir* **2004**, 20, 9227.
- (144) Sehgal, D.; Vijay, I. K. *Anal. Biochem.* **1994**, 218, 87.
- (145) Hermanson, G. T., in *Bioconjugate Techniques*.
- (146) Boukherroub, R.; Wojtyk, J. T. C.; Wayner, D. D. M.; Lockwood, D. J. *J. Electrochem. Soc.* **2002**, 149, H59.
- (147) Voicu, R.; Boukherroub, R.; Bartzoka, T.; Ward, J. T. C.; Wojtyk, J. T. C.; Wayner, D. D. M. *Langmuir* **2004**, 20, 11713.
- (148) Kilian, K.; Böcking, T.; Gaus, K.; Gooding, J. J. *Angew. Chem., Int. Ed.* **2008**, 47, 2697.
- (149) Moraillon, A.; Gouget-Laemmel, A. C.; Ozanam, F.; Chazalviel, J. N. *J. Phys. Chem. C* **2008**, 112, 7158.
- (150) Wei, F.; Sun, B.; Liao, W.; Ouyang, J. H.; Zhao, X. S. *Biosens. Bioelectron.* **2003**, 18, 1149.
- (151) Liao, W.; Wei, F.; Qian, M. X.; Zhao, X. S. *Sens. Actuators, B* **2004**, 101, 361.
- (152) Liu, Y.-J.; Navasero, N. M.; Yu, H. Z. *Langmuir* **2004**, 20, 4039.
- (153) Wojtyk, J. T. C.; Morin, K. A.; Boukherroub, R.; Wayner, D. D. M. *Langmuir* **2002**, 18, 6081.
- (154) Böcking, T.; James, M.; Coster, H. G. L.; Chilcott, T. C.; Barrow, K. D. *Langmuir* **2004**, 20, 9227.
- (155) Yin, H. B.; Brown, T.; Wilkinson, J. S.; Eason, R. W.; Melvin, T. *Nucleic Acids Res.* **2004**, 32, e118.
- (156) Yang, M.; Teeuwen, R. L. M.; Giesbers, M.; Baggerman, J.; Arafat, A.; de Wolf, F. A.; van Hest, J. C. M.; Zuilhof, H. *Langmuir* **2008**, 24, 7931.

- (157) Mitchell, S. A.; Ward, J. T. C.; Wayner, D. D. M.; Lopinski, G. P. *J. Phys. Chem. B* **2002**, *106*, 9873.
- (158) Sam, S.; Touahir, L.; Salvador Andres, J.; Allongue, P.; Chazalviel, J. N.; Gouget-Laemmel, A. C.; Henry de Villeneuve, C.; Moraillon, A.; Ozanam, F.; Gabouze, N.; Djebbar, S. *Langmuir* **2010**, *26*, 809.
- (159) Perring, M.; Dutta, S.; Arafat, S.; Mitchell, M.; Kenis, P. J. A.; Bowden, N. B. *Langmuir* **2005**, *21*, 10537.
- (160) Coffinier, Y.; Olivier, C.; Perzyna, A.; Grandidier, B.; Wallart, X.; Durand, J.-O.; Melnyk, O.; Stiévenard, D. *Langmuir* **2005**, *21*, 1489.
- (161) Scheres, L.; Klingebiel, B.; ter Maat, J.; Giesbers, M.; de Jong, H.; Hartmann, N.; Zuilhof, H. *Small* **2010**, *6*, 1918.
- (162) Jun, Y.; Le, D.; Zhu, X. Y. *Langmuir* **2002**, *18*, 3415.
- (163) Mizuno, H.; Buriak, J. M. *J. Am. Chem. Soc.* **2008**, *130*, 17656.
- (164) Ravoo, B. J. *J. Mater. Chem.* **2009**, *19*, 8902.
- (165) Kolb, H.; Finn, M.; Sharpless, K. *Angew. Chem., Int. Ed.* **2001**, *40*, 2004.
- (166) Iha, R. K.; Wooley, K. L.; Nystrom, A. M.; Burke, D. J.; Kade, M. J.; Hawker, C. J. *Chem. Rev.* **2009**, *109*, 5620.
- (167) Ciampi, S.; Bocking, T.; Kilian, K.; James, M.; Harper, J. *Langmuir* **2007**, *23*, 9320.
- (168) Ciampi, S.; Eggers, P. K.; Le Saux, G.; James, M.; Harper, J. B.; Gooding, J. J. *Langmuir* **2009**, *25*, 2530.
- (169) Haensch, C.; Erdmenger, T.; Fijten, M. W. M.; Hoeppener, S.; Schubert, U. S. *Langmuir* **2009**, *25*, 8019.
- (170) Hoyle, C.; Lowe, A.; Bowman, C. *Chem. Soc. Rev.* **2010**, *41*.
- (171) Kade, M. J.; Burke, D. J.; Hawker, C. J. *J. Polym. Sci., Part A: Polym. Chem.* **2010**, *48*, 743.
- (172) Nebhani, L.; Barner-Kowollik, C. *Adv. Mater.* **2009**, *21*, 3442.
- (173) Bertin, A.; Schlaad, H. *Chem. Mater.* **2009**, *21*, 5698.
- (174) Jonkheijm, P.; Weinrich, D.; Köhn, M.; Engelkamp, H.; Christianen, P. C. M.; Kuhlmann, J.; Maan, J. C.; Nüsse, D.; Schroeder, H.; Wacker, R.; Breinbauer, R.; Niemeyer, C. M.; Waldmann, H. *Angew. Chem., Int. Ed.* **2008**, *47*, 4421.
- (175) Weinrich, D.; Köhn, M.; Jonkheijm, P.; Westerlind, U.; Dehmelt, L.; Engelkamp, H.; Christianen, P. C. M.; Kuhlmann, J.; Maan, J. C.; Nüsse, D.; Schröder, H.; Wacker, R.; Voges, E.; Breinbauer, R.; Kunz, H.; Niemeyer, C. M.; Waldmann, H. *ChemBioChem* **2010**, *11*, 235.
- (176) Hensarling, R. M.; Doughty, V. A.; Chan, J. W.; Patton, D. L. *J. Am. Chem. Soc.* **2009**, *131*, 14673.
- (177) Wendeln, C.; Rinnen, S.; Schulz, C.; Arlinghaus, H. F.; Ravoo, B. J. *Langmuir* **2010**, *26*, 15966.
- (178) Caipa Campos, M. A.; Paulusse, J. M. J.; Zuilhof, H. *Chem. Commun.* **2010**, *46*, 5512.
- (179) de Smet, L. C. P. M.; Stork, G. A.; Hurenkamp, G. H. F.; Sun, Q. Y.; Topal, H.; Vronen, P. J. E.; Sieval, A. B.; Wright, A.; Visser, G. M.; Zuilhof, H.; Sudholter, E. J. R. *J. Am. Chem. Soc.* **2003**, *125*, 13916.

- (180) Vericat, C.; Vela, M. E.; Benitez, G.; Carro, P.; Salvarezza, R. C. *Chem. Soc. Rev.* **2010**, 39, 1805.
- (181) Quayum, M. E.; Kondo, T.; Nihonyanagi, S.; Miyamoto, D.; Uosaki, K. *Chem. Lett.* **2002**, 208.





## Chapter 3

### Mimicking the Silicon Surface: Reactivity of Silyl Radical Cations towards Nucleophiles

**Abstract.** Radical cations of selected low molecular-weight silicon model compounds were obtained by photoinduced electron transfer. These radical cations react readily with a variety of nucleophiles, regularly used in monolayer fabrication onto hydrogen-terminated silicon. From time-resolved kinetics it was concluded that the reactions proceed via a bimolecular nucleophilic attack to the radical cation. A secondary kinetic isotope effect indicated that the central Si-H bond is not cleaved in the rate-determining step. Apart from substitution products also hydrosilylation products were identified in the product mixtures. Observation of the substitution products, combined with the kinetic data, point to an bimolecular reaction mechanism involving Si-Si bond cleavage. The products of this nucleophilic substitution can initiate radical chain reactions leading to hydrosilylation products, which can independently also be initiated by dissociation of the radical cations. Application of these data to the attachment of organic monolayers onto hydrogen-terminated Si surfaces via hydrosilylation leads to the conclusion that the delocalized Si radical cation (a surface-localized hole) can initiate the hydrosilylation chain reaction at the Si surface. Comparison to monolayer experiments shows that this reaction only plays a significant role in the initiation, and not in the propagation steps of Si-C bond making monolayer formation.

**This chapter is published as:**

“Mimicking the Silicon Surface: Reactivity of Silyl Radical Cations towards Nucleophiles”, Rijksen, B.; van Lagen, B.; Zuilhof, H. *J. Am. Chem. Soc.*, 2011, 133, 4998-5008.

### 3.1 Introduction

Over the past two decades extensive research has been performed on the formation of self-assembled organic monolayers on silicon and silicon-related surfaces. Typical examples are addition of alkenes and alkynes onto silicon<sup>1-6</sup> and germanium.<sup>6,7</sup> The passivation and functionalization of flat silicon surfaces has attracted a lot of attention because of their potential application in electronic devices.<sup>2-4,6,8</sup> In search of increasingly milder and faster attachment conditions, several fabrication methods were developed, making use of elevated temperatures,<sup>9,10</sup> UV irradiation,<sup>11-14</sup> hydrosilylation catalysts,<sup>6,15,16</sup> Grignard and alkyl lithium reagents,<sup>17,18</sup> electrochemistry,<sup>19-21</sup> and chemomechanical scribing.<sup>22-25</sup> These methods, however, still require a substantial input of energy to initiate monolayer formation, which can trigger side reactions. The search for lower energy input has led to the development of the mildest method yet for fabrication of high-quality monolayers, which can be performed at room temperature in the dark.<sup>26</sup> Recent studies showed that alkynes react faster than alkenes, and lead to higher packing densities.<sup>27,28</sup> Also the exclusion of oxygen during the fabrication process brings oxidation of the surface well below the detection limit of X-ray photoelectron spectrometry (XPS),<sup>29</sup> which opens the way for electronic devices.<sup>30-35</sup> However, the reaction times, in the range of hours, are too long for industrial application. In order to speed up monolayer formation, more detailed mechanistic knowledge is required.

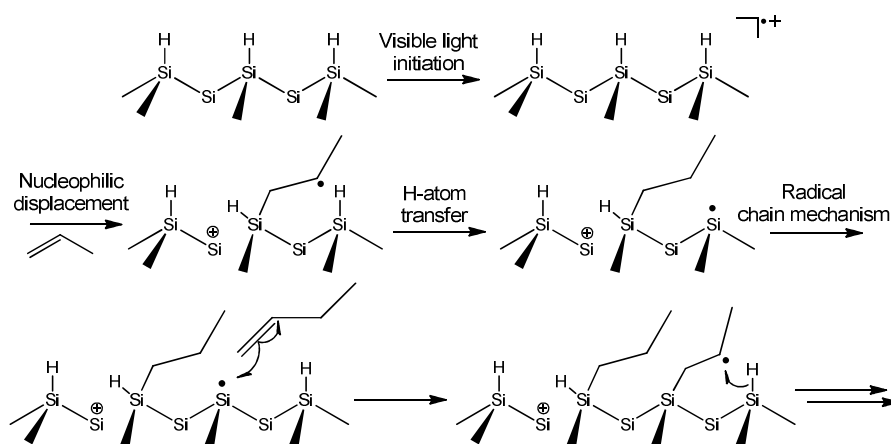


**Figure 1.** Monolayer formation onto H-terminated Si: radical cation-induced initiation,<sup>37</sup> followed by the radical chain mechanism.

For methods using UV irradiation ( $\lambda < 350$  nm) it has been shown that a radical chain reaction is initiated by homolytic cleavage of Si-H bonds at the surface.<sup>36</sup> Recently it was indicated that UV irradiation also causes photoemission of electrons from the Si surface

into electron-acceptor levels in adjacent alkenes.<sup>12</sup> Mild attachment of 1-alkynes, however, takes place under conditions that will not allow regular crossing of high activation barriers, rendering direct cleavage of a Si-H bond unlikely. In earlier work from our lab we proposed a mechanism<sup>37</sup> in which holes originating from excitons, migrate to the surface forming delocalized radical cations. These radical cations are then attacked by nucleophiles. Upon alkylation, the resulting  $\beta$ -radical in the alkyl chain abstracts hydrogen atom from a neighboring Si-H site, leaving a radical at the silicon surface (Figure 1). A radical chain reaction similar to the mechanism described above is then initiated. This mechanism was further supported by island formation, observed with scanning tunneling microscopy (STM),<sup>38-40</sup> during monolayer fabrication. A dedicated mechanistic study of radical cation initiation via measurements and analysis of the kinetics has, however, not been undertaken yet.

The goal of the current work is to provide more detailed kinetic and product-based information regarding the reactivity of Si-based radical cations using small molecular models ( $\text{Si}_4$ ,  $\text{Si}_7$  and  $\text{Si}_9$  derivatives). Examples of radical cations of disilanes,<sup>41,42</sup> and cyclic and linear oligosilanes<sup>43</sup> are known in literature.<sup>44</sup> The models in this study, however, require a central Si-H site to mimic the top layer of the hydrogen-terminated silicon surface, and silicon atoms connected to this site to mimic the bulk (Figure 2, top). To our knowledge, radical cations of these branched silanes have not been studied before.

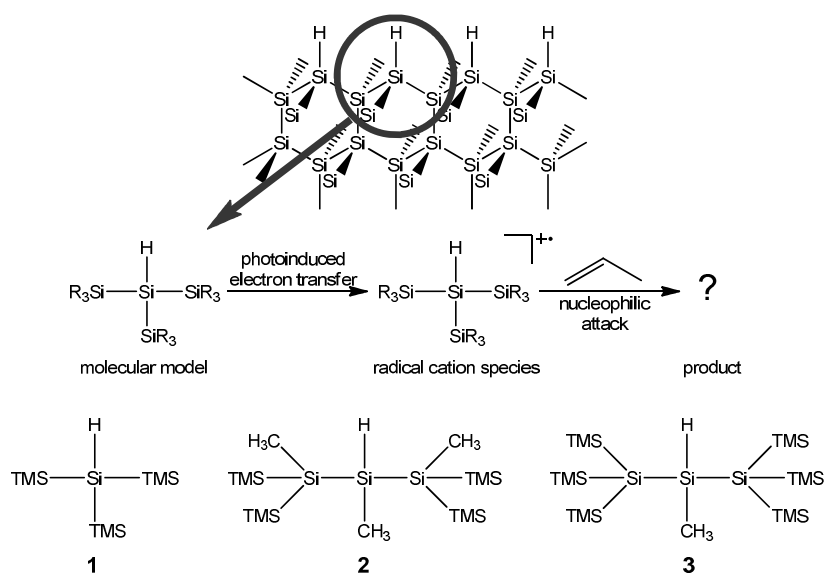


**Figure 2.** Representation of the selection of the models used in the current study (1 - 3) and the subsequent study of the silyl radical cations. Note: TMS =  $\text{Si}(\text{CH}_3)_3$ .

Tris(trimethylsilyl)silane (**1**), a Si<sub>4</sub> derivative, has proven its use in modeling surface reactions,<sup>36,45,46</sup> although the stability of the radical cation may be problematic due to its relatively small silicon backbone structure (branched Si<sub>4</sub>; TMS = Si(CH<sub>3</sub>)<sub>3</sub>). Therefore the model was extended by using a Si<sub>3</sub> structure with a central Si-H center, which was either appended with four or six TMS groups (compounds **2** and **3**, respectively; Figure 2, bottom), to combine a more extended delocalization with a tailor-made variation of the steric bulk around the Si-H site.

## 3.2 Experimental Section

### 3.2.1 Materials

Toluene and THF were distilled from resp. CaH<sub>2</sub> and from Na/benzophenone before use. The nucleophiles that were commercially available were analyzed by GC-MS and did not need any further purification except for the aldehydes which were purified by column chromatography (Si-60, hexane/ethylacetate). 10-Undecynyl aldehyde was synthesized according to literature procedures.<sup>47</sup> Hexafluoro-iso-propanol (HFIP), 1,2-dichloroethane (DCE) and tris(trimethylsilyl)silane were used as obtained from Sigma-Aldrich. NMQ was synthesized according to a literature procedure,<sup>48</sup> and recrystallized before use. All solutions were stored over molecular sieves. All sample preparations were performed in a glovebox to ensure dry and oxygen-free conditions.

### 3.2.2 Equipment

Low-resolution mass spectra were obtained using an Agilent technologies 7890A GC, equipped with Alltech ATTM-5ms column, in conjunction with a 5975C VL Mass Selective Detector. High-resolution mass spectra were obtained by direct probe measurements on a Fisons (VG) 7070. Nanosecond flash photolysis studies were carried out at 355 nm using the third harmonic of a Nd:YAG laser (Brilliant, Quantel Inc.) Transient spectra were obtained with an LP920 spectrophotometer (Edinburgh Instruments Limited) fitted with a 450 W Xe arc lamp as probe-light source and a red-sensitive photomultiplier (R928, Hamamatsu) and ICCD camera (DH720, Andor technology) as detectors. All NMR spectra were recorded on a Bruker Avance III with an inverse broadband probe running at 400 MHz, with C<sub>6</sub>D<sub>6</sub> as solvent. Cyclic voltammograms were recorded on a  $\mu$ AutoLAB type III Potentiostat/Galvanostat (Eco Chemie BV). The working electrode consisted of an inlaid glassy carbon disk (2.0 mm diameter). A glassy carbon rod served as a counter electrode. To ensure non-aqueous conditions, a double junction Ag/AgCl electrode was used. The inner chamber was filled with a 3 M KCl solution and the outer chamber with 0.1 M tetrabutylammonium hexafluorophosphate in acetonitrile.

### 3.2.3 Transient absorption spectroscopy

For each data point, a 4 mL vial was filled with NMQ in DCE (0.8 mL 2.0 O.D. solution in DCE), silane (0.8 mL 40 mM in toluene), DCE (0.8 mL) and HFIP (1.6 mL) and the required amount of nucleophile (max. 100  $\mu$ L). The sample was taken out of the glovebox immediately before starting the experiment. After loading the sample in a 5 mL syringe it was connected to the flow cell in the laser setup. The cell was flushed with 1.5 mL of the sample and then the experiment was started. A typical data point was collected by averaging a series of six consecutive measurements which consisted of twelve scans and twelve background scans.

### 3.2.4 Calculations

All calculations were performed with the B3LYP functional,<sup>49</sup> using the Gaussian 09 suite of programs.<sup>50</sup> All geometries were optimized at the 6-311G(d,p) level and were shown to be global minima on the potential energy surface by frequency analysis. The energies were determined by single-point calculations at the 6-311++G(2d,2p) level and corrected with the zero-point energy determined from the 6-311G(d,p) geometry. The lowest-energy conformers for **2** and **2**<sup>•+</sup> were found by stepwise rotations of the TMS groups and pre-optimizing at the B3LYP/3-21G level, before optimization each rotamer at the B3LYP/6-311G(d,p) level of theory.

### 3.2.5 Cyclic voltammetry

In a glovebox under argon atmosphere, a CV-cell was filled with a 5 mL solution of tetrabutylammonium hexafluorophosphate in acetonitrile (0.1 M). The counter and working electrode were placed and the cell was closed. After taking the cell from the box it was immediately connected to a nitrogen line to keep the solution dry. The reference electrode, which was kept in dry acetonitrile stored over mol sieves, was placed in the CV cell under nitrogen flow. After recording the baseline, 40  $\mu$ L of a silane solution in toluene (10 mM) was added with a syringe. Measurements were performed in single cycles.

### 3.2.6 Photochemistry product analysis

In a typical experiment for GC analysis, NMQ (0.5 mL 2.0 O.D. solution in DCE), *n*-decane (internal standard 5  $\mu$ L), silane (0.5 mL 40 mM in toluene) and nucleophile were mixed in a 4 mL vial with screwcap. The vial was then illuminated with a mercury lamp ( $\lambda \approx 340$  nm) for the required time. Afterwards the mixture was analyzed by GC and GC-MS.

### 3.2.7 Radical chemistry product analysis

In a typical experiment for GC analysis, 1,1'-azobiscyclohexanecarbonitrile (20 mg in 0.5 mL toluene), *n*-decane (internal standard 5  $\mu$ L), silane (0.5 mL 40 mM in toluene) and nucleophile were mixed in a 4 mL vial with screw cap. The vial was then placed in an oven at 100 °C for 1 h. Afterwards the mixture was analyzed by GC and GC-MS.

### 3.2.8 Syntheses

**Methyl-bis(methyl-bis(trimethylsilyl)silyl)silane (2):** This compound was synthesized following a modified literature procedure.<sup>51</sup> First methyl-tris(trimethylsilyl)silane<sup>52</sup> and methyl-bis(trimethylsilyl)silyl-potassium<sup>53</sup> were prepared according to literature. The solvent was removed in vacuo and replaced by freshly distilled toluene. After cooling the mixture to -78 °C, a solution of dichloromethylsilane in toluene was added dropwise. The mixture was allowed to warm to room temperature and stirred for another 2 h. The product was purified by prep-HPLC (C18 reverse phase, methanol). <sup>29</sup>Si NMR (C<sub>6</sub>D<sub>6</sub>): -11.84 (Si(CH<sub>3</sub>)<sub>3</sub> ~ 0.24 (<sup>1</sup>H)), -12.18 (Si(CH<sub>3</sub>)<sub>3</sub> ~ 0.26 (<sup>1</sup>H)), -67.06 (HSiCH<sub>3</sub>), -83.16 (Si(TMS)<sub>2</sub>CH<sub>3</sub>).

**Methyl-bis(tris(trimethylsilyl)silyl)silane (3):** This compound was synthesized following a modified literature procedure.<sup>51</sup> First tetra(trimethylsilyl)silane<sup>54</sup> and tris(trimethylsilyl)silyl-potassium<sup>53</sup> were prepared according to literature. The solvent was removed in vacuo and replaced by freshly distilled toluene. After cooling the mixture to -78 °C, a solution of dichloromethylsilane in toluene was added dropwise. The mixture was allowed to warm to room temperature and stirred for another 2 h. The product was recrystallized from ethyl acetate/acetonitrile: <sup>29</sup>Si NMR (C<sub>6</sub>D<sub>6</sub>): -9.49 (Si(CH<sub>3</sub>)<sub>3</sub>), -65.49 (HSiCH<sub>3</sub>), -124.61 (SiTMS<sub>3</sub>).

**Deuterated Methyl-bis(tris(trimethylsilyl)silyl)silane (3-D):** First [(Me<sub>3</sub>Si)<sub>3</sub>Si]<sub>2</sub>SiHClMe was prepared from **3** according to a literature procedure.<sup>55</sup> In the subsequent step this compound was reduced with an excess of LiAlD<sub>4</sub> in pentane until GC-MS showed complete conversion. The mixture was then filtrated over a silica plug and the solvent was evaporated, yielding pure **3-D**. <sup>1</sup>H NMR (400 MHz, C<sub>6</sub>D<sub>6</sub>): 0.35 (s, 54H), 0.59 (s, 3H); <sup>13</sup>C NMR (100 MHz, C<sub>6</sub>D<sub>6</sub>): -0.50 (HSiCH<sub>3</sub>), 3.48 (Si(CH<sub>3</sub>)<sub>3</sub>); <sup>29</sup>Si NMR (C<sub>6</sub>D<sub>6</sub>): -9.35 (Si(CH<sub>3</sub>)<sub>3</sub>), -24.73 (Si-(SiTMS<sub>3</sub>)<sub>3</sub>), -65.89 (DSiCH<sub>3</sub>). MS (EI) *m/z* (%): 524 (1) [M<sup>+</sup>-CH<sub>3</sub>], 464 (34) [M<sup>+</sup>-HSi(CH<sub>3</sub>)<sub>3</sub>], 232 (56), 217(100), 73 (80) [Si(CH<sub>3</sub>)<sub>3</sub>]<sup>+</sup>.

**Decane-tris(trimethylsilyl)silane (4a), decane-bis(trimethylsilyl)silane (4b):** A solution of tris(trimethylsilyl)silane (0.5 g, 2.0 mmol) and potassium tert-butoxide (0.25 g, 2.2 mmol) in freshly distilled THF (5 mL) was stirred for 1 hour at room temperature. A solution of 1-bromodecane (0.5 g, 2.3 mmol) in THF (5 mL) was added dropwise and the

reaction was left to stir for another hour. After removal of the solvent, the solid residue was extracted with pentane, which after evaporation gave a colorless oil. The products were isolated with prep-HPLC (C-18 reverse phase, methanol). **4a**: Characteristics were similar to literature.<sup>45</sup> <sup>29</sup>Si NMR (C<sub>6</sub>D<sub>6</sub>): -13.22 (Si(CH<sub>3</sub>)<sub>3</sub>), -82.11 (Si-TMS<sub>3</sub>). **4b**: <sup>1</sup>H NMR (400 MHz, C<sub>6</sub>D<sub>6</sub>): 3.90 (t, 1H), 1.51-1.58 (m, 2H), 1.29-1.40 (m, 14H), 0.86-0.93 (m, 5H), 0.23 (s, 18H); <sup>13</sup>C NMR (400 MHz, C<sub>6</sub>D<sub>6</sub>): 34.20, 32.69, 30.45, 30.43, 30.16, 30.12, 29.53, 23.46, 14.71, 7.87, 0.73. <sup>29</sup>Si NMR (C<sub>6</sub>D<sub>6</sub>): -15.87 (Si(CH<sub>3</sub>)<sub>3</sub>), -66.66 (Si-TMS<sub>2</sub>). MS (EI) *m/z* (%): 316 (5) [M<sup>+</sup>], 301 (3) [M<sup>+</sup>-CH<sub>3</sub>], 242 (11) [M<sup>+</sup>-HSi(CH<sub>3</sub>)<sub>3</sub>], 168 (31), 140 (36), 112 (33), 102 (74), 73 (100) [Si(CH<sub>3</sub>)<sub>3</sub><sup>+</sup>]. HR-MS (EI): 316.2442, calc. for [M]<sup>+</sup>: 316.2438.

**Decene-tris(trimethylsilyl)silane (5a)**: A solution of tris(trimethylsilyl)silane (1.0 g, 4.0 mmol), 1-decyne (2.5 mL, 14 mmol) and 1,1'-azobiscyclohexanecarbonitrile (0.25 g, 1.0 mmol) in heptane (20 mL) was refluxed for 2 h. Purification by flash column chromatography (C-18 reverse phase, methanol/MTBE) yielded a 1:1 mixture of cis/trans isomers. The isomers were isolated by prep-HPLC (C-18 reverse phase, methanol). HR-MS (EI): 386.2678, calc for [M]<sup>+</sup>: 386.2677. (**E**): <sup>1</sup>H NMR (400 MHz, C<sub>6</sub>D<sub>6</sub>): δ 6.19 (m, 1H), 5.73 (d, 1H), 2.13 (q, 2H), 1.28-1.47 (m, 12H), 0.91 (t, 3H), 0.29 (s, 27H). <sup>13</sup>C NMR (400 MHz, C<sub>6</sub>D<sub>6</sub>): δ 150.46 (=CH-CH<sub>2</sub>), 121.42 (Si-CH=), 38.43, 32.62, 30.19, 30.13, 29.99, 29.77, 23.43, 14.70 (CH<sub>2</sub>-CH<sub>3</sub>), 1.42 (Si(CH<sub>3</sub>)<sub>3</sub>). <sup>29</sup>Si NMR (C<sub>6</sub>D<sub>6</sub>): -13.24 (Si(CH<sub>3</sub>)<sub>3</sub>), -86.18 (Si-TMS<sub>3</sub>). MS *m/z* (%): 386 (6) [M<sup>+</sup>], 371 (1) [M<sup>+</sup>-CH<sub>3</sub>], 313 (2) [M<sup>+</sup>-Si(CH<sub>3</sub>)<sub>3</sub>], 297 (8), 174 (100) [Si(Si(CH<sub>3</sub>)<sub>3</sub>)<sub>2</sub><sup>+</sup>], 73 (63) [Si(CH<sub>3</sub>)<sub>3</sub><sup>+</sup>]. (**Z**): <sup>1</sup>H NMR (400 MHz, C<sub>6</sub>D<sub>6</sub>): δ 6.49 (q, 1H, J = 13 Hz), 5.67 (2t, 1H, J = 13 Hz), 2.19 (q, 2H), 1.28-1.45 (m, 12H), 0.91 (t, 3H), 0.29 (s, 27H). <sup>13</sup>C NMR (400 MHz, C<sub>6</sub>D<sub>6</sub>): δ 150.30 (=CH-CH<sub>2</sub>), 120.32 (Si-CH=), 36.56, 32.62, 30.64, 30.47, 30.44, 30.05, 23.43, 14.70 (CH<sub>2</sub>-CH<sub>3</sub>), 1.74 (Si(CH<sub>3</sub>)<sub>3</sub>). <sup>29</sup>Si NMR (C<sub>6</sub>D<sub>6</sub>): -12.64 (Si(CH<sub>3</sub>)<sub>3</sub>), -93.22 (Si-TMS<sub>3</sub>). MS (EI) *m/z* (%): 386 (7) [M<sup>+</sup>], 371 (1) [M<sup>+</sup>-CH<sub>3</sub>], 313 (2) [M<sup>+</sup>-Si(CH<sub>3</sub>)<sub>3</sub>], 297 (9), 174 (100) [Si(Si(CH<sub>3</sub>)<sub>3</sub>)<sub>2</sub><sup>+</sup>], 73 (66) [Si(CH<sub>3</sub>)<sub>3</sub><sup>+</sup>].

**Decene-bis(trimethylsilyl)silane (5b, E/Z)**: A mixture of decene-tris(trimethylsilyl)silane (0.6 mmol) and potassium tert-butoxide (0.6 mmol) in THF (0.5 mL) was stirred for 1 h at room temperature. Then a cooled solution of 10% HCl in water (10 mL) was added and the mixture was stirred for another hour. The mixture was extracted with ether, and the combined organic fractions were dried over magnesium sulfate. Removal of the solvents gave a colorless oil which was purified by prep-HPLC (C-18 reverse phase, methanol). HR-MS (EI): 314.2277, calc for [M]<sup>+</sup>: 314.2281. (**E**): <sup>1</sup>H NMR (400 MHz, C<sub>6</sub>D<sub>6</sub>): δ 6.28 (m, 1H, J = 18 Hz), 5.72 (m, 1H, J = 18 Hz), 3.81 (d, 1H, J = 5 Hz), 2.12 (q, 2H), 1.26-1.45 (m, 12H), 0.91 (t, 3H), 0.25 (s, 18H). <sup>13</sup>C NMR (400 MHz, C<sub>6</sub>D<sub>6</sub>): 150.95, 119.99, 37.80, 32.28, 29.85, 29.75, 29.46, 29.38, 23.10, 14.35, 0.11. <sup>29</sup>Si NMR (C<sub>6</sub>D<sub>6</sub>): -15.71 (Si(CH<sub>3</sub>)<sub>3</sub>), -70.20 (Si-TMS<sub>2</sub>). MS (EI) *m/z* (%): 314 (23) [M<sup>+</sup>], 299 (2) [M<sup>+</sup>-CH<sub>3</sub>], 255 (6) [M<sup>+</sup>-HSi(CH<sub>3</sub>)<sub>3</sub>], 141 (43), 116 (69), 73 (100). (**Z**): <sup>1</sup>H NMR (400 MHz, C<sub>6</sub>D<sub>6</sub>): δ 6.52 (q, 1H, J = 13 Hz), 5.61 (m, 1H, J = 13 Hz), 3.90 (d, 1H, J = 8 Hz), 2.27 (q, 2H), 1.26-1.45 (m, 12H), 0.91 (t,

3H), 0.25 (s, 18H).  $^{13}\text{C}$  NMR (400 MHz,  $\text{C}_6\text{D}_6$ ): 150.28, 119.11, 34.19, 32.28, 30.08, 30.01, 29.80, 29.72, 23.10, 14.35, 0.11.  $^{29}\text{Si}$  NMR ( $\text{C}_6\text{D}_6$ ): -15.24 ( $\text{Si}(\text{CH}_3)_3$ ), -81.94 ( $\text{Si-TMS}_2$ ). MS (EI)  $m/z$  (%): 314 (24) [ $\text{M}^+$ ], 299 (2) [ $\text{M}^+-\text{CH}_3$ ], 255 (7) [ $\text{M}^+-\text{HSi}(\text{CH}_3)_3$ ], 141 (39), 116 (62), 73 (100).

**Undeca-oxy-tris(trimethylsilyl)silane (8):** In a 4 mL vial, chloro-tris(trimethylsilyl)silane (0.25 g, 0.9 mmol) was dissolved in a mixture of pentane (1 mL) and triethylamine (2 mL). After addition of 1-undecanol (1 mL), the mixture was shaken and left at room temperature for 2 h. After removal of the solvents, the semi-solid residue was extracted with pentane. Evaporation of the pentane yielded a colorless oil which was purified by flash-column chromatography (Si-60, hexane).  $^1\text{H}$  NMR (400 MHz,  $\text{C}_6\text{D}_6$ ): 3.58 (t, 2H), 1.56 (p, 2H), 1.28-1.41 (m, 16H) 0.92 (t, 3H), 0.30 (s, 27H).  $^{13}\text{C}$  NMR (400 MHz,  $\text{C}_6\text{D}_6$ ): 68.46, 33.59, 32.34, 30.14, 30.08 (2 C), 29.94, 29.81, 26.41, 23.12, 14.37, 0.58.  $^{29}\text{Si}$  NMR ( $\text{C}_6\text{D}_6$ ): 0.22 ( $\text{Si-TMS}_3$ ), -16.46 ( $\text{Si}(\text{CH}_3)_3$ ). MS (EI)  $m/z$  (%): 403 (8) [ $\text{M}^+-\text{CH}_3$ ], 345 (8) [ $\text{M}^+-\text{Si}(\text{CH}_3)_3$ ], 263 (100), 191 (48), 175 (39), 131 (24), 73 (69) [ $\text{Si}(\text{CH}_3)_3^+$ ]. HR-MS (EI) [ $\text{M}$ ] $^{+x}$ : 418.2941, calc for [ $\text{M}$ ] $^{+x}$ : 418.2939.

**Undeca-oxy-bis(trimethylsilyl)silane (9):** MS (EI)  $m/z$  (%): 331 (2) [ $\text{M}^+-\text{CH}_3$ ], 272 (2) [ $\text{M}^+-\text{His}(\text{CH}_3)_3$ ], 159 (22), 117 (100), 73 (56).

### 3.3 Results and Discussion

#### 3.3.1 Formation and Identification of Silyl Radical Cations

Both **2** and **3** were synthesized according to modified literature procedures.<sup>51</sup> Silyl-potassium intermediates were prepared from tetrakis(trimethylsilyl)silane and methyl-tris(trimethylsilyl)silane and potassium tert-butoxide.<sup>53</sup> Branched oligosilane structures were obtained by reaction of the resulting silyl-potassium building blocks with methylchlorosilane. Efficient generation of the radical cations of **1** – **3** for time-resolved absorption measurements was achieved via photo-induced electron transfer using a positively charged sensitizer and toluene (1 M) as co-sensitizer: irradiation of N-methyl quinolinium (NMQ; 355 nm) in the presence of toluene yields the formation of toluene radical cation in high yields even in apolar solvents,<sup>48</sup> which can subsequently oxidize **1** – **3** to yield the silane radical cations **1** $^{\bullet+}$ , **2** $^{\bullet+}$  and **3** $^{\bullet+}$  (see Appendix 1 for details). This method is highly superior over direct irradiation of the silanes, which yields significant amounts of photochemical side products, as below 300 nm photo-ionization competes with direct homolytic Si-H bond cleavage.



The oxidation potentials of **1** – **3** were obtained by cyclic voltammetry to ensure efficient electron transfer from the silanes to toluene<sup>•+</sup> ( $E_{\text{ox}}(\text{toluene}) = 2.32 \text{ V vs. Ag/AgCl}$ ).<sup>56</sup> From the results in Table 1 it becomes clear that all three compounds have a sufficiently lower oxidation potential than toluene (peak potentials  $E_p$  from 1.34 to 1.67 V vs Ag/AgCl). In more detail it shows that **1**, with the smallest silicon ‘backbone’, has the highest potential. Interestingly **3** has a slightly higher oxidation potential than **2**, while having more silicon atoms. This may be explained by differences in the effective conjugation lengths, which is highly dependent on the conformation of the silicon backbone. Anti-conformation of the silicon atoms contributes the most to conjugation, whereas small dihedral angles (syn to gauche) do not contribute significantly.<sup>57</sup> Due to steric hindrance of the bulky TMS groups, **3** can not fully optimize the  $\sigma$  delocalization to the degree available for **2**. This steric effect is visible in the bond angle between the central Si and the two adjacent Si atoms. For **2** and **3**, this was calculated (B3LYP/6-311G(d,p)) to be 118° and 132° (experimental value: 128.3°),<sup>51</sup> respectively, i.e. significantly larger than the 109° for unstrained  $\text{sp}^3$  Si atoms. Calculated vertical ionization potentials (Table 1), obtained from the difference in absolute energies between the optimized neutral species and the corresponding radical cation in that geometry, confirm the significantly higher oxidation potential found for **1**. For **2** and **3**, the calculated potentials are close to each other, with the ordering in line with the experimental data. Finally, also the ordering of the ease of oxidation obtained using Koopmans’ theorem<sup>58</sup> (Table 3, bottom row) correlates nicely with the oxidation potentials found.

**Table 1.** Oxidation potentials of molecular models **1**, **2** and **3**.

	1	2	3
$E_p^a$	$1.67 \pm 0.01$	$1.34 \pm 0.01$	<b><math>1.42 \pm 0.01</math></b>
$IP_{\text{vert}}^b$	190	172	<b>173</b>
$IP_{\text{Koopmans}}^c$	<b>154</b>	<b>143</b>	<b>146</b>

<sup>a</sup>Peak potential in V vs. Ag/AgCl (3M KCl), 60 mV/s; <sup>b</sup>Vertical ionization potential (in kcal mol<sup>-1</sup>; B3LYP/6-311++G(2d,2p)//B3LYP/6-311G(d,p) calculations); <sup>c</sup>Ionization potential according to Koopmans’ theorem (in kcal mol<sup>-1</sup>; B3LYP/6-311++G(2d,2p)//B3LYP/6-311G(d,p) calculations).

The effect of the steric hindrance is also visible in Figure 3, which shows the relaxed geometries of the radical cations. In **1**<sup>•+</sup> two of the three Si-Si bonds are lengthened significantly more than the third bond (from 2.38 Å in the neutral precursor **1** to 2.50/2.50

and 2.40 Å, respectively). The charge is also predominantly present on the TMS moieties that are bound by a more lengthened Si-Si bond (from 0.027 in the precursor molecule **1** to 0.385 and 0.202 for the more and less lengthened Si-Si bonds, respectively). Also the angle  $\angle\text{Si2-Si1-Si3}$  becomes smaller going from  $113^\circ$  to  $99^\circ$  as the radical cation is formed, while the other angles,  $\angle\text{Si2-Si1-Si4}$  and  $\angle\text{Si3-Si1-Si4}$ , increase from  $113^\circ$  to  $118^\circ$ . Also **2<sup>•+</sup>** (and **3<sup>•+</sup>**) shows relaxation of the central angle  $\angle\text{Si2-Si1-Si3}$ , as it decreases from  $118^\circ$  ( $132^\circ$ ) to  $107^\circ$  ( $119^\circ$ ). The positive charge on the molecule is mainly localized on the TMS groups (from 0.062 in the precursor molecule **2** to 0.260 and 0.231 for the TMS moieties centered on atoms Si5 and Si7, respectively, and to 0.149 and 0.150 for those on Si4 and Si6, respectively). Most charge is localized on the TMS groups that are part of the w-shaped silicon chain (e.g. Si5-Si2-Si1-Si3-Si7 in **2**). This is also shown by the Si-Si bond orders, which are about 0.77 in this chain and 0.89 for the remaining two Si-Si bonds. Also bond lengths are increased from 2.38 to 2.44 Å in this chain, whereas the other bonds are only marginally lengthened to 2.40 Å. The w-shape (dihedrals: 7-3-1-2,  $143^\circ$ ; 3-1-2-5,  $147^\circ$ ) is distinctive for the previously mentioned  $\sigma$  conjugation in silicon chains. Silicon atoms bound in this conformation can attribute to the conjugation and thus stabilize the molecule. The geometry of **3<sup>•+</sup>** resembles that of **2<sup>•+</sup>**, including the relaxation of the angle strain ( $\angle\text{Si2-Si1-Si3}$  = from  $132^\circ$  in the neutral to  $119^\circ$  in the radical cation) and the w-shaped chain. The conjugated ‘backbone’ shows a better anti-conformation than **2<sup>•+</sup>** (dihedrals:  $\angle 8-3-1-2 = 172^\circ$ ;  $\angle 3-1-2-5 = 154^\circ$ ). However, bond orders show that the charge is mainly localized on two TMS-groups on Si5 and Si8. This is also reflected by the bond lengths, which are longer for Si3-Si8 and Si2-Si5 (2.49 Å) than for Si1-Si3 and Si1-Si2 (2.45 Å). The bonds not significantly involved in the sigma conjugation are only slightly longer (2.42 Å) than in the neutral molecule (2.39 - 2.40 Å).

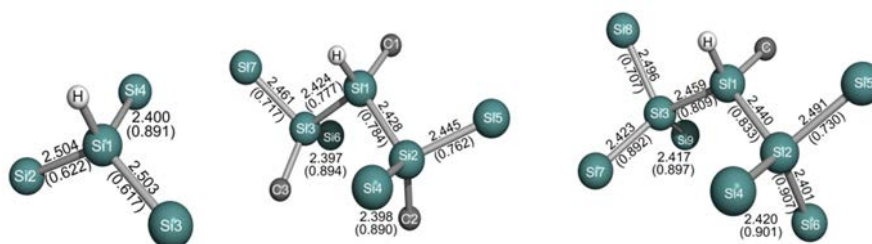


**Figure 3.** Silicon backbones and relevant carbon and hydrogen atoms of relaxed geometries of **1<sup>•+</sup>**, **2<sup>•+</sup>** and **3<sup>•+</sup>**. Bond distances and Wiberg bond orders (between parentheses) are depicted near the corresponding bonds (B3LYP/6-311++G(2d,2p)//B3LYP/6-311G(d,p) calculations).

Time-resolved absorption measurements were performed in a laser transient absorption setup. To avoid interference of absorption of the NMQ radical, these experiments were performed in oxygen-saturated solutions of 1,2-dichloroethane (DCE) and hexafluoroisopropanol (HFIP). Oxygen reacts rapidly with the NMQ radical (diffusion controlled) to photo-inactive products. HFIP was reported to stabilize radical cations,<sup>59</sup> and silane radical cations specifically.<sup>48</sup> As shown in Figure 4(left), toluene radical cation can be observed with absorption maxima at 425 and 825 nm. Upon addition of **3**, the absorption of toluene radical cation disappears, while a new transient appears at 690 nm. This indicates electron transfer between toluene radical cation and **3**. The transients resulting from **1**, **2** and **3** ( $\lambda_{\text{max}}$  is 520, 670 and 690 nm, respectively) are depicted in Figure 4(right). The stability of the transient in the presence of oxygen points towards a radical cationic transient, since organic radical cations typically react slowly with oxygen. To exclude the possibility of a radical mechanism, 1-bromohexane was added to the mixture, as bromoalkanes are known to react very fast with silicon-centered radicals.<sup>7,60</sup> This addition did not lead to any quenching and the lifetime of the transient remained the same, thus excluding the involvement of a radical transient and supporting the assignment of the transients in Figure 4(right) to **1**<sup>•+</sup>, **2**<sup>•+</sup> and **3**<sup>•+</sup>, respectively.

The radical cationic nature of these transients was further confirmed by investigating their ability to oxidize tris-*p*-tolylamine (TTA), a well-known electron donor with a low oxidation potential,<sup>48</sup> to yield the highly stable TTA radical cation ( $\lambda_{\text{max}} = 670 \text{ nm}$ <sup>61</sup>). Directly after the laser pulse, electron transfer occurs primarily between sensitizer (7 mM) and the co-sensitizer toluene (1 M), because of their higher concentrations. Subsequently, toluene radical cation will quickly oxidize a silane, yielding a still relatively fast build-up of the silyl radical cation concentration and a simultaneous depletion of toluene radical cation. Under the conditions used, this process is finished after ca. 20 nanoseconds. Finally, after this process is nearly complete TTA, which is present in a much lower concentration (1  $\mu\text{M}$ ), will transfer an electron to the silyl radical cations. As depicted in Figures 5 (left) and 5 (right), a clear shift from respectively from 520  $\rightarrow$  670 nm (from **1**<sup>•+</sup> to TTA<sup>•+</sup>) and 695  $\rightarrow$  670 nm (from **3**<sup>•+</sup> to TTA<sup>•+</sup>), indicates electron transfer and TTA to **3**<sup>•+</sup>. This confirms that the transients in Figure 4b can be attributed to the silyl radical cations.

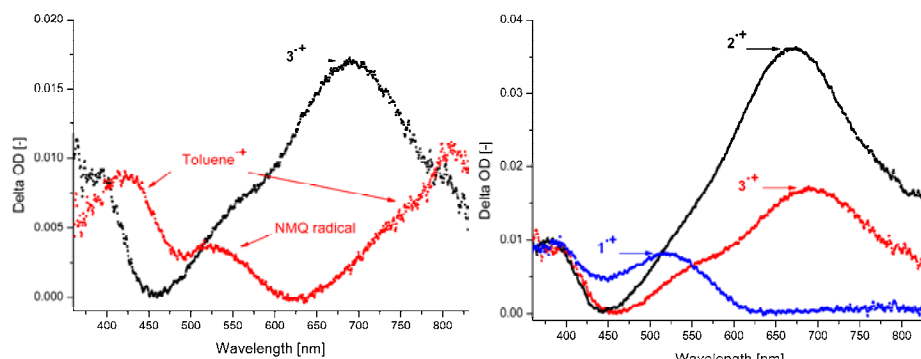


**Figure 4.** Left) UV-Vis absorption spectra of the mixtures of NMQ (7 mM) and toluene (1.0 M) in 1,2-dichloroethane in presence (10 mM) and absence of **3** in the reaction mixture (50 ns after laser pulse @ 355 nm). Right) UV-Vis absorption spectra of **1**<sup>•+</sup>, **2**<sup>•+</sup> and **3**<sup>•+</sup> (50 ns after 355 nm laser pulse).

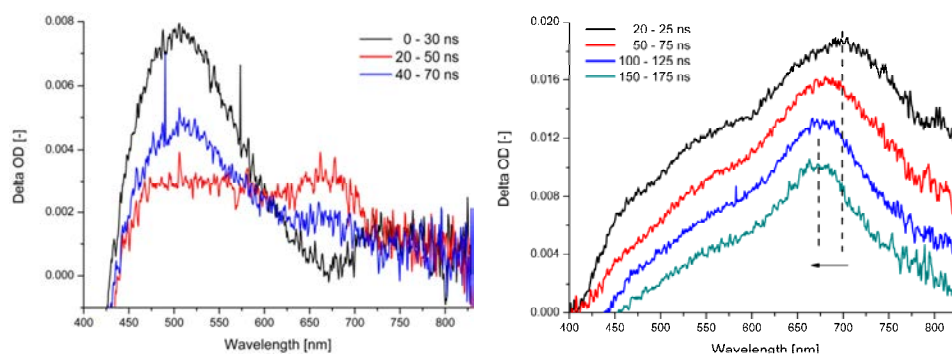


**Figure 5.** Absorption spectra of **1**<sup>•+</sup> (left) and **3**<sup>•+</sup> (right) in the presence of TTA recorded at increasing intervals after the laser pulse.

### 3.3.2 Reactivity of Silyl Radical Cations

The lifetime of **1**<sup>•+</sup> was measured in an oxygen-saturated solution to minimize the interference of NMQ<sup>•</sup>, and was found to be  $50 \pm 5$  ns. This proved to be too short to accurately determine the kinetics of reactions with nucleophiles using the current set-up. Reproducibility of the lifetime measurements proved highly dependent on small amounts of water present. To prepare ultra-dry solutions, all samples were prepared under water-free conditions in a glovebox under argon atmosphere. The maxima of **2**<sup>•+</sup> and **3**<sup>•+</sup> did not overlap with the absorption of NMQ<sup>•</sup>, and the exclusion of oxygen did not affect the

lifetimes. Under these conditions, the lifetimes for  $2^{\bullet+}$  and  $3^{\bullet+}$  were found to be  $1250 \pm 150$  ns and  $367 \pm 17$  ns, respectively. These lifetimes correlate with the ease of oxidation (Table 1) and the degree of delocalization that followed from the quantum chemical calculations: increased delocalization of the charge leads to decreased reactivity, i.e. prolonged lifetime.

The rate of reaction of both transients was subsequently studied with a series of nucleophiles, which were selected based on their relevance for monolayer formation onto H-terminated silicon surfaces.<sup>6</sup> The decay of both transients was mono-exponential (Figure 6, left), while the lifetimes of the radical cations became linearly shorter with increasing nucleophile concentration (Figure 6, right). This dependence on nucleophile concentration indicates a bimolecular reaction, since the silyl radical cation concentration is constant as this is only determined by the (near-constant) intensity of the laser pulse. The reaction rate constants obtained from a Stern-Volmer type plot are pseudo first-order constants (Table 2). From entries 1 and 2, it becomes clear that 1-alkynes react approximately a factor two faster with both silyl radical cations than 1-alkenes, which resembles the faster monolayer formation for 1-alkynes.<sup>27,29,30</sup> Entries 3 to 6 show that water, alcohols, acids and aldehydes, which are generally better nucleophiles than unsaturated carbons, react significantly faster with silyl radical cations.<sup>62,63</sup> This increased reactivity of these nucleophiles is similar for  $2^{\bullet+}$  and  $3^{\bullet+}$ , and nucleophilic attack onto the radical cation is further substantiated by the high reaction rate of 1-decanethiol with  $3^{\bullet+}$ . The significant difference in reactivity of  $2^{\bullet+}$  and  $3^{\bullet+}$  parallels the stability of the radical cations, and apparently outweighs the reduced steric hindrance around the Si-H site in  $2^{\bullet+}$ . As was discussed earlier, bromoalkanes (entry 8) show no significant reactivity towards the radical cations, excluding a radical reaction.

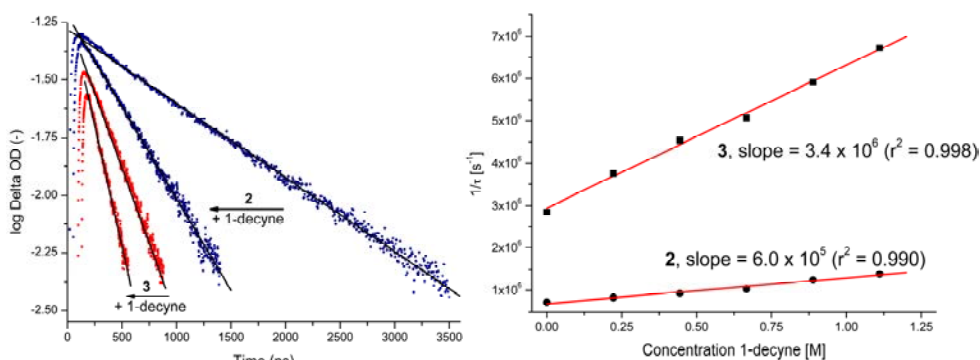


**Figure 6.** Decay of  $2^{\bullet+}$  and  $3^{\bullet+}$  in the absence or presence of 0.44 M 1-decyne (left) and; Stern-Volmer type plots obtained for  $2^{\bullet+}$  and  $3^{\bullet+}$  in the presence of 1-decyne (right).

The high reactivity of alcohols, acids and aldehydes is, at first sight, not in line with monolayer-forming experiments, where these moieties are commonly used for further functionalization of the monolayers. Also the reactivity of water is striking, because it is commonly used to rinse hydrogen-terminated Si samples after etching steps. For a better comparison with these monolayer experiments, the reactivity of doubly functionalized alkenes and alkynes was tested, as can be seen in entries 9 to 12. From these results it becomes clear that the reactivity of these doubly functionalized nucleophiles is similar to the reactivity of the mono-functionalized aldehydes and acids (Table 2, entries 5 and 6), and that the contribution of alkene and alkyne moieties is small. This implies that if the radical cation reaction would be the rate-limiting step in the attachment to the silicon surface, the monomers would attach via the aldehyde and acid functionalities rather than via the alkene or alkyne moieties. This is in contrast to what was found for example for aldehyde-functionalized monolayers prepared from  $\omega$ -unsaturated-1-aldehydes.<sup>64</sup> These materials were reported to show 90% attachment via Si-C bonds, and only 10% attachment via Si-O-C bonds. Even more so, in the case of acid-functionalized monolayers, prepared from  $\omega$ -unsaturated-1-acids, close to 100% attachment via Si-C bonds was reported.<sup>65-68</sup> According to these monolayer-forming experiments at least the large majority of chains attaches via the alkene and alkyne moieties.

These data thus show that alkenes and alkynes do react rapidly with delocalized Si-centered radical cationic materials, which is consistent with efficient initiation of monolayer formation onto H-terminated Si via a Si-centered radical cation. In the case of Si surfaces the absolute rates are, of course, expected to be significantly lower due the larger extent of delocalization, but the current experiments show that surface-localized radical cations on the H-Si surfaces can in principle initiate the reaction with 1-alkenes and 1-alkynes. The still much higher reaction rates of oxygen-centered nucleophiles with these Si-centered radical cations additionally show that – while initiation via this route may be feasible – the largest fraction of monolayer-forming molecules does not react via this mechanism, as this would yield extensive Si-O-C formation with  $\omega$ -unsaturated-1-carboxylic acids and  $\omega$ -unsaturated-1-aldehydes, which is not observed. The majority of Si-C bonds in a monolayer must therefore be formed via a different reaction.

**Table 2.** Pseudo first-order rate constants for the reactions of **2**<sup>•+</sup> and **3**<sup>•+</sup> with various nucleophiles.

Entry	Nucleophile	$k_2^a$	$k_3^a$
1	1-Decene	$0.24 \pm 0.02$	$1.7 \pm 0.06$
2	1-Decyne	$0.61 \pm 0.05$	$3.5 \pm 0.2$
3	H <sub>2</sub> O	-	$33 \pm 0.2$
4	1-Undecanol	$9.7 \pm 0.2$	$25 \pm 0.4$
5	1-Undecanal	$22 \pm 0.7$	$41 \pm 2$
6	1-Undecanoic acid	$6.5 \pm 0.04$	$22 \pm 0.4$
7	1-Decanethiol	-	$> 100^b$
8	1-Bromohexane	-	$< 0.1^c$
9	10-Undecenoic acid	-	$25 \pm 0.4$
10	10-Undecynoic acid	-	$21 \pm 1$
11	10-Undecenal	-	$55 \pm 1$
12	10-Undecynal	-	$45 \pm 1$

<sup>a</sup> Rates  $\pm$  standard deviation (in  $10^6 \text{ M}^{-1}\text{s}^{-1}$ ); <sup>b/c</sup> Rates too high/low to measure accurately with the set-up used.

To obtain more information about the exact reaction mechanism kinetic isotope effects (KIEs) were studied. Therefore the hydrogen at the central Si-H site of **3** was replaced by deuterium to give **3-D**. This did not cause noticeable changes in the absorption spectrum or in the lifetime of the radical cation in the absence of added nucleophiles. The results of the kinetics experiment of **3-D** with 1-decene and 1-decyne are depicted in Table 3. It becomes clear that the reactions of **3** are a factor 1.2 faster than reactions of **3-D**. This excludes Si-H bond cleavage in the rate-determining step, as then typically a primary isotope effect with  $k_H/k_D > 2$  would have been observed.<sup>69</sup> This thus also excludes a concerted mechanism with simultaneous Si-H bond cleavage and Si-C bond formation.<sup>70</sup> On the other hand, a KIE of 1.2 indicates a secondary kinetic isotope effect (SKIE), which places the hydrogen

connected to the reaction center ( $\alpha$ -position) or next to it ( $\beta$ -position). The SKIE can be caused by a change in hybridization, going from  $sp^3$  to  $sp^2$  in the transition state, or by hyperconjugation as deuterium is less able to stabilize the resulting cation. From these kinetic results it is not possible to determine the exact reaction center, but Si-H bond cleavage in the TS of the substitution reaction is unlikely, which points to Si-Si cleavage as the bond-breaking process that accompanies Si-C bond formation.

**Table 3.** Kinetic isotope effects for reactions of **3**<sup>•+</sup> with 1-decene and 1-decyne (in DCE/HFIP; 20 °C).

Entry	Nucleophile	$k_{\text{Si-H}}^*$	$k_{\text{Si-D}}^*$	<i>KIE</i>
1	1-Decene	$1.72 \pm 0.057$	$1.42 \pm 0.17$	$1.21 \pm 0.12$
2	1-Decyne	$3.53 \pm 0.17$	$3.01 \pm 0.28$	$1.17 \pm 0.11$

\*Rates  $\pm$  standard deviation (in  $10^6 \text{ M}^{-1} \text{ s}^{-1}$ ).

### 3.3.3 Product analysis

To substantiate this hypothesis, the reactivity of the radical cations of **1** - **3** was subsequently studied by their reaction with 1-decene and 1-decyne, and the reaction products were analyzed with GC-MS. Photochemical reactions ( $\lambda_{\text{exc}} \geq 350 \text{ nm}$ ) were performed in identical reaction mixtures (NMQ sensitized) as the transient absorption experiments. Product studies are typically performed with neutral sensitizers such as 9-cyanoanthracene and 9,10-dicyanoanthracene as they give less products of side reactions. However, it is well-documented that the nucleophilic reaction with the silyl radical cation competes with return electron transfer in the radical ion pair, resulting in the neutral sensitizer and silane.<sup>71</sup> In addition, it has been shown that disilanes are fragmented in a dissociative return electron transfer (DRET) process, resulting in the formation of radicals.<sup>41</sup> After confirming this for a 9-cyanoanthracene-sensitized test reaction (see below), we resorted to NMQ sensitization in these preparative reactions, specifically of **1**, as in the NMQ-sensitized reactions of **2** and **3** side reactions again precluded identification of reaction products resulting from nucleophilic attack. The reactions with **1** yielded reaction products in larger amounts, which could be analyzed and identified by GC-MS after independent synthesis of the most likely structures as reference compounds. Co-injection on the GC-MS and comparison of the mass spectra confirmed the identity of the



products (Figure 7). The reaction of **1** with 1-decene resulted in a substitution of the silicon-bound hydrogen (**4a**) or a TMS group (**4b**) in a ratio of 2:1. The reaction of **1** with 1-decyne, yielded similar hydrosilylation (**5a**) and substitution products (**5b**) (Figure 7b). In addition, the ratio of cis/trans isomers was similar to the products of radical reactions performed with **1**.<sup>45</sup> This observation of **4a** and **5a** seems at variance with the findings of the kinetic study discussed earlier, as the secondary kinetic isotope effect indicates a bimolecular nucleophilic attack on the silicon backbone and rules out substitution of the Si-H in the reaction of the radical cations with nucleophiles. However, it is likely that **4a** and **5a** are the products of a hydrosilylation side reaction, which proceeds via a radical mechanism. In a 9-cyanoanthracene-sensitized test reaction with alkenes and alkynes, *only* hydrosilylation products **4a** and **5a** were found. This can be explained by DRET, which results in the efficient formation of silyl radicals that can subsequently react with unsaturated moieties. The absence of the substitution products in these product mixtures indicates that such substitution products are formed via a different route than a radical reaction, and the question arises whether the substitution products **4b** and **5b** are the result of a nucleophilic attack onto a radical cation.

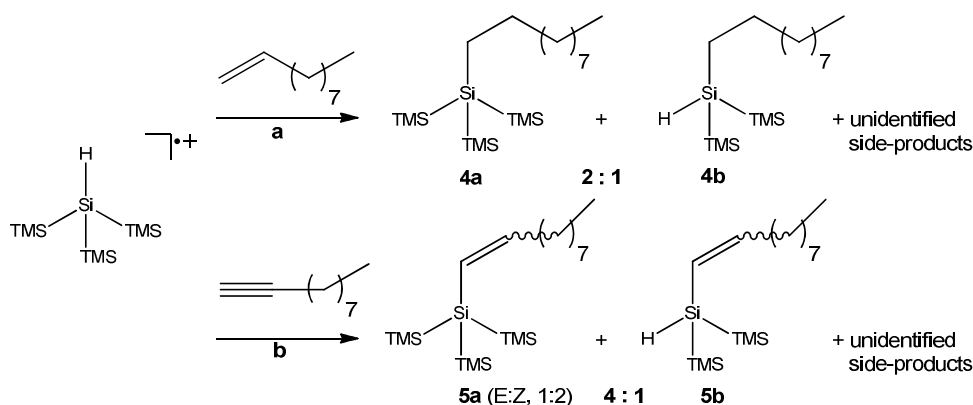


**Figure 7.** Products found in the reaction mixture for 1-decene (a) and 1-decyne (b).

In order to further distinguish between the radical and the radical cation reaction, the radical reaction was considered first. From the literature it is known that silyl radicals react rapidly with alkenes<sup>45</sup> and even faster with bromine-containing compounds,<sup>60</sup> such as 1-bromohexane. In order to obtain a better insight, radical reactions of **1**<sup>•</sup> with 1-decene, 1-bromohexane and 1-undecanol were performed. A thermal radical initiator, 1,1'-azobiscyclohexanecarbonitrile, was used to generate **1**<sup>•</sup>.<sup>72</sup> First, reaction with alkene did not result in any Si-Si cleavage (Figure 8a): only a hydrosilylation product was formed, which

after co-injection proved to be identical to **4a**. In a second reaction 1-bromohexane reacted very fast with **1<sup>•</sup>**, resulting in exclusive formation of **6**. Again no products resulting from cleavage of the Si-Si bond were observed (Figure 8b). The third reaction of **1<sup>•</sup>** in the presence of 1-undecanol demonstrates that alcohols do not react with silyl radicals, since **8** – which was synthesized independently to function as reference compound – was completely absent from the reaction mixture (Figure 8c). The only product present in the mixture is the termination product (**7**) of two silyl radicals. In order to distinguish between radical and radical cation products, 1-undecanol was also reacted with **1<sup>•+</sup>**, resulting in Si-Si cleavage products **9** and **10** (Figure 8d). These products can only be the result of a reaction with the silyl radical cation, as the previous reaction showed that 1-undecanol does not react with silyl radicals.

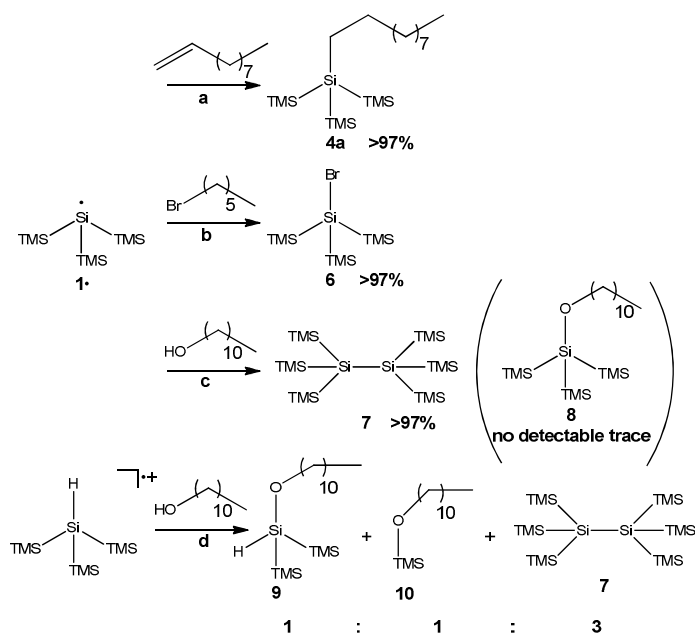


**Figure 8.** Products of reactions of **1<sup>•</sup>** (a-c) and of **1<sup>•+</sup>** with 1-undecanol (d).

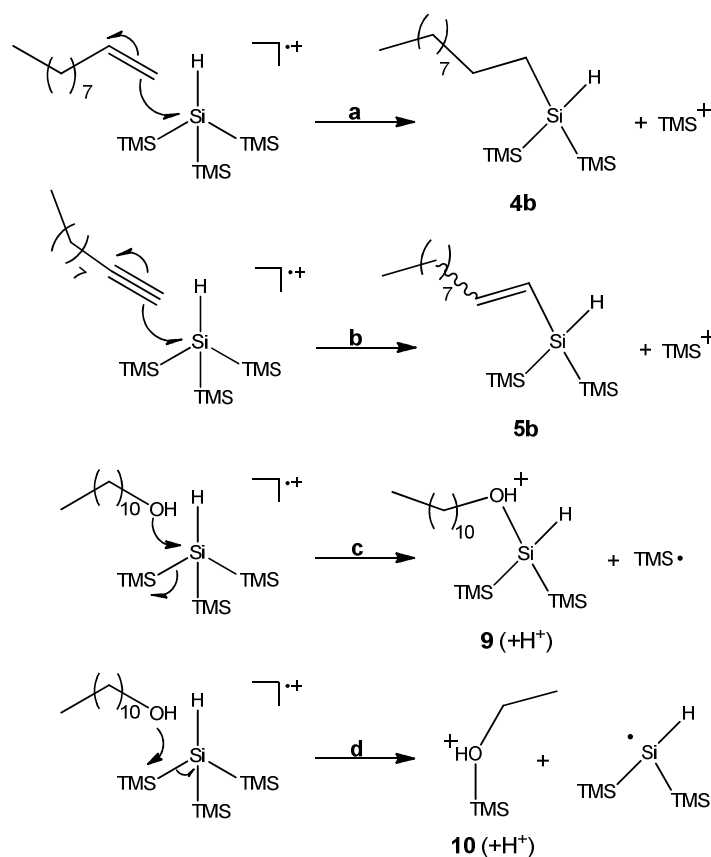


**Figure 9.** Reaction mechanisms of  $1^{\bullet+}$  with 1-decene (a), 1-decyne (b) and 1-undecanol (c,d).

After identifying the trapping products of the silyl radical cation, it is possible to look more detailed at the substitution at the central Si atom. For alkenes and alkynes it becomes clear that nucleophilic attack to the silyl radical cation results in dissociation and the formation of a TMS cation. The resulting  $\beta$ -carbon radical can subsequently initiate a radical chain reaction via abstraction of a hydrogen atom from a neighboring silane, yielding substitution products **4b** and **5b** and the silicon-centered radical  $1^{\bullet}$ . In the case of 1-alkenes and 1-alkynes the mechanism of this reaction is likely to be similar (Figure 9, a and b). However, for alcohols a different mechanism must be in effect since two substitution products (**9** and **10**) are observed. Nucleophilic attack on the central Si-H moiety in the radical cation leads to loss of a TMS radical and formation of **9** (Figure 9c). However, attack on the TMS group will result in the formation of **10** and silyl radical **11** (Figure 9d). Routes 10c and 10d again

show how a parallel radical chain reaction can be initiated. The observed 1 : 1 ratio of **9** and **10** suggests that both substitution pathways are in this case equally likely to occur. Interestingly, the cleavage of a Si-Si backbond is not observed by Chabal and coworkers who prepared monolayers on Si(111) from methanol, using mild conditions (65 °C, 12h).<sup>73</sup> This reaction is likely to proceed via a concerted mechanism, where the methoxy group attaches to the surface under expulsion of H<sub>2</sub>, with a calculated activation barrier of 33.7 kcal mol<sup>-1</sup>.<sup>74</sup> These findings are in line with calculations performed by Re and coworkers, who found activation barriers of 64.6 and 57.7 kcal mol<sup>-1</sup> for the concerted attachment of alkenes and alkynes respectively.<sup>75</sup> However, these barriers are significantly higher than the barriers estimated from the rates in Table 2 (7.4, 9.0 and 8.5 kcal mol<sup>-1</sup> for 1-undecanol, 1-decene and 1-decyne resp., for more details see Appendix 2). This indicates that the radical cation reactions proceed via a different pathway which lead to different products than the concerted mechanism.

Besides radical formation as a result of nucleophilic attack on the radical cation, also several other routes for initiation of the radical reaction could in principle be operative (see Figure 10). For instance, instability of **1**<sup>•+</sup> may result in spontaneous dissociation. Loss of H<sup>+</sup>, resulting in the silicon-centered radical **1**<sup>•</sup> (Figure 10a) may be a viable option, although it can only occur as a side reaction, since otherwise products **9** and **10** would not predominantly form. A second option is the dissociation of a TMS<sup>+</sup> group, resulting in the silicon-centered radical **11**<sup>•</sup> (Figure 10b). The TMS<sup>+</sup> fragment would in turn react with 1-undecanol to form **10**, but the radical fragment cannot react with the alcohol to form **9**. Since both products **9** and **10** are present in equal amounts in the reaction mixture, also this pathway can only occur as a minor side reaction. The third possibility, a TMS radical splitting off, yielding the silicon-centered cation **11**<sup>+</sup> is also unlikely (Figure 10c), as the resulting TMS radical would react rapidly with 1-decene, and the product of this reaction was not observed. Also this pathway would lead to unequal amounts of **9** and **10**, which is not the case, as described above. Finally, dissociation may also occur as a result of return electron transfer from the sensitizer to the silane (Figure 10d). As mentioned earlier, dissociative return electron transfer (DRET) is the major mechanism in the degradation of radical cations of disilanes to monosilyl radicals.<sup>41</sup> Since this mechanism would also generate a TMS radical that should lead to products that were not observed, this mechanism is in our case unlikely as well. The above observations indicate that the Si radicals are predominantly formed by nucleophilic attack to the Si radical cation, rather than by spontaneous dissociation or DRET. This also demonstrates the feasibility of the formation of silicon-centered radicals at the silicon surface by nucleophilic attack to a delocalized radical cation. Such formation of radicals as a result of an initiating radical cation process has been hypothesized before,<sup>37</sup> and the data above provide further support for such a route. This more detailed mechanistic insight will be valuable to attempts to further improve monolayer formation onto hydrogen-terminated Si surfaces, both with respect to the rate of

the reaction as well as in regard of the quality of the monolayer. Such studies are currently ongoing in our laboratories.

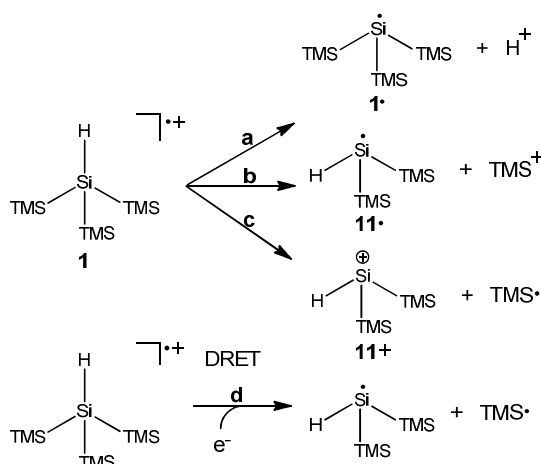


**Figure 10.** Dissociation pathways of  $1^{\bullet+}$  due to instability (a-c) or return electron transfer (d).

### 3.4 Conclusions

Small Si-H centered models (with 4, 7 and 9 Si atoms, respectively) were prepared and studied to gain insight in the mechanisms of formation of Si-C linked monolayers by 1-alkenes and 1-alkynes onto hydrogen-terminated silicon surfaces. Si-centered radical cations of these Si<sub>4</sub>, Si<sub>7</sub> and Si<sub>9</sub> compounds react with high rates ( $k_2 \sim 10^6 \text{ M}^{-1}\text{s}^{-1}$ ) in a bimolecular reaction with 1-alkynes and 1-alkenes, but do not react with 1-bromoalkanes. The reactivity with alkenes and alkynes is in line with initiation of Si-C linked monolayer formation by 1-alkenes and 1-alkynes onto H-terminated silicon surfaces via positively charged surfaces.<sup>37</sup> Such a bimolecular reaction is expected to yield a cation and a radical as products. Better, oxygen-centered nucleophiles (aldehydes/carboxylic acids) react appreciably faster with the Si radical cations. These increasing reaction rates for stronger nucleophiles contrast with the small to insignificant reactivity of these moieties observed in the preparation of aldehyde-functionalized and acid-functionalized monolayers onto H-terminated Si. A radical cation mechanism does not account for the Si-C bond formation on H-terminated Si surfaces that is predominant also for  $\omega$ -unsaturated 1-carboxylic acids and -1-aldehydes. This shows that the majority of monolayer-forming materials yields Si-C formation via another mechanism. The observation of hydrosilylation products for the

model systems under current study indicates a radical side reaction. This radical formation proceeds predominantly via nucleophilic attack on the silyl radical cation, and only to a minor degree to spontaneous dissociation of the radical cations or dissociative return electron transfer. Radical cation-initiated attachment onto a H-terminated Si surface thus is the rate-limiting step in Si-C attached monolayer formation, but the majority of molecules is attached via a purely radical propagation reaction.

## References

- (1) Ciampi, S.; Harper, J. B.; Gooding, J. J. *Chem. Soc. Rev.* **2010**, 39, 2158.
- (2) Boukherroub, R. *Curr. Opin. Solid St. M.* **2005**, 9, 66.
- (3) Shirahata, N.; Hozumi, A.; Yonezawa, T. *Chem. Rec.* **2005**, 5, 145.
- (4) Wayner, D. D. M.; Wolkow, R. A. *J Chem Soc Perk T 2* **2002**, 23.
- (5) Sieval, A. B.; Linke, R.; Zuilhof, H.; Sudhölter, E. J. R. *Adv. Mater.* **2000**, 12, 1457.
- (6) Buriak, J. M. *Chem. Rev.* **2002**, 102, 1271.
- (7) Choi, K.; Buriak, J. M. *Langmuir* **2000**, 16, 7737.
- (8) Sieval, A. B.; Huisman, C. L.; Schoenecker, A.; Schuurmans, F. M.; Van der Heide, A. S. H.; Goossens, A.; Sinke, W. C.; Zuilhof, H.; Sudhölter, E. J. R. *J. Phys. Chem. B* **2003**, 107, 6846.
- (9) Linford, M. R.; Fenter, P.; Eisenberger, P. M.; Chidsey, C. E. D. *J. Am. Chem. Soc.* **1995**, 117, 3145.
- (10) Sieval, A. B.; Demirel, A. L.; Nissink, J. W. M.; Linford, M. R.; van der Maas, J. H.; de Jeu, W. H.; Zuilhof, H.; Sudhölter, E. J. R. *Langmuir* **1998**, 14, 1759.
- (11) Shestopalov, A. A.; Clark, R. L.; Toone, E. J. *Langmuir* **2010**, 26, 1449.
- (12) Wang, X. Y.; Ruther, R. E.; Streifer, J. A.; Hamers, R. J. *J. Am. Chem. Soc.* **2010**, 132, 4048.
- (13) Cicero, R. L.; Linford, M. R.; Chidsey, C. E. D. *Langmuir* **2000**, 16, 5688.
- (14) Terry, J.; Mo, R.; Wigren, C.; Cao, R. Y.; Mount, G.; Pianetta, P.; Linford, M. R.; Chidsey, C. E. D. *Nucl. Instrum. Meth. B.* **1997**, 133, 94.
- (15) Buriak, J. M.; Stewart, M. P.; Geders, T.; Choi, H. C. *Abstr. Pap. Am. Chem. S.* **1999**, 218, U457.
- (16) Holland, J. M.; Stewart, M. P.; Allen, M. J.; Buriak, J. M. *J. Solid State Chem.* **1999**, 147, 251.
- (17) Hurley, P. T.; Nemanick, E. J.; Brunschwig, B. S.; Lewis, N. S. *J. Am. Chem. Soc.* **2006**, 128, 9990.
- (18) Juang, A.; Scherman, O. A.; Grubbs, R. H.; Lewis, N. S. *Langmuir* **2001**, 17, 1321.
- (19) Allongue, P.; de Villeneuve, C. H.; Pinson, J.; Ozanam, F.; Chazalviel, J. N.; Wallart, X. *Electrochim. Acta* **1998**, 43, 2791.
- (20) deVilleneuve, C. H.; Pinson, J.; Bernard, M. C.; Allongue, P. *J. Phys. Chem. B* **1997**, 101, 2415.
- (21) Robins, E. G.; Stewart, M. P.; Buriak, J. M. *Chem. Commun.* **1999**, 2479.

- (22) Lee, M. V.; Guo, D. W.; Linford, M. R.; Zuilhof, H. *Langmuir* **2004**, *20*, 9108.
- (23) Niederhauser, T. L.; Jiang, G. L.; Lua, Y. Y.; Dorff, M. J.; Woolley, A. T.; Asplund, M. C.; Berges, D. A.; Linford, M. R. *Langmuir* **2001**, *17*, 5889.
- (24) Niederhauser, T. L.; Lua, Y. Y.; Jiang, G. L.; Davis, S. D.; Matheson, R.; Hess, D. A.; Mowat, I. A.; Linford, M. R. *Angew. Chem. Int. Ed.* **2002**, *41*, 2353.
- (25) Yang, L.; Lua, Y. Y.; Lee, M. V.; Linford, M. R. *Acc. Chem. Res.* **2005**, *38*, 933.
- (26) Scheres, L.; Arafat, A.; Zuilhof, H. *Langmuir* **2007**, *23*, 8343.
- (27) Ng, A.; Ciampi, S.; James, M.; Harper, J. B.; Gooding, J. J. *Langmuir* **2009**, *25*, 13934.
- (28) Scheres, L.; Giesbers, M.; Zuilhof, E. *Langmuir* **2010**, *26*, 10924.
- (29) Scheres, L.; Giesbers, M.; Zuilhof, H. *Langmuir* **2010**, *26*, 4790.
- (30) Zigah, D.; Herrier, C.; Scheres, L.; Giesbers, M.; Fabre, B.; Hapiot, P.; Zuilhof, H. *Angew. Chem. Int. Edit.* **2010**, *49*, 3157.
- (31) Popoff, R. T. W.; Asanuma, H.; Yu, H. Z. *J. Phys. Chem. C* **2010**, *114*, 10866.
- (32) Campos, M. A. C.; Paulusse, J. M. J.; Zuilhof, H. *Chem. Commun.* **2010**, *46*, 5512.
- (33) Yaffe, O.; Scheres, L.; Puniredd, S. R.; Stein, N.; Biller, A.; Lavan, R. H.; Shpaisman, H.; Zuilhof, H.; Haick, H.; Cahen, D.; Vilan, A. *Nano Lett.* **2009**, *9*, 2390.
- (34) Seitz, O.; Vilan, A.; Cohen, H.; Hwang, J.; Haeming, M.; Schoell, A.; Umbach, E.; Kahn, A.; Cahen, D. *Adv. Funct. Mater.* **2008**, *18*, 2102.
- (35) Seitz, O.; Bocking, T.; Salomon, A.; Gooding, J. J.; Cahen, D. *Langmuir* **2006**, *22*, 6915.
- (36) Stewart, M. P.; Buriak, J. M. *J. Am. Chem. Soc.* **2001**, *123*, 7821.
- (37) Sun, Q.-Y.; De Smet, L. C. P. M.; Van Lagen, B.; Giesbers, M.; Thuene, P. C.; Van Engelenburg, J.; De Wolf, F. A.; Zuilhof, H.; Sudhölter, E. J. R. *J. Am. Chem. Soc.* **2005**, *127*, 2514.
- (38) Lopinski, G. P.; Wayner, D. D. M.; Wolkow, R. A. *Nature* **2000**, *406*, 48.
- (39) Eves, B. J.; Sun, Q.-Y.; Lopinski, G. P.; Zuilhof, H. *J. Am. Chem. Soc.* **2004**, *126*, 14318.
- (40) Cicero, R. L.; Chidsey, C. E. D.; Lopinski, G. P.; Wayner, D. D. M.; Wolkow, R. A. *Langmuir* **2002**, *18*, 305.
- (41) Al-Kaysi, R. O.; Goodman, J. L. *J. Am. Chem. Soc.* **2005**, *127*, 1620.
- (42) Guirado, G.; Haze, O.; Dinnocenzo, J. P. *J. Org. Chem.* **2010**, *75*, 3326.
- (43) Karatsu, T.; Kanayama, K.; Takahashi, M.; Ishigohoka, N.; Fukui, K.; Kitamura, A. *Heteroatom Chem.* **2001**, *12*, 269.
- (44) Karatsu, T. *J. Photoch. Photobio. C* **2008**, *9*, 111.
- (45) Kopping, B.; Chatgililoglu, C.; Zehnder, M.; Giese, B. *J. Org. Chem.* **1992**, *57*, 3994.
- (46) Sommer, L. H.; Pietrusza, E. W.; Whitmore, F. C. *J. Am. Chem. Soc.* **1947**, *69*, 188.
- (47) Kabalka, G. W.; Zhou, L. L.; Wang, L.; Pagni, R. M. *Tetrahedron* **2006**, *62*, 857.
- (48) Dockery, K. P.; Dinnocenzo, J. P.; Farid, S.; Goodman, J. L.; Gould, I. R.; Todd, W. P. *J. Am. Chem. Soc.* **1997**, *119*, 1876.
- (49) Becke, A. D. *J. Chem. Phys.* **1993**, *98*, 5648.

- (50) M. J. Frisch, G. W. T., H. B. Schlegel, G. E. Scuseria, ; M. A. Robb, J. R. C., G. Scalmani, V. Barone, B. Mennucci, ; G. A. Petersson, H. N., M. Caricato, X. Li, H. P. Hratchian, ; A. F. Izmaylov, J. B., et al. *Gaussian09* **2009**, revision A.02; Gaussian.
- (51) Gross, T.; Reinke, H.; Oehme, H. *Can. J. Chem.* **2000**, 78, 1399.
- (52) Kollegger, G.; Hassler, K. *J. Org. Chem.* **1995**, 485, 233.
- (53) Marschner, C. *Eur. J. Inorg. Chem.* **1998**, 221.
- (54) Gilman, H.; Smith, C. L. *J. Org. Chem.* **1967**, 8, 245.
- (55) Apeloig, Y.; Yuzefovich, M.; Bendikov, M.; BravoZhvotovskii, D.; Klinkhammer, K. *Organometallics* **1997**, 16, 1265.
- (56) Montalti, M.; Credi, A.; Prodi, L.; Gandolfi, M. T. *Handbook of photochemistry*; Third ed.; Taylor & Francis Group LLC, 2006.
- (57) Krempner, C.; Reinke, H. *Organometallics* **2007**, 26, 2053.
- (58) Koopmans, T. *Physica* **1934**, 1, 104.
- (59) Ebersson, L.; Hartshorn, M. P.; Persson, O. *J. Chem. Soc. Perk. T. 2* **1995**, 1735.
- (60) Chatgililoglu, C.; Griller, D.; Lesage, M. *J. Org. Chem.* **1989**, 54, 2492.
- (61) Shida, T. *Electronic Absorption Spectra of Radical Ions*; Elsevier: Amsterdam, The Netherlands, 1988.
- (62) Todd, W. P.; Dinnocenzo, J. P.; Farid, S.; Goodman, J. L.; Gould, I. R. *J. Am. Chem. Soc.* **1991**, 113, 3601.
- (63) Dinnocenzo, J. P.; Simpson, T. R.; Zuilhof, H.; Todd, W. P.; Heinrich, T. *J. Am. Chem. Soc.* **1997**, 119, 987.
- (64) Hong, Q.; Rogero, C.; Lakey, J. H.; Connolly, B. A.; Houlton, A.; Horrocks, B. R. *Analyst* **2009**, 134, 593.
- (65) Bin, X. M.; Mischki, T. K.; Fan, C. Y.; Lopinski, G. P.; Wayner, D. D. M. *J. Phys. Chem. C* **2007**, 111, 13547.
- (66) Aureau, D.; Ozanam, F.; Allongue, P.; Chazalviel, J. N. *Langmuir* **2008**, 24, 9440.
- (67) Perring, M.; Dutta, S.; Arafat, S.; Mitchell, M.; Kenis, P. J. A.; Bowden, N. B. *Langmuir* **2005**, 21, 10537.
- (68) Faucheux, A.; Gouget-Laemmel, A. C.; de Villeneuve, C. H.; Boukherroub, R.; Ozanam, F.; Allongue, P.; Chazalviel, J. N. *Langmuir* **2006**, 22, 153.
- (69) Carey, F. A.; Sundberg, R. J. *Advanced Organic Chemistry Part A: Structure and Mechanisms*; Fifth ed.; Springer, 2008.
- (70) de Lijser, H. J. P.; Snelgrove, D. W.; Dinnocenzo, J. P. *J. Am. Chem. Soc.* **2001**, 123, 9698.
- (71) Dinnocenzo, J. P.; Farid, S.; Goodman, J. L.; Gould, I. R.; Todd, W. P. *Mol. Cryst. Liq. Cryst.* **1991**, 194, 151.
- (72) Postigo, A.; Kopsov, S.; Ferreri, C.; Chatgililoglu, C. *Org. Lett.* **2007**, 9, 5159.
- (73) Michalak, D. J.; Amy, S. R.; Aureau, D.; Dai, M.; Esteve, A.; Chabal, Y. J. *Nat. Mater.* **2010**, 9, 266.
- (74) Solares, S. D.; Michalak, D. J.; Goddard, W. A.; Lewis, N. S. *J. Phys. Chem. B* **2006**, 110, 8171.
- (75) Coletti, C.; Marrone, A.; Giorgi, G.; Sgamellotti, A.; Cerofolini, G.; Re, N. *Langmuir* **2006**, 22, 9949.



## Chapter 4

# Reactivity of Silyl Radicals Towards Unsaturated Hydrocarbons: Understanding Monolayer Formation on H-Terminated Silicon (111)

**Abstract.** Radical reactions of silyl radicals with unsaturated species (including a series of alkenes, alkynes, and aldehydes) were studied experimentally and theoretically using model compounds that represent the hydrogen-terminated silicon surface (H-Si). Competition reactions of precursors, typically employed in monolayer formation on H-Si, with the tris(trimethylsilyl)silyl radical, yielded reactivity ratios that are in line with monolayer experiments from the literature. Alkynes were shown to react 8-fold faster than alkenes, whereas aldehydes were shown to react 30-fold slower than alkenes. Introduction of alkenes in conjugation with the reactive unsaturated moiety ( $C=C$  or  $C\equiv C$ ) led to a significant increase in reactivity, due to stabilization of the formed  $\beta$ -carbon radical. Since monolayer fabrication may possibly be speeded up in this way, two additional classes of compounds,  $HC\equiv C-CH=CHR$  and  $HC\equiv C-C\equiv CR$  ( $R$  = alkyl), were synthesized and reacted with the silicon model compounds revealing promising 200 to 1400-fold increases in reactivity, respectively. A theoretical  $Si_4$  model was constructed to calculate reaction barriers and free energies. The thus derived reaction rates showed excellent correlation with experimentally determined rates, demonstrating the usefulness of this simple model as a tool for predicting outcomes of monolayer experiments with hetero-bifunctional precursors. The model was subsequently extended to a  $Si_7$ -system to study hydrogen transfer at the H-Si surface in more detail. The calculated barriers for these transfer reactions showed that Si-C bond forming monolayer formation from alkene or alkyne derivatives is rate-limited by this H-transfer reaction, rather than by the Si-C bond-forming addition step. Improved monolayer formation (faster, higher monolayer density) requires addressing both propagation steps.

**This chapter is submitted as:**

“Reactivity of Silyl Radicals Towards Unsaturated Hydrocarbons: Understanding Monolayer Formation on H-Terminated Silicon (111)”, Rijkssen, B.; Paulusse, J.M.J.; Zuilhof, H.

## 4.1 Introduction

The development of novel sensing devices relies on the functionalization of inorganic surfaces with self-assembled monolayers.<sup>1-6</sup> Covalently attached monolayers on hydrogen-terminated silicon (H-Si) provide for a robust platform that may be easily incorporated into the existing electronic infrastructure of a sensing device. Recent synthetic developments have led to high-quality monolayers on oxygen-free Si, bringing application in electronic devices within reach.<sup>7-12</sup> The attachment of terminal alkenes or alkynes onto the H-Si surface, at elevated temperatures<sup>13,14</sup> or by UV irradiation,<sup>15-18</sup> is commonly accepted to proceed via a radical chain mechanism.<sup>4,14,19</sup> Also the significantly milder attachment methods, which make use of white light or do not even require irradiation or heating,<sup>20</sup> were shown to proceed via this mechanism.<sup>21</sup> Initiation of this chain reaction can occur in several different ways, depending on the reaction conditions.<sup>4,14-16,20,22-26</sup> The radical chain propagation consists of two reactions steps: reaction of a C=C or C≡C bond with a Si radical at the surface, resulting in formation of a Si-C bond and a  $\beta$ -carbon-centered radical, and subsequent transfer of a hydrogen atom of a neighboring Si-H site to the carbon chain resulting in a new Si radical, which is available for the next addition reaction (see Figure 1). These reactions are not limited to alkenes or alkynes, as radical attachment and the subsequent propagation steps have also been demonstrated for unsaturated heteroatom bonds such as carbonyls.<sup>27-30</sup>

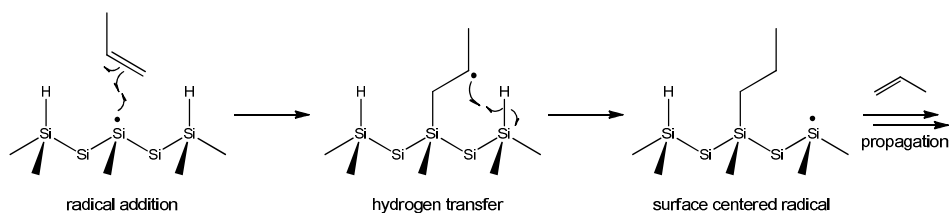


**Figure 1.** Propagation steps in the radical chain mechanism as proposed by Chidsey and coworkers.<sup>14</sup>

Over the past few years silyl radical reactions have been investigated both by experimental and computational methods. Reactions of the tris(trimethylsilyl)silyl radical **2** with a large variety of reagents have been studied in great detail (see Figure 2).<sup>31-35</sup> However, these reactions were not specifically aimed at better understanding surface radical reactions, but rather with precursor **1** being a radical-based reducing agent,<sup>35,36</sup> or serving as a radical mediator in polymerization reactions.<sup>31,32</sup> As such, linear alkenes and alkynes, commonly used in monolayer fabrication, were not included in these studies. Radical reactions at the H-Si surface have indeed been studied in detail by quantum chemical calculations performed on both small silicon clusters and larger silicon slabs.<sup>37-42</sup> These studies reveal

important differences in reactivity of various functional groups in the two propagation steps. Extensive silicon models ensure a good representation of the Si surface. However, in view of computational cost, most studies are limited to small reagent molecules (ethylene and acetylene), which consequently results in a limited view of the reactivity of actual monolayer precursor molecules.

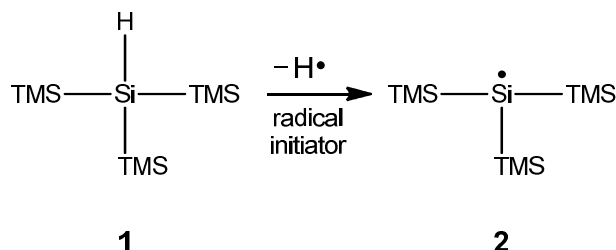


**Figure 2.** Tris(trimethylsilyl)silane (**1**) and the tris(trimethylsilyl)silyl radical (**2**). (TMS = Si(CH<sub>3</sub>)<sub>3</sub>)

While the previous study showed initiation by Si-centered radical cations is feasible, it was also shown from the relative reactivity of representative nucleophiles that this initiation was not the rate-limiting step in monolayer formation onto H-Si. In order to gain more detailed insights into the reactivity of precursor molecules commonly used in the fabrication of organic monolayers on H-Si (alkenes, alkynes, etc.), the present study focuses on their experimental reactivity in competition reactions with radical **2**, and a comparison is made between these findings and those of monolayer assembly. The driving forces and rates of the addition and hydrogen transfer reactions are subsequently modeled with DFT calculations on the experimentally employed alkene or alkyne in conjunction with a Si<sub>4</sub> model that resembles the top layer of the H-Si(111) surface. This leads to the discovery of a novel lead compound for monolayer formation onto H-Si(111), a delineation of the rate-determining step in such monolayer formation and detailed guidelines for the development of more reactive monolayer-forming molecules.

## 4.2 Experimental Section

### 4.2.1 Materials

Di-*tert*-butylperoxide (98%), 1-decene (99%), 1-decyne (99%), bis(trimethylsilyl)-1,3-butadiyne (96%), 1-bromododecane (99%), potassium fluoride dehydrate (98%), DMF (99.8%), HMPA (99%), methyl lithium/LiBr in diethylether (1.6 M), di-isobutylaluminum hydride in pentane (1.6 M), DME (anhydrous), n-butyl lithium in pentane (1.6 M), and

hexadecane (99%) were obtained from Sigma-Aldrich. Tris(trimethylsilyl)silane (97%) was obtained from VWR. All reagents were used without further purification unless stated otherwise. Phenylacetylene (96%) was obtained from Sigma-Aldrich and further purified by filtration over Si-60 and aluminum oxide before use. 1-Undecanal (97%) was obtained from Alfa-Aesar and was purified over a small Si-60 column to remove oxidation products and stabilizer. THF was obtained from VWR (technical grade) and distilled from Na/benzophenone. All reagents and stock solutions used in the radical experiments were de-oxygenated by three freeze-pump-thaw cycles and stored in a glovebox under argon atmosphere.

#### 4.2.2 Equipment

GC-MS analysis was performed on an Agilent technologies 7890A GC, equipped with Alltech ATTM-5ms column, in conjunction with a 5975C VL Mass Selective Detector. All NMR spectra were recorded on a Bruker Avance III with an inverse broadband probe running at 400 MHz, with C<sub>6</sub>D<sub>6</sub> as solvent.

#### 4.2.3 Computational Procedure

All DFT calculations were performed using the Gaussian 09 package<sup>43</sup> and all geometries (Si<sub>4</sub>- and Si<sub>7</sub>-model) were optimized with the B3LYP functional as implemented in there using a 6-311G(d,p) basis set. The Si<sub>4</sub>-model geometries were confirmed to be minima on the potential energy surface via calculation of the vibrational frequencies. Some surface-model geometries showed one or more imaginary frequencies, which may be attributed to vibrations in the silicon backbone, and are a result of the set constraints to maintain the surface rigid. The absolute energies of both models were corrected with the zero-point energy, obtained from the vibrational frequency analysis.

**Procedure for Obtaining Surface Model:** The geometry of the silicon backbone of the surface models was obtained from Materials Studio. A silicon crystal was cleaved along the 111-plane, from which a unit cell, containing one surface atom and being four atoms deep, was built. This unit cell was expanded in the x and y directions to obtain a 12 × 12 slab. This slab was optimized using PCFF<sup>44</sup> and the smart minimizer routine as implemented in the Discover package in the Materials Studio software.<sup>45,46</sup> The surface model was cut from the middle of the slab, leaving the positions of silicon and hydrogen atoms intact. All dangling bonds were replaced with hydrogen atoms and constraints were put on all silicon and original hydrogen atoms before optimizing the geometry in Gaussian09.

#### 4.2.4 Radical Competition Reactions

A solution of  $\text{Si}_4$  and hexadecane in benzene (respective concentrations: 50 mM and 10 mM, 2 mL) and the desired reagent (100  $\mu\text{L}$ ) and di-*tert*-butyl peroxide (10  $\mu\text{L}$ ) were mixed in a 4 mL vial, and divided into separate aliquots. These aliquots were irradiated for different time intervals, ranging from 5 to 15 min, at  $\lambda = 320$  nm, after which the reaction mixtures were analyzed by GC-MS.

#### 4.2.5 Syntheses

**Synthesis of 1-trimethylsilyl-hexadeca-1,3-diyne and hexadeca-1,3-diyne (4):** These compounds were synthesized following modified literature procedures.<sup>47-49</sup> A solution of 1,4-bis(trimethylsilyl)-1,3-butadiyne (20.0 mmol) in anhydrous THF (50 mL) was cooled to  $-78$  °C before dropwise addition of a solution of methyl lithium – lithium bromide complex in diethyl ether (1.6 M, 20 mmol). The mixture was left to warm up to room temperature, and stirred for another 4 h. After cooling the solution again to  $-78$  °C, a solution of 1-bromododecane (22 mmol) in anhydrous HMPA (50 mL) was added dropwise, and the mixture was left to warm up to room temperature and was stirred for another 30 min. The solution was neutralized with a suspension of crushed ice in aqueous HCl (100 mL, 3M) and subsequently extracted with diethyl ether. The combined organic fractions were washed with a saturated bicarbonate solution and brine, and dried over  $\text{MgSO}_4$ . The resulting liquid was further purified by flash-column chromatography (Si-60/hexane). Yield 92%, MS(EI)  $m/z$ (%) 290 (1)  $[\text{M}^+]$ , 275 (42)  $[\text{M}^+ - \text{CH}_3]$ , 163 (26), 133 (26), 97 (28), 73 (100), 59 (28). For the preparation of **4**, the combined fractions were not washed, and solvents were removed under reduced pressure. To the resulting brown liquid was added a suspension of  $\text{KF} \cdot \text{H}_2\text{O}$  in DMF (200 mol% in 50 mL), after which the mixture was stirred vigorously at room temperature for 1 h. The reaction mixture was quenched by pouring it into a suspension of crushed ice in aqueous HCl (100 mL, 3M). The mixture was extracted with diethyl ether, and the combined fractions were washed with a saturated bicarbonate solution and brine, and dried over  $\text{MgSO}_4$ . Solvents were removed under reduced pressure, and the resulting liquid was purified by flash-column chromatography (Si60/hexane) yielding the product as a yellow oil (92%).<sup>47-49</sup>

**Synthesis of (E)-hexadeca-3-en-1-yne (3):** This compound was synthesized according to a literature procedure,<sup>50</sup> using **4** as precursor, and purified by prep-HPLC ( $\text{C}_{18}$  reversed phase/MeOH) to achieve 99.9% purity as determined with GC-MS. Yield: 90%.  $^1\text{H}$ -NMR (400 MHz,  $\text{C}_6\text{D}_6$ )  $\delta$  0.91 (t,  $J = 6.8$  Hz, 3H), 1.13-1.29 (m, 20H), 1.82 (m, 2H), 3.01 (s, 1H), 5.52 (d,  $J = 15.6$  Hz, 1H), 6.18 (m, 1H).  $^{13}\text{C}$ -NMR (100 MHz,  $\text{C}_6\text{D}_6$ )  $\delta$  14.39 ( $\text{CH}_3$ ), 23.15, 29.00, 29.14, 29.42, 29.59, 29.85, 30.01, 30.13, 30.16, 30.74, 33.31, 92.79 ( $\text{HC}\equiv\text{C}$ -), 105.08

( $\text{HC}\equiv\text{C}-$ ), 110.58 ( $\equiv\text{C}-\text{CH}=\text{}$ ), 146.12 ( $\text{C}=\text{CH}-\text{CH}_2$ ). MS (EI)  $m/z(\%)$  220 (1) [ $\text{M}^+$ ], 135 (23), 121 (37), 107 (38), 93 (74), 79 (100), 67 (54), 55 (54).

### 4.3 Results and Discussion

#### 4.3.1 Radical addition

The kinetics of the addition of an unsaturated carbon chain to silyl radical **2** were determined via competition reactions. Such reactions were carried out with known initial reagent concentrations (alkenes, alkynes and aldehydes), in degassed benzene at ambient temperature. The radical reaction was initiated by UV-induced homolytic cleavage of di-*tert*-butylperoxide ( $\lambda_{\text{exc}} = 320 \text{ nm}$ ), which was present at low concentrations ( $27 \mu\text{M}$ ) in the reaction mixture. The formed *t*-butoxyl radicals reacted with **1** generating a silyl radical (**2**;  $[(\text{CH}_3)_3\text{Si})_3\text{Si}\cdot]$ ), which subsequently reacted with the unsaturated compounds present (Figure 3).

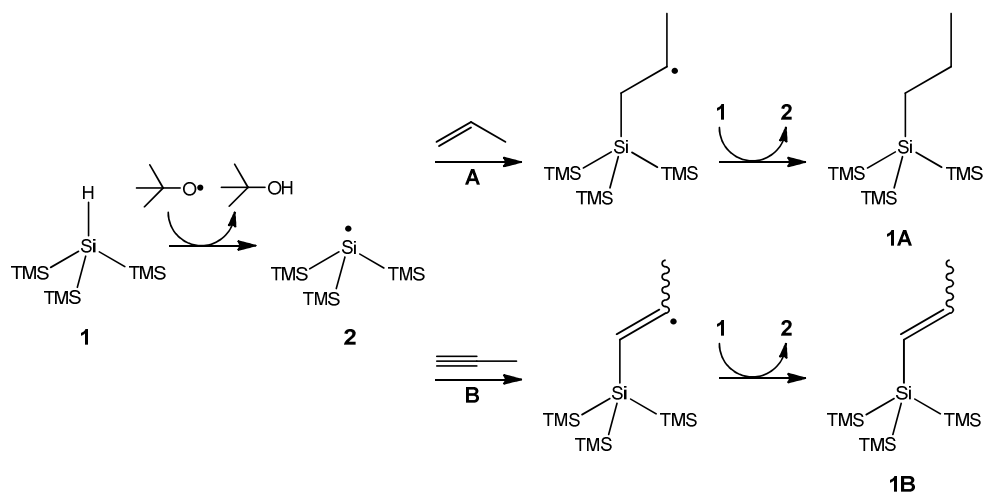


**Figure 3.** Formation of silyl radicals and subsequent competition reactions with alkenes and alkynes leading to hydrosilylation products **1A** and **1B**.

The radical addition reaction is a bimolecular process and thus dependent on the concentration of both the silyl radical as well as the reagent. From Figure 1 and Eq 1 it follows that at low conversion ( $< 5 \%$  of **1** reacted) the ratio of rate constants for alkenes

and alkynes, the so-called reactivity ratio  $r$ ,<sup>51</sup> can be derived from the ratio of product concentrations:

$$\text{Product ratio} = \frac{k_A}{k_B} = r \quad (1)$$

Product formation, as well as conversion of **1**, were determined by GC-MS analysis of the product mixture using hexadecane as an internal standard. Table 1 depicts the product ratios of various reagents versus 1-decene (Entry 1). Since alkenes have traditionally been most commonly employed in monolayer fabrication,<sup>1,4,13,15</sup> 1-decene is set to a reactivity of 1. Competition reactions employing 1-decyne revealed a 7.5-fold increase in reactivity as compared to 1-decene (Entry 2). This is in good agreement with the findings of Gooding and coworkers, who found that alkynes are up to 9 times more reactive than alkenes upon reaction with hydrogen-terminated Si(100).<sup>52</sup> This difference in reactivity was also demonstrated for Si(111) surfaces, where alkynes were shown to react faster, and also led to more densely packed monolayers.<sup>53,54</sup> Interestingly, the reactivity of 1-undecanal showed a dramatic 30-fold decrease as compared to 1-decene (Entry 3). A similar difference in reactivity for aldehydes and alkenes was observed for monolayer experiments on H-Si(111), where monolayers prepared from  $\omega$ -functional  $\alpha$ -alkenal showed 10% attachment via an Si-O bond versus 90% attachment via an Si-C bond.<sup>55</sup>

**Table 1.** Product ratios of the reaction of **2** with different nucleophiles.

Entry	Nucleophile	Ratio
1	1-decene	1
2	1-decyne	7.50 ( $\pm$ 0.07)
3	1-undecanal	$3.3 (\pm 0.1) \times 10^{-2}$
4	phenylacetylene	$91 \pm 5$
5	( <i>E</i> )-hexadec-3-en-1-yne ( <b>3</b> )	$2.0 (\pm 0.1) \times 10^2$
6	hexadeca-1,3-diyne ( <b>4</b> )	$1.40 (\pm 0.07) \times 10^3$

The reactivity of unsaturated hydrocarbons has been suggested earlier to depend on the stabilization of the  $\beta$ -radical that forms upon addition, and that better stabilization of this radical may be achieved by introducing conjugation.<sup>38</sup> Hence, phenylacetylene was predicted to be more reactive than alkenes and alkynes.<sup>38,39</sup> A remarkable 100-fold increase in reactivity with respect to 1-decene was observed for phenylacetylene (Entry 4). Comparison of these results with monolayer experiments is naturally very interesting, but not trivial. Densely packed monolayers have indeed been prepared from phenylacetylene and styrene, due to the  $\pi\pi$ -stacking of the phenyl rings.<sup>56</sup> However, the footprint of the phenyl ring is appreciably bigger than that of an alkyl chain and also of a single Si-H site on the surface. As a result the density of such monolayers cannot be compared directly with that of linear species, while the thus modified surfaces are also more prone to oxidation. This combination of desirable high rates due to conjugation effects, but undesirably large footprints led us to define alternative precursor molecules with longer alkyl chains to study the effects of molecular conjugation on monolayer formation. Therefore, the doubly unsaturated linear hydrocarbons (*E*)-hexadec-3-en-1-yne (**3**) and hexadeca-1,3-diyne (**4**) were prepared. These compounds have a significantly smaller Van der Waals radius and may be more suitable for monolayer fabrication than phenylacetylene. From the reactions between these compounds and **2**, it becomes clear that molecular conjugation plays a significant role, as **3** displays a promising 200-fold increase of reactivity as compared to 1-decene (Entry 5). Interestingly, **4** even shows a dramatic increase in reactivity of a factor 1400 versus 1-decene (Entry 6). Hence, these compounds **3** and **4** are the first compounds that show real promise to further improve upon the quality of monolayer formation (both in terms of rate of formation and packing density) in comparison to the currently most favorable agent, 1-alkynes. This would be a big step forward, since monolayer formation can in that case compete better with device-disturbing oxidation processes, and thus further enhance the potential of modified silicon surfaces. Such monolayer formation is currently being studied in our labs.

Although the discussed reactivity ratios observed for our Si<sub>4</sub>-radical model (entries 1-4) correspond to earlier observed differences in the rates of monolayer formation, they only reflect the overall result of a radical reaction, and the detailed activation barriers of the two propagation steps may show a different picture for the individual reactions. Indeed, calculations performed by Selloni and coworkers revealed that acetylene requires a higher activation energy (3.5 kcal mol<sup>-1</sup>) for the addition step than ethylene (0.92 kcal mol<sup>-1</sup>).<sup>39</sup> If this would be rate limiting, then it would imply that alkenes react faster than alkynes, which is in contrast with experimental findings.<sup>53,54</sup> For the subsequent hydrogen abstraction from the Si surface, a lower activation barrier was calculated for alkynes (-2.3 kcal mol<sup>-1</sup> vs. initial situation) than for alkenes (+7.6 kcal mol<sup>-1</sup> vs. initial situation). In fact, for alkenes this activation barrier is even higher than the barrier for the reverse reaction, i.e. desorption from the surface. It was therefore suggested that alkenes are equally likely to desorb from



the surface as they are to pick up an adjacent hydrogen atom from the surface. This would lead to slower monolayer formation for alkenes, in agreement with the monolayer experiments mentioned above.<sup>52-54</sup> Such a dissociative reverse reaction may also influence our current experimental data, as only the final products are studied and reversible product formation (i.e. involving dissociation) cannot be monitored. The here obtained reactivity ratios reflect the net reactivity, which may differ from the actual rate for addition. However, the significantly lower reactivity of 1-undecanal (Entry 3) with respect to 1-decene contrasts with the calculations of Selloni and coworkers, which suggest a higher reactivity of aldehydes than alkenes or even alkynes.<sup>38</sup> The calculated activation barrier for addition of formaldehyde (+0.69 kcal mol<sup>-1</sup>) is significantly lower, than the aforementioned barrier for ethylene. The activation barrier for the subsequent hydrogen shift, from the Si surface to the  $\beta$ -siloxyl radical, was calculated to be even lower than the barrier for alkynes.<sup>38</sup> According to our experiments, however, aldehydes are less reactive towards the silyl radical than alkenes or alkynes (Entry 3), showing the need for an additional theoretical approach.

#### 4.3.2 Addition of unsaturated species to Si radicals: theory versus experiment

In order to investigate the discrepancies between the theoretical data available from the literature and our experimental results concerning the silyl radical, quantum chemical calculations were performed using a model derived from **1**. The methyl groups of **1** were replaced by hydrogen atoms, resulting in the Si<sub>4</sub>-model as depicted in Figure 4. Reaction enthalpies ( $\Delta H_{\text{reagent}}$ ) and activation enthalpies ( $\Delta H^\ddagger$ ) were calculated using the B3LYP/6-311G(d,p) level of theory as the difference between the enthalpies of the product and reagents, and between those of the transition state (TS) and the reagents, respectively. Reaction rates were calculated using equation 2.<sup>57</sup>

$$k(T) = \frac{k_B T}{hc} e^{\frac{-\Delta G^\ddagger}{RT}} = \frac{k_B T}{hc} e^{\frac{\Delta S^\ddagger}{R}} e^{\frac{-\Delta H^\ddagger}{RT}} = \frac{k_B T}{hc} \frac{Q^\ddagger}{\prod_i Q_i^{\text{reagents}}} e^{\frac{-\Delta H^\ddagger}{RT}} \quad (2)$$

where  $T$  is temperature (in K; here  $T = 298$  K),  $c$  is concentration (here  $c = 1$  M),  $k_B$  is Boltzmann's constant,  $h$  is Planck's constant,  $\Delta G^\ddagger$  is Gibbs free energy of activation,  $Q$  is the partition function of the TS and the separately optimized reagents, and  $\Delta H^\ddagger$  is the enthalpy-corrected energy difference of the TS and the reagents when optimized together.

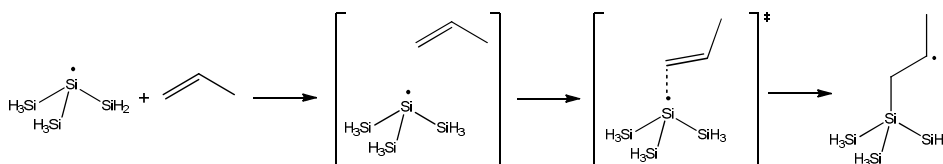


**Figure 4.** Si<sub>4</sub>-model used for calculating barrier and reaction enthalpy.

Application of the approach outlined in Equation 2 leads to a highly accurate prediction of reaction rates. Table 2 shows the Gibbs free barrier energies and the calculated reaction rates; in Figure 5, the calculated relative reactions rates (with respect to 1-decene) are plotted against the experimental data. An excellent correlation ( $r^2 = 0.993$ ) between the experimental and theoretical data sets is observed, showing the predictive power of this computational approach. In more detail, it is e.g. observed that the theoretical rates for 1-butene and 1-butyne show a near 5-fold difference, which is close to the experimentally determined ratio of 7. However, not only the ratios are predicted correctly as indicated by the high correlation coefficient and the slope close to unity (0.94), but also the absolute values are calculated with high accuracy. For example, the *ab initio*-calculated rate for 1-butene,  $6.5 \times 10^5 \text{ M}^{-1} \text{ s}^{-1}$  ( $\Delta G^\ddagger = 9.52 \text{ kcal mol}^{-1}$ ), is close to the experimental rate of approximately  $1 \times 10^5 \text{ M}^{-1} \text{ s}^{-1}$  ( $\Delta G^\ddagger = 10.6 \text{ kcal mol}^{-1}$ ) for the addition of **2** to an alkene.<sup>32</sup> Also the rate calculated for 1-propanal closely matches the experimental rate for addition of **2** to a carbonyl group ( $8 \times 10^4 \text{ M}^{-1} \text{ s}^{-1}$  vs.  $4.2 \times 10^4 \text{ M}^{-1} \text{ s}^{-1}$  [or  $\Delta G^\ddagger = 10.8 \text{ kcal mol}^{-1}$  vs.  $11.1 \text{ kcal mol}^{-1}$ ] for the acetone/**2** system).<sup>34</sup> The observed correlation between calculated and experimental rates extends to the conjugated system, as the calculated reaction rate for styrene  $1.8 \times 10^7 \text{ M}^{-1} \text{ s}^{-1}$  ( $\Delta G^\ddagger = 7.55 \text{ kcal mol}^{-1}$ ) closely matches the experimentally determined reaction rates  $\sim 5 \times 10^7 \text{ M}^{-1} \text{ s}^{-1}$  ( $\Delta G^\ddagger = 6.9 \text{ kcal mol}^{-1}$ ),<sup>31,36</sup> Finally, entries 6 and 7 show a significant increase of reactivity, which is consistent with the reactivities reported in Table 1. We therefore conclude that the free energy calculations obtained via Equation 2 for the Si<sub>4</sub>-model provide for the first time an accurate approach to predict the rates of such Si-C bond-forming radical reactions. Analogous approaches using only the theoretical enthalpy data of this model, or using Carr-Parinello data<sup>31,36</sup> showed significantly poorer correlations with experiment (see Appendix 2). Furthermore, the model allows *in silico* testing of reactivity of newly designed precursors for monolayer formation before synthesizing these compounds, which speeds up the experiments.

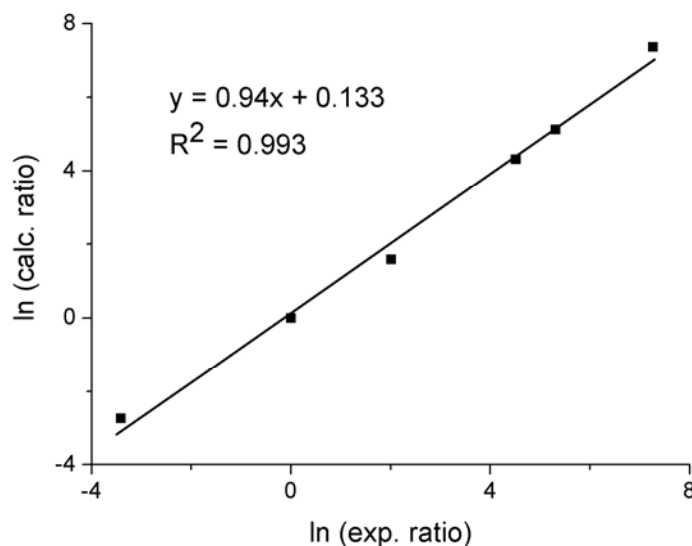


**Figure 5.** Correlation plot of the experimental reaction ratios versus the relative reaction ratio obtained with the Si<sub>4</sub>-model.

**Table 2.** Calculated (B3LYP/6-311G(d,p)) Gibbs free barrier energies and the resulting theoretical reaction rates for radical addition to the Si<sub>4</sub>-model.

Entry	Compound	$\Delta G^\ddagger$ (kcal mol <sup>-1</sup> )	$k$ (M <sup>-1</sup> s <sup>-1</sup> )
1	1-butene	9.52	$6.5 \times 10^5$
2	1-butyne	8.58	$3.2 \times 10^6$
3	1-propanal	11.1	$4.2 \times 10^4$
4	styrene	7.55	$1.8 \times 10^7$
5	phenylacetylene	6.97	$4.8 \times 10^7$
6	penta-1,3-diyne ( <b>5</b> )	5.16	$1.0 \times 10^9$
7	( <i>E</i> )-pent-3-en-3-yne ( <b>6</b> )	6.48	$1.1 \times 10^8$

### 4.3.3 Hydrogen atom transfer at the H-silicon(111) surface.

Optimum monolayer formation hinges partly on a low activation barrier for H-atom transfer, which drives further investigations into the factors governing this. In order to calculate the energies involved in H-atom transfer at the silicon surface, i.e. the second propagation step, a model of a H-Si(111) surface was constructed. This Si<sub>7</sub>-model consists of a silicon backbone that was isolated from a silicon surface slab that was constructed and optimized in the PCFF force field in Materials Studio (Figure 6).<sup>44,58</sup> In order to preserve the surface geometry of the Si-H sites, the positions of the five back-bonded SiH<sub>3</sub> groups were fixed during the optimizations, while the two central Si-H sites were allowed to relax. Vibrational frequency analysis on the resulting geometries showed small imaginary frequencies that were not related to transition states, but arise from these constraints set on the molecule. To rule out any errors resulting from these vibrations, calculations were also performed without any set constraints. This did not result in significant differences in the energy levels of the reagent and product geometries, but geometrical fixation of these five Si atoms is essential to mimic the TS for chemisorption, as otherwise the ring strain that develops is alleviated by significant repositioning of these backbone Si atoms.

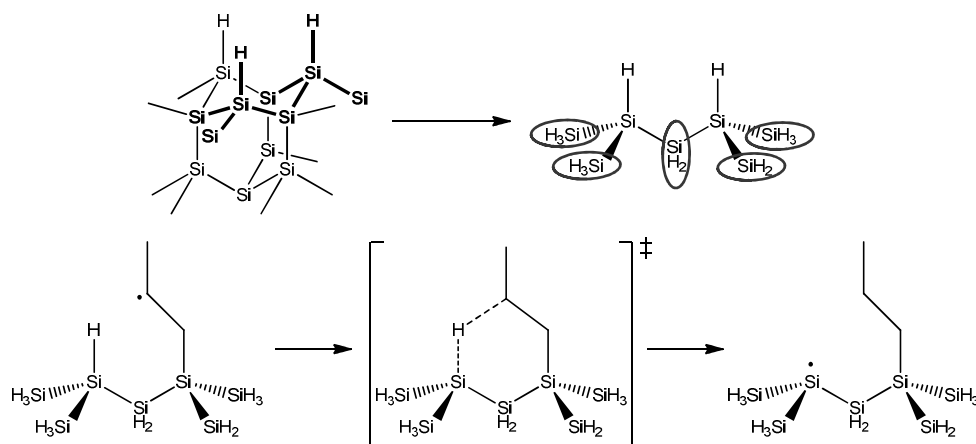


**Figure 6.** Silicon structure isolated from surface slab (top left), and fixation of back-bonded silicon groups (encircled; top right); schematic input geometries for DFT calculations (bottom).

The results of these calculations on the hydrogen-transfer reaction are summarized in Table 3. Entries 1 and 2 demonstrate that the reaction energies of 1-butene and 1-butyne lie far apart (-9.48 and -18.58 kcal mol<sup>-1</sup>, respectively). Moreover, the barrier for the alkyne is significantly smaller than that found for the alkene (12.71 vs. 18.17 kcal mol<sup>-1</sup>, respectively). These trends are consistent with literature values obtained from calculations

on a larger surface-slab,<sup>39</sup> and with the appreciably faster formation of alkyne-derived monolayers.<sup>53,54</sup> The differences in the calculated energies between the reactivity of alkynes and alkenes presented here may be explained by the high C-H bond strength on an sp<sup>2</sup>-hybridized carbon atom in comparison to an sp<sup>3</sup>-hybridized carbon atom (characteristic difference of ~13 kcal/mol).<sup>59,60</sup> This results in a large energy gain when a H-atom is transferred from an Si-H site at the surface to the vinyl radical. Interestingly, the reaction and barrier energies for 1-butene and 1-propanal (Entry 3) differ much less, with e.g. H-transfer energy barriers for alkenes and aldehydes of 18.17 and 18.85 kcal/mol, respectively. Apparently, the oxygen atom next to the  $\beta$ -carbon radical results only in minor stabilization, which is supported by C-H BDEs determined for comparable structures (97.8 kcal mol<sup>-1</sup> for alkyl-H and 95.9 kcal mol<sup>-1</sup> for an alkoxy-H, respectively).<sup>60,61</sup> These data imply that the H-transfer reaction at the surface proceeds faster with alkynes than with alkenes or aldehydes. This is in contrast with earlier literature findings, where the barrier for aldehydes was calculated to be significantly smaller than for alkenes or alkynes by 8 and 4 kcal mol<sup>-1</sup>, respectively.<sup>38</sup> However, only with our current data – predicting a higher barrier for Si-C bond formation and a similar barrier for H-atom transfer – it becomes evident why aldehydes react slower in monolayer formation as observed experimentally in Gooding's competition reaction.<sup>52</sup>

**Table 3.** Reaction and activation energies calculated for the surface model.

Entry	Compound	$\Delta E_{\text{react}}$	$\Delta E^\ddagger$	BDE
<b>1</b>	1-butene	-9.48	18.17	<b>97.8</b>
<b>2</b>	1-butyne	-18.58	12.71	<b>111.2</b> <sup>59</sup>
<b>3</b>	butanal	-8.45	18.85	<b>95.9</b>
<b>4</b>	styrene	2.55	25.09	<b>85.4</b>
<b>5</b>	phenylacetylene	-7.88	18.31	-
<b>6</b>	penta-1,3-diyne ( <b>5</b> )	-7.61	19.39	-
<b>7</b>	<b>(E)-pent-3-en-1-yne (6)</b>	<b>-7.32</b>	<b>21.89</b>	-

B3LYP/6-311G(d,p) calculations; all energies in kcal mol<sup>-1</sup>. BDEs obtained from literature.<sup>59-62</sup>

The influence of stabilization of the  $\beta$ -radical becomes apparent in the case of hydrogen transfer from the silicon surface to a styryl radical, which is calculated to be slightly endothermic (Entry 4). The reaction barrier is also considerably higher than for other precursor molecules, indicating that the propagation reaction is relatively slow. Another indication of the stabilization effects of the  $\pi$ -system is the BDE of the vinylic  $\alpha$ -C-H bond in styrene. In this respect, phenylacetylene is an interesting precursor molecule as it contains both a radical-stabilizing  $\pi$ -system as well as the ability to form an intrinsically less stable vinyl radical upon Si-C bond formation. The increased reactivity with respect to styrene is demonstrated by the differences in reaction energies and barrier energies with styrene, which are roughly of the same order as the differences between 1-butyne and 1-butene (10.4 and 6.8 kcal mol<sup>-1</sup> for phenylacetylene and styrene, as compared to 9.4 and 5.5 kcal mol<sup>-1</sup> for 1-butyne and 1-butene, respectively). The extent of conjugation does not significantly influence the reaction energy, as phenylacetylene, **5** and **6** all display approximately the same reaction energies of -7 kcal mol<sup>-1</sup>. This means that the lower barriers found for the Si-C bond formation step for **5** and **6** are offset by higher activation barriers for the H-transfer step. As a result, detailed experimental studies are needed to see how the balance between these two factors works out in actual monolayer formation, in which packing energies also play a role in determining the driving force of the reactions, and will likely thus influence the experimentally observed reaction times that are needed to form a densely packed monolayer. Figure 7 displays the good correlation of the calculated reaction barriers obtained using this Si<sub>7</sub>-model, with available experimental BDEs. This allows for prediction of the order of reactivity of the carbon radicals in the hydrogen abstraction reaction. From the above results we conclude that the non-stabilized vinyl radical (resulting from the Si-C bond forming reaction of an alkyne) is the most reactive, while styrene is by far the least reactive. Surprisingly, all other barriers in Table 4 show actually only little variation.

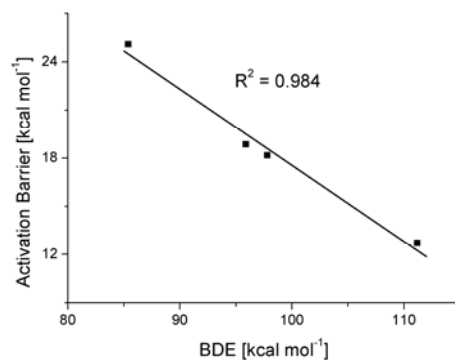


**Figure 7.** Correlation plot of experimental BDEs vs. activation barriers calculated with the Si<sub>7</sub>-model.

The entropy contribution to the activation barrier, however, could not be calculated. The geometric constraints that were used during the calculations resulted in imaginary frequencies that affected the entropy values. The reaction rate for the abstraction of hydrogen from **1** by a simple alkyl radical was determined to be  $1 - 3 \times 10^5 \text{ M}^{-1} \text{ s}^{-1}$ .<sup>63</sup> This rate is of the same order of magnitude as the rate for addition of an alkene to **1**, as discussed in the previous paragraph. However, as this H-transfer rate is based on freely moving molecules of **1** instead of on an intramolecular reaction with a fixed silicon chain, the actual H-transfer rate is most likely lower. This is also confirmed by calculations that were performed on the unconstrained Si<sub>7</sub>-model. Indeed, the reaction barriers were lowered considerably if the Si<sub>7</sub>-model was allowed to fully relax in the TS, thereby releasing the ring strain caused by that fact that in reality this is a surface-bound reaction. Based on the comparison of calculated activation barriers for the addition reaction and the H-transfer we conclude that the rate of propagation in organic monolayer formation on the H-Si(111) surface is limited by the H-transfer step. This insight allows a more precise focus on the further improvement of monolayer formation. During this process other effects than the ones discussed here may also affect the rate of chemisorption, such as the efficiency of the initiation of the monolayer formation process,<sup>26,37</sup> as well as the energetics of the packing of the monolayer. In addition, when the formation of the monolayer has progressed to a significant degree, the entropy factor in the Si-C bond forming reaction (“finding the empty spots on the almost filled surface”) starts to play a growing role. Recent studies show that the efficiency of packing is partly dependent on the Bohr radius of the precursors used,<sup>45,64</sup> suggesting that the newly designed compounds **3** and **4** are excellent candidates for improved monolayer formation; this is currently under investigation in our labs. Given the high demand for well-defined monolayers onto silicon surfaces, the further development of such materials will likely push the development of the field of hybrid electronics an important step forward.

#### 4.4 Conclusions

A combined experimental and theoretical study of silicon-centered radical **2** [ $((\text{CH}_3)_3\text{Si})_3\text{Si}\bullet$ ] shows that the formation of Si-C bonded monolayers onto hydrogen-terminated silicon surfaces is rate-limited by the rate of hydrogen transfer in one of the propagation steps. The experimental and calculated reactivities of **2** towards alkenes, alkynes and aldehydes are in excellent agreement with results of monolayer formation in earlier literature reports. The theoretical Si<sub>4</sub>-model proves highly accurate, and predicts the usefulness of novel precursors ( $\text{H-C}\equiv\text{C-C}\equiv\text{C-R}$  and  $\text{H-C}\equiv\text{C-CH=CH-R}$ ) for improved monolayer formation.

The calculated activation barriers for the rate-limiting hydrogen abstraction reaction, as modeled with an Si<sub>7</sub>-cluster, display a very good correlation with experimental BDEs of the newly formed C-H bond. This allows for predicting the reactivity of carbon-centered radicals towards the surface-bound hydrogen (Si-H). Speeding up the monolayer formation process by introducing radical-stabilizing groups is therefore unlikely. However, selectivity in the attachment of  $\alpha$   $\omega$ -functional precursors (attachment via the  $\alpha$  or  $\omega$  moiety) or mixed monolayers is solely determined by the radical addition reaction. As the rate thereof can be predicted accurately, combinations of functionalities may be tested *in silico*, and thus minimize synthetic efforts and surface-related experiments. In this respect, the newly designed ene-yne (**3**) and di-yne (**4**) precursors are predicted to yield an improved monolayer formation.

## References

- (1) Ciampi, S.; Harper, J. B.; Gooding, J. J. *Chem. Soc. Rev.* **2010**, *39*, 2158.
- (2) Boukherroub, R. *Curr. Opin. Solid St. M.* **2005**, *9*, 66.
- (3) Wayner, D. D. M.; Wolkow, R. A. *J. Chem. Soc. Perk. Trans. 2* **2002**, 23.
- (4) Buriak, J. M. *Chem. Rev.* **2002**, *102*, 1271.
- (5) Shirahata, N.; Hozumi, A.; Yonezawa, T. *Chem. Rec.* **2005**, *5*, 145.
- (6) Sieval, A. B.; Huisman, C. L.; Schoenecker, A.; Schuurmans, F. M.; Van der Heide, A. S. H.; Goossens, A.; Sinke, W. C.; Zuilhof, H.; Sudhölter, E. J. R. *J. Phys. Chem. B* **2003**, *107*, 6846.
- (7) Zigah, D.; Herrier, C.; Scheres, L.; Giesbers, M.; Fabre, B.; Hapiot, P.; Zuilhof, H. *Angew. Chem. Int. Edit.* **2010**, *49*, 3157.
- (8) Popoff, R. T. W.; Asanuma, H.; Yu, H. Z. *J. Phys. Chem. C* **2010**, *114*, 10866.
- (9) Caipa Campos, M. A.; Paulusse, J. M. J.; Zuilhof, H. *Chem. Commun.* **2010**, 46, 5512.
- (10) Yaffe, O.; Scheres, L.; Puniredd, S. R.; Stein, N.; Biller, A.; Lavan, R. H.; Shpaisman, H.; Zuilhof, H.; Haick, H.; Cahen, D.; Vilan, A. *Nano Lett.* **2009**, *9*, 2390.
- (11) Seitz, O.; Vilan, A.; Cohen, H.; Hwang, J.; Haeming, M.; Schoell, A.; Umbach, E.; Kahn, A.; Cahen, D. *Adv Funct Mater* **2008**, *18*, 2102.
- (12) Seitz, O.; Bocking, T.; Salomon, A.; Gooding, J. J.; Cahen, D. *Langmuir* **2006**, *22*, 6915.
- (13) Sieval, A. B.; Demirel, A. L.; Nissink, J. W. M.; Linford, M. R.; van der Maas, J. H.; de Jeu, W. H.; Zuilhof, H.; Sudhölter, E. J. R. *Langmuir* **1998**, *14*, 1759.
- (14) Linford, M. R.; Fenter, P.; Eisenberger, P. M.; Chidsey, C. E. D. *J. Am. Chem. Soc.* **1995**, *117*, 3145.
- (15) Wang, X. Y.; Ruther, R. E.; Streifer, J. A.; Hamers, R. J. *J. Am. Chem. Soc.* **2010**, *132*, 4048.
- (16) Cicero, R. L.; Linford, M. R.; Chidsey, C. E. D. *Langmuir* **2000**, *16*, 5688.
- (17) Shestopalov, A. A.; Clark, R. L.; Toone, E. J. *Langmuir* **2010**, *26*, 1449.
- (18) Terry, J.; Mo, R.; Wigren, C.; Cao, R. Y.; Mount, G.; Pianetta, P.; Linford, M. R.; Chidsey, C. E. D. *Nucl. Instrum. Meth. B.* **1997**, *133*, 94.



- (19) Cicero, R. L.; Chidsey, C. E. D.; Lopinski, G. P.; Wayner, D. D. M.; Wolkow, R. A. *Langmuir* **2002**, *18*, 305.
- (20) Scheres, L.; Arafat, A.; Zuilhof, H. *Langmuir* **2007**, *23*, 8343.
- (21) Eves, B. J.; Sun, Q.-Y.; Lopinski, G. P.; Zuilhof, H. *J. Am. Chem. Soc.* **2004**, *126*, 14318.
- (22) Mischki, T. K.; Lopinski, G. P.; Wayner, D. D. M. *Langmuir* **2009**, *25*, 5626.
- (23) Stewart, M. P.; Buriak, J. M. *J. Am. Chem. Soc.* **2001**, *123*, 7821.
- (24) Sun, Q.-Y.; De Smet, L. C. P. M.; Van Lagen, B.; Giesbers, M.; Thuene, P. C.; Van Engelenburg, J.; De Wolf, F. A.; Zuilhof, H.; Sudhölter, E. J. R. *J. Am. Chem. Soc.* **2005**, *127*, 2514.
- (25) Sun, Q.-Y.; de Smet, L. C. P. M.; van Lagen, B.; Wright, A.; Zuilhof, H.; Sudhölter, E. J. R. *Angew. Chem. Int. Ed.* **2004**, *43*, 1352.
- (26) Rijksen, B.; van Lagen, B.; Zuilhof, H. *J. Am. Chem. Soc.* **2011**, *133*, 4998.
- (27) Hacker, C. A.; Anderson, K. A.; Richter, L. J.; Richter, C. A. *Langmuir* **2005**, *21*, 882.
- (28) Boukherroub, R.; Morin, S.; Sharpe, P.; Wayner, D. D. M.; Allongue, P. *Langmuir* **2000**, *16*, 7429.
- (29) Boukherroub, R.; Morin, S.; Wayner, D. D. M.; Bensebaa, F.; Sproule, G. I.; Baribeau, J. M.; Lockwood, D. J. *Chem. Mater.* **2001**, *13*, 2002.
- (30) Effenberger, F.; Gotz, G.; Bidlingmaier, B.; Wezstein, M. *Angew. Chem. Int. Edit.* **1998**, *37*, 2462.
- (31) Lalevee, J.; Allonas, X.; Fouassier, J. P. *J. Org. Chem.* **2007**, *72*, 6434.
- (32) Lalevee, J.; Blanchard, N.; Graff, B.; Allonas, X.; Fouassier, J. P. *J. Organomet. Chem.* **2008**, *693*, 3643.
- (33) Chatgililoglu, C.; Griller, D.; Lesage, M. *J. Org. Chem.* **1989**, *54*, 2492.
- (34) Alberti, A.; Chatgililoglu, C. *Tetrahedron* **1990**, *46*, 3963.
- (35) Chatgililoglu, C. *Chem-Eur. J.* **2008**, *14*, 2310.
- (36) Ballestri, M.; Chatgililoglu, C.; Clark, K. B.; Griller, D.; Giese, B.; Kopping, B. *J. Org. Chem.* **1991**, *56*, 678.
- (37) Lee, M. V.; Scipioni, R.; Boero, M.; Silvestrelli, P. L.; Ariga, K. *Phys. Chem. Chem. Phys.* **2011**, *13*, 4862.
- (38) Kanai, Y.; Takeuchi, N.; Car, R.; Selloni, A. *J. Phys. Chem. B* **2005**, *109*, 18889.
- (39) Takeuchi, N.; Kanai, Y.; Selloni, A. *J. Am. Chem. Soc.* **2004**, *126*, 15890.
- (40) Kanai, Y.; Tilocca, A.; Selloni, A.; Car, R. *J. Chem. Phys.* **2004**, *121*, 3359.
- (41) Coletti, C.; Marrone, A.; Giorgi, G.; Sgamellotti, A.; Cerofolini, G.; Re, N. *Langmuir* **2006**, *22*, 9949.
- (42) Yan, H.; Shi, Y. C.; Liu, G.; Yuan, S. L. *Mol. Simulat.* **2008**, *34*, 525.
- (43) Frisch, M. J.; Trucks, G. W.; Schlegel, H. B.; Scuseria, G. E.; Robb, M. A.; Cheeseman, J. R.; Scalmani, G.; Barone, V.; Mennucci, B.; Petersson, G. A.; Nakatsuji, H.; Caricato, M.; Li, X.; Hratchian, H. P.; Izmaylov, A. F.; Bloin, J.; al., e. *Gaussian09* **2009**, revision A.02; Gaussian.
- (44) Maple, J. R.; Hwang, M. J.; Stockfisch, T. P.; Dinur, U.; Waldman, M.; Ewig, C. S.; Hagler, A. T. *J. Comp. Chem.* **1994**, *15*, 162.
- (45) Pei, Y.; Ma, J.; Jiang, Y. S. *Langmuir* **2003**, *19*, 7652.
- (46) Materials Studio 5.0, Accelrys Software Inc, 2009.

- (47) Kim, T.; Crooks, R. M. *Tetrahedron Lett.* **1994**, 35, 9501.
- (48) Li, F.; Shishkin, E.; Mastro, M. A.; Hite, J. K.; Eddy, C. R.; Edgar, J. H.; Ito, T. *Langmuir* **2010**, 26, 10725.
- (49) Xu, Z. C.; Byun, H. S.; Bittman, R. J. *Org. Chem.* **1991**, 56, 7183.
- (50) Miller, J. A.; Zweifel, G. *J. Am. Chem. Soc.* **1983**, 105, 1383.
- (51) Mayo, F. R.; Lewis, F. M. *J. Am. Chem. Soc.* **1944**, 66, 1594.
- (52) Ng, A.; Ciampi, S.; James, M.; Harper, J. B.; Gooding, J. J. *Langmuir* **2009**, 25, 13934.
- (53) Scheres, L.; Giesbers, M.; Zuilhof, H. *Langmuir* **2010**, 26, 4790.
- (54) Scheres, L.; Giesbers, M.; Zuilhof, H. *Langmuir* **2010**, 26, 10924.
- (55) Hong, Q.; Rogero, C.; Lakey, J. H.; Connolly, B. A.; Houlton, A.; Horrocks, B. R. *Analyst* **2009**, 134, 593.
- (56) Kondo, M.; Mates, T. E.; Fischer, D. A.; Wudl, F.; Kramer, E. J. *Langmuir* **2010**, 26, 17000.
- (57) Vos, A. M.; De Proft, F.; Schoonheydt, R. A.; Geerlings, P. *Chem. Comm.* **2001**, 1108.
- (58) Sieval, A. B.; Vleeming, V.; Zuilhof, H.; Sudholter, E. J. R. *Langmuir* **1999**, 15, 8288.
- (59) Ervin, K. M.; Gronert, S.; Barlow, S. E.; Gilles, M. K.; Harrison, A. G.; Bierbaum, V. M.; Depuy, C. H.; Lineberger, W. C.; Ellison, G. B. *J. Am. Chem. Soc.* **1990**, 112, 5750.
- (60) Seetula, J. A.; Slagle, I. R. *J. Chem. Soc. Faraday T.* **1997**, 93, 1709.
- (61) Johnson, R. D.; Hudgens, J. W. *J. Phys. Chem.* **1996**, 100, 19874.
- (62) Mcmillen, D. F.; Golden, D. M. *Annu. Rev. Phys. Chem.* **1982**, 33, 493.
- (63) Chatgililoglu, C.; Dickhaut, J.; Giese, B. *J. Org. Chem.* **1991**, 56, 6399.
- (64) Scheres, L.; Rijksen, B.; Giesbers, M.; Zuilhof, H. *Langmuir* **2011**, 27, 972.

## Chapter 5

### Hexadecadienyl Monolayers on H- Si(111): Faster Monolayer Formation and Improved Surface Coverage Using the Enyne Moiety

**Abstract.** To further improve the coverage of organic monolayers on hydrogen-terminated silicon (H-Si) surfaces with respect to the hitherto best agents (1-alkynes), it was hypothesized that enynes ( $\text{H-C}\equiv\text{C-HC=CH-R}$ ) would be even better reagents for dense monolayer formation. To investigate whether the increased delocalization of  $\beta$ -carbon radicals by the enyne functionality indeed lowers the activation barrier, the kinetics of monolayer formation by hexadec-3-en-1-yne and 1-hexadecyne on H-Si(111) were followed by studying partially incomplete monolayers. Ellipsometry and static contact angle measurements indeed showed a faster increase of layer thickness and hydrophobicity for the hexadec-3-en-1-yne-derived monolayers. This more rapid monolayer formation was supported by IRRAS and XPS measurements that for the enyne show a faster increase of the  $\text{CH}_2$  stretching bands and the amount of carbon at the surface (C/Si ratio), respectively. Monolayer formation at room temperature yielded plateau values for hexadec-3-en-1-yne and 1-hexadecyne after 8 and 16 h, respectively. Additional experiments were performed for 16 h at  $80^\circ$  to ensure full completion of the layers, which allows comparison of the quality of both layers. Ellipsometry thicknesses (2.0 nm) and contact angles ( $111 - 112^\circ$ ) indicated a high quality of both layers. XPS, in combination with DFT calculations, revealed terminal attachment of hexadec-3-en-1-yne to the H-Si surface, leading to dienyl monolayers. Moreover, analysis of the  $\text{Si}_{2p}$  region showed no surface oxidation. Quantitative XPS measurements - obtained via rotating Si samples - showed a higher surface coverage for  $\text{C}_{16}$  dienyl layers than  $\text{C}_{16}$  alkenyl layers (63% vs. 59%). The dense packing of the layers was confirmed by IRRAS and NEXAFS results. Molecular mechanics simulations were undertaken to understand the differences in reactivity and surface coverage. Alkenyl layers show more favorable packing energies for surface coverages up to 50 - 55%. At higher coverages this packing energy rises quickly, and there the dienyl packing becomes more favorable. When the binding energies are included the difference becomes more pronounced, and dense packing of dienyl layers becomes more favorable by 2-3 kcal/mol. These combined data show that enynes provide the highest-quality organic monolayers reported on H-Si onto now.

**This chapter is submitted as:**

“Hexadecadienyl Monolayers on Hydrogen-terminated Si(111): Faster Monolayer Formation and Improved Surface Coverage Using the Enyne Moiety”, Bart Rijkse & Sidharam Pujari, Luc Scheres, Cees J. M. van Rijn, J.E. Baio, Tobias Weidner, and Han Zuilhof 2012.

## 5.1 Introduction

Long-term passivation of oxide-free silicon surfaces can be achieved by the covalent attachment of self-assembled monolayers onto hydrogen-terminated silicon surfaces (H-Si). Not only can these thin organic layers protect the surface from oxidation, they also form a versatile scaffold for (bio)functionalization.<sup>1-6</sup> Many methods and procedures to produce these layers have been described in literature, including thermal<sup>7,8</sup> and UV<sup>9-12</sup> methods, electrochemistry,<sup>13,14</sup> and chemomechanical scribing.<sup>15,16</sup> However, under those reaction conditions side reactions might occur, thereby reducing the quality of the produced layers.<sup>17,18</sup> Milder methods, which invoke a substantially lower energy input, have been shown to overcome these issues, though at cost of longer reaction times.<sup>19,20</sup> Hence, a reduction of the reaction time under these mild reaction conditions, while maintaining the oxide-free nature of the organic monolayer-silicon interface, might bring application of these layers in (bio)electronic devices within reach.<sup>21-25</sup>

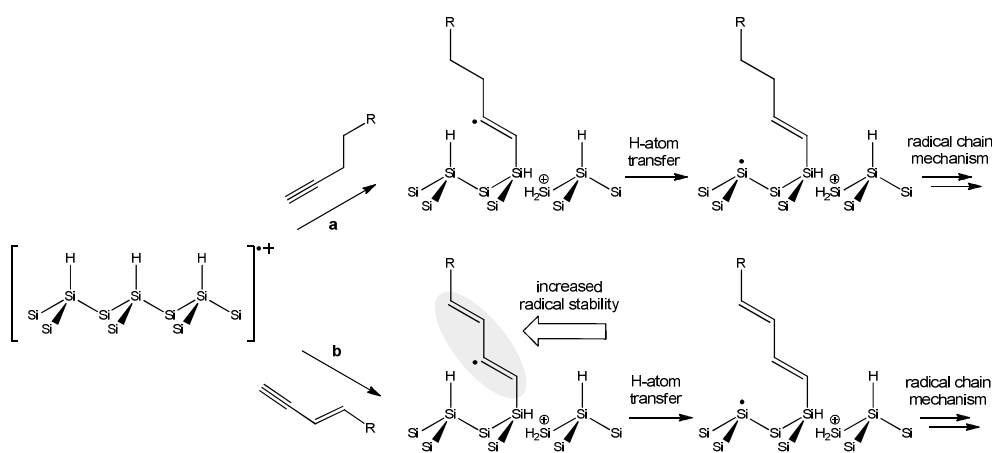
For these potential applications the stability of the oxide-free monolayer-silicon interface is one of the most important properties, for which oxidation is a hampering factor both during and after the modification process.<sup>26,27</sup> During the formation of the – not yet complete – monolayer, oxidation by traces of oxygen present in the precursor or reaction flask might be relatively fast, and competes with the precursors for reactive surface sites. After completion of the monolayer the oxidation rate is relatively slow due to the limited diffusion of oxygen through the monolayer<sup>28</sup> but even there, only a small fraction of defects in the monolayer is already sufficient to cause detectable amounts of oxide after prolonged storage in ambient conditions.<sup>29</sup> In order to further improve the stability of the oxide-free monolayer-silicon interfaces, both oxidation routes need to be suppressed via a combination of faster attachment and a higher packing density.

One of the current theories that explains mild attachment, involves initiation by nucleophilic attack of the precursors to delocalized silyl radical cations at the H-Si surface (see Figure 1).<sup>5,6,30</sup> Hence, better nucleophiles will improve the initial attack on the delocalized radical cations and therefore facilitate C-Si bond formation. In addition, recent studies have shown that stabilizing the  $\beta$ -carbon radical intermediate by a neighboring  $\pi$ -system speeds up the propagation of the radical chain mechanism and thereby monolayer formation.<sup>31-33</sup> In accordance with the above, a significant higher reactivity of  $\omega$ -alkynes compared to  $\omega$ -alkenes has been demonstrated on H-Si(100) and H-Si(111) surfaces.<sup>34,35</sup>

Besides the reactivity, also the shape and footprint of the precursor are important parameters, as both can have a tremendous influence on the packing, and thus on the stability of the layer.<sup>36</sup> Limited by steric constraints and unfavorable conformations of the carbon chains near the surface, numerous studies have reported a maximum surface

coverage of 50-55% for alkyl monolayers on Si(111).<sup>7,9,35,37-42</sup> However, by introducing moieties with a smaller Van der Waals radius than a regular CH<sub>2</sub>-group, i.e., a smaller footprint, packing densities as high as ~67% have been obtained for long alkoxy (Si-O-C) monolayers<sup>40,43,44</sup> and for C<sub>18</sub> alkenyl (Si-C=C) monolayers on H-Si(111).<sup>19,35,36</sup> Obviously, this is a clear indication that even minor structural differences in the linkage can have a major effect on the overall monolayer structure. In addition, regarding the long term stability of the oxide-free interface, we note that a higher surface coverage will not only slow down diffusion of water and oxygen through the monolayer, but will also result in slightly reduced numbers of unreacted H-Si sites at the interface.

All these findings encouraged us to design two new precursors with a further increased reactivity and the proper geometrical requirements. As can be seen in Scheme 1, both candidate structures (hexadec-3-en-1-yne and 1,3-hexadecadiyne) possess a conjugated reactive terminal functionality, which is expected to enhance the nucleophilic attack at the silicon surface and might improve subsequent stabilization of the  $\beta$ -carbon radical intermediate by the neighboring  $\pi$ -system. Furthermore, since CH=CH moieties have a significantly smaller footprint than CH<sub>2</sub>-CH<sub>2</sub> moieties, the smaller Van der Waals radius of both linkages to the silicon surface (Si-HC=CH-HC=CH- and Si-HC=CH-C $\equiv$ C-, respectively) meet the requirements to obtain high surface coverage organic monolayers.



**Scheme 1.** Mechanistic hypothesis that initiated study of enynes for monolayers on H-Si(111): Nucleophilic attack of (a) 1-alkynes and (b) 3-en-1-ynes to delocalized radical cations at the silicon surface result in the formation of  $\beta$ -carbon radicals. Subsequent transfer of a hydrogen atom from a neighboring Si-H site then results in the formation of a surface-centered radical.

In a recent photospectroscopic study the reactivity of these two candidate structures towards silyl radicals has been investigated.<sup>31</sup> It was shown that hexadec-3-en-1-yne and 1,3-hexadecadiyne are both at least 30 times more reactive than 1-alkynes. However, preliminary results of monolayer-forming experiments showed that diynes polymerize under monolayer-forming conditions, which precludes their use in this.

The above ideas and results stimulated us to investigate the kinetics of monolayer formation with hexadec-3-en-1-yne on hydrogen-terminated Si(111) in detail. To visualize a possible enhanced reactivity of the 3-en-1-yne functionality compared to 1-alkynes, 1-hexadecyne-derived monolayers were used as a reference. The kinetics of the surface attachment reactions were followed by studying partially complete monolayers obtained after fixed times by static contact angle measurements, ellipsometry, infrared reflective absorption spectroscopy (IRRAS), and x-ray photoelectron spectroscopy (XPS). Next, in order to reveal the influence of the structurally different linkage to the H-Si(111) substrate (Si-C=C-C=C versus Si-C=C) on the quality and structure of the final monolayers, fully completed hexadecadienyl and hexadecenyl monolayers were thoroughly studied by additional quantitative XPS measurements involving rotating Si samples to exclude crystal reflection effects,<sup>35,39</sup> DFT calculations and near-edge x-ray absorption fine structure (NEXAFS) measurements. Finally, a combined *ab initio* and molecular mechanics molecular modeling study was undertaken to provide insight into the subtle chemical and structural differences responsible for the observed reactivity and quality difference between alk-3-en-1-yne and in 1-alkyne-derived monolayers. The resulting picture clarifies the potential of novel, high-reactivity moieties for the attachment of organic monolayers onto H-Si surfaces.

## 5.2 Experimental Section

### 5.2.1 Materials

Bis(trimethylsilyl)-1,3-butadiyne (96%), 1-bromododecane (99%), potassium fluoride dihydrate, DMF, HMPA, methyllithium/LiBr in diethylether (1.6 M), diisobutylaluminumhydride in pentane (1.6 M), DME (anhydrous), and n-butyllithium in pentane (1.6 M), acetone (semiconductor grade VLSI PURANAL Honeywell 17617) and sulfuric acid (95-97%) were obtained from Sigma-Aldrich. From other sources we purchased hydrogen peroxide (Acros Organics, 35%) ammonium fluoride (Riedel-de Haën, 40%, semiconductor grade VLSI PURANAL Honeywell 17600), deionized water (resistivity 18.3 MΩ cm), pentane (VWR, 95%). 1-Hexadecyne (90%, ABCR, Germany) was purified by column chromatography (hexane) to remove trace amounts of 1-bromoalkane, and subsequently distilled twice under reduced pressure before use. Silicon

wafers were (111)-oriented, single-side or doubly polished (500-550  $\mu\text{m}$  thick, n-type doping by phosphorus), and have a resistivity of 2.0 - 8.0  $\Omega\text{ cm}$  (Siltronix, France).

### 5.2.2 Equipment

NMR spectra were recorded on a Bruker Avance III with an inverse broadband probe running at 400 MHz, with  $\text{C}_6\text{D}_6$  as solvent. Hexadeca-3-en-1-yne was purified by HPLC (Shimadzu, ALLTIMA C18 5U column, MeOH, 15 mL/min, UV detection at 215 nm).

### 5.2.3 Preparation of Materials

**Synthesis of hexadeca-3-en-1-yne:** This compound was synthesized according to a literature procedure,<sup>45</sup> using 1-tris(trimethyl)silyl-1,3-hexadeca-di-yne<sup>46,47</sup> as precursor, and purified by prep-HPLC ( $\text{C}_{18}$  reversed phase/MeOH) to achieve 99.9% purity as determined with GC-MS. Yield: 90%.  $^1\text{H-NMR}$  (400 MHz,  $\text{C}_6\text{D}_6$ )  $\delta$  0.91 (t,  $J = 6.8\text{ Hz}$ , 3H), 1.13-1.29 (m, 20H), 1.82 (m, 2H), 3.01 (s, 1H), 5.52 (d,  $J = 15.6\text{ Hz}$ , 1H), 6.18 (m, 1H).  $^{13}\text{C-NMR}$  (100 MHz,  $\text{C}_6\text{D}_6$ )  $\delta$  14.39 ( $\text{CH}_3$ ), 23.15, 29.00, 29.14, 29.42, 29.59, 29.85, 30.01, 30.13, 30.16, 30.74, 33.31, 92.79 ( $\text{HC}\equiv\text{C-}$ ), 105.08 ( $\text{HC}\equiv\text{C-}$ ), 110.58 ( $\equiv\text{C-CH=}$ ), 146.12 ( $\text{C=CH-CH}_2$ ). MS (EI)  $m/z(\%)$  220 (1) [ $\text{M}^+$ ], 135 (23), 121 (37), 107 (38), 93 (74), 79 (100), 67 (54), 55 (54).

**Hydrogen-terminated Si(111) surfaces (H-Si(111)):** H-Si(111) was prepared by chemical etching as previously reported.<sup>48,49</sup> All liquid reagents were continuously purged with an argon flow. An n-type Si (111) wafer with a  $0.2^\circ$  miscut angle along  $\langle 112 \rangle$ , was first cut ( $10 \times 10\text{ mm}^2$ ) and subsequently cleaned in a sonication bath with acetone and then with Milli-Q water (resistivity  $>18\text{ M}\Omega\text{ cm}$ ). The Si wafer was oxidized in freshly prepared piranha solution ( $\text{H}_2\text{SO}_4/\text{H}_2\text{O}_2$  3:1) for at least 20 min. After piranha treatment, the substrates were immersed immediately in water and rinsed thoroughly, followed by drying with a stream of argon. Subsequently, the substrates were etched in an argon-saturated 40% aqueous  $\text{NH}_4\text{F}$  solution for 15 min, rinsed by Milli-Q water, and finally dried with a stream of argon. The H-Si surfaces were studied by X-ray photoelectron spectroscopy (XPS) and atomic force microscopy.

### 5.2.4 Preparation of Hexadec-3-en-1-yne and 1-Hexadecyne Monolayers on H-Si(111).

**Kinetic studies:** After being etched, the samples were rinsed with argon-saturated water, and finally blown dry with a stream of argon. These samples were then immediately transferred to the inert atmosphere glove box. Next, the surface was covered with a few drops of neat 1-hexadecyne or hexadeca-3-en-1-yne. The reactions were performed at room temperature under ambient light (i.e., standard fluorescent lamps in the fume hood were on). To stop the reaction, the sample was removed from the glovebox and immediately

extensively rinsed with pentane and  $\text{CH}_2\text{Cl}_2$ . The sample was then sonicated for 5 min in  $\text{CH}_2\text{Cl}_2$  to remove physisorbed molecules, after which the samples were blown dry with a stream of dry argon.

**Quality studies:** High-quality monolayers were produced in a fume hood setup described in literature.<sup>35,48</sup> A three-necked flask was charged with 2 mL of 1-hexadecyne or hexadeca-3-en-1-yne, and was purged with argon under reduced pressure for 30 min, while being heated up to 80 °C. The freshly etched and dried surface was then quickly transferred into the flask, which was immediately depressurized again. The reaction mixture was kept at 80 °C overnight. The sample was then removed from the flask and immediately extensively rinsed with pentane and  $\text{CH}_2\text{Cl}_2$ , sonicated for 5 min in  $\text{CH}_2\text{Cl}_2$  to remove physisorbed molecules, and blown dry with a stream of dry argon.

### 5.2.5 Monolayer Characterization

**Contact Angle Measurements:** Contact angle measurements were performed on a Krüss DSA 100 contact angle goniometer with an automated drop dispenser and image video capture system. The static contact angles of six small droplets, (3.0  $\mu\text{L}$  volume of deionized water) dispensed on modified silicon surfaces, were determined using the implemented Tangent 2 fitting model. The digital drop images were processed by the image analysis system, which calculated both the left and right contact angles from the drop shape with an accuracy of  $\pm 1.0^\circ$ .

**Ellipsometry:** The thickness of the modified silicon surfaces (in the dry state) was measured using a rotating analyzer ellipsometer of Sentech Instruments (Type SE-400), operating at 632.8 nm (He-Ne laser), and an angle of incidence of 70°. The optical constants of the substrate were determined with a piece of freshly etched H-Si(111) ( $n = 3.819$  and  $k = 0.057$ ). The thicknesses of the monolayers were determined with a planar three-layer (ambient, monolayer, substrate) isotropic model with a refractive index for the organic monolayers of 1.46. The reported values for the layer thickness are the average of eight measurements taken at different locations on the substrate with an error  $< 1 \text{ \AA}$ .

**X-ray Photoelectron Spectroscopy (XPS):** XPS measurements were performed using a JPS-9200 photoelectron spectrometer (JEOL, Japan). A monochromatic Al  $K\alpha$  X-ray source ( $h\nu = 1486.7 \text{ eV}$ ) 12 kV and 20 mA using an analyzer pass energy of 10 eV was used. The base pressure in the chamber during measurements was  $3 \times 10^{-7} \text{ Torr}$ , and spectra were collected at room temperature. The intensity of XPS core level electron was measured as the peak area after standard background subtraction according to the linear procedure. The takeoff angle  $\phi$  (angle between sample and detector) of 80° is defined with a precision 1°. The typical sample size was  $1 \times 1 \text{ cm}^2$ . For a precise determination of the atomic C/Si ratio of organic monolayers on Si(111), the influence of X-ray photo diffraction (XPD) on



the XPS signal had to be accounted for.<sup>35,39</sup> Therefore, the samples were rotated 360° around the surface normal, yielding rotationally averaged C<sub>1s</sub> and Si<sub>2p</sub> emissions to obtain a truly quantitative C/Si ratio which is now independent of the orientation of the sample. As our sample holder only allows rotation of the samples at a takeoff angle of 90°, we used non-monochromatic Al-K $\alpha$  ray radiation (twin source) at 10 kV and 15 mA with analyzer pass energy of 50 eV and a takeoff angle of 90° for these measurements. All spectra were corrected with a slight linear background before fitting. All XPS spectra were evaluated using the Casa XPS software (version 2.3.15). All binding energies are referenced relative to the main hydrocarbon (CH<sub>2</sub>) peak with a binding energy of 285.0 eV.

**Near Edge X-ray Absorption Fine Structure (NEXAFS):** NEXAFS spectra were collected at the National Synchrotron Light Source (NSLS) U7A beamline at Brookhaven National Laboratory, using an elliptically polarized beam with ~85% p-polarization. This beam line utilizes a monochromator and 600 l/mm grating providing a full-width at half-maximum (FWHM) resolution of ~0.15 eV at the carbon K-edge. The monochromator energy scale was calibrated using the intense C 1s -  $\pi^*$  transition at 285.35 eV of a graphite transmission grid placed in the path of the X-rays. Partial electron yield was monitored by a detector with the bias voltage maintained at -150 V. Samples were mounted to allow rotation and allow changing the angle between the sample surface and the synchrotron X-rays. The NEXAFS angle is defined as the angle between the incident light and the sample surface. The spectra were brought to the standard form by linear pre-edge background subtraction and normalizing to the unity edge jump defined by a horizontal plateau 40–50 eV above the absorption edge.

**Fourier Transform Infrared Reflection Absorption Spectroscopy (FT-IRRAS):** IRRAS spectra were recorded on a Bruker Tensor 27 FT-IR spectrometer using a variable angle reflection unit (Auto Seagull, Harrick Scientific). A Harrick grid polarizer was installed in front of the detector and was used to record spectra with p-polarized (parallel) radiation with respect to the plane of incidence at the sample surface. All spectra were obtained at an incident angle of 68° (2048 scans). The resolution was set at 1 cm<sup>-1</sup> per modulation center. The final spectra were obtained using a piranha-oxidized reference surface as background. Data were collected as differential reflectance versus wavenumber. All spectra were recorded at room temperature in dry atmosphere. A linear baseline correction was applied.

### 5.2.6 Computational Procedures

**XPS binding energies:** XPS binding energies were estimated by calculating the orbital energies of molecular analogues of chains attached to a silicon surface which was mimicked by a Si(SiH<sub>3</sub>)<sub>3</sub> group.<sup>50</sup> The geometries were optimized with B3LYP/6-

311G(d,p), using the Gaussian 09 package.<sup>34</sup> The carbon binding energies were then estimated by calculating the 1s core energy versus the average of the 2p valence orbital energies (mimicking the Fermi level).

**Monolayer simulations:** Unit cells were constructed, and expanded to supercells of  $12 \times 12$  units (33, 50, 67 and 75% surface coverage) and  $10 \times 15$  units (60% surface coverage), following literature procedures.<sup>35</sup> The geometries were optimized using the polymer consistent force field (PCFF) (bottom two rows of Si atoms were constrained) as implemented in the Discover package in Materials Studio, using the ultrafine settings of the smart minimizer routine (line width 0,01 and convergence  $10^{-5}$ , VdW and coulomb, atom centered and long-range correction switched off).<sup>35</sup> All G3 calculations of the binding energies of the chains to the surface were performed using the Gaussian 09 package.

## 5.3 Results and Discussion

### 5.3.1 Reactivity difference of 3-en-1-yne and 1-alkynes onto H-Si(111)

To study the reactivity difference of alkynes and alk-3-en-1-yne towards oxide-free hydrogen-terminated Si(111) (H-Si(111)) surfaces, the kinetics of monolayer formation under ambient conditions were explored by analyzing the resulting (partial) monolayers after different reaction times. To minimize the effect of competing oxidation reactions induced by water and oxygen, the experiments were performed in a glovebox under argon atmosphere. Precursors and freshly etched H-Si(111) were deoxygenized by three or more freeze-pump-thaw cycles before transferring them into the glovebox. The reaction was started by covering the freshly etched surfaces with 1 or 2 drops of precursor. The surfaces were then allowed to react for the appropriate time at a constant temperature of 20 °C. Subsequently, the resulting (partial) monolayers were analyzed by water contact angle measurements (static, advancing and receding angles), ellipsometry and x-ray photoelectron spectroscopy (XPS) and infrared reflection-absorption spectroscopy (IRRAS). As shown in Figure 1A, for both precursors, the static contact angles gradually increase in time, while monolayer formation proceeds faster with hexadec-3-en-1-yne than with 1-hexadecyne. With hexadec-3-en-1-yne, the plateau value of 111 - 112°, indicative of hydrophobic and densely packed organic monolayers,<sup>7,19,35,48,51</sup> was already reached after 8 h, while for 1-hexadecyne these values were only obtained after increasing the reaction time to 16 h. This demonstrates a considerable reactivity difference between both precursors. As expected, this difference in reactivity was also displayed by the ellipsometry measurements (See Figure 1B), which show significant differences in the growth of the layer thickness over time. The hexadecadienyl monolayers reached a thickness of 1.9 nm after 2 h, while hexadecenyl monolayers were then only 1.5 nm thick. The plateau value 2.1 ( $\pm$  0.1 nm) nm

for hexadec-3-en-1-yne was reached after 8 h, whereas it took the 1-hexadecyne at least 16 h.

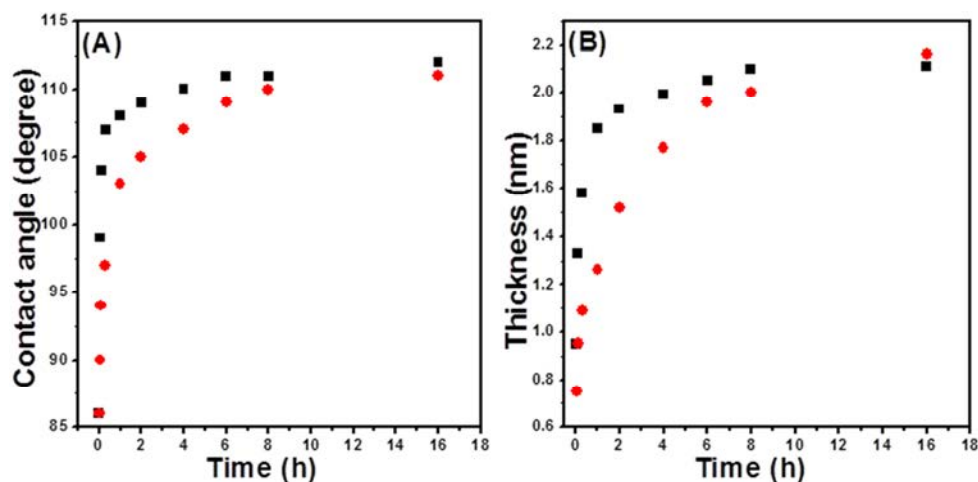


**Figure 1.** (A) Static water contact angles ( $\pm 1^\circ$ ), and (B) layer ellipsometric thicknesses ( $\pm 0.1$  nm) of hexadec-3-en-1-yne (■) and 1-hexadecyne (●) layers versus the reaction times at room temperature.

In order to monitor the actual formation of the organic monolayer, the contributions of the  $\text{Si}_{2p}$  and  $\text{C}_{1s}$  core levels were studied in time by XPS narrow scans. For both precursors, the  $\text{Si}_{2p}$  signal rapidly decreases in time, which coincides with an increase of the carbon signal at 285 eV (Figure 2A and B). This is a clear indication of the formation of an organic monolayer. Furthermore, the  $\text{Si}_{2p}$  narrow scans of both partial and complete organic monolayers, show no visible traces of oxygen at the silicon surface, demonstrating the success of the stringent oxygen-excluding conditions required to study the kinetics of monolayer formation in detail, and to obtain high-quality organic monolayers on oxide-free H-Si (see Figure 2C and D).<sup>20,35</sup>

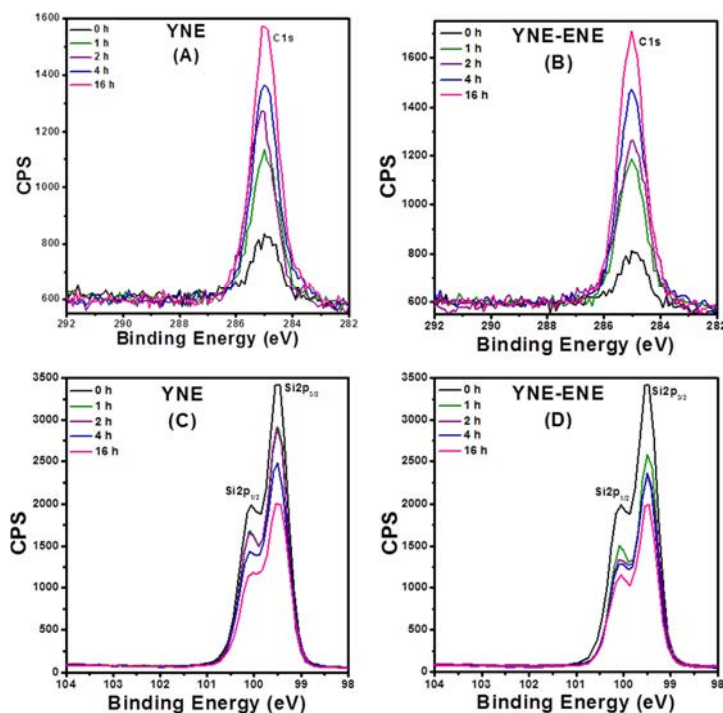


**Figure 2.** XPS spectra of the C<sub>1s</sub> (A and B) and Si<sub>2p</sub> region (C and D) of monolayers on H-Si(111) derived from 1-hexadecyne and hexadec-3-en-1-yne, respectively.

To obtain detailed information about the molecular order of the (partial) monolayers in time, IRRAS measurements were carried out. As can be seen in Figures 3A and 3B, the intensities of the antisymmetric ( $\nu_a$ ) and symmetric ( $\nu_s$ ) methylene stretching vibrations grow gradually in time for both precursors, clearly displaying the increasing amount of carbon chains at the surface. Furthermore, upon completion of the monolayers, for both types of monolayer the antisymmetric and symmetric CH<sub>2</sub> stretching frequencies shift from 2923 to 2918 cm<sup>-1</sup> and from 2853 to 2848 cm<sup>-1</sup>, respectively. In line with the contact angle and ellipsometry data in Figure 1, these optimal frequencies were obtained after 8 h for the hexadec-3-en-1-yne and after 16 h for the 1-hexadecyne. We note that these frequencies correspond to highly ordered organic monolayers and are for 1-hexadecyne in good agreement with literature.<sup>51-53</sup> Moreover, the gradual disappearance of a detectable Si-H stretching vibration at 2083 cm<sup>-1</sup> (Fig. 3C and D) confirms the formation of a chemical bond rather than physical adsorption of the precursors onto H-Si(111).<sup>19,35</sup>

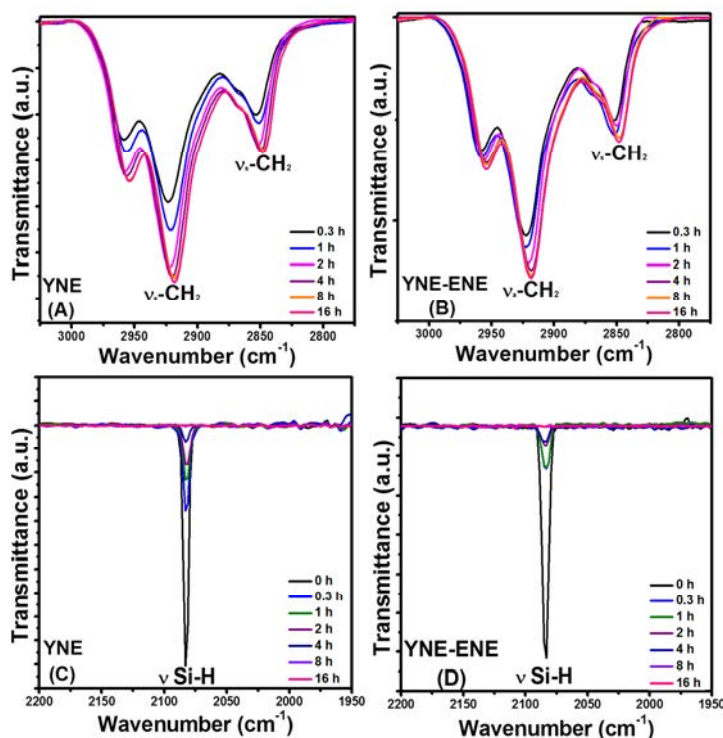


**Figure 3.** IRRAS data of 1-alkyne-derived (A, C) and 3-en-1-yne-derived (B, D) monolayers on H-Si(111) at ambient condition as a function of reaction time.

### 5.3.2 High-quality hexadecadienyl and hexadecenyl monolayers on H-Si(111)

After confirming the considerably higher reactivity of the 3-en-1-yne moiety towards H-Si(111) compared to the 1-yne moiety, the quality of the both final monolayers was studied in more detail. To ensure completion of the monolayer formation, i.e., to minimize the number of defects, more stringent reaction conditions (16 h at 80 °C) were chosen. Static water contact angles of 111 - 112°, advancing contact angles of 116 - 117°, receding contact angles of 109 - 110°, and ellipsometric thicknesses of  $2.1 \pm 0.1$  and  $2.2 \pm 0.1$  nm for monolayers derived from hexadec-3-en-1-yne and 1-hexadecyne, respectively, compare well with literature values (111° and 2.1 nm for 1-hexadecyne) and confirm the high quality of both organic monolayers.<sup>35</sup> The theoretical layer thickness can be determined via equation 1 (see Appendix 3 for derivation). By inserting a tilt angle ( $\theta$ ) of 30°, which is the experimentally determined tilt angle of high-quality organic monolayers on gold,<sup>54</sup> a

theoretical thickness of 1.90 nm for hexadecenyl and 1.89 nm for hexadecadienyl monolayers was calculated. This is somewhat lower than the ellipsometric values, which is likely caused by the assumed tilt angle of 30°. A smaller tilt angle, indicating more upright positioned chains, will result in thicker layers.

1-hexadecyne (nm):

$$d_{Th} = 0.188 + 1772 \cos \theta + 0.156 \sin(35.5 + \theta) \quad (1a)$$

hexadeca-3-en-1-yne (nm):

$$d_{Th} = 0.188 + 1765 \cos \theta + 0.156 \sin(35.5 + \theta) \quad (1b)$$

IRRAS measurements show the anti-symmetric and symmetric CH<sub>2</sub> stretching vibrations at 2918.2 cm<sup>-1</sup> and 2850.2 cm<sup>-1</sup> (hexadecenyl), and 2917.7 cm<sup>-1</sup> and 2848.2 cm<sup>-1</sup> (hexadecadienyl), respectively for both monolayers (see Figure 4). The value for hexadecenyl monolayers is in line with literature values,<sup>35</sup> and indicative of a highly ordered monolayer in which the chains adopt an all-trans conformation. In this regard it should be noted that these hexadecadienyl monolayers have two methylene groups less for favorable interchain Van der Waals interactions compared to hexadecenyl monolayers and even four methylene groups less compared to hexadecyl monolayers. Therefore it is remarkable that such a highly ordered organic monolayer can be obtained with only 12 CH<sub>2</sub> groups (cf. dodecyl termination), especially when comparing these low wavenumbers with those of a dodecyl monolayer on H-Si(111) (2922 cm<sup>-1</sup>).<sup>35</sup>

To study the linkage to the Si(111) substrate in more detail, XPS C<sub>1s</sub> narrow scans were recorded. In addition, density functional theory (DFT) calculations were used to calculate the binding energies of the distinct carbon atoms in the linkage. As shown in Figure 5A and B, both C<sub>1s</sub> spectra are deconvoluted into three contributions. The components at 283.8, 285.0 and 285.7 eV have been assigned to the carbons directly attached to the relatively electropositive silicon (C-Si, E<sub>calc</sub> = 283.9 eV), the aliphatic carbons (C-C, E<sub>calc</sub> = 285.0 eV), and the more electronegative sp<sup>2</sup> hybridized carbons (C=C, E<sub>calc</sub> = 285.6 and 285.8 eV), respectively. In combination with DFT calculations on other possible binding conformations (see Appendix 3), the relative intensities of these distinct carbons disclose the linkage of both monolayer types to the H-Si(111) surface, i.e., 1 : 12 : 3 for hexadec-1-en-3-yne-derived monolayers with a Si-C=C-C=C linkage and 1 : 14 : 1 for 1-hexadecyne-derived monolayers with a Si-C=C linkage. In addition, in the Si 2p narrow scans obtained for the dienyl and alkenyl layers (see Figure 5C and D), no silicon oxide was identified in the 101 - 103.5 eV region. This again confirms the monolayer quality and its ability to prevent appreciable oxidation of the underlying Si substrate.<sup>36</sup>

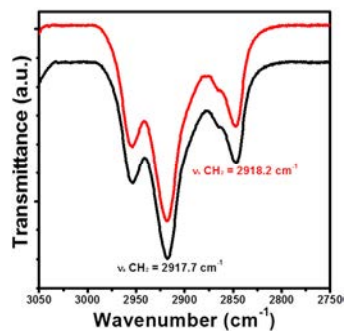


**Figure 4.** IRRAS of hexadec-3-en-1-yne (black) and 1-hexadecyne (red) derived monolayers on H-Si(111) at 80 °C.

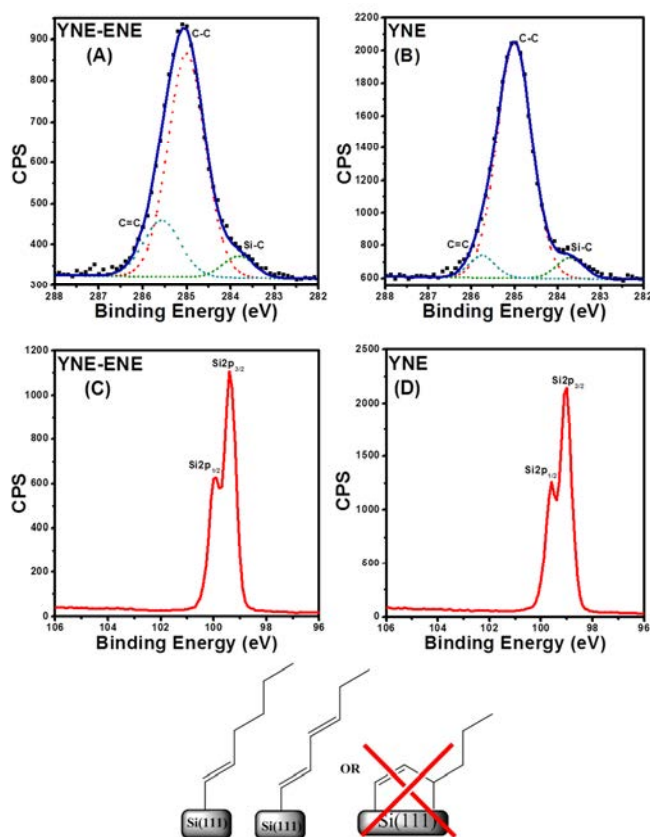


**Figure 5.** C<sub>1s</sub> (A,B) and Si<sub>2p</sub> (C,D) XPS narrow scan spectra of the H-Si(111) surface after modification (80 °C, 16 h) with hexadec-3-en-1-yne and 1-hexadecyne, respectively.

Moreover, in order to extract the packing densities, also the exact composition of monolayers was determined by quantitative XPS measurements. To overcome the signal dependency on the orientation of the crystal, i.e., to remove any influence of X-ray diffraction, the XPS samples were rotated 360° around the surface normal, in steps of 10°. <sup>35,39</sup> The obtained C/Si ratios display the expected periodicity of 120°, and reveal an increased amount of carbon for the hexadecadienyl monolayers as compared to the hexadecenyl monolayers (Table 1). The surface coverage and monolayer thickness were calculated from these C/Si ratios using the following equations: <sup>27,56</sup>

$$\text{Thickness:} \quad d_{\text{ML}} (\text{\AA}) = \lambda_{\text{ML}}^{\text{Si}} \sin(\phi) \ln(1 + C_{\text{C}}/C_{\text{Si}}) \quad (2),$$

$$\text{Surface coverage:} \quad \theta_{\text{ML}} = \frac{d_{\text{ML}} \times D_{\text{Au}}}{d_{\text{TH}(30)} \times D_{\text{Si}}} \quad (3),$$

In which  $\lambda_{\text{ML}}^{\text{Si}}$  is the attenuation length of Si<sub>2p</sub> photoelectron in the organic monolayer (39.5 Å), and  $\phi$  is the angle between the surface plane and the detector (90°). The surface coverage is estimated by comparison to the literature value of a fully characterized alkanethiol monolayer on gold, where  $d_{\text{TH}}$  is the theoretical thickness of an organic monolayer on H-Si(111) with a tilt angle of 30° (1.90 and 1.89 nm for alkenyl and dienyl layers, respectively), and  $D_{\text{Si}}$  and  $D_{\text{Au}}$  are the number of sites per cm<sup>2</sup> ( $7.8 \times 10^{14}$  cm<sup>-2</sup> and  $4.65 \times 10^{14}$  cm<sup>-2</sup>, respectively). <sup>35,39</sup> From the results in Table 1, it shows that the dienyl layers, with a surface coverage of 63% ( $\pm 1\%$ ), are significantly more densely packed than the hexadecenyl monolayers, while the XPS-derived thickness of both layers is the same within the experimental error ( $1.9 \pm 0.1$  and  $2.0 \pm 0.1$  nm, for enyne-derived and alkyne-derived C<sub>16</sub> monolayers, respectively). The thickness and surface coverage of 59% for the hexadecenyl monolayers are in excellent agreement with previous findings. <sup>35</sup> These results clearly show that, besides an increased reactivity, the 3-en-1-yne moiety also leads to a significant higher surface coverage, fulfilling both prerequisites for improvement of quality in monolayers.

**Table 1.** Quantitative XPS Data; Atomic C/Si ratios, resulting monolayer thickness and surface coverage of hexadecadienyl and hexadecenyl monolayers on H-Si(111).

Reactant	XPS C <sub>1s</sub> /Si <sub>2p</sub> ratios	Surface coverage %
C <sub>16</sub> Enyne	40.2/59.8	63%
C <sub>16</sub> Alkyne	37.7/62.3	59%



Finally, to investigate the ordering of the monolayer in more detail, high-quality Near Edge X-Ray Absorption Fine Structure (NEXAFS) measurements were performed. NEXAFS spectra provide information about the electronic structure of the surface species by measuring characteristic absorption resonances corresponding to electronic transitions from atomic core levels to unoccupied molecular orbitals.<sup>55</sup> Carbon *K*-edge spectra for the hexadecadienyl and hexadecenyl layers on silicon, acquired at 70°, 55° and 20°, are presented in Figure 6 along with the difference between the 70° and 20° spectra. The adsorption near 285.0 eV,  $\pi^*(C=C)$  clearly indicates resonance of the aromatic alkene moieties, whereas the strong Rydberg/C-H ( $R^*$ ) resonance near 287.9 eV and the broad  $\sigma^*$  resonances are related to the alkyl chains and the C-C bonds at higher photon energies, respectively. The spectra show no signs of chemical impurities such as C=O, nor any traces of unreacted C $\equiv$ C moieties (expected near 285.9 eV) for any of the monolayers.<sup>55-59</sup> The pronounced linear dichroism for the C=C, C-C and C-H related resonances (highlighted by the 70° – 20° difference spectra) indicates significant order and molecular alignment in both monolayers. The positive polarity of the observed difference peaks for the  $\pi^*$  resonance implies a strongly tilted orientation of the  $\pi^*(C=C)$  orbitals, which is expected for an upright chain orientation, since the  $\pi^*(C=C)$  orbitals are perpendicular to the C=C-C plane. The  $R^*$  features also show an appreciable positive linear dichroism while the C-C difference peaks are negative, which is again a clear indication of an upright orientation of the alkyl chain.

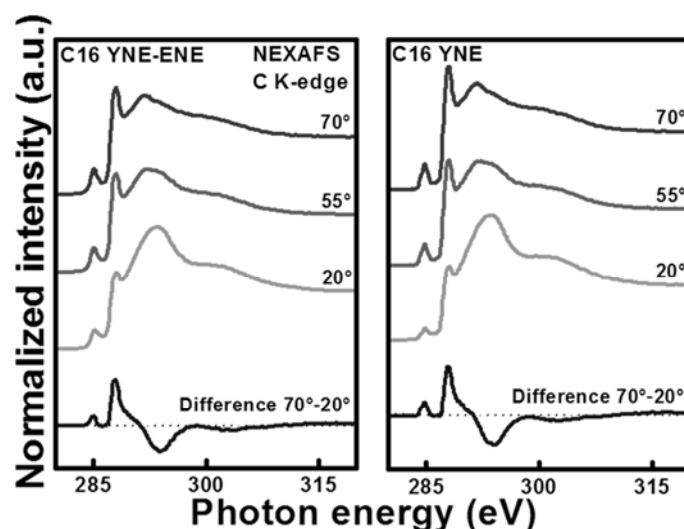


**Figure 6:** NEXAFS carbon *K*-edge spectra for hexadecadienyl and hexadecenyl monolayers on Si(111), acquired at 70°, 55° and 20°. The difference spectra between the 70° and the 20° data are shown in blue.

A quantitative analysis of the C *K*-edge NEXAFS spectra was performed to determine the average molecular tilt and twist angles. The orientation of the carbon chains with respect to the surface normal were determined using the  $R^*$  transitions. The intensities of these resonances as a function of the X-ray incidence angle  $\Theta$  were evaluated using literature procedures for a planar orbital.<sup>55</sup> This analysis yields average tilt angles versus the surface normal of  $28^\circ \pm 5^\circ$  and  $25^\circ \pm 5^\circ$  for dienyl and alkenyl layers, respectively. These values are slightly similar to those observed for alkane thiols on gold ( $28^\circ$ ).<sup>60</sup> In addition, these NEXAFS data can be used (via Eq. 2) to derive monolayer thicknesses, and these agree within experimental error with the XPS thicknesses. The tilt angle of the alkene  $\pi^*(C=C)$  orbitals was determined using the  $\pi^*$  resonance intensity variations and a standard methods for vector orbitals.<sup>55</sup> The orientations of the orbitals ( $\rho$ ) were found to be  $66^\circ \pm 5^\circ$  and  $76^\circ \pm 5^\circ$  for dienyl and alkenyl chains, respectively. These values can be used, together with equation 4, to determine the twist angle of the chains.<sup>61</sup> The twist angle  $\psi$  can be described as the rotation over the long molecular axis of the chains.

$$\rho = \arccos(\sin \phi \cos \psi) \quad (4)$$

This evaluation yields twist angles of  $\psi = 60^\circ$  and  $\psi = 45^\circ$  for dienyl and alkene chains, respectively. These values are in line with geometries observed for related alkanethiols on gold ( $53^\circ$ ) and other metal surfaces.<sup>54</sup> Overall, the NEXAFS data indicate that the structure of the hexadecadienyl and hexadecenyl layers is very similar. Both are densely packed, highly ordered and contamination free. The structure and orientation of the monolayers are also very similar to the binding geometry observed for alkanethiols on gold.

### 5.3.3 Molecular modeling

The obtained difference in surface coverage stimulated us to perform a comparative molecular modeling study of monolayers derived from 1-hexadecyne and hexadec-3-en-1-yne. Unit cells containing hexadecadienyl and hexadecenyl (both  $C_{16}$ ) chains were constructed, and used to create large simulation cells with various substitution percentages and substitution patterns analogous to those described in literature.<sup>38,40,41,62-64</sup> Energy minimizations were performed using a polymer consistent force field (PCFF) with high-convergence criteria and periodic boundaries conditions to eliminate the edge effects and to mimic an infinitely large monolayer.

The structure of the resulting optimized monolayers was compared in detail with the available experimental data. Reported data are the average observed for the chains (48 at 33% coverage to 108 at 75% coverage) in the periodically repeating unit cells at a specific

substitution pattern. As shown in Table 2 for one of the substitution patterns, at a coverage of approximately 60 – 67%, the alkenyl and dienyl layers display a calculated thickness of 1.9 and 2.0 nm, respectively. These values agree with the thicknesses derived from the XPS and NEXAFS measurements discussed above ( $1.9 \pm 0.1$  nm for both layers). The differences between both types of layers become clear after comparison of the tilt and the layer thicknesses at the various surface coverages. At low coverage (33-50%), the dienyl chains are more upright oriented than the alkenyl chains, resulting in a higher layer thickness. However, the tilt angles for alkenyl layers decrease rapidly when going to a higher surface coverage, while the dienyl layers show a more gradual decrease. This behavior can be explained by the rigidity of the dienyl moiety, which is caused by the two double C=C bonds and their overlapping p-orbitals, which keep the four carbons in an almost planar conformation (typical dihedral C=C-C=C  $\sim 170^\circ$  for 33 - 60% coverage). At low coverage, the dienyl will thus keep its upright orientation, whereas the alkenyl moiety has more rotational freedom, resulting in a more flat orientation of alkyne-derived monolayers. Both layers show a slight increase of the Si-C=C bond angles with increasing coverage, likely caused by the optimization of the interchain Van der Waals interactions between CH<sub>2</sub> moieties at the expense of such minor distortions at the surface.

**Table 2.** Calculated characteristics of hexadecenyl and hexadecadienyl monolayers on H-Si(111).

Unit Cell	Hexadecenyl			Hexadecadienyl		
	Thickness (nm)	Tilt angle chain	$\angle$ Si-C=C (in $^\circ$ )	Thickness (nm)	Tilt angle chain	$\angle$ Si-C=C (in $^\circ$ )
<b>33A</b>	1.2	$61 \pm 2$	$123 \pm 1$	1.3	$56 \pm 2$	$121 \pm 1$
<b>50A</b>	1.7	$48 \pm 2$	$123 \pm 2$	1.8	$26 \pm 4$	$124 \pm 2$
<b>60A</b>	2.0	$19 \pm 6$	$125 \pm 3$	1.8	$27 \pm 3$	$124 \pm 4$
<b>67A</b>	2.0	$17 \pm 2$	$124 \pm 3$	2.0	$11 \pm 4$	$126 \pm 3$
<b>75A</b>	2.1	$8 \pm 3$	$124 \pm 3$	2.0	$5 \pm 3$	$127 \pm 2$

Next to the structural parameters of the monolayers, also the packing energies were determined. After optimization of the layer, the chains were cut loose from the surface. The carbon atoms that were attached to silicon were left uncapped since capping with hydrogen led to distortion of the geometry. The resulting dangling carbon bonds were subsequently neglected by the used PCFF forcefield. The average packing energy per chain was then calculated according to:

$$E_{\text{packing}} = \frac{E_{\text{chains}}}{n} - E_{\text{single}} \quad (5),$$

in which  $E_{\text{chains}}$  is the total packing energy of the layer,  $n$  is the number of chains in the layer, and  $E_{\text{single}}$  is the energy of a separately optimized chain.<sup>62</sup> The resulting average packing energies per chain are shown in Figure 7 (dotted lines). At low surface coverage, hexadecenyl layers are energetically more favorable than dienyl layers. This difference can be explained by the upright position of the rigid dienyl moiety that pushes the CH<sub>2</sub> chain up, to an orientation in which the  $\pi$ - $\pi$  overlap of the resulting diene moiety competes with the interchain Van der Waals interactions between CH<sub>2</sub> moieties. For the alkyne-derived monolayer, such competition is absent, yielding a more flat orientation of the CH<sub>2</sub> chains with concomitantly increased attractive Van der Waals interactions.

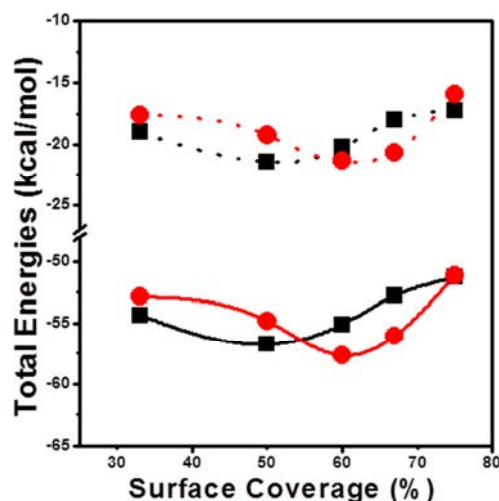


**Figure 7.** Packing energy (dotted lines) and total energy (solid lines) per chain for hexadecenyl (■) and hexadecadienyl (●) monolayers, as a function of surface coverage.

The optimum for the C<sub>16</sub> alkenyl layers is found around 50% coverage, while for the C<sub>16</sub> dienyl monolayer this is close to 60%. This difference corresponds to the experimental finding that hexadecadienyl layers can achieve a higher surface coverage (63%) than hexadecenyl layers (59%). This can largely be attributed to the volumes of the atoms close to the silicon surface (-CH=CH-CH=CH- versus -CH=CH-CH<sub>2</sub>-CH<sub>2</sub>-), which for the -CH=CH-CH=CH- moiety is ~5% smaller, with concomitant reduction of steric repulsions as increased surface coverages.

The optimum packing, however, is still lower than the experimentally observed packing of both the alkenyl and dienyl layers. The likely dominant part of the explanation for this phenomenon lies in the fact that the binding of the chains to the surface is energetically highly favorable and irreversible, yielding an experimental density that is higher than the optimum for the non-covalent interchain interactions.

The second aspect controlling the experimentally observed packing density relates to the Si-C binding energy. For the monolayers under study this was calculated via high-quality G3 *ab initio* calculations of the reaction of 1-pentyne and pent-3-en-1-yne with a small hydrogen-terminated silicon cluster (HSi(SiH<sub>3</sub>)<sub>3</sub>), analogous to literature procedures.<sup>62,63</sup> For fully relaxed structures this would favor the reaction of the enyne by 2.6 kcal.mol<sup>-1</sup>. However, the situation is slightly more complicated, as for varying coverages the precise structures near the surface vary slightly. To take this into account properly, the product geometries for the G3 calculations were isolated from the PCFF-optimized monolayer structures discussed earlier. Isolated Si<sub>4</sub> clusters were cut out of the surface slabs, and the chains were truncated to five carbon atoms, in order to lower the computational cost. The atoms were then constrained, in order to perform single-point G3 energy calculations (see Appendix 3 for a more detailed description). The binding energy was then calculated as the difference of the energy of the chain attached to the surface and the fully relaxed reactant complexes, and corrected for the energy contribution of the deformation of the C<sub>5</sub> chain, according to literature procedures.<sup>62</sup> Figure 7 (continuous lines) then shows the sum of packing and binding energies at the various degrees of surface coverage for enyne-derived and alkyne-derived C<sub>16</sub> monolayers. This profile of the total energy resembles the profile of the packing energy, but show a more distinct preference for the reactivity of the C<sub>16</sub> enyne. For the calculated total energies of 60% and 67%, i.e., close to what is experimentally observed, the energy gap between the alkenyl and the dienyl layers increases to 2.5 and 3.2 kcal mol<sup>-1</sup>. This overall higher reaction exothermicity and higher optimum packing density for enyne-derived monolayers fits very well with the experimental observation of the faster reaction of the C<sub>16</sub> enyne than of hexadecyne (Figure 1), and the observed higher denser packing of the dienyl layers (Figure 4).

## 5.4 Conclusions

In summary, we successfully developed a novel precursor, hexadeca-3-en-1-yne ( $\text{HC}\equiv\text{C}-\text{HC}=\text{CH}-\text{C}_{12}\text{H}_{25}$ ), for the formation of high-quality monolayers on H-terminated silicon surfaces. Detailed kinetics studies show that this enyne reacts faster than the corresponding  $\text{C}_{16}$  alkyne, while quantitative XPS studies show that the resulting dienyl monolayers also display a higher packing density than had been reported up to now on H-Si(111). Infrared and NEXAFS measurements confirm the formation of highly ordered, densely packed enyne-derived monolayers. Finally, a molecular modeling study (combination of molecular mechanics calculations on complete monolayers and G3 *ab initio* calculations on well-defined model systems) shows that for  $\text{C}_{16}$  monolayers an enyne-derived monolayer is both more stable and more densely packed than the monolayer derived from the corresponding  $\text{C}_{16}$  alkyne (hexadecyne).

This enhanced monolayer quality and rate of formation of enyne-derived monolayers, compared with the best performing reagent up to now (1-alkynes), makes enynes  $\text{HC}\equiv\text{C}-\text{HC}=\text{CH}-\text{R}$  the agent of choice if a supreme monolayer quality is desired, which also enhances the stability of the oxide-free silicon interface. This development further increases the chance of a successful application of organic monolayers on silicon in electronic and biosensor devices.

## References

- (1) Gooding, J. J.; Ciampi, S.; Harper, J. B. *Chem. Soc. Rev.* **2010**, 39, 2158.
- (2) Buriak, J. M. *Chem. Rev.* **2002**, 102, 1271.
- (3) Yonezawa, T.; Shirahata, N.; Hozumi, A. *Chem. Rec.* **2005**, 5, 145.
- (4) Gooding, J. J.; Ciampi, S. *Chem. Soc. Rev.* **2011**, 40, 2704.
- (5) Rijksen, B.; Caipa Campos, M. A.; Paulusse, J. M. J.; Zuilhof, H. In *Encyclopedia of Radicals in Chemistry, Biology and Materials*; Chatgililoglu, C., Struder, A., Eds.; Wiley: Chichester, 2012.
- (6) Scheres, L.; ter Maat, J.; Giesbers, M.; Zuilhof, H. *Small* **2010**, 6, 642.
- (7) Linford, M. R.; Fenter, P.; Eisenberger, P. M.; Chidsey, C. E. D. *J. Am. Chem. Soc.* **1995**, 117, 3145.
- (8) Sieval, A. B.; Huisman, C. L.; Schoenecker, A.; Schuurmans, F. M.; Van der Heide, A. S. H.; Goossens, A.; Sinke, W. C.; Zuilhof, H.; Sudhölter, E. J. R. *J. Phys. Chem. B* **2003**, 107, 6846.
- (9) Cicero, R. L.; Linford, M. R.; Chidsey, C. E. D. *Langmuir* **2000**, 16, 5688.
- (10) Shestopalov, A. A.; Clark, R. L.; Toone, E. J. *Langmuir* **2010**, 26, 1449.
- (11) Terry, J.; Mo, R.; Wigren, C.; Cao, R. Y.; Mount, G.; Pianetta, P.; Linford, M. R.; Chidsey, C. E. D. *Nucl. Instrum. Meth. B.* **1997**, 133, 94.

- (12) Wang, X. Y.; Ruther, R. E.; Streifer, J. A.; Hamers, R. J. *J. Am. Chem. Soc.* **2010**, *132*, 4048.
- (13) G. Robins, E.; P. Stewart, M.; M. Buriak, J. *Chem. Commun.* **1999**, 2479.
- (14) Belanger, D.; Pinson, J. *Chem. Soc. Rev.* **2011**, *40*, 3995.
- (15) Niederhauser, T. L.; Jiang, G. L.; Lua, Y. Y.; Dorff, M. J.; Woolley, A. T.; Asplund, M. C.; Berges, D. A.; Linford, M. R. *Langmuir* **2001**, *17*, 5889.
- (16) Yang, L.; Lua, Y.-Y.; Tan, M.; Scherman, O. A.; Grubbs, R. H.; Harb, J. N.; Davis, R. C.; Linford, M. R. *Chem. Mater.* **2007**, *19*, 1671.
- (17) Buriak, J. M.; Stewart, M. P.; Geders, T. W.; Allen, M. J.; Choi, H. C.; Smith, J.; Raftery, D.; Canham, L. T. *J. Am. Chem. Soc.* **1999**, *121*, 11491.
- (18) Jin, H.; Kinser, C. R.; Bertin, P. A.; Kramer, D. E.; Libera, J. A.; Hersam, M. C.; Nguyen, S. T.; Bedzyk, M. J. *Langmuir* **2004**, *20*, 6252.
- (19) Scheres, L.; Arafat, A.; Zuilhof, H. *Langmuir* **2007**, *23*, 8343.
- (20) Caipa Campos, M. A.; Paulusse, J. M. J.; Zuilhof, H. *Chem. Commun.* **2010**, *46*, 5512.
- (21) Popoff, R. T. W.; Asanuma, H.; Yu, H. Z. *J. Phys. Chem. C* **2010**, *114*, 10866.
- (22) Seitz, O.; Bocking, T.; Salomon, A.; Gooding, J. J.; Cahen, D. *Langmuir* **2006**, *22*, 6915.
- (23) Seitz, O.; Vilan, A.; Cohen, H.; Hwang, J.; Haeming, M.; Schoell, A.; Umbach, E.; Kahn, A.; Cahen, D. *Adv. Funct. Mater.* **2008**, *18*, 2102.
- (24) Yaffe, O.; Scheres, L.; Puniredd, S. R.; Stein, N.; Biller, A.; Lavan, R. H.; Shpaisman, H.; Zuilhof, H.; Haick, H.; Cahen, D.; Vilan, A. *Nano Lett.* **2009**, *9*, 2390.
- (25) Zigah, D.; Herrier, C.; Scheres, L.; Giesbers, M.; Fabre, B.; Hapiot, P.; Zuilhof, H. *Angew. Chem. Int. Ed.* **2010**, *49*, 3157.
- (26) Chatgililoglu, C. *Organosilanes in Radical Chemistry* **2004**.
- (27) Chatgililoglu, C.; Guarini, A.; Guerrini, A.; Seconi, G. *J. Org. Chem.* **1992**, *57*, 2207.
- (28) Wayner, D. D. M.; Wolkow, R. A. *J. Chem. Soc. Perk. T. 2* **2002**, 23.
- (29) Lehner, A.; Steinhoff, G.; Brandt, M. S.; Eickhoff, M.; Stutzmann, M. *J. Appl. Phys.* **2003**, *94*, 2289.
- (30) Sun, Q.-Y.; de Smet, L. C. P. M.; van Lagen, B.; Wright, A.; Zuilhof, H.; Sudhölter, E. J. R. *Angew. Chem. Int. Ed.* **2004**, *43*, 1352.
- (31) Rijkssen, B.; Paulusse, J. M. J.; Zuilhof, H. *Submitted*.
- (32) Takeuchi, N.; Kanai, Y.; Selloni, A. *J. Am. Chem. Soc.* **2004**, *126*, 15890.
- (33) Lalevée, J.; Blanchard, N.; Graff, B.; Allonas, X.; Fouassier, J. P. *J. Organomet. Chem.* **2008**, *693*, 3643.
- (34) Frisch, M. J. T., G. W.; Schlegel, H. B.; et al, In *Gaussian 09, Revision A.1*; Gaussian, Inc., Wallingford CT.: 2009.
- (35) Scheres, L.; Giesbers, M.; Zuilhof, H. *Langmuir* **2010**, *26*, 4790.
- (36) Puniredd, S. R.; Assad, O.; Haick, H. *J. Am. Chem. Soc.* **2008**, *130*, 13727.
- (37) Nemanick, E. J.; Solares, S. D.; Goddard, W. A.; Lewis, N. S. *J. Phys. Chem. B* **2006**, *110*, 14842.
- (38) Sieval, A. B.; van den Hout, B.; Zuilhof, H.; Sudhölter, E. J. R. *Langmuir* **2001**, *17*, 2172.

- (39) Wallart, X.; De Villeneuve, C. H.; Allongue, P. *J. Am. Chem. Soc.* **2005**, *127*, 7871.
- (40) Pei, Y.; Ma, J.; Jiang, Y. *Langmuir* **2003**, *19*, 7652.
- (41) Zhang, L.; Wesley, K.; Jiang, S. *Langmuir* **2001**, *17*, 6275.
- (42) Barone, V.; Cacelli, I.; Ferretti, A.; Monti, S.; Prampolini, G. *J. Phys. Chem. C* **2011**, *115*, 4145.
- (43) Sano, H.; Maeda, H.; Ichii, T.; Murase, K.; Noda, K.; Matsushige, K.; Sugimura, H. *Langmuir* **2009**, *25*, 5516.
- (44) Hacker, C. A.; Anderson, K. A.; Richter, L. J.; Richter, C. A. *Langmuir* **2004**, *21*, 882.
- (45) Miller, J. A.; Zweifel, G. *J. Am. Chem. Soc.* **1983**, *105*, 1383.
- (46) Kim, T.; Crooks, R. M. *Tetrahedron Lett.* **1994**, *35*, 9501.
- (47) Xu, Z.; Byun, H. S.; Bittman, R. *J. Org. Chem.* **1991**, *56*, 7183.
- (48) Sieval, A. B.; Linke, R.; Zuilhof, H.; Sudholter, E. J. R. *Adv. Mater.* **2000**, *12*, 1457.
- (49) Allongue, P.; de Villeneuve, C. H.; Morin, S.; Boukherroub, R.; Wayner, D. D. M. *electrochem. acta* **2000**, *45*, 4591.
- (50) Yang, M.; Teeuwen, R. L. M.; Giesbers, M.; Baggerman, J.; Arafat, A.; De Wolf, F. A.; Van Hest, J. C. M.; Zuilhof, H. *Langmuir* **2008**, *24*, 7931.
- (51) de Smet, L. C. P. M.; Pukin, A. V.; Sun, Q.-Y.; Eves, B. J.; Lopinski, G. P.; Visser, G. M.; Zuilhof, H.; Sudhölter, E. J. R. *Appl. Surf. Sci.* **2005**, *252*, 24.
- (52) Brunner, H.; Mayer, U.; Hoffmann, H. *App. Spectrosc.* **1997**, *51*, 209.
- (53) Hasegawa, T.; Takeda, S.; Kawaguchi, A.; Umemura, J. *Langmuir* **1995**, *11*, 1236.
- (54) Love, J. C.; Estroff, L. A.; Kriebel, J. K.; Nuzzo, R. G.; Whitesides, G. M. *Chem. Rev.* **2005**, *105*, 1103.
- (55) Stöhr, J. *NEXAFS Spectroscopy*; Springer-Verlag: Berlin, 1992; Vol. 25.
- (56) Outka, D. A.; Stöhr, J.; Rabe, J. P.; Swalen, J. D. *J. Chem. Phys.* **1988**, *88*, 4076.
- (57) Weiss, K.; Bagus, P. S.; Wöll, C. *J. Chem. Phys.* **1999**, *111*, 6834.
- (58) Väterlein, P.; Fink, R. *J. Chem. Phys.* **1998**, *108*, 3313.
- (59) Cabarcos, O. M.; Shaporenko, A.; Weidner, T.; Uppili, S.; Dake, L. S.; Zharnikov, M.; Allara, D. L. *J. Phys. Chem. C* **2008**, *112*, 10842.
- (60) Laibinis, P. E.; Whitesides, G. M. *J. Am. Chem. Soc.* **1992**, *114*, 1990.
- (61) Rong, H.-T. F., S.; Yang, Y.-J.; Zharnikov, M.; Buck, M.; Wuhn, M.; Wöll, C.; Helmchen, G. *Langmuir* **2001**, *17*, 1582.
- (62) Scheres, L.; Rijksen, B.; Giesbers, M.; Zuilhof, H. *Langmuir* **2011**, *27*, 972.
- (63) Sieval, A. B.; van den Hout, B.; Zuilhof, H.; Sudhölter, E. J. R. *Langmuir* **2000**, *16*, 2987.
- (64) Yuan, S.-L.; Cai, Z.-T.; Jiang, Y.-S. *New J. Chem.* **2003**, *27*, 626.



# Chapter 6

## General Discussion

Over the past two decades a lot of progress has been made in understanding the attachment reactions of organic species onto hydrogen-terminated silicon surfaces. This has led to many novel methods for monolayer fabrication, each addressing important issues such as, speed of formation, selectivity of the precursors towards the surface, milder reaction conditions, and prevention of surface oxidation. Formation of self-assembled covalently attached organic monolayers on silicon surfaces is based on a complex interplay of various processes taking place at the surface. Using the organic chemistry toolbox, there are several ways to link the chains to the substrate. This thesis focused mainly on the radical chain mechanism that allows direct formation of Si-C bonds. Chapter 2 provided an overview of those methods that, either directly or indirectly, steer the radical reactions taking place at the surface. A general trend among these methods is that an improvement of one characteristic often goes at the expense of another. For example, speed-up of the monolayer formation often goes hand in hand with a loss of quality of the monolayer or versatility of the method used (due to side reactions taking place). Conversely, using novel techniques that allow very mild attachment (no side reactions or degradation of the precursors) and give the highest quality of monolayers on oxide-free surfaces, will take up to 16 hours of reaction time. The question which is the best technique, depends mostly on the application in mind. Organic monolayers on silicon are most often used as scaffolds for further functionalization of the surface. If the goal is to immobilize functional molecules onto relatively stable layers, and surface oxidation is unimportant, there is no need to spend too much time and effort on a high-quality layer. Widely available alkene-based precursors are then probably the precursors of first choice. On the other hand, time and effort are well spent in the case of electronic devices where surface oxidation has to be taken to a minimum, and high-quality monolayers with specified (bio-)functionalities at the top are needed.

Recent advances in producing monolayers on oxide-free silicon surfaces have enabled thorough electronic characterization studies of organic monolayers.<sup>1-3</sup> This has led to

surprising discoveries that the type of charge transport across the monolayer is dependent on the level of doping. And that the temperature dependency of the conductivity resembles the behavior of metals to a remarkably high degree. The robustness of the silicon platform combined with the highly ordered structure of the layers ensures the role of organic monolayers in the development of biosensors, molecular electronic and photovoltaic devices.<sup>1,4-6</sup>

With regard to the processes taking place at the silicon surface during monolayer formation, many questions remain unanswered. Especially, in the case of mild attachment, the initiation of the radical chain mechanism has been under much debate in recent years.<sup>7-11</sup> Key issue here is the formation of a surface-centered radical, which apparently takes place without any significant input of energy. There is general consensus that homolytic cleavage of Si-H and Si-Si bonds at the surface, which require a significant activation energy, can be excluded under these conditions. However, for the actual initiation mechanism several theories are under discussion. Some explanations state that radical initiation at the surface is catalyzed by impurities or adventitious oxygen in the reaction mixture.<sup>12</sup> Other groups find strong evidence for side reactions with the glass surface of the reaction vessel, creating reactive species that can induce the formation of radicals at the silicon surface.<sup>7</sup> Among these mechanisms under discussion, however, only a few mechanisms take the electronic band structure of silicon, that is responsible for charge separation, into account.<sup>9,10</sup> According to the radical cation mechanism, due to the band structure in silicon, positively charged delocalized holes are spontaneously created at the silicon surface upon photoexcitation. These holes in turn, which behave in some respects analogous to delocalized radical cations, are susceptible to nucleophilic attack of olefins. This theory, already proposed in 2005, formed the starting point for a more in-depth study of silyl radical cations, which is described in Chapter 3.

In this study, low-molecular weight branched silanes were used as molecular models of the top atomic layers of the silicon surface. The delocalized holes at the silicon surface were mimicked by the radical cationic species of these models, and these indeed showed a high reactivity towards various oxygen-centered nucleophiles. Most importantly, however, the significant reactivity of these silicon radical cations towards alkenes and alkynes supports the feasibility of this reaction taking place at the silicon surface during monolayer formation. The obtained knowledge about this possible initiation mechanism may help in the development of new methods for monolayer preparation, which hopefully allow an even further increased degree of control over the process. For instance, the migration of holes to the surface is at equilibrium with recombination of the electron/hole pairs. Stabilization of the charge separation may shift this equilibrium, resulting in a larger concentration of holes at the surface, and thus enhancing the monolayer formation. This may be achieved by applying a bias voltage over the surface, or by placing the substrate in a magnetic field (see

Figure 1A and B). The idea is that upon formation of the exciton in an electric field, the holes are more efficiently separated from the electrons. In the case of the bias voltage, the electrons will then move towards the positively charged electrode. A magnetic field will have a similar effect on the electrons, which will move perpendicular to the direction of the magnetic field. A third option is illumination with light in the visible region, which will strongly increase the exciton formation. In fact, the white light reaction,<sup>9,13</sup> provided the basis for the radical cation theory in the first place. Use of a cut-off filter to block low wavelengths prevents undesired side-reactions from occurring, and ensures mild reaction conditions. In combination with the new techniques to remove oxygen from the reaction vessel,<sup>14</sup> a significant speed-up of the formation of high-quality layers lies within reach.

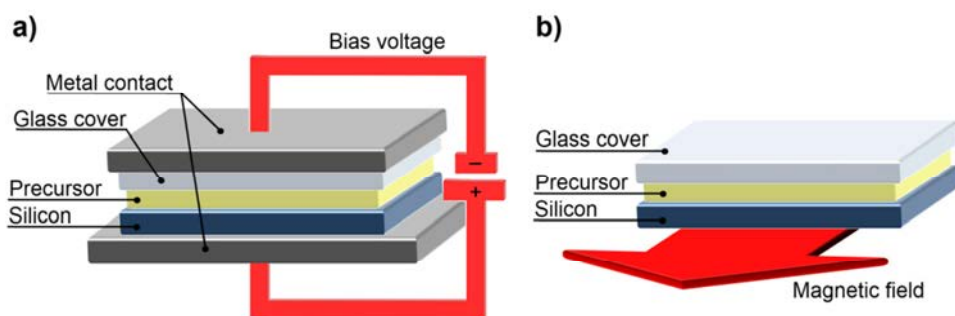


**Figure 1.** Stabilization of delocalized holes at the silicon surface by **a.** applying a bias voltage, or **b.** performing the monolayer formation in a magnetic field.

An alternative route for speeding up monolayer formation lies in enhancing the reactivity of the precursors used. By increasing the reactivity, also the chance of capturing a hole at the silicon surface increases. The observed difference in reactivity between alkenes and alkynes is a result of the higher electron density in a C $\equiv$ C bond as compared to the C=C bond, which makes it a better nucleophile. Introduction of electron donating groups next to these reactivity centers may further increase reactivity. However, changing the geometry of the chains will also result in a change in the packing of the monolayer. Another option is to blend a more reactive species, with the precursors. The high reactive species will capture the hole resulting in a surface centered radical, which is the initiation for the radical chain mechanism. The challenge here is to find such a reactive species that does not interfere with the radical mechanism, nor causes any extra deformation in the packing of the layer.

In Chapter 4 the radical chain mechanism was studied in more detail, and particularly the idea of stabilizing the  $\beta$ -carbon radical was investigated. Similar to Chapter 3, the surface was mimicked by a low-molecular weight branched silane (tris[trimethylsilyl]silane). The

reactivity of the resulting silyl radical was measured in competition reactions with various monolayer precursors. The stabilizing effect of conjugation on the  $\beta$ -radical was demonstrated both experimentally and by theoretical calculations. Two structures (novel to the area of monolayers), a 1,3-di-yne and a 3-en-1-yne species, showed drastically enhanced reactivity towards silyl radicals. Moreover the linear structures of both molecules are in line with the linear structures of alkenes and alkynes that are typically used. The good agreement between the experiments and the theoretical model allows an accurate prediction of the reactivity of precursors, which may prove useful in the development of even faster precursors. An additional use of this model may lie in predicting the degree of upside-down attachment of bi-functional precursors. For instance aldehyde-terminated alkenes show 10% attachment via Si-O-C bonds,<sup>15</sup> when alkynes are used this percentage of upside-down attachment is likely to decrease by a factor 7. The novel enyne-derived precursors may, because of their enhanced reactivity, shift the balance even more towards Si-C linkage. In a similar fashion, the monolayer structure that can be expected based on new combinations of functionalities can be predicted before the actual molecule is synthesized.

In Chapter 5, the newly designed molecules were tested in monolayer fabrication. The solution-phase reactivity of the 1,3-diyne was too high, resulting in polymerization reactions interfering with the surface reactions. The 3-en-1-yne precursor, however, showed to be a highly successful candidate for improved monolayer formation on silicon. The speed-up (factor 2) is modest but significant in line with theoretical data, and shows that the knowledge obtained by the mechanistic studies does indeed give a better understanding of the processes at the surface. Based on this success, it can be hoped that a further speed-up lies within reach. Moreover, the increased surface coverage of the resulting dienyl layers shows that tuning the molecular structure of the chains can also favorably influence the monolayer packing, and thus the stability of the monolayer itself. In fact, it is fair to say that the enyne-derived C<sub>16</sub> monolayers on H-Si that are described in this thesis are simply the best monolayers ever made on H-Si in oxygen content and packing density, and form a significant improvement with respect to the previously best result of 1-alkyne-derived monolayers.<sup>14,16,17</sup>

In summary, the research described in this thesis has contributed to the understanding of the processes that take place at the hydrogen-terminated silicon surface during monolayer formation. At a fundamental level it has refined ideas and theories of radical cation initiation at the silicon surface. From a practical point of view, it has also led to the development of even denser monolayers, and to the speed-up of monolayer formation itself, which further minimizes the formation of silicon oxide. As such, these insights and new materials – the typically desired core results of any chemical endeavor – enlarge the toolbox of silicon surface chemistry, and are thus expected to further decrease the barrier

towards application of functionalized monolayers in silicon-based sensory and electronic devices.

## References

- (1) Haensch, C.; Hoepfner, S.; Schubert, U. S. *Chem. Soc. Rev.* **2010**, *39*, 2323.
- (2) Fraxedas, J. *Adv. Mater.* **2002**, *14*, 1603.
- (3) Yaffe, O.; Scheres, L.; Segev, L.; Biller, A.; Ron, I.; Salomon, E.; Giesbers, M.; Kahn, A.; Kronik, L.; Zuilhof, H.; Vilan, A.; Cahen, D. *J. Phys. Chem. B* **2010**, *114*, 10270.
- (4) Zotti, G.; Vercelli, B.; Berlin, A. *Acc. Chem. Res.* **2008**, *41*, 1098.
- (5) Park, J.-W.; Kim, H.; Han, M. *Chem. Soc. Rev.* **2010**, *39*, 2935.
- (6) Maldonado, S.; Knapp, D.; Lewis, N. S. *J. Am. Chem. Soc.* **2008**, *130*, 3300.
- (7) Mischki, T. K.; Lopinski, G. P.; Wayner, D. D. M. *Langmuir* **2009**, *25*, 5626.
- (8) Stewart, M. P.; Buriak, J. M. *J. Am. Chem. Soc.* **2001**, *123*, 7821.
- (9) Sun, Q.-Y.; De Smet, L. C. P. M.; Van Lagen, B.; Giesbers, M.; Thuene, P. C.; Van Engelenburg, J.; De Wolf, F. A.; Zuilhof, H.; Sudhölter, E. J. R. *J. Am. Chem. Soc.* **2005**, *127*, 2514.
- (10) Wang, X. Y.; Ruther, R. E.; Streifer, J. A.; Hamers, R. J. *J. Am. Chem. Soc.* **2010**, *132*, 4048.
- (11) Vilan, A.; Yaffe, O.; Biller, A.; Salomon, A.; Kahn, A.; Cahen, D. *Advanced Materials* **2010**, *22*, 140.
- (12) Linford, M. R.; Fenter, P.; Eisenberger, P. M.; Chidsey, C. E. D. *J. Am. Chem. Soc.* **1995**, *117*, 3145.
- (13) de Smet, L. C. P. M.; Pukin, A. V.; Sun, Q. Y.; Eves, B. J.; Lopinski, G. P.; Visser, G. M.; Zuilhof, H.; Sudholter, E. J. R. *Appl. Surf. Sci.* **2005**, *252*, 24.
- (14) Scheres, L.; Arafat, A.; Zuilhof, H. *Langmuir* **2007**, *23*, 8343.
- (15) Hong, Q.; Rogero, C.; Lakey, J. H.; Connolly, B. A.; Houlton, A.; Horrocks, B. R. *Analyst* **2009**, *134*, 593.
- (16) Scheres, L.; Giesbers, M.; Zuilhof, H. *Langmuir* **2010**, *26*, 4790.
- (17) Scheres, L.; Giesbers, M.; Zuilhof, H. *Langmuir* **2010**, *26*, 10924.



## Appendix 1

### More detailed discussion on stabilization of $2^{\bullet+}$ and $3^{\bullet+}$ by sigma conjugation

The positive charge on  $2^{\bullet+}$  is mainly localized on the TMS groups (from 0.062 in the precursor molecule 2 to 0.260 and 0.231 for the TMS moieties centered on atoms Si5 and Si7, respectively, and to 0.149 and 0.150 for those on Si4 and Si6, respectively).

The geometry of  $3^{\bullet+}$  resembles that of  $2^{\bullet+}$ , including the relaxation of the angle strain ( $\angle\text{Si2-Si1-Si3}$  = from  $132^\circ$  in the neutral to  $119^\circ$  in the radical cation) and the w-shaped chain. The conjugated ‘backbone’ shows a better anti-conformation than  $2^{\bullet+}$  (dihedrals:  $\angle 8-3-1-2 = 172^\circ$ ;  $\angle 3-1-2-5 = 154^\circ$ ). However, bond orders show that the charge is mainly localized on two TMS-groups on Si5 and Si8. This is also reflected by the bond lengths, which are longer for Si3-Si8 and Si2-Si5 (2.49 Å) than for Si1-Si3 and Si1-Si2 (2.45 Å). The bonds not significantly involved in the sigma conjugation are only slightly longer (2.42 Å) than in the neutral molecule (2.39 - 2.40 Å).

### Full citation of reference of Gaussian 09, Revision A.02.

M. J. Frisch, G. W. Trucks, H. B. Schlegel, G. E. Scuseria, M. A. Robb, J. R. Cheeseman, G. Scalmani, V. Barone, B. Mennucci, G. A. Petersson, H. Nakatsuji, M. Caricato, X. Li, H. P. Hratchian, A. F. Izmaylov, J. Bloino, G. Zheng, J. L. Sonnenberg, M. Hada, M. Ehara, K. Toyota, R. Fukuda, J. Hasegawa, M. Ishida, T. Nakajima, Y. Honda, O. Kitao, H. Nakai, T. Vreven, J. A. Montgomery, Jr., J. E. Peralta, F. Ogliaro, M. Bearpark, J. J. Heyd, E. Brothers, K. N. Kudin, V. N. Staroverov, R. Kobayashi, J. Normand, K. Raghavachari, A. Rendell, J. C. Burant, S. S. Iyengar, J. Tomasi, M. Cossi, N. Rega, J. M. Millam, M. Klene, J. E. Knox, J. B. Cross, V. Bakken, C. Adamo, J. Jaramillo, R. Gomperts, R. E. Stratmann, O. Yazyev, A. J. Austin, R. Cammi, C. Pomelli, J. W. Ochterski, R. L. Martin, K. Morokuma, V. G. Zakrzewski, G. A. Voth, P. Salvador, J. J. Dannenberg, S. Dapprich, A. D. Daniels, O. Farkas, J. B. Foresman, J. V. Ortiz, J. Cioslowski, and D. J. Fox, Gaussian, Inc., Wallingford CT, 2009

**Estimation of barrier energies**

**Table A1.** Gibb's free activation barriers for the reactions of  $2^{\bullet+}$  and  $3^{\bullet+}$  with various nucleophiles, estimated using  $k(T) = \frac{k_B T}{h} e^{\frac{-G_{act}}{RT}}$ .

Entry	Nucleophile	$G_{act, 2}$	$G_{act, 3}$
1	1-Decene	18.3	9.0
2	1-Decyne	17.7	8.5
3	H <sub>2</sub> O	-	7.2
4	1-Undecanol	16.1	7.4
5	1-Undecanal	15.6	7.1
6	1-Undecanoic acid	16.3	7.4
7	1-Decanethiol	-	< 6.5
8	1-Bromohexane	-	> 10.6
9	10-Undecenoic acid	-	7.4
10	10-Undecynoic acid	-	7.5
11	10-Undecenal	-	6.9
12	10-Undecynal	-	7.0

Activation barriers in kcal mol<sup>-1</sup>.



## Appendix 2

### Correlation of barrier energies to reactivity ratios

Figure A1 shows the correlation of the zero-point energy-corrected barrier energies to the reactivity ratios. The correlation is rather poor compared to Figure 5 in Chapter 4, demonstrating the influence of the entropy to the reaction barriers. The barriers for alkene and alkyne are virtually the same, and the barrier for the ene-yne is even lower than that for the diyne.

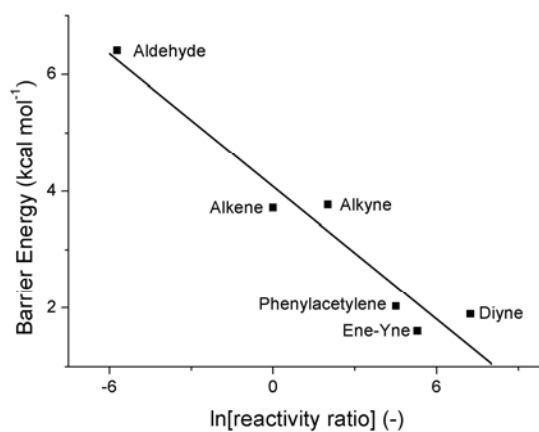


**Figure A1.** Correlation of the zero-point energy-corrected barrier energies to the reactivity ratios.

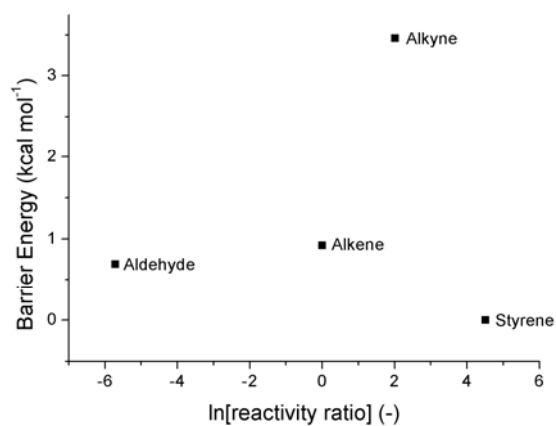


**Figure A2.** Correlation of barrier energies obtained from literature to the reactivity ratios.



## Appendix 3

### Derivation of equation for monolayer thickness

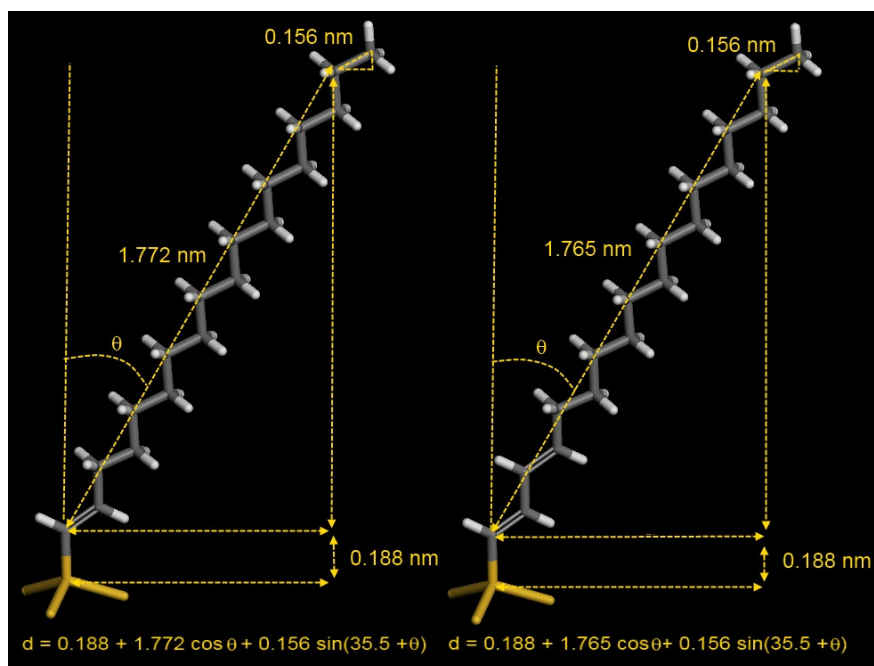


**Figure A1.** Derivation of the monolayer thickness by using the length of the carbon chain, the Si-C bond length and the tilt angle ( $\theta$ ).

### Modeling studies in Materials Studio

The modeling of the monolayers on silicon was performed following the procedures as described previously.<sup>1,2</sup> Since the packing energies were combined with the binding energies, only one series of coverage patterns was used. Unit cells were constructed, with dimensions  $a = b = 3.840 \text{ \AA}$ ,  $c = 35 \text{ \AA}$ ,  $a = b = 90^\circ$ , and  $g = 120^\circ$  (See Figure A2). The cells were expanded to larger cells ( $2 \times 2$ ,  $2 \times 3$ ,  $2 \times 4$  or  $2 \times 5$ ) and chains were replaced by hydrogen to achieve the desired pattern. The cells were then expanded to supercells of  $12 \times 12$  units (33, 50, 67 and 75% surface coverage) and  $10 \times 15$  units (60% surface coverage).<sup>3</sup>

The geometries were optimized using the polymer consistent force field (PCFF) (bottom two rows of Si atoms were constrained) as implemented in the Discover package in

Materials Studio, using the ultrafine settings of the smart minimizer routine (line width 0,01 and convergence  $10^{-5}$ , VdW and coulomb, atom centered and long-range correction switched off).

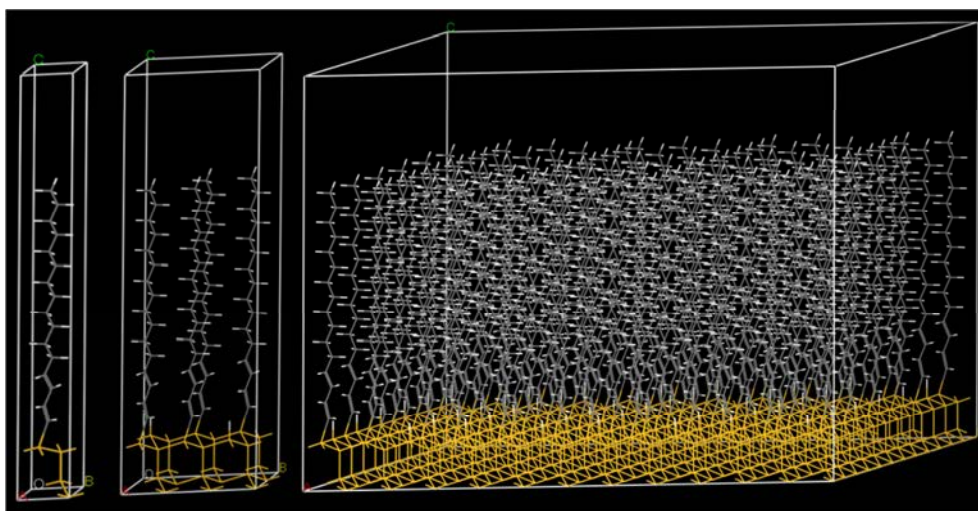


**Figure A2.** Construction of monolayer geometries from a single unit cell (left) to the desired pattern (middle), and finally the entire monolayer (right).

#### **DFT calculations of XPS binding energies.**

XPS binding energies were estimated by calculating the orbital energies of molecular analogues of chains attached to a silicon surface which was mimicked by a  $\text{Si}(\text{SiH}_3)_3$  group (See Figure A3). The geometries were optimized with B3LYP/6-311G(d,p), using the Gaussian 09 package.<sup>4</sup> The carbon binding energies were then estimated by calculating the 1s core energy versus the average of the 2p valence orbital energies (mimicking the Fermi level).

The calculations show that the peaks at 283.8 eV can be attributed to carbons attached to silicon. (both 283.9 eV, See Figure S3).  $\text{Sp}^2$  hybridized carbons, show a binding energy around 285.7 eV, as the stronger electronegativity will increase the binding energy. Regular  $\text{sp}^3$  hybridized carbons give a binding energy of 295.0 eV. Calculations of the binding energies of the hexadecenyl chain attached to the surface give three peaks: at 283.9 eV for

the carbon attached to the silicon, at 285.0 eV for the aliphatic carbons, and at 285.8 eV for the  $sp^2$  carbons, in the ratio of 1 : 14 : 1 (See Fig. A3A). The different attachment modes of the 3-en-1-yne give a very different pattern of binding energies. Terminal attachment (Fig. A3B) gives three peaks (binding energies for the  $sp^2$  hybridized carbons at 285.6-285.8 eV) in a ratio of 1:3:14. Double attachment (Fig. A3C) gives two carbons attached to silicon, which results in a ratio of 2:1:15. Another possibility is terminal attachment with retention of the triple bond (Fig. A3D). The triple bond results in distinct peaks at 284.3 eV for the carbon connected to silicon, and at 286.5 eV for the other  $sp$  hybridized carbon.

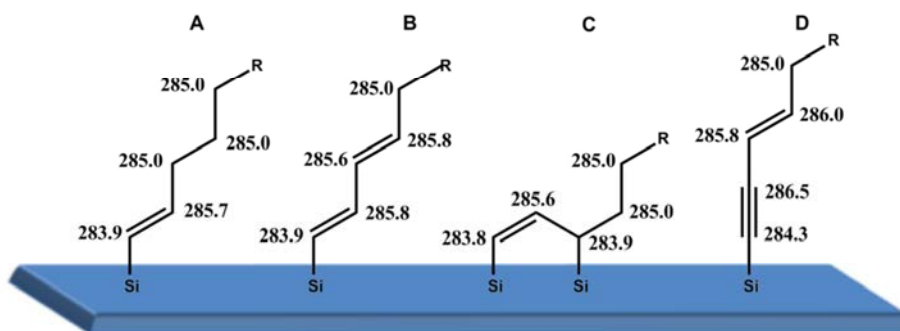


**Figure A3.** Self-Assembled monolayers on Si(111); **a.** hexadecenyl layers and **b-d.** possible modes of attachment of hexadeca-3-en-1-ynes. Calculated binding energies per carbon atom are depicted in eV ( $R = C_{11}H_{23}$ ).

## References

- (1) Scheres, L.; Rijksen, B.; Giesbers, M.; Zuilhof, H. *Langmuir* **2011**, 27, 972.
- (2) Sieval, A. B.; Opitz, R.; Maas, H. P. A.; Schoeman, M. G.; Meijer, G.; Vergeldt, F. J.; Zuilhof, H.; Sudhölter, E. J. R. *Langmuir* **2000**, 16, 10359.
- (3) Scheres, L.; Giesbers, M.; Zuilhof, H. *Langmuir* **2010**, 26, 10924.
- (4) Frisch, M. J. T., G. W.; Schlegel, H. B.; Scuseria, G. E.; Robb, M. A.; Cheeseman, J. R.; et al In *Gaussian 09, Revision A.1*; Gaussian, Inc., Wallingford CT.: 2009.



## Summary

Covalently attached organic monolayers on silicon surfaces form thermally and chemically stable platforms for (bio)functionalization of the surface. Recent advances in monolayer formation – yielding increases in monolayer quality and the complete exclusion of oxygen at modified surfaces – have paved the way for the future development of biosensors, photovoltaics, and molecular electronic devices. Despite these successful innovations in monolayer formation (including patterning and functionalization) over the last two decades, the actual knowledge of the processes at the silicon surface still lags behind. Yet, a good understanding of the mechanisms of initiation and propagation will help in finding new tunable parameters for further speed-up, and new strategies for attaching interesting biomolecules to the silicon surface.

In the search for even faster synthetic methods to build monolayers of even higher quality, this thesis presented a combined systematic experimental and theoretical study of the mechanisms underlying monolayer formation.

Chapter 1 serves as a general introduction to this thesis by explaining the concept of self-assembly, and by giving examples of self-assembled monolayers on different types of surfaces, namely: thiol-based monolayers on metal surfaces, organosilane-based monolayers on oxide surfaces, and organic monolayers directly attached to silicon surfaces via Si-C bonds. It compares several properties of such monolayers and the formation thereof, to introduce the focus on Si-C based monolayers in the rest of the thesis.

A more detailed overview of the current knowledge regarding the mechanisms that underlie monolayer formation onto hydrogen-terminated silicon (H-Si) is presented in Chapter 2. Typically three types of silicon surfaces are used in literature: H-Si(111), H-Si(100), and porous silicon (H-pSi). These different surface geometries require different strategies for surface etching and monolayer formation, which are explained. The focus of this chapter is mainly directed to H-Si(111) and H-Si(100) surfaces, where silyl radicals play a key role in the formation of Si-C bonds that link the monolayers to the surface. These radicals also readily react with oxygen leading to oxidation of the surface. Several initiation mechanisms that induce the formation of these radicals are discussed, along with supporting theoretical and experimental modeling studies. A distinction is made between ‘high energy’ methods that make use of elevated temperatures or UV irradiation to directly cleave Si-H bonds, and ‘mild’ methods that use very little energy input (too little for direct Si-H cleavage) and indirectly lead to formation of surface-centered radicals. This chapter also gives an overview of the current state of affairs with respect to further surface functionalization and patterning, as well as perspectives for further research and applications.

The radical cation initiation mechanism is studied in more detail in Chapter 3. This chapter describes how radical cations of low molecular-weight silicon model compounds, which were synthesized to represent the H-Si surface, were obtained by photo-induced electron transfer. The stability and the nature of the radical cations were investigated with lifetime and secondary electron transfer studies. The radical cations showed high reactivity towards various oxygen-centered nucleophiles ( $\sim 10^7 \text{ M}^{-1}\text{s}^{-1}$ ), and significant reactivity towards 1-alkenes and 1-alkynes ( $\sim 10^5 - 10^6 \text{ M}^{-1}\text{s}^{-1}$ ). Time-resolved kinetics revealed a bimolecular nucleophilic attack to the radical cation, while a secondary isotope effect indicated that the central Si-H bond is close to the reaction center but is not cleaved in the rate-determining step. Both findings are in good agreement with the radical cation initiation mechanism. Moreover, product analysis showed substitution products that confirmed the cleavage of a Si-Si bond, whereas the presence of hydrosilylation products could be explained by the formation of a  $\beta$ -carbon radical. This carbon radical subsequently initiates a radical chain mechanism by abstracting a hydrogen atom from unreacted silane. In conclusion, this chapter shows that radical cation initiation at the silicon surface is feasible. However, given the differences in reactivity between oxygen-centered and carbon-centered nucleophiles, this reaction is likely to only play a significant role in the initiation steps of monolayer formation, and not in the propagation of the Si-C bond formation.

Chapter 4, describes the experimental and theoretical study of the radical chain mechanism, and in particular the effect of stabilization of the  $\beta$ -carbon radical. Analogously to Chapter 3, the H-Si surface was represented by a low molecular-weight silane. The radical reactivity was studied by performing competition reactions of precursors (alkenes, alkynes, etc.) with the tris(trimethylsilyl)silyl radical, and via high-level theoretical calculations on a theoretical  $\text{Si}_4$ -model to obtain the activation barrier and overall free energy changes. In line with results from monolayer experiments in literature, 1-alkynes were found to react 8-fold faster than 1-alkenes, whereas aldehydes reacted 30-fold slower than 1-alkene. Moreover, a dramatic increase of reactivity was observed for molecules with an extended  $\pi$ -conjugation. These findings were supported by the calculated reaction rates, which showed an excellent correlation with the experimental rates, and confirmed the effect of delocalization of the  $\beta$ -carbon radical on the reactivity. Lowering the energy of the radical intermediate, however, may have an adverse effect on the second step of the reaction, the hydrogen transfer from the surface. In order to study this second reaction in more detail, the theoretical model was extended to a  $\text{Si}_7$ -cluster. These calculations revealed that the barriers for hydrogen transfer were, in general, higher than the barriers for the radical addition, which indicated that for monolayer formation, hydrogen transfer is likely to be the rate-limiting step.

Based on the insights obtained in the research described in Chapters 3 and 4, Chapter 5 describes in a combined experimental and theoretical study a significant improvement of



surface coverage and speed-up of monolayer formation on H-Si. The newly designed enyne moiety (from Chapter 4) was tested against the agent that gives the highest quality monolayers on H-Si(111) known in literature, namely a 1-alkyne. The first part of the chapter describes the monolayer kinetics that were obtained by studying partly completed monolayers from hexadec-3-en-1-yne and 1-hexadecyne. Ellipsometry and contact angle measurements, showed a faster increase of layer thickness and hydrophobicity for the hexadec-3-en-1-yne-derived monolayers. Plateau values for both characteristics were obtained after 8 and 16 hours at room temperature for hexadec-3-en-1-yne and 1-hexadecyne, respectively. This difference in reaction speed was confirmed by IRRAS and XPS measurements.

In the second part of the chapter, fully completed layers (obtained after 16 h at 80 °C) were studied to determine and compare the quality (packing and order) of both monolayers. Ellipsometry thickness, contact angles, IRRAS, and NEXAFS indicated a high quality and dense packing of both layers. Quantitative XPS revealed a higher surface coverage for C<sub>16</sub> dienyl layers than C<sub>16</sub> alkenyl layers (63% vs. 59%).

In the third and final part of Chapter 5, molecular mechanics simulations in combination with G3 calculations revealed a more favorable packing for alkenyl layers for surface coverages up to 55%. At higher surface coverages, dienyl packing becomes more favorable, which is thus again in line with experiments.

Finally, chapter 6 discusses the overall outcomes of this research and gives suggestions for further work in this field.



## Samenvatting

Covalent gebonden organische monolagen op silicium oppervlakken vormen een thermisch en chemisch stabiel platform voor (bio) functionalisatie van het oppervlak. Recente ontwikkelingen in monolaag formatie – resulterend in toenemende kwaliteit en de volledige uitsluiting van zuurstof op deze gemodificeerde oppervlakken – hebben de deur geopend voor toekomstige ontwikkelingen van biosensoren, photovoltaïsche cellen en moleculaire elektronische apparaten. Ondanks deze succesvolle innovaties op het gebied van monolaag formatie (o.a. ook het maken van patronen en functionalisatie) in de laatste twintig jaar, blijft de eigenlijke kennis van de processen die zich afspelen aan het oppervlak achter. Een goed begrip van de mechanismen voor initiatie en propagatie kan helpen in het vinden van nieuwe parameters die leiden tot een versnelling van het proces, en tot nieuwe strategieën voor het binden van nieuwe interessante biomoleculen aan het silicium oppervlak.

In de zoektocht naar nog snellere synthese methoden voor het maken van monolagen van nog hogere kwaliteit, beschrijft dit proefschrift een gecombineerde experimentele en theoretische studie van de onderliggende mechanismes van monolaag formatie.

Hoofdstuk 1 geeft een algemene inleiding tot dit proefschrift, waarbij het concept van “self-assembly” (zichzelf ordenende systemen) uitgelegd wordt. Tevens worden er voorbeelden gegeven van deze geordende monolagen op verschillende soorten oppervlakken zoals: thiol monolagen op metal oppervlakken, organosilaan monolagen op oxide oppervlakken en organische monolagen die direct via Si-C bindingen vastzitten aan silicium oppervlakken. Deze laatste groep vormt het belangrijkste aandachtspunt van dit proefschrift, en ter inleiding worden enkele eigenschappen van de verschillende monolaag systemen vergeleken.

Hoofdstuk 2 geeft een meer gedetailleerd overzicht van de hedendaagse kennis van de mechanismes die ten grondslag liggen aan monolaag formatie op waterstof getermineerd silicium. In de literatuur worden overwegend drie soorten silicium oppervlakken beschreven: H-Si(111), H-Si(100) en poreus silicium (H-pSi). Deze drie verschillende oppervlakken vereisen elk hun eigen methodes voor het etsen van het oppervlak en het vormen van de monolagen, die worden toegelicht. De nadruk van dit hoofdstuk ligt voornamelijk bij H-Si(111) en H-Si(100) oppervlakken, waarbij silicium radicalen de kern vormen in de vorming van Si-C bindingen die de monolagen verankeren aan het oppervlak. Deze radicalen zijn ook erg reactief ten opzichte van zuurstof, hetgeen leidt tot oxidatie van het oppervlak. Diverse mechanismen die de formatie van deze radicalen initiëren, worden samen met ondersteunende theoretische en experimentele studies in dit hoofdstuk besproken. Er wordt een onderscheid gemaakt tussen ‘hoog energetische’ methodes die gebruik maken van hoge temperaturen en UV straling om rechtstreeks Si-H bindingen te

verbreken, en ‘milde’ methodes die veel minder energie gebruiken (te weinig om rechtstreeks Si-H bindingen te verbreken) en indirect leiden tot de formatie van radicalen aan het oppervlak. Dit hoofdstuk geeft tevens een overzicht van de huidige stand van zaken met betrekking tot het verder functionaliseren en aanbrengen van patronen, alsook een perspectief naar toekomstige applicaties en onderzoek.

Het radicaal kation initiatie mechanisme wordt in meer detail bestudeert in hoofdstuk 3. Dit hoofdstuk beschrijft hoe radicaal kationen van silicium modelverbindingen met een laag molecuulair gewicht, die gesynthetiseerd zijn om het H-Si oppervlak na te bootsen, werden verkregen met behulp van licht geïnduceerde elektronen overdracht. De stabiliteit en de aard van de radicaal kationen werden onderzocht door de levensduur en secundaire elektronen overdracht te bestuderen. De radicaal kationen vertoonden een sterke reactiviteit ten aanzien van diverse op zuurstof gebaseerde nucleofielen ( $\sim 10^7 \text{ M}^{-1}\text{s}^{-1}$ ), en een significante reactiviteit ten aanzien van 1-alkenen en 1-alkynen ( $\sim 10^5 - 10^6 \text{ M}^{-1}\text{s}^{-1}$ ). Verder toonde tijds-opgeloste kinetiek een bimoleculaire nucleofiele aanval op het radicaal kation aan. Een secundair isotoop effect geeft verder aan dat de centrale Si-H binding vlak naast het reactiecentrum ligt, maar dat deze niet wordt verbroken in de snelheidsbepalende stap. Beide bevindingen zijn in overeenstemming met het radicaal kation mechanisme. Analyse van de reactieproducten toonde bovendien substitutie producten aan die het verbreken van een Si-Si binding bevestigden. De aanwezigheid van hydrosilyleringsproducten kon verklaard worden door de vorming van een  $\beta$ -koolstof radicaal. Dit radicaal initieert vervolgens een kettingreactie door een waterstof atoom af te pakken van een niet-gereageerd silaan. Tot slot laat dit hoofdstuk zien dat radicaal kation initiatie op het silicium oppervlak mogelijk is. Gezien het verschil in reactiviteit tussen zuurstof en koolstof gebaseerde nucleofielen, zal deze reactie waarschijnlijk alleen een aanzienlijke rol spelen in de initiatiestap, en niet in de propagatie van de vorming van de Si-C bindingen.

Hoofdstuk 4 beschrijft vervolgens een experimentele en theoretische studie naar de radicaal kettingreactie, en in het bijzonder het effect van het stabiliseren van het  $\beta$ -koolstof radicaal. Het H-Si oppervlak wordt, analoog aan hoofdstuk 3, nagebootst door een silaan met een laag molecuulair gewicht. De reactiviteit van het radicaal werd indirect bepaald door het volgen van competitie reacties tussen uitgangsstoffen (alkenen, alkynen, etc.) en het tris(trimethylsilyl)silyl radicaal, en via berekeningen van de activerings- en de reactie-energie aan een theoretisch  $\text{Si}_4$ -model. Geheel in lijn met experimentele resultaten uit de literatuur, bleken 1-alkynen 8 maal sneller te reageren dan 1-alkenen, terwijl aldehyden 30 maal langzamer waren dan 1-alkenen. Verder werd er een drastische toename van reactiviteit waargenomen voor verbindingen met een uitgebreid systeem van  $\pi$ -conjugatie. Deze bevindingen werden ondersteund door de berekende reactie snelheden, die een uitstekende correlatie toonden met de experimentele resultaten. Dit bevestigde het effect van delocalisatie van het  $\beta$ -koolstof radicaal op de reactiviteit. Echter, verlaging van de

energietoestand van het radicaal intermediair kan een tegengesteld effect hebben op de waterstof overdracht in de tweede stap van de reactie. Om deze reactie meer in detail te kunnen onderzoeken is het theoretische model uitgebreid tot een  $\text{Si}_7$  cluster. Deze berekeningen toonden aan dat de reactie barrière voor waterstof overdracht in het algemeen hoger waren dan de barrières voor de additie stap. Dit is een sterke aanwijzing dat deze tweede stap waarschijnlijk snelheidsbeperkend is.

Gebaseerd op de inzichten uit hoofdstukken 3 en 4, geeft hoofdstuk 5 een beschrijving van een gecombineerde experimentele en theoretische studie naar een significante verbetering van de bedekkingsgraad en reactiesnelheid van monolagen op H-Si. De nieuwe ene-yne groep (uit hoofdstuk 4) werd vergeleken met een 1-alkyne, een precursor die op het moment de hoogste kwaliteit monolagen geeft of H-Si die bekend zijn in de literatuur. Het eerste deel van het hoofdstuk beschrijft de kinetiek van monolaag vorming, die werd gevolgd door onvolledige monolagen te bestuderen. Ellipsometrie en contacthoek metingen toonden een snellere toename van laagdikte en hydrofobiciteit aan voor de hexadec-3-en-1-yne monolagen. Plateau waarden voor beide karakteristieken werden verkregen na 8 en 16 uur reactie op kamertemperatuur. Dit verschil in reactiesnelheid werd bevestigd door IRRAS en XPS metingen.

In het tweede gedeelte van het hoofdstuk werd de kwaliteit van volledig uitgereageerde monolagen (verkregen na 16 uur bij 80 °C) bestudeerd en vergeleken. Laagdiktes, contacthoeken, IRRAS en NEXAFS wezen voor beide monolagen op een hoge kwaliteit en dichte pakking. Kwantitatieve XPS toonde vervolgens aan dat de bedekkingsgraad voor  $\text{C}_{16}$  dienylynen groter was dan voor  $\text{C}_{16}$  alkenylynen (63% tegen 59%).

In het derde en laatste deel van hoofdstuk 5 wijzen “molecular mechanics” simulaties in combinatie met G3 berekeningen naar een gunstigere pakking voor alkenylynen voor bezettingsgraden tot 55%. Bij hogere bezetting is de pakking van de dienylynen gunstiger, hetgeen wederom in lijn is met de experimentele resultaten.

Tot slot geeft hoofdstuk 6 een beschrijving van de algemene resultaten van dit onderzoek. Tevens worden er suggesties gegeven voor verder onderzoek.



## **Curriculum Vitae**

Bart Rijkse werd op 5 juli 1979 in Venlo geboren. Na het behalen van het VWO-diploma aan het Thomascollege in Venlo begon hij in 1998 aan de studie moleculaire wetenschappen aan de Wageningen Universiteit. Hij deed afstudeervakken bij de leerstoelgroepen Fysische Chemie en Kolloïdkunde, en Organische Chemie. In 2006 begon hij aan een promotie onderzoek bij de leerstoelgroep Organische Chemie aan de Wageningen Universiteit, onder leiding van Prof. dr. H. Zuilhof. De belangrijkste resultaten van dit onderzoek staan beschreven in proefschrift. Sinds maart 2011 is hij werkzaam bij DOW Benelux B.V. als onderzoeker in de materials science & engineering groep in Terneuzen.

Bart Rijkse was born on July 5, 1979 in Venlo. After finishing pre-university education at the Thomascollege in Venlo, he started his study molecular sciences at the Wageningen University in 1998. He did internships in the departments for Physical Chemistry and Colloid Sciences, and Organic Chemistry. In 2006, Bart started his PhD research in the department of Organic Chemistry at Wageningen University. The most important results of this research are described in this thesis. Since March 2011 he is working for DOW Benelux B.V. in the materials science & engineering group in Terneuzen.





## List of Publications

*Molecular Modeling of Alkyl and Alkenyl Mono layers on Hydrogen-Terminated Si(111)*

L. Scheres, B. Rijksen, M. Giesbers, and H. Zuilhof, *Langmuir*, **2011**, 27, 972-980

*Mimicking the Silicon Surface: Reactivity of Silyl Radical Cations toward Nucleophiles*

B. Rijksen, B. van Lagen, and H. Zuilhof, *Journal of the American Chemical Society*, **2011**, 133, 4998-5008

*Silyl Radical Surface Chemistry*

B. Rijksen, M.A. Caipa Campos, J.M.J. Paulusse, and H. Zuilhof, **2012**, In *Encyclopedia of Radicals in Chemistry, Biology and Materials*; Eds.: C. Chatgililoglu, A. Struder, Wiley, Chichester

*Reactivity of Silyl Radicals towards Unsaturated Hydrocarbons: Understanding Monolayer Formation on H-Terminated Silicon (111)*

B. Rijksen, J.M.J. Paulusse, and Han Zuilhof, **2012**, submitted

*Hexadecadienyl Monolayers on Hydrogen-terminated Si(111): Faster Monolayer Formation and Improved Surface Coverage Using the Enyne Moiety*

B. Rijksen & S. Pujari, L. Scheres, C. van Rijn, J. Baio, T. Weidner, and H. Zuilhof, **2012**, submitted



## Overview Training Activities

### Discipline specific activities

#### Courses:

Photophysics, photochemistry & photobiology, HRSMC, VU Amsterdam, 2007

Molecular modeling, HRMSC, UvA, Amsterdam, 2008

Advanced Macromolecular Systems Across the Length Scales (AMSALS) III, Mesa+, Enschede, 2008

Advanced Organic Chemistry, Laboratory of Organic Chemistry, Wageningen, 2010

#### Meetings:

Annual NWO Conference Structure and Reactivity, NWO, Lunteren, 2006-2010

Annual MicroNano Conference, 2006-2010

NanoNed Meetings, Nanofabrication, 2006-2010

Organic Chemistry Symposium, KNCV, Wageningen, 2008 & 2010

### General Courses

Vlag PhD week, 2007

PhD Scientific Writing, Centa, Wageningen, 2009

Career Perspectives, Wageningen Graduate Schools, 2010

### Optionals

Group Meetings, Laboratory of Organic Chemistry, 2006-2010

Colloquia, Laboratory of Organic Chemistry, 2006-2010

PhD studytrip, Laboratory of Organic Chemistry, Sweden, 2007

PhD studytrip, Laboratory of Organic Chemistry, China, 2009

Organizing committee PhD studytrip China, 2009



## Dankwoord

Mijn promotieonderzoek was een sprong in het diepe. Er kwamen best veel nieuwe dingen op mij af. Gelukkig waren er altijd mensen om me heen die me hielpen en wilden samenwerken, waardoor mijn onderzoek al snel vorm kreeg. Ik heb erg veel plezier gehad tijdens mijn aioschap bij ORC, omdat ik onderzoeken leuk vind, maar vooral ook door de steun van familie, vrienden en collega's! Daarom deze laatste pagina's om iedereen te bedanken voor hun steun en hulp.

In de eerste plaats wil ik mijn promotor, Prof. dr. Han Zuilhof, bedanken. Han, ik herinner me ons eerste gesprek over een mogelijk aioschap. Je zocht iemand die niet vies was van organische synthese, maar die ook de kinetiek wilde induiken. Je dacht dat dergelijk fundamenteel onderzoek wel bij mij zou passen, en je hebt gelijk gehad! Ik heb het erg naar mijn zin gehad, en ben dankbaar voor de kans die je me gegeven hebt. Het resultaat van alle inspanningen ligt nu voor je. Ik heb veel van je geleerd over chemie, en over wetenschap in het algemeen. Ook op persoonlijk vlak ben je altijd zeer betrokken geweest, en dat heb ik erg gewaardeerd! Verder wil ik je bedanken voor de extra tijd die je in de laatste fase vrij hebt gemaakt (avonden, weekenden en vooral de kerstvakantie...).

Vervolgens wil ik graag Jos Paulusse bedanken voor de vele nuttige gesprekken en zijn bijdrage aan artikelen. Jos, hoewel je eigenlijk niet mijn begeleider was, heb je veel tijd vrij gemaakt om me met van alles en nog wat te helpen. Je hebt eerste versies gecorrigeerd, goede vragen gesteld, en vooral bijgedragen aan een hele prettige werksfeer bij ORC. Ik wens je heel veel succes in Twente!

Bij deze wil ik ook graag de leden van de promotiecommissie, Frans Leermakers, Fred Brouwer, Leo Jenneskens en Louis de Smet bedanken voor het beoordelen van mijn proefschrift. Tevens wil ik graag alle deelnemers van het Flagship Nanofabrication van NanoNed bedanken voor een leuke en leerzame tijd! De halfjaarlijkse bijeenkomsten en vooral de jaarlijkse symposia waren legendarisch!

Barend, bedankt voor de prettige samenwerking. Zonder jouw hulp was de radicaal kation paper nooit geworden tot wat het nu is. Dat is niet alleen te danken aan je zeer nauwkeurige metingen, maar ook aan het engelengeduld dat je getoond hebt tijdens het eindeloos sleutelen aan de laser om überhaupt een signaal te krijgen. Verder heb ik erg veel van je geleerd over NMR, en heb ik je betrokkenheid zeer gewaardeerd!

Luc, samen met Han en Ahmed heb je er voor gezorgd dat ik begonnen ben aan een promotieonderzoek bij ORC. Ik had eigenlijk andere plannen, maar jullie enthousiasme voor monolagen heeft me aangestoken. En daar heb ik de afgelopen jaren geen moment spijt van gehad! Dank je voor de regelmatige 'werkoverleggen' en je inspanningen voor de laatste paper. Ik ben blij dat je verder bent gegaan in de monolagen business en wens je veel succes met het op de kaart zetten van SurFix! Hopelijk ben je volgend jaar met vastelaovend weer van de partij ☺.

Het schrijven van een hoofdstuk voor een boek over radicaal chemie is een hele uitdaging, maar gelukkig hoefde ik het niet alleen te doen. Mabel, ik wil je dan ook van harte bedanken voor je bijdrage aan dit hoofdstuk. Het was een ware uitputtingsslag, met mailtjes over en weer tot diep in de nacht. Maar we hebben de deadline gehaald, en ik ben erg tevreden met het resultaat! Verder wil ik je ook bedanken voor de gezellige tijd in het lab.

Sidhu, I really liked working with you. I like your curiosity and your adventurous spirit, which takes you all over the world. Also, I think your lab skills make you the new monolayer king of ORC! I am convinced that you will do great, and I am looking forward to reading your future papers.

Loes en Kim, jullie wil ik in het bijzonder bedanken voor de gezellige tijd. Als kamergenoten (aangrenzende kamers via open tussendeur tellen als één ;) ) hebben we het nodige meegemaakt. Gelukkig vooral leuke dingen zoals de aio-reizen, de borrels en niet te vergeten de studiereis naar de Efteling ☺ Ik wens jullie heel veel succes in jullie verdere carrière bij Stahl en de Hogeschool Utrecht!

Natuurlijk wil ik ook mijn andere kamergenoten, Wouter en Sourav, bedanken voor de gezellige tijd. Jacob, mede dankzij jou heb ik een goede start kunnen maken bij ORC. Ik heb veel van je geleerd, met als voornaamste punt de beginselen van QM berekeningen, die uiteindelijk een substantieel deel van mijn onderzoek zijn geworden. Ruud en Rokus, naast gezelligheid hebben ook jullie een bijdrage geleverd aan mijn modeling carrière. Van jobjes starten op een van de moores tot aan waarschuwingen voor relativistische effecten. Remco, Jurjen, TuHa, Tijs (als je NMR samples had afgeleverd), Nagendra, Ahmed, Michel en Milena bedankt voor de gezellige tijd in de kelder van ORC!

Verder wil ik graag de mensen bedanken die mijn leven qua specialistische metingen en hand en spandiensten een stuk makkelijker hebben gemaakt: Marcel voor hulp bij XPS metingen, Frank, Elbert en Teris voor hulp bij de nodige chromatografische vraagstukken, Ronald voor de bestellingen en het verzinnen van ad hoc oplossingen voor praktische problemen!, Maarten Posthumus en Peter van Galen voor exacte massa bepalingen, Erik voor de carpool, en last but not least Elly en Aleida voor hulp bij de administratieve zaken (zeker in de eindfase was ik erg blij met jullie hulp). Verder wil ik iedereen binnen ORC bedanken voor de gezellige tijd!

Vervolgens wil ik graag mijn paranimfen Monique en David bedanken voor hun steun tijdens de laatste fase van dit traject. Monique, ik vind het echt supertof dat je paranimf wil zijn! David, al tijdens mijn studie, maar vooral ook tijdens mijn aio-schap heb je altijd veel interesse getoond in mijn voortgang. Relativeren met een biertje erbij, of lekker stoom afblazen tijdens een rugby training of wedstrijd gaat toch het best met vrienden er bij! Ik vind het erg fijn dat jullie allebei naast me staan tijdens mijn verdediging.

Trees, Simon & Catja, Dorien en Rik bedankt voor de vele gezellige borrels in Wageningen! Verder wil ik ook iedereen van rugbyclub Wageningen bedanken voor een leuke tijd.

Pap en mam, jullie wil ik graag bedanken voor jullie steun en interesse. Zonder jullie vertrouwen en steun in het begin was ik er waarschijnlijk niet eens aan begonnen. Hoewel het onderwerp ver van jullie af stond, hebben jullie toch altijd geprobeerd te begrijpen wat ik nou eigenlijk aan het doen was daar in Wageningen. Dat heb ik altijd erg fijn gevonden! Bij deze wil ik ook Frans en Joke, die er ineens een schoonzoon met zijn tijdrovende hobby bijkregen, bedanken voor hun betrokkenheid en interesse in mijn vorderingen.

Lieve Veerle, deze laatste regels zijn voor jou bestemd. Jouw vertrouwen en begrip heeft heel veel voor me betekend. Vooral als het even niet meezat wist je me op te beuren en me te motiveren. Nu de aio-dingen bijna achter de rug zijn, kijk ik er erg naar uit om samen met jou in het aanstaande avontuur te duiken!

Bart

The research in this thesis was financially supported by NanoNed, funded by the Dutch Ministry of Economic Affairs (project WPC 7123).

Printed by De Budelse BV, Budel, The Netherlands